

https://dspace.org/

The characterization of Mycobacterium tuberculosis amidase-like proteins

Matlhabe, Ofentse

2024
https://hdl.handle.net/10539/37592

Downloaded from a DSpace repository. https://dspace.org/

The characterization of

Mycobacterium tuberculosis amidase-like proteins

Ofentse Matlhabe

682609

A thesis submitted to the Faculty of Health Sciences, University of the Witwatersrand, Johannesburg, in fulfilment of the requirements for the degree of Doctor of Philosophy.

Johannesburg, 2023

Declaration

I, Ofentse Matlhabe, am a student registered for the degree of Doctor of Philosophy at the University of the Witwatersrand in the academic year 2023.

I hereby declare the following:

- I am aware that the use of someone else's literature and work without their permission and/or without acknowledging the original source is unacceptable.
- I confirm that the work submitted for assessment for the above-mentioned degree is my own unaided work except where explicitly indicated otherwise.
- I have not submitted this work before for any other degree or examination at any other university.
- I have followed the required conventions in referencing the thoughts and ideas of others.
- I understand that the University of the Witwatersrand may take disciplinary action against me if there is a belief that this is not my own unaided work or that I have failed to acknowledge the source of the ideas or words in my writing.

Signature of candidate: O. Matlhabe Date: 14/06/23

Dedications

I would like to dedicate this work to my wife, Thato Moloisana-Matlhabe for the love, patience and support that she has given me throughout this journey. My parents, Annah and Thomas Mabunda for their support and for allowing me to follow my own path. To my friend Mthembeni Dumisa for his support and encouragement**.**

Acknowledgements

I would like to thank my family for the support they have provided. Without you all, I would not have the strength to walk this journey.

I would like to thank Prof Bavesh Kana, not only for your supervision, but also for your mentorship and support, which has been beyond the scope of your prescribed duties as supervisor. I thank you for your patience and for allowing me to the room to drive this project. Although you say I do not listen to you, I hold your words in high esteem.

I would like to thank Dr Christopher Ealand for the support that you have provided me, for your patience, and for making time to assist me, even when you are busy. I thank you for challenging how I think as a scientist and for making sure that I succeed in whatever I set out to do in the lab.

The staff at the CBTBR. Thank-you for all your support and assistance and for making sure that the lab is running at all times. To my PhD colleagues, Moagi and Itumeleng, thank you both for your inputs and for the moral support.

I would like to thank the South African National Research foundation for the financial support

To the following researchers for contributing materials:

Prof. Michael VanNieuwenhze, Department of Chemistry, Indiana University Bloomington, for gifting us TADA.

Prof. Tom Bernhardt, Department of Microbiology and Immunobiology, Harvard Medical School, for donating the E. coli ΔenvCΔnlpD to us strain.

Dr. Gavin Owen, HIV Pathogenesis Research Unit, Department of Molecular Medicine and Haematology, Wits University for gifting us the *E. coli* BL21 (DE3) strain.

Dr Shuyi Ma, Department of Microbiology, University of Washington, Seattle, WA, USA. For gifting us the TFI library plasmids (including pEXNF_Rv1423 and pEXNF_Rv1776c).

Presentations from this dissertation

1. Matlhabe, O.D., Ealand, C., and Kana, B. Characterizing the biological function of Rv3717 (Ami1), a *Mycobacterium tuberculosis*, amidase. Molecular Biosciences Research Thrust Postgraduate Research Day, Wits University, Johannesburg. December 2022. Oral presentation
2. Matlhabe, O.D., Ealand, C., and Kana, B. Characterizing Rv3717 (Ami1), a *Mycobacterium tuberculosis*, amidase. 13th Cross-faculty Postgraduate Symposium, Wits University, Johannesburg. October 2022. Oral presentation
3. Matlhabe, O.D., Ealand, C., and Kana, B. Characterizing Rv3717 (Ami1), a *Mycobacterium tuberculosis*, amidase. Molecular Biosciences Research Thrust Postgraduate Research Day, Wits University, Johannesburg. December 2021. Grad flash presentation
4. Matlhabe, O.D., Ealand, C., and Kana, B. The activation mechanism of mycobacterial amidase proteins. Molecular Biosciences Research Thrust Postgraduate Research Day, Wits University, Johannesburg. December 2019. Poster presentation

Abstract

Tuberculosis (TB), a disease caused by the bacterium *Mycobacterium tuberculosis*, is a significant global threat to human health. The emergence of drug resistant *M. tuberculosis* necessitates the identification of new drug targets for the development of new, shorter regimens. The peptidoglycan (PG) core of the *M. tuberculosis* cell wall is a potential source of drug targets because it is unique to bacteria and plays a vital role in a multitude of cellular processes and host-mediated immune responses. PG is constantly remodelled by PG synthases and hydrolases in response to external stimuli. This research focuses on *N*-acetylmuramyl-L-alanine amidases (amidases), PG hydrolases that are implicated in bacterial growth, cell division, virulence and antibiotic tolerance. More specifically, this PhD aims to characterize the *M. tuberculosis* Ami1 (Rv3717) homologue and to highlight its potential as a drug target. Genotypic characterization of a previously generated *M. tuberculosis* mutant strain lacking *ami1* (H37*Δami1S*) was conducted prior phenotypic assessments. The deletion of *ami1* had no significant effect on growth rate and cell division in standard 7H9 media. In contrast, the growth rate of H37*Δami1S* was significantly reduced when grown in Sauton's minimal media with (1%) or without glycerol as a carbon source. We then surmised that Ami1 possibly plays a role in intracellular survival, where host-derived carbon sources support bacterial growth. The survival of H37*Δami1S* was reduced in IFN-γ stimulated U937 macrophages.

H37*Δami1S* displayed increased susceptibility to rifampicin when assessed by broth microdilution. This observation was credited to a weakened, more permeable cell wall. Consistent with this, H37*Δami1S* exhibited an increased ethidium bromide uptake. Subsequently, we hypothesized that H37*Δami1S* may display alterations in antibiotic tolerance/persistence. In a 7-day time-course experiment, H37*Δami1S* displayed increased susceptibility to vancomycin, ethionamide and isoniazid as evidenced by declining bacterial survival. We interrogated the isoniazid-associated phenotype further, by assessing the transcription of all three amidase-encoding genes. Only *ami1* was induced following exposure to isoniazid whereas the expression of *ami3* and *ami4* remained at basal levels. The regulation of the *ami1* gene was explored further through bioinformatics, which revealed two putative transcriptional regulators predicted to bind upstream of *ami1*, namely Rv1423 and Rv1776c. Protein homology modelling detected HTH DNA binding domains in both proteins. These proteins were then cloned for recombinant expression in the pET29a+ system for purification. Rv1776c was successfully expressed and purified. Electrophoretic mobility shift assays yielded preliminary data that suggested that Rv1776c binds the promoter region of the *ami1* gene.

Attempts to optimize binding were unsuccessful. To further evaluate the role of Rv1776c and Rv1423 in regulating *ami1* gene expression, we over-expressed the regulators, using the tetracycline operator, and assessed effect on cell wall stability, via an ethidium bromide diffusion assay. Over-expression of Rv1776c was not achieved despite increasing concentrations of anhydrotetracycline, suggesting possible downstream regulation of Rv1776c; however, over-expression of Rv1423 was achieved. An increase in ethidium bromide uptake was observed in strains over-expressing Rv1776c and Rv1423. Increasing anhydrotetracycline concentrations in both strains resulted in marginal decreases in the transcription of *ami1*. Overall, this study has demonstrated that Ami1 plays a vital role in how *M. tuberculosis* utilizes a carbon source during normal growth and survival *in vitro*. Moreover, the transcription of *ami1* is specifically and directly responsive to isoniazid exposure, possibly via two transcriptional repressors. This work therefore supports further characterization and development of Ami1 as novel drug target in *M. tuberculosis*.

Table of Contents

Declaration i
Dedications ii
Acknowledgements iii
Presentations from this dissertation iv
Abstract v
List of Figures xi
List of tables xiv
Nomenclature xv
Chapter 1: General Literature Review 1
1. General Literature Review 1
1.1. The burden of TB 1
1.2. Pathogenesis 2
1.3. Methods used by Mtb to evade host immune responses 3
1.4. TB prevention 4
1.5. Diagnosis of TB: current tools, limitations and the development of novel tools 7
1.6. Treatment of TB 11
1.7. Mechanisms of drug resistance/tolerance in Mtb 13
1.8. The mycobacterial cell wall 15
1.9. PG modifications and their roles in mycobacterial cell walls 20
1.10. PG remodelling during cell growth and division 21
1.11. PG polymerization and PG synthases 23
1.12. PG hydrolases 24
1.12.1. Glycosidases 25
1.12.2. Peptidases 25
1.12.3. Amidases 26
Chapter 2: General Experimental Methods and Associated Materials 28
2. General experimental methods and associated materials 28
2.1. Bacterial growth conditions 28
2.1.1. Growth conditions for *E. coli* strains 28
2.1.2. Growth conditions for Msm strains 28
2.1.3. Growth conditions of Mtb strains 28
2.2. DNA extractions 29

2.2.1. Mtb genomic DNA (gDNA) extraction 29
2.2.1.2. Small scale gDNA extraction for PCR in Mtb 29
2.2.2. Plasmid DNA extraction from *E. coli* 30
2.2.3. Ethanol precipitation for purification of genomic and plasmid DNA 31
2.3. DNA manipulation/cloning 31
2.3.1. Polymerase Chain Reaction (PCR) 31
2.3.2. Restriction digests 32
2.3.3. Plasmid dephosphorylation 32
2.3.4. Agarose gel electrophoresis 33
2.3.5. DNA fragment purification 33
2.3.5. DNA ligation 34
2.4. Bacterial Transformations 34
2.4.1. Transformation of chemically competent *E. coli* DH5α cells 34
2.4.2. Mtb electroporations 35
2.5. Monitoring gene expression 35
2.5.1. RNA Extraction in Mtb 35
2.5.2. Complementary DNA (cDNA) synthesis from total RNA 36
2.5.3. Quantitative PCR (qPCR) 37
Chapter 3: Characterization of an *ami1*-deficient mutant of *Mycobacterium tuberculosis* 38
3.1. Introduction 38
3.1.1. Amidases in *E. coli* 38
3.1.2. Amidases in *Bacillus subtilis* 39
3.1.3. Amidases is *Staphylococcus* species 41
3.1.4. Mycobacterial amidases 43
3.1.5. Amidases and the immune response 43
Hypothesis 46
Aims and Objectives 46
3.2. Methods 48
3.2.1. Confirmation of ami1 deletion and complementation 52
3.2.2. Determining the role of Ami1 in Mtb cell growth and division 54
3.2.3. Assessing H37*Δami1S* Survival under carbohydrate limiting conditions 55
3.2.4. Monitoring the effect of *ami1* deletion on Mtb cell wall permeability 55
3.2.5. Survival under antibiotic stress 56

3.2.6. Transposon mutagenesis for identifying genes that are conditionally essential with *ami1* under isoniazid stress 58
3.2.6.1. Phage Stock Preparation and titering 59
3.2.6.2. Bacterial transduction and transposon library construction 59
3.2.7. Assessing the role of Ami in Mtb intracellular survival 60
3.3. Results 62
3.3.1. Confirmation of *ami1* gene deletion in the mutant strain H37*Δami1S* 63
3.3.2. Deletion of *ami1* has no effect on *in vitro* cell growth, elongation, and division in nutrient rich media 65
3.3.3. H37*Δami1S* displayed poor growth in Sauton's media (1% and 0% glycerol) 72
3.3.4. H37*Δami1S* displays increased EtBr uptake 73
3.3.5. The *ami1* mutant of Mtb displays increased susceptibility to Lysozyme, Vancomycin, Ethionamide and INH in time-kill assays 74
3.3.6. INH exposure induces *ami1* transcription in H37RvS 81
3.3.8. The survival of H37*Δami1S* is reduced in activated U937Mϕ 87
Chapter 4: Characterization of putative regulators of the *ami1* gene in *Mycobacterium tuberculosis* 92
4.1. Introduction 92
4.1.1. Regulation of amidase activity at protein level 92
4.1.2. Regulation of amidase activity at transcriptional level 94
4.2. Methods 97
4.2.1. Investigating Ami1 transcription regulator 101
4.2.2. Expression and purification of FLAG-tagged Rv1423 and Rv1776c 101
4.2.3. Expression and purification of His-tagged Rv1423 and Rv1776c 102
4.2.6. Electrophoretic mobility shift assay (EMSA) 106
4.2.7. EtBr uptake 107
4.2.8 RT-qPCR for monitoring ami1, ami3 and ami4 expression post INH exposure 107
4.2.9. Heterologous expression of Ami1 in *E.coli* 107
4.3. Results 108
4.3.1. Preliminary data to determine regulatory mechanisms for Ami1 in Mtb. 109
4.3.2. Identification and characterization of putative *ami1* transcriptional regulators 111
4.3.2. Expression and purification of Rv1423 and Rv1776c using *E. coli* expression systems 113
4.3.3. Assessing *ami1* promoter DNA binding ability 118

4.3.4. Monitoring phenotypic effects of over expressing putative Ami1 regulators 119
Chapter 5: Conclusion, limitations and future experiments.....125
Chapter 6: References.....128
Chapter 7: Appendices.....148
Appendix A: Growth Media Formulations.....148
Appendix B: Solutions.....149
Appendix C: Molecular weight Marker.....152
Appendix D: Hain-line probe assay data sheet.....153
Appendix E: Optimization of Rv1423 IPTG inductions.....154
Appendix F: Optimization of EMSA Rv1776c-500bp UP *ami1* binding.....155
Appendix G: Ethics waiver.....160
Appendix H: Turn it in similarity report.....161

List of Figures

Figure 1.1. The estimated TB incidence in 2021.

Figure 1.2. TB vaccine candidates and their progression through clinical trials.

Figure 1.3. Estimated incidences of MDR-TB as determined by the WHO in 2021.

Figure 1.4. Schematic diagram representing the mycobacterial cell wall

Figure 1.5. Biosynthetic pathways that result in the formation of the mycolic acid-arabinogalactan-peptidoglycan complex (MAPc) in Mtb.

Figure 1.6. The biosynthesis of PG in *Mycobacterium tuberculosis*.

Figure 1.7. Schematic diagram showing *N*-glycolyl modifications in mycobacterial PG.

Figure 1.8. Various PG synthases and the bonds arising from their actions on the PG molecule.

Figure 1.9. Various PG hydrolases and their cleavage locations on the PG molecule.

Figure 3.2. An overview of the methodology used in this study.

Figure 3.3. An overview of the findings of this study.

Figure 3.3.1. Genotyping and *ami1* transcriptional analysis in H37RvS, H37*Δami1S*, and H37*Δami1S*::ami1.

Figure 3.3.2. Growth kinetics of Mtb strains.

Figure 3.3.3. Schematic diagrams showing the PG incorporation mechanism of fluorescent D-ala analogue TADA.

Figure 3.3.4. Assessment of TADA staining and cell lengths of *Mtb* strains.

Figure 3.3.5. PTweety_DivIV_GFP restriction mapping to confirm plasmid integrity.

Figure 3.3.6. pFtsZGFP restrictions to confirm plasmid integrity.

Figure 3.3.7. DivIVA-GFP localization in *M. tuberculosis* strains

Figure 3.3.8. FtsZ-GFP localization in *M. tuberculosis* strains.

Figure 3.3.9. Schematic showing pMV_FtsZGFP integration into H37RvS and H37Δami1S.

Figure 3.3.10. Confirmation of pMV_FtsZGFP integration into H37RvS and H37Δami1S.

Figure 3.3.11. Growth assessment of the ami1 mutant strains under nutrient limited conditions.

Figure 3.3.12. Assessment of ethidium bromide uptake in the *ami1* mutant of Mtb.

Figure 3.3.13. Drug susceptibility assessments of the ami1 mutants using time-kill curves.

Figure 3.3.14. Biofilm formation and associated drug tolerance in the *ami1* mutant.

Figure 3.3.15. TADA fluorescence microscopy of *Mtb* strains exposed to INH.

Figure 3.3.16. Transcriptional analysis of amidase-encoding genes in Mtb.

Figure 3.3.17. Restriction digests of -5C*ami1*_EGFP and -5C*sigA*_EGFP to confirm successful cloning.

Figure 3.3.18. Fluorescence intensity of H37_-5C*ami 1*_EGFP and H37_-5C*sigA*_EGFP strains reporting on the expression of the *ami1* and *sigA*.

Figure 3.3.19. Transposon mutagenesis in the *ami1* mutant.

Figure 3.3.20. Survival of the ami1 mutant in macrophages.

Figure 4.1. An overview of the methodology used in this study.

Figure 4.2. An overview of the findings of this study.

Figure 4.3.1. Restriction digests of pMV_-4CAmi1.

Figure 4.3.2. The activity of Ami1 is not dependent on amidase activators, EnvC and NlpD.

Figure 4.3.3. Two transcriptional regulators for *ami1* gene expression in Mtb.

Figure 4.3.4. Predicted structural and DNA binding models for Rv1776c and Rv1423.

Figure 4.3.5. Restriction digests of pRv1423FLAG.

Figure 4.3.6. Restriction digests of pRv1776FLAG.

Figure 4.3.7. Expression and purification of Rv1423 and Rv1776 using the pFLAG system.

Figure 4.3.8. Restriction digests of pETRv1776c and pETRv1423 confirming successful cloning.

Figure 4.3.9. Induction of Rv1776c and Rv1423 protein expression.

Figure 4.3.10. Purification of the Rv1776c protein.

Figure 4.3.11. EMSA assessing the DNA binding ability of Rv1776c to the -500bp upstream promoter region of *ami1* of Rv1776c.

Figure 4.3.12. EtBr uptake of Mtb strains.

Figure 4.3.13. Assessment of *ami1* transcription in *Mtb* strains overexpressing Rv1423 and Rv1776c.

Figure 5.1. Proposed model for the possible role of *ami1* in Mtb.

List of tables

Table 1.1. Various methods that are currently used for the clinical diagnosis of TB (Table adapted from Mabhula and Singh, 2019).

Table 1.2. Various drugs used for TB treatment, their mechanisms of action, and the types of mutations in *M. tuberculosis* that confer resistance (Hoagland et al., 2016, Almeida Da Silva and Palomino, 2011).

Table 3.2.1. Bacterial strains used in this study.

Table 3.2.2. Standard PCR primers used in this study.

Table 3.2.3. PCR primers for confirming pMV306 (and it variations) integration into the Mtb genome.

Table 3.2.4. Plasmids used in this study.

Table 3.2.5. Standard RT-qPCR primers used in this study.

Table 3.3.1. Minimum inhibitory concentration (MIC) values for antibiotics targeting various biological processes, such as DNA replication, protein translation and cell wall synthesis.

Table 3.3.2. Hain line probe assay to determine drug susceptibility of strains exposed to INH (sampled from the time-kill assays at day zero [T0] day 7 [T7]). See Appendix D for data sheet.

Table 4.2.1. Bacterial strains used in this study.

Table 4.2.2. Standard PCR primers used in this study.

Table 4.2.3. Plasmids used in this study.

Table 4.2.4. Primers used for qPCR in this study

Table 4.2.5. SDS-PAGE gel recipes.

Table 4.2.6. PAGE gel recipes for a 10 ml gel.

Table 4.3.1. Attributes of Rv1776c and Rv1423 as determined by Mycobrowser.

Nomenclature

α:	Alpha
β:	Beta
Δ:	Delta
γ:	Gamma
μ:	Micro
Ω:	Ohm
ϕ:	Phi
Ami:	Amidase
Amp:	Ampicillin
AG:	Arabinogalactan
ATP:	Adenosine triphosphate
BCG:	Bacilli Calmette-Guérin
$CaCl_2$:	Calcium chloride
cDNA:	Complementary Deoxyribonucleic acid
CFU:	Colony forming unit
CSF-1:	Colony Stimulating factor 1
CSPD:	Chloro-5-substituted adamantyl- 1, 2-dioxetane phosphate
CR3:	Complement Receptor type 3
CTAB:	Cetyltrimethylammonium bromide
CW:	Cell wall
DIG:	Digoxigenin
DNA:	Deoxyribonucleic acid
dNTPs:	Deoxynucleoside triphosphate
EDTA:	Ethylenediaminetetraacetic acid
EMB:	Ethambutol
gDNA:	Genomic DNA
GlcNAc:	*N*-acetyl glucosamine
HCL:	Hydrochloric acid
HIV:	Human Immunodeficiency Virus
Hyg:	Hygromycin
IGRA:	Interferon-gamma (IFN-γ) release assay

Isoniazid:	INH
Kan:	Kanamycin
LA:	LB agar
LB:	Luria-Bertani broth
LTBI:	Latent TB infections
MAs:	Mycolic acids
MBD:	Membrane desalting buffer
m-DAP:	meso-Diaminopimelic acid
MDR:	Multidrug-resistant
$MgCl_2$:	Magnesium chloride
Msm:	*Mycobacterium smegmatis*
Mtb:	*Mycobacterium tuberculosis*
MurNAc:	*N*-acetyl muramic acid
NaCl:	Sodium chloride
NADPH:	Nicotinamide adenine dinucleotide phosphate
NaOH:	Sodium hydroxide
OADC:	Oleic Albumin Dextrose Catalase
OD:	Optical density
PAMPs:	Pathogen-associated molecular patterns
PAS:	Para-aminosalicylic acid
PCR:	Polymerase chain reaction
PG:	Peptidoglycan
PPRs:	Pattern recognition receptors
PZA:	Pyrazinamide
qPCR:	Quantitative PCR
RIF:	Rifampicin
RNA:	Ribonucleic acid
RRDR:	RIF-resistance determining region
RT-PCR:	Reverse Transcriptase PCR
SDS:	Sodium Dodecyl Sulfate
SSC:	Saline sodium citrate
TB:	Tuberculosis

TBE:	Tris borate EDTA
Tris:	Tris (hydroxymethyl) aminomethane
TY broth:	Tryptone Yeast extract broth
UV:	Ultra violet
WGS:	Whole-genome sequencing
WHO:	World health organisation
XDR:	Extensively drug-resistant

Chapter 1: General Literature Review

1. General Literature Review

1.1. The burden of TB

Tuberculosis (TB), a disease caused by *Mycobacterium tuberculosis* (Mtb), is the leading cause of death due to an infectious bacterial agent, claiming an estimated 1.4 – 1.6 million lives annually (WHO, 2022). In addition, approximately 1.7 billion people are thought to be latently infected with Mtb, and 5 – 15% of those will likely develop active TB disease during their lifetime (WHO, 2022). The global incidence of TB remains high, despite it being a curable disease. This has been attributed to several factors, including poor compliance to treatment, unfavourable socio-economic conditions, an increased proportion of undiagnosed infections driving transmission, and TB-HIV coinfection (Pai et al., 2016). In 2021, the global TB incidence was an estimated 10.6 million new infections, with sub-Saharan Africa accounting for 23% of the global incidences, Figure 1.1 (WHO, 2022).

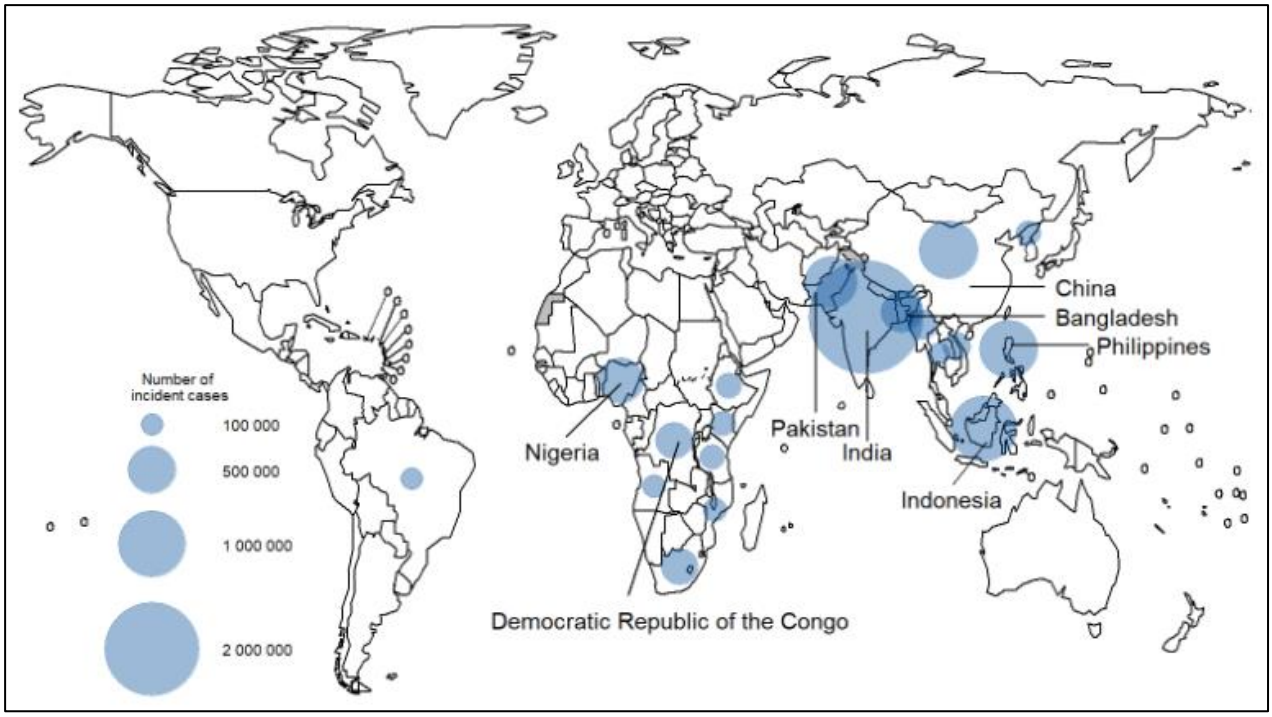


Figure 1.1. **The estimated TB incidence in 2021.** The annotated world map only reports on countries with a minimum of 100 000-incident cases. Developing nations in Sub-Saharan Africa and South-East Asia are associated with the highest burden of disease (figure extracted from WHO 2022 TB report).

1.2. Pathogenesis

The initial stages of Mtb infection involve the inhalation of aerosolized particles, containing as little as ten Mtb bacilli, that were released into the air by an infected individual through coughing or sneezing (Hoagland et al., 2016). The pathogen then encounters alveolar macrophages and/or dendritic cells in the lung, and may be detected through opsonic, non-opsonic or non-specific recognition immune systems (Hmama et al., 2015). Opsonic recognition involves recognition of bacterial cells coated with antibodies (such as immunoglobulin G), complement factors and/or other surfactants by complement receptor type 3 (CR3) and Fcγ receptors; this type of recognition may lead to phagosome-lysosome fusion, resulting in the death of bacteria (Thau et al., 2022, Schäfer et al., 2009). Non-opsonic recognition involves the use of pattern recognition receptors (PRRs) to detect pathogen-associated molecular patterns (PAMPs), in this case, these are highly conserved bacterial structures such as peptidoglycan (PG) (Hmama et al., 2015, Schäfer et al., 2009). This type of recognition is associated with intracellular survival of Mtb (Schäfer et al., 2009). Non-specific recognition includes bactericidal macropynocytosis of the pathogen by host cells (BoseDasgupta and Pieters, 2014). Macropynocytosis is a form of endocytosis that entails the indiscriminate engulfment of extracellular fluids (Lin et al., 2020). Macrophages constantly use macropynocytosis to capture antigens, and this process may be enhanced in response to stimuli such as the colony stimulating factor (CSF-1) and pathogen-derived molecules such as lipopolysaccharide (Lin et al., 2020, Canton, 2018, Condon et al., 2018). The pathogenesis of Mtb will be discussed from the perspective of the non-opsonic recognition pathway because it favours bacterial survival. Pathogen recognition triggers phagocytosis in the alveolar macrophage. Phagocytosis then triggers a pro-inflammatory response, which involves the release of cytokines and chemokines to recruit immune cells (foamy cells, epithelioid cells and multinucleated giant cells) around the infected macrophage to form the cell body called the granuloma (Smith, 2003, Guirado et al., 2013). Granulomas serve to regulate the growth of intracellular Mtb and to limit the spread of bacilli to other locations within the lung or as disseminated TB (Guirado et al., 2013). Latent TB infection occurs when granulomas contain the pathogen and prevent tissue damage but the bacteria remain viable. In instances where the granulomas fail to contain Mtb, active pulmonary TB may develop. In cases where the host's immune system in compromised, such as in HIV-AIDS and TB co-infection, the risk of reactivation or progression to active TB is high (Bruchfeld et al., 2015).

1.3. Methods used by Mtb to evade host immune responses

Mtb has developed various strategies for evading the host immune system, including the prevention of phagosome-lysosome fusion; the hindering of antigen presentation; and modulating various cell death pathways in macrophages (Stutz et al., 2018a). Typically, when a bacterium is engulfed by a macrophage, it is encapsulated in the phagosome (an endocytic vacuole), which will mature following fusion with the lysosome. Fusion will expose the bacterium and other phagocytosed contents to antibacterial effectors such as defensins, lysozyme, acidic pH, nitric oxide, toxic peptides, and reactive oxygen intermediates, all of which result in bacterial death (Mohanty et al., 2015). Deng et al. (2020) reported that the overexpression of Mtb Rv1096 (a mannosylated peptidoglycan deacetylase) in *Mycobacterium smegmatis* (Msm) resulted in the inhibition of phagosome-lysosome fusion following infection of RAW264.7 macrophages. Additionally, Rv1096 inhibited NADPH oxidase activity (an enzyme that produces superoxide anions that are subsequently converted to hydrogen peroxide) and blocked the production of reactive oxygen species (ROS). This study further showed that Mtb produces virulence factors that promote intracellular survival because the secretion of interleukin-12 and tumour necrosis factor-α was impaired by Rv1096 when expressed in Msm. Five putative interaction partners of Rv1096 were identified, all of which may co-operate with Rv1096 to affect cell division and immune evasion during mycobacterial infections (Deng et al., 2020). Mtb prevents infected cells from presenting antigens that might lead to the recruitment of pathogen degradative T cells (Stutz et al., 2018a). In addition, the pathogen produces several other virulence factors including PE-PGRS47, which inhibits autophagosomal processing, thus preventing the presentation of bacterial peptides by MHC class II (Saini et al., 2016). Hip1 (Rv2224C) lowers the expression of surface receptors (such as chemokine receptors, CD40, integrins) required for antigen presentation (Madan-Lala et al., 2014). Various studies have shown that Mtb prevents apoptotic cell death in infected cells, whilst promoting necrosis, which favours bacterial dissemination (Wong and Jacobs, 2013, Amaral et al., 2022, Stutz et al., 2018b). These combined events result in a spectrum of clinical outcomes that include asymptomatic infection, which can take the form of latent TB infection (LTBI) [no clear radiological/ microbiological evidence of disease], subclinical TB [radiological/microbiological evidence of TB] or incipient TB [radiological/microbiological evidence of TB, in addition to the presence of an evolving host biomarker signature that predicts progression to active TB] (Drain et al., 2018, Peters et al., 2019). In subset of individuals, active TB disease, with symptoms emerges. Several approaches are used to prevent

progression of latent infection to active disease, whilst treatment of active TB involves administration of combination chemotherapy.

1.4. TB prevention

The prevention of TB infection and progression to active disease is vital to reducing disease burden in public health systems. Currently, there are three clinical approaches for the prevention of TB. (1) The vaccination of children with the Bacillus Calmette-Guérin (BCG) vaccine; (2) the treatment of individuals with LTBI and (3) the prevention of Mtb transmission via infection prevention and control measures targeted at active TB cases (WHO, 2022). Currently, the WHO recommends four types of drug regimens for the treatment of LTBI, which involve several antibiotics including isoniazid (INH) and rifampicin (RIF or other rifamycins): 3HP (3 months of weekly doses of rifapentine and INH), 3RH (3 months involving daily doses of RIF and INH), 4R (daily doses of RIF for 4 months), and 6H (6-month treatment with daily doses of INH) (WHO, 2022). For the prevention of transmission and control of active TB, the WHO recommends approaches such as administrative, environmental and personal protection measures. Treatment for active TB will be discussed later.

The BCG vaccine used for TB recently celebrated 100 years of use. BCG is effective at protecting infants and young children, particularly with respect to disseminated infection, but displays variable efficacy in adults, as reviewed by Kumar (2021). As a result, widespread use of this vaccine has not resulted in eradication of TB, necessitating the development of new vaccine candidates. The TuBerculosis Vaccine Initiative (TBVI) assesses the effectiveness of potential TB vaccines by observing efficacy across three categories of people, namely (1) infants and neonates, (2) adolescents and adults, and (3) infected individuals. TB vaccine development makes use of various approaches, including the use of live-attenuated or dead whole cell, protein/adjuvant, and viral vector vaccines, (Fatima et al., 2020). These are shown in Figure 1.2.

VPM1002, VACCAE^{TM}, and MIP are three promising potential TB vaccines, which are in phase 3 clinical trials (https://www.tbvi.eu/). VPM1002 is a recombinant BCG strain in which the *urease C* gene is replaced with a *Listeria monocytogenes* gene, *Hly*, encoding listeriolysin O (Grode et al., 2005, Nieuwenhuizen et al., 2017, Fatima et al., 2020, Schrager et al., 2020). In addition to the BCG based induction of CD4+ T-cell response, VPM1002 secretes listeriolysin O, to disturb the phagosomal membrane, leading to the release of VPM1002

components into the cytosol, resulting in antigen processing through the MHC-I pathway and the induction of immune response processes such as apoptosis, and autophagy (Lewinsohn et al., 2017, Grode et al., 2005, Saiga et al., 2015, Schaible et al., 2003). This vaccine represents one of the more promising variations of BCG produced to date, with promising preliminary safety data (Cotton et al., 2022).

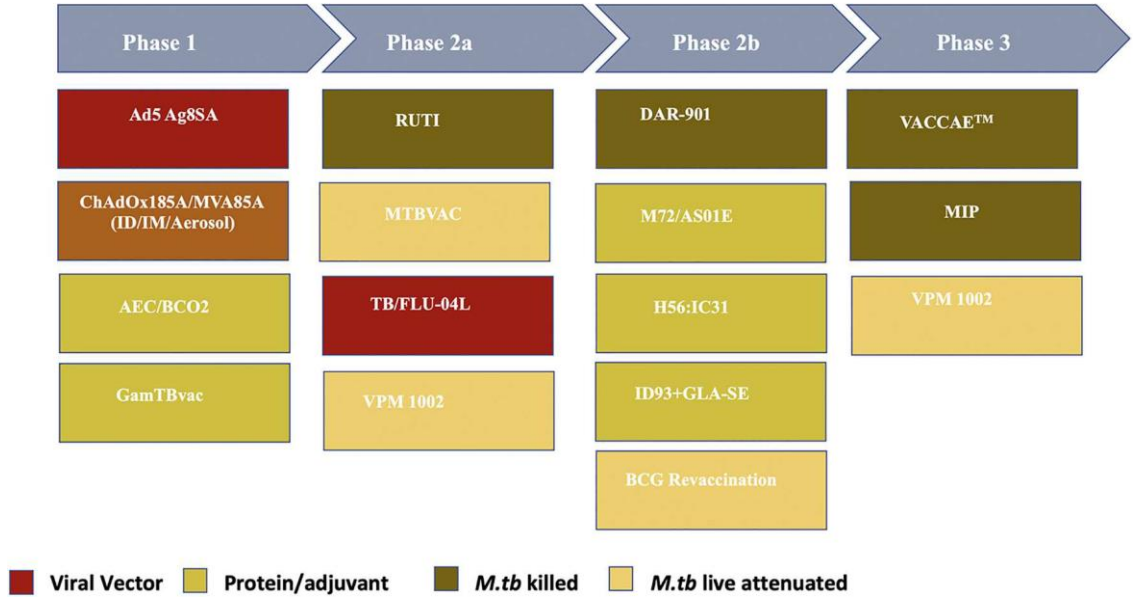


Figure 1.2: TB vaccine candidates and their progression through clinical trials. Shown are different vaccine candidate, based on various delivery platforms, and their progress in clinical development. TB vaccine candidates include live-attenuated mycobacterial vaccine candidates (VPM1002, BCG revaccination, and MTBVAC); mycobacterial killed, whole-cell candidates (VACCAE^{TM}, MIP, DAR-901, and RUTI); protein/adjuvant candidates (M72:AS01E, H56:IC31, ID93: GLA-SE, AEC/BCO2 and GamTBvac); viral vector candidates (TB/FLU-04L, Ad5Ag85A and ChAdOx1.85A/MVA85A). Additional information on vaccine candidates is included in the text. Taken from Fatima et al., 2020).

VACCAE^{TM} is a killed *Mycobacterium vaccae* (*M. vaccae*) candidate that is in phase III trials and is licensed as an adjunctive therapeutic vaccine in TB patients in China (Sable et al., 2019). *M. vaccae* is a non-pathogenic saprophytic NTM. In mouse models it was shown to induce immune response against Mtb by generating CD8+ cytotoxic T lymphocytes which kill Mtb infected macrophages (Gröschel et al., 2014). MIP is a killed *Mycobacterium indicus pranii* that is phase III trials in India, however; it is currently licensed as MIP Immuvac, a leprosy vaccine (Martin et al., 2020). In guinea pig models of tuberculosis, the combination of MIP

and first-line TB drugs enhanced bactericidal activity (Gupta et al., 2012). Moreover, the same study showed that guinea pigs that had received MIP immunotherapy displayed an increase in protective Th1 immune response (Gupta et al., 2012).

There are several candidates in phase IIB trials, and most are protein/adjuvant candidates, including M72/AS01$_E$, H56:IC31 and ID93:GLA-SE. M72/AS01$_E$, was shown to significantly decrease reactivation of TB in individuals with LTBI, with an efficacy of 54.0% protection against active pulmonary tuberculosis disease (Van Der Meeren et al., 2018, Tait et al., 2019). M72/AS01$_E$ is comprised of two components: The first is an M72 antigen, a recombinant protein constructed from the immunogenic Mtb antigens, Mtb32A (*Rv0125*) and Mtb39A) (*Rv1196*), encoding PepA and PPE 18 respectively (Skeiky et al., 1999, Dillon et al., 1999, Ji et al., 2019). The second components the liposome-based AS01$_E$, consisting of monophosphoryl lipid A and the QS-21 adjuvant (Ji et al., 2019, Baldridge et al., 2006). The M72 component elicits T-cell response whereas; the AS01$_E$ component mediates TLR4 receptors and cytotoxic lymphocyte cells (Skeiky et al., 1999, Dillon et al., 1999, Ji et al., 2019, Baldridge et al., 2006). H56:IC31 is comprised of the antigens Ag85B, ESAT-6 and Rv2660c, with the IC31 adjuvant, and developed for TB prevention in adults (Luabeya et al., 2015). This vaccine induces antigen-specific IgG response and Th1 cytokine-expressing CD4+ T cells (Luabeya et al., 2015). ID93: GLA-SE is the third of the subunit vaccines in phase II trials. The ID93 component of this vaccine candidate consists of four Mtb antigens (Rv1813, Rv2608, Rv3619 and Rv3620) with a GLA-SE adjuvant. This vaccine induces antigen-specific IgG response and polyfunctional CD4 T cells (Day et al., 2021).

Other vaccine candidates in phase IIB trials include DAR-901 and BCG revaccination which are Mtb killed and live-attenuated vaccines, respectively (Fatima et al., 2020). DAR-901 is a killed *Mycobacterium obuense*, which is targeted towards TB prevention in adolescents (Munseri et al., 2020). BCG revaccination is targeted at adolescents and adults that have previously received the BCG vaccine and it has been shown to reduce the rate of upper respiratory tract infections in adults (Nemes et al., 2018).

With the exception of VPM 1002, which has been discussed above, there are three more candidates undergoing phase IIA trials, namely, RUTI, MTBVAC and TB/FLU-04L. RUTI is formulated as a liposomal structure that contain killed Mtb that cultured in stressful conditions (Vilaplana et al., 2010). IT was found to immunogenic in people with LTBI at 1 month post isoniazid treatment (Nell et al., 2014). MTBVAC is a live attenuated Mtb vaccine consisting of a double deletion of the *phoP* and *fadD26* virulence genes, subsequently disrupting

phthiocerol dimycocerosate biosynthesis and leading to defects in the ESX-1 system (Sable et al., 2019). This vaccine induces a wide range of immune response, including the production of polyfunctional CD4+ and CD8+ T-cells (Sable et al., 2019). TB/FLU-04L. is a recombinant virus-vectored candidate, making use of live attenuated influenza A virus as a vector to express the Mtb antigens, Ag85A and ESAT-6 (Martin et al., 2020). It has been found to be immunogenic to individuals that were previously vaccinated with BCG (WHO, 2012). The protein vaccine, GamTBvac was phase I trials but has recently undergone phase IIa trials (Martin et al., 2020). It consists of Mtb antigens Ag85A and ESAT6–CFP-10 with the dextran immobilized binding domain, and similarly to TB/FLU-04L, its boosts immunity in people previously vaccinated with BCG (Tkachuk et al., 2017).

Phase I clinical trials include a few vaccine candidates such as the viral vector vaccine, ChAdOx1.85A/MVA85A that encodes Antigen 85A, and the recombinant protein vector AEC/BC02, which expresses g85B and ESAT6-CFP10 as Mtb antigens (Fatima et al., 2020). Another candidate currently in phase 1 clinical trials is the viral vector vaccine, Ad5Ag85A, expressing the immunogenic diacylglycerol acyltransferase, Ag85A, is (Jeyanathan et al., 2022). The vaccine is composed of a recombinant replication-deficient human Ad5 vector expressing Ag85A proteins, and has been shown to stimulate polyfunctional T-cells (Smaill and Xing, 2014). Furthermore, the same study revealed that Ad5Ag85A increased CD4+ and CD8+ T-cell immunity in previously BCG-vaccinated volunteers compared with their non-vaccinated counterparts. These efforts are encouraging as an effective TB vaccine in adults is expected to reduce new infections and achieve the WHO target of eradicating TB by 2035.

1.5. Diagnosis of TB: current tools, limitations and the development of novel tools

Detection of TB in the clinical setting involves a variety of approaches. Prior to the widespread use of molecular diagnostics, routine clinical laboratories testing for TB typically relied on the presence of acid-fast bacilli using smear microscopy. In addition, culture-based methods and nucleic acid amplification tests (NAATs) have been subsequently introduced (Machado et al., 2019, MacLean et al., 2020). Mtb can be isolated from several types of biological samples for testing, including sputum, bronchial secretions, bronchoalveolar lavage fluid, gastric lavage, blood, bone marrow, urine, biopsies or cerebrospinal fluid (Machado et al., 2019). Smear microscopy has been used for TB diagnosis for at least 100 years. This test exploits the acid-fast nature of Mtb for detection using Ziehl-Neelsen or Auramine stains with high specificity.

However, while smear microscopy is simple, quick and cheap, it has a low sensitivity (20 – 80%) (Steingart et al., 2006), with a limit of detection ranging between 5,000 to 10,000 bacteria per ml of sputum in unprocessed smears (Rasool et al., 2019). An additional limitation associated with the detection of acid-fast bacilli (AFB) is that the presence these organisms may not necessarily indicate Mtb infection specifically as other mycobacterial species such as Non-tuberculous mycobacteria (NTMs) are also acid-fast (Table 1.1) (Sia and Rengarajan, 2019). NTMs are saprophytic mycobacterial species that are commonly found across various environments, but are opportunistic pathogens particularly in people living with HIV (PLWH) (Ratnatunga et al., 2020). Recently, NTM lung infections have been on the rise due to the emergence of drug resistance (Ratnatunga et al., 2020). An added limitation with smear microscopy is that it does not report on response to TB treatment as it strains both live and dead bacteria. Novel metabolic stains, specifically report on the quantum of live bacterial organisms have emerged and are expected to bolster the benefit of smear microscopy (Kamariza et al., 2018, Kamariza et al., 2021).

Culture-based approaches to TB diagnosis remain the clinical gold standard due to higher sensitivity and specificity, particularly when combined with molecular-based techniques such nucleic acid detection (discussed below).

The ability to culture Mtb enables the identification of species, drug susceptibility profiles, the capacity to transmit and more importantly, response to treatment. In the case of the latter, consecutive negative cultures late during treatment are an indication of treatment success. Culture methods have also enabled isolation of tubercle bacilli for use in transmission linkage studies, thus enabling the broad field of TB epidemiology. However, there are drawbacks associated with culture-based approaches for TB detection. These include higher costs; the slow growth rate of Mtb delays detection and may result in inadequate treatment regimens if infecting strains are resistant to antibiotic treatment; contamination from other oral microbiota; and specialized BSL3 facilities/staff (Table 1.1). For isolation of Mtb, specialist media such as Lowenstein-Jensen (LJ), agar-based Middlebrook 7H10 or 7H11 formulations, and liquid-based formulations including 7H9 and 7H12 mycobacterial growth indicator tubes (MGIT). MGITs are commercial tests and can be manual, semi-automated or fully automated. These tests use radiation and more recently, fluorescent-based detection method. Examples include the BACTEC MB9000, BACTEC MGIT 960 and 320 and the manual MGIT, the Septi-Chek AFB systems (Becton Dickinson, Sparks, MD, USA), the ESP (Extra Sensing Power) Myco-ESPculture System II (Trek Diagnostic Systems, USA) and the BacT/ALERT MB

(bioMérieux, Marcy-l'Etoile, France) (Machado et al., 2019, Afsar et al., 2018, Cohen et al., 2019).

Rapid molecular tests targeting nucleic acids, particularly the GeneXpert MTB/RIF® (Cepheid, Sunnyvale, CA) have gained traction globally as tools of TB diagnosis due to increased sensitivity compared to smear microscopy (WHO, 2022). This is a PCR-based assay that detects Mtb and rifampicin (RIF) resistance concurrently (Cohen et al., 2019). The setbacks with GeneXpert MTB/RIF® is it only detects RIF resistant strains within the RIF-resistance determining region (RRDR) of the *rpoB* gene and thus is incapable of detecting strains with *rpoB* RIF-resistance outside the RRDR (Table 1.1) (Mabhula and Singh, 2019). Furthermore, the sensitivity of Xpert MTB/RIF® is lower in patients with HIV or paucibacillary disease. To address this limitation, the GeneXpert MTB/RIF ULTRA® assay was developed, which has improved sensitivity (Dorman et al., 2018). Another drawback to the GeneXpert is high cost, which has limited broader use in the health systems of endemic countries.

Line probe assays (LPAs) detect resistance to first-line drugs (RIF and INH) and second-line drugs (fluoroquinolones and injectable second-line drugs) but are limited in that they only target a select number of resistance alleles (Table 1.1) (Heyckendorf et al., 2018). To circumvent these limitations, whole-genome sequencing (WGS) can be used, as it is able to detect mutations on a genome-wide scale (Table 1.1). WGS is expensive, which makes it less feasible in the clinical settings of low-middle income countries (Mabhula and Singh, 2019). The paucibacillary nature of TB infections in young children and HIV patients makes TB detection in sputum difficult and unreliable and therefore, methods such as the lateral-flow lipoarabinomannan assay can be used to detect Mtb from urine samples (Table 1.1) (Marais and Pai, 2007, Schramm et al., 2021, Lawn et al., 2012).

The above-mentioned tests have largely been directed at detecting TB in individuals with symptomatic active disease. Assays such as the Mantoux tuberculin skin test and the Interferon-gamma (IFN-γ) release assay (IGRA) can be used for the detection of LTBI. The Mantoux tuberculin skin test depends on the hypersensitivity of the immune system to purified protein derivative (PPD) of mycobacterial origin (Sia and Rengarajan, 2019). However, the test may result in false positives, as it can detect other mycobacterial species, including the BCG vaccine, and thus it should be used along with the IGRA (Table 1.1).

Table 1.1. Various methods that are currently used for the clinical diagnosis of TB (Table adapted from Mabhula and Singh, 2019).

Diagnostic tool	Type of detection	Period of diagnosis	Limitations	References
Smear microscopy	Acid fast staining (Ziehl-Neelsen and Auramine-rhodamine staining)	A few hrs	Positive results may not mean Mtb infection	Kommareddi et al. (1984)
Culture-based methods	Mycobacterial growth	~ 12 weeks	Time-consuming Requires special facilities Contamination	Cohen et al. (2019)
Rapid molecular tests: • Gene-Xpert MTB/RIF • First-line Line probe assay • Second-line Line probe assay • Lateral-flow lipoarabinomannan assay	• RIF resistance • INH and RIF resistance in patients positive for smear microscopy and culture methods • Resistance to fluoroquinolones and second-line injectable agents • Mtb in urine samples of HIV positive individuals	≤ 2 hrs	Cost Line probe assay target a limited number of resistance variants	Heyckendorf et al. (2018), Lawn et al. (2012), WHO (2019)
Mantoux tuberculin skin test	Sensitivity to mycobacterial purified protein derivative (PPD)	2-3 days	Positive result not specific to Mtb infection	Sia and Rengarajan (2019)
Interferon-gamma (IFN-γ) release assays	Immune response to Mtb	8-30 hrs	Expensive, cannot differentiate between LTBI and active infection	Sia and Rengarajan (2019)
Whole-genome sequencing	Alterations in the genome of *M. tuberculosis*	-	-	Cohen et al. (2019)

The IGRA detects the kinetics of production of IFN-γ by white blood cells in response to TB antigens and is thus able to distinguish immune responses from BCG and TB infection (Sia and Rengarajan, 2019). This is based on using antigen for stimulation of cells that are specific to Mtb and missing in BCG strains. Accurate and timeous diagnosis of LTBI enables efficient treatment and reduces the burden on health systems. Despite these advances, a low-cost, point of care test for TB that can be used at the bedside is still lacking. There are several exciting initiatives underway including the use of metabolic probes, new antigen tests and novel microfluidic culture systems.

1.6. Treatment of TB

Streptomycin, para-aminosalicylic acid (PAS) and isoniazid (INH) were amongst the first effective drugs against TB but were developed approximately 70 years ago (Mabhula and Singh, 2019). The use of streptomycin has been discontinued due to the rapid emergence of drug resistance (Crofton and Mitchison, 1948). Currently, treatment for drug-susceptible TB, as recommended by the WHO, is a 6-month regimen consisting of four drugs: RIF, INH, pyrazinamide (PZA) and ethambutol (EMB). The regimen involves a 2-month treatment period with all four drugs followed by 4 months of treatment with INH and RIF only (WHO, 2022). The regimen is effective for clearance of the pathogen in drug susceptible individuals provided there is adequate adherence and health systems support to patients. To counter non-adherence, and some severe side effects associated with prolonged TB chemotherapy, recent clinical trials have tested shorter regimens. The TBTC Study (S31/A5349) compared 3 separate regimens: 1) The standard 6-month regimen, 2) a 2-month treatment with RIF, INH, PZA and EMB, followed by 9 weeks of INH and RIF and 3) a 2-month treatment with RIF, INH, PZA and moxifloxacin, followed by 9 weeks of RIF, INH and moxifloxacin (Dorman et al., 2020, Dorman et al., 2021, Pettit et al., 2023). The four month moxifloxacin-containing regimen was non-inferior compared to the standard treatment, and was safe, suggesting that shorter treatment durations for TB are possible (Dorman et al., 2020, Dorman et al., 2021, Pettit et al., 2023).

The greatest threat to the eradication of TB is the emergence of drug resistance, particularly composite forms of resistance where the disease-causing strains is resistant to multiple drugs. The 2022 World Health Organisation TB report (WHO, 2022) indicated that in addition to South Africa having one of the highest incidences of TB, it is also one of the countries that are heavily burdened with drug-resistant TB, Figure 1.3. The emergence of multidrug-resistant

(MDR) and extensively drug-resistant (XDR) forms of TB has rendered the first-line treatment regimen ineffective (Black et al., 2014). MDR-TB is associated with strains that are resistant to RIF and INH, whereas XDR-TB is associated with MDR strains that are additionally resistant to any fluoroquinolone and any injectable drug used for MDR treatment (WHO, 2019). In 2018, there were 186 772 and 13 068 new cases of MDR-TB, respectively (WHO, 2019). The 2020 WHO guidelines recommend a reduced treatment period for drug-resistant TB of 9-11 months compared to the previous 9-20-month treatment regimen with second-line drugs and injectable drugs such as fluoroquinolones and aminoglycosides (Mirzayev et al., 2021). Fluoroquinolones inhibit mycobacterial DNA replication (Mabhula and Singh, 2019). Aminoglycosides inhibit the 30S ribosomal subunit of Mtb, thus blocking protein synthesis (Cambau et al., 2015). Aminoglycosides continue to be used in several settings regardless of the potential hearing loss as a side effect (Mabhula and Singh, 2019). Bedaquiline, a diarylquinolone that prevents ATP synthesis, is the first novel TB drug to be approved by the US Food and Drug Administration (FDA) in over 40 years (Mahajan, 2013). Delamanid, a drug targeting mycolic acid synthesis is another novel drug that has recently been approved by the FDA (Ahmed et al., 2020). However, Mtb has already developed resistance to both bedaquilinine and delaminid via mutations in the *atpE* and *Rv3547*genes, respectively (Koul et al., 2007).

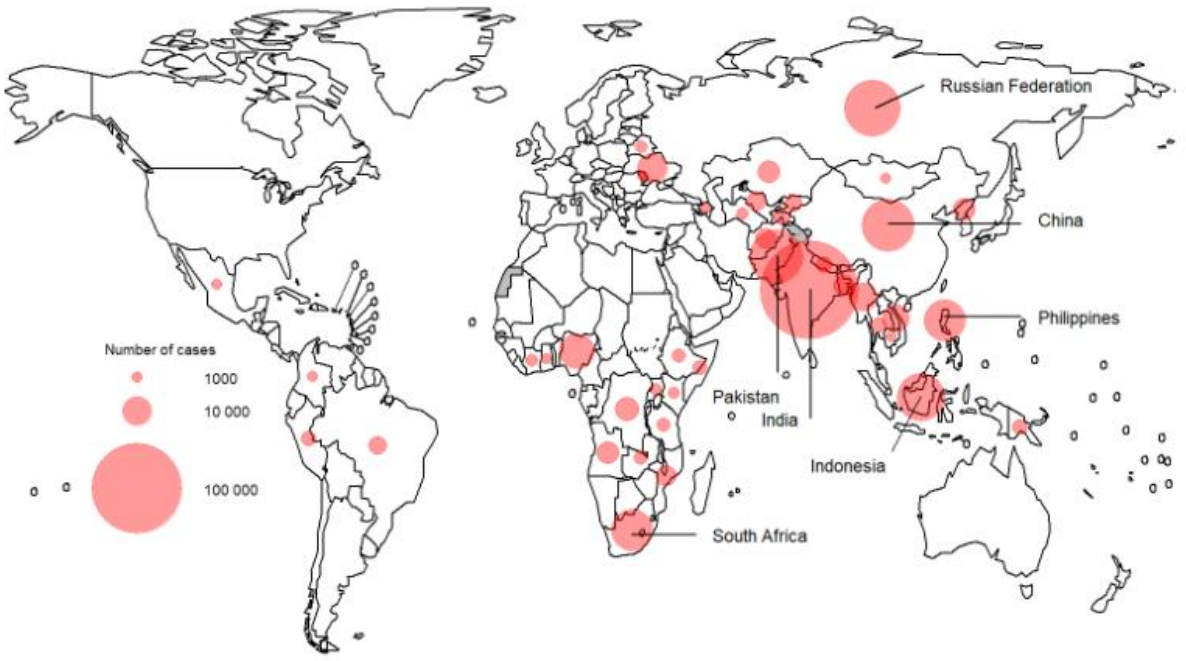


Figure 1.3. Estimated incidences of MDR-TB as determined by the WHO in 2021. South Africa, is reported to be burdened by at least 20 000 cases of drug-resistant TB. The figure is taken from WHO 2022 TB report.

1.7. Mechanisms of drug resistance/tolerance in Mtb

In Mtb, drug resistance arises as a consequence of chromosomal mutations (short nucleotide polymorphisms, insertions and deletions) rather than horizontal gene transfer (Cohen et al., 2019, Portelli et al., 2018). These mutations may interfere with the binding affinity of drugs to their target proteins, reduce enzymes that activate prodrugs, lead to the overexpression of efflux pumps that reduce drug concentrations or reduce drug permeability (Koch et al., 2018). Apart from resistance-conferring mutations, Mtb has inherent traits that make it drug tolerant. For example, efflux pumps can remove anti-tubercular drugs from the cytoplasm, including EMB, INH, RIF, bedaquiline and fluoroquinolones (Malinga and Stoltz, 2016). Mtb can also enter a reversible, non-replicative state of persistence, which is characterised by low metabolic activity when exposed to stresses such as immune suppression or antibiotics (Caño-Muñiz et al., 2018). When the adverse conditions are removed, mycobacteria resume metabolic activity, which may ultimately lead to the development of active pulmonary TB or worsening of disease in individuals who have been on inappropriate therapy (Caño-Muñiz et al., 2018). Mtb persister cells are thought to be associated with latent TB infection, though definitive evidence for this is currently lacking (Scanga et al., 1999). Lastly, the presence of a complex cell wall (CW) reduces permeability to small molecules, rendering Mtb more refractory to treatment.

Space left intentionally blank

Table 1.2. Various drugs used for TB treatment, their mechanisms of action, and the types of mutations in *M. tuberculosis* that confer resistance (Hoagland et al., 2016, Almeida Da Silva and Palomino, 2011).

Drug	Target/mechanism of action	Source of resistance
Isoniazid	Prevents mycolic acid synthesis by inhibiting Enoyl-ACP reductase (InhA)	*katG* and *inhA* mutations
Rifampicin	Attaches to the β subunit of RNA polymerase leading to the prevention of RNA synthesis	Mutation in the *rpoB* gene reduces binding affinity by changing the conformation of the RNA polymerase β subunit.
Ethambutol	Inhibits arabinosyl transferase, an enzyme that polymerizes arabinogalactan	Mutations in the *embB* gene of the *embCAB* operon encoding for arabinosyl transferase
Pyrazinamide	Disrupts and inhibits membrane energetics and membrane transport respectively	*pncA* mutations reduce the conversion of Pyrazinamide to its active form
Ethionamide	Prevents mycolic acid synthesis by inhibiting Enoyl-ACP reductase (InhA).	Mutations in *ndh*, *ethA*, *ethR* or *inhA* genes
Cycloserine	Targets alanine racemase (*alrA*), resulting in the inhibition of PG synthesis	Overexpression *alrA* reduces drug efficacy
Delamanid	Mycolic acid synthesis inhibition	Rv3547 mutation

Space left intentionally blank

1.8. The mycobacterial cell wall

The mycobacterial cell wall (CW) is a multi-layered structure that provides a highly selective barrier that is essential for cell growth, virulence and resistance to antibiotics (Kieser and Rubin, 2014). In addition to the CW, the surface of Mtb has a capsule-like material, which is predominantly composed of polysaccharides (glucans, arabinans and arabinomannans), proteins and lipids (Daffé and Draper, 1997). The capsule has been shown to play a role in immune evasion due to inherent immuno-regulatory and anti-phagocytic activities (Kaur et al., 2009).The inner structure of the CW consists of three components, namely, long-chain mycolic acids (MAs), a highly branched arabinogalactan (AG) polysaccharide layer, and a cross-linked peptidoglycan polymer (Figure 1.4). The biosynthesis and chemical structure of these different components is discussed next.

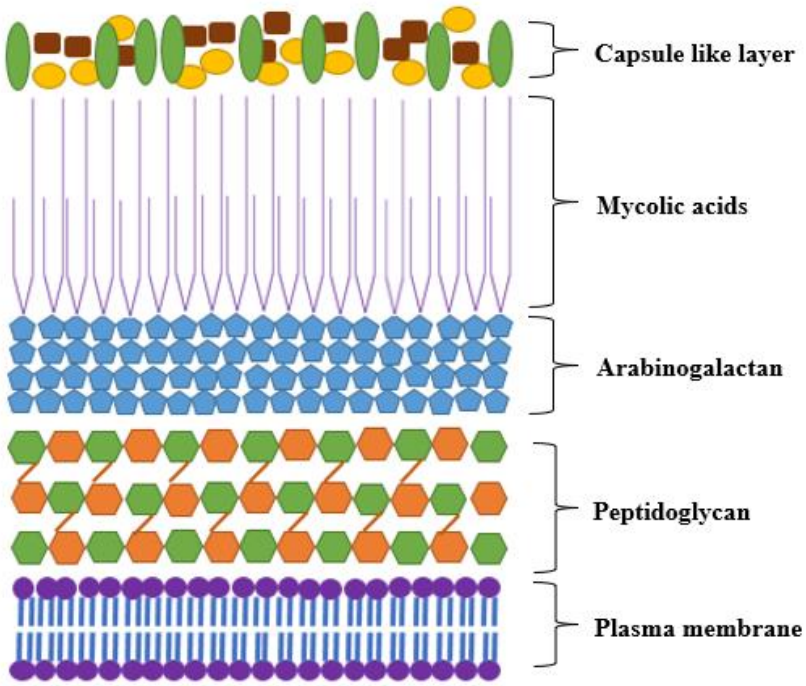


Figure 1.4. Schematic diagram representing the mycobacterial cell wall. Green oval shapes represent capsule proteins; yellow and brown represent capsule polysaccharides. Branch-like structures in pink represent mycolic acids, and blue pentagons represent arabinogalactan. Green and orange hexagons represent the *N*-acetylglucosamine and *N*-acetylmuramic acid components of the PG respectively. The orange lines represent the crosslinks between PG residues, and the purple circle and blue lines represent the phospholipid bilayer of the plasma membrane. Adapted from Squeglia et al. (2018).

Biosynthesis of arabinogalactan (AG)

AG is made up of arabinan and galactan (Hett and Rubin, 2008). This structure has approximately 30 arabinosyl residues, three of which are attached to galactan (Barry et al., 2007). AG is covalently bonded to PG by a phosphoryl-*N*-acetylglucosaminosyl-rhamnosyl linkage (Hett and Rubin, 2008). Arabinogalactan anchors MA to PG; thus, it plays important role in cell wall stability (Hett and Rubin, 2008). In Mtb, approximately 10% of the PG NAM residues are covalently linked to AG. A comprehensive outline of AG biosynthesis has been reviewed in (Hett and Rubin, 2008, Crick et al., 2001, Jankute et al., 2015). Briefly, the first step, which occurs on the cytoplasmic side of the plasma membrane, in AG synthesis is the formation of linker region or unit: α-L-Rhap-(1→3)-α-D-GlcNAc-(1→P) (McNeil et al., 1990). GlcNAc-1-phosphate is transferred from UDP-GlcNAc to prenyl phosphate by WecA (Rv1302) followed by the addition of rhamnose (Rha) from dTDP-Rha, by WbbL (Rv3265c), making up the linker. The next two steps occur independently and result in the formation of AG units that will incorporated into the existing CW. In the reactions, UDP-galactofuranose is generated from UDP-galactopyranose and decaprenylphosphoryl-arabinofuranose is generated from the pentose phosphate pathway. Galactofuranose is then added to the linker and polymerized to form long, linear chains. Arabinofuranose residues are added to the polymerized galactose as either linear or branched chains. These residues originate from the pentose phosphate pathway/hexose monophosphate shunt and the intermediate precursor of the polymerized arabinofuranose is decaprenylphosporyl-Arabinofuranose. Finally, the AG complex is ligated to PG and decaprenylphophate. It was recently shown that Lcp1, a phosphotransferase, is responsible for ligating AG to PG (Harrison et al., 2016). Several anti-TB drug target AG biosynthesis including ethambutol.

Biosynthesis of mycolic acids (MAs)

MAs are long chains ($C_{60\text{-}90}$) of β-hydroxy and α-alkyl fatty acids with 70–90 carbons per chain, which are highly hydrophobic (Boshoff and Barry III, 2006, Hett and Rubin, 2008). MAs determine the permeability of the outer cell envelope and have been shown to play a role in bacterial pathogenicity and resistance to antibiotics such as β-lactams (Barry et al., 2007, Boshoff and Barry III, 2006). MAs are attached to AG via long meromycolate and short α-

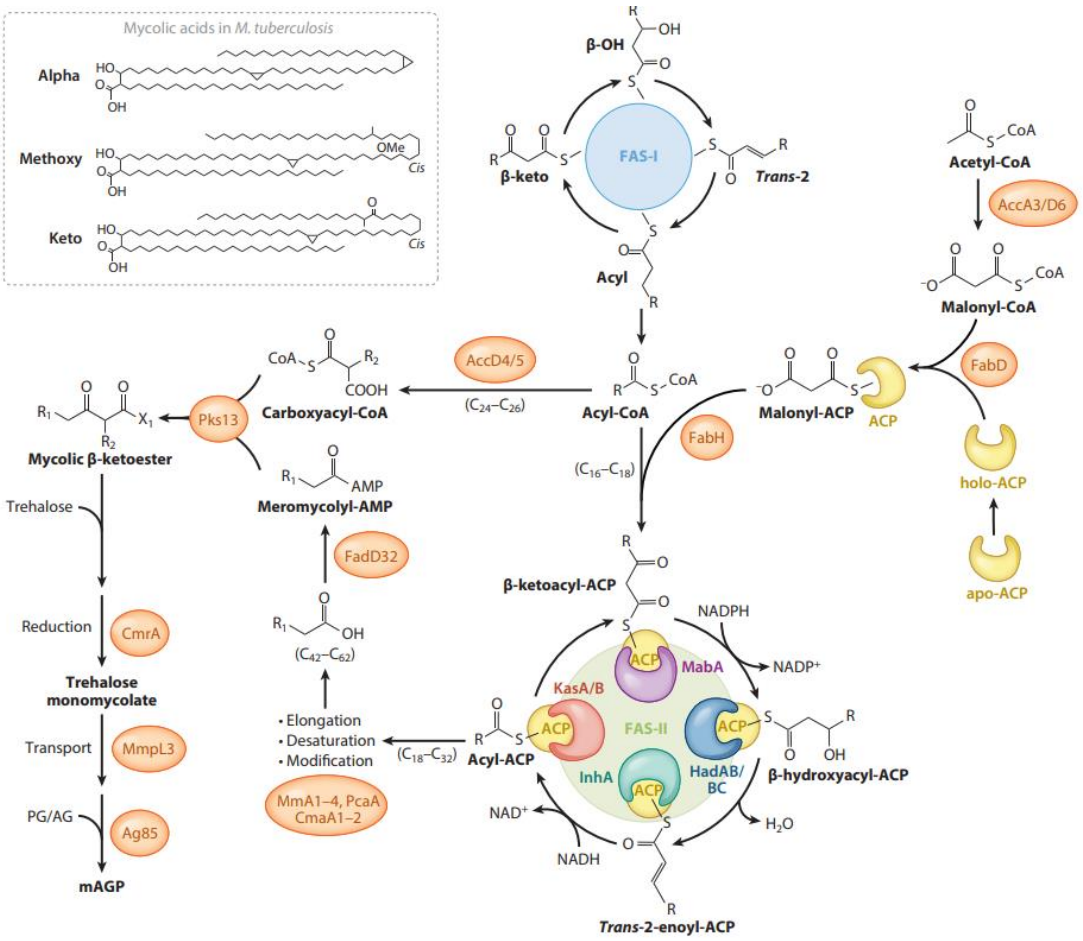


Figure 1.5. **Biosynthetic pathways that result in the formation of the mycolic acid-arabinogalactan-peptidoglycan complex (MAPc) in Mtb.** Figure taken from Crick et al., 2001. Some enzymes along the pathways have subsequently been identified.

chains (Brennan, 2003). The majority of MAs are covalently linked to the AG layer by ester bonds and exist as tetramycolyl-pentaarabinofuranosyl clusters on the AG or as trehalose mycolates (Hett and Rubin, 2008; Jankute et al., 2015). The basic biosynthesis pathway for Mas is given in Figure 1.5. The transport of MAs from the cytoplasm is catalyzed by MmpL3 and the antigen 85 complex (Jackson et al., 1999). There are three distinct types of MAs, namely α- MAs, methoxy-MAs and keto-MAs. The α-MAs are most abundant and are only found in a *cis*-cyclopropane configuration whereas methoxy- and keto-MAs contain cycloprone rings in either *cis*- or *trans*-configurations (Jankute et al., 2015). The biosynthesis of MAs can be achieved via two main mechanisms: FAS-I or FAS-II. The short-chain fatty acids (C_{16-24}) are produced *de novo* in the FAS-I pathway (Takayama et al., 2005) (Figure 1.5). These saturated fatty acids (FAs) can form the α-alkyl MAs (C_{24}) or can be extended by the

FAS-II pathway. This is initiated by a condensation reaction catalyzed by FabH, which uses malonyl-AcpM and palmitoyl-CoA to yield a β-ketacyl-AcmP intermediate. This is then reduced by MabA to produce β-hydroxyacyl-AcpM, which is then dehydrated by HadAB/BC to yield a *trans*-2-enol AcpM intermediate. This is subsequently reduced by InhA to produce an acyl-AcpM extended by two carbons. The FAS-II cycle continues with more condensation, which is facilitated by KasA/B returning to the above via MabA, HadAB/BC and InhA. Cycling continues to extend the acyl chain until $C_{42\text{-}62}$, which forms the saturated long-chain meromycolate (Jankute et al., 2015). Following MA biosynthesis via the FAS-II pathway, various modifications can be made to the saturated FA chains, including the addition of functional groups via *cis*-/*trans*-cyclopropnation or keto and methoxy groups via CmaA1-2-, MmaA1-4- and PcnA-type enzymes (Dubnau et al., 2000, Glickman, 2003, Glickman et al., 2000). These modifications are thought to alter cell wall fluidity/permeability and offer protection against host immune responses such the suppression of inflammation caused by Mtb infection (Yuan et al., 1995, Rao et al., 2005).

Biosynthesis of peptidoglycan

PG is a complex polymer that surrounds the plasma membrane. It is common across almost all eubacteria but absent in eukaryotic organisms (Do et al., 2020a). The mesh-like arrangement of this structure confers rigidity, which facilitates with resistance to osmotic pressure and maintenance of cell shape (Alderwick et al., 2015). PG consists of long strands of alternating *N*-acetyl muramic acid (MurNAc) and *N*-acetyl glucosamine (GlcNAc) connected via β-1, 4 glycosidic bonds (Squeglia et al., 2018). PG synthesis is initiated in the cytoplasm, where a series of reactions lead to the biosynthesis of the PG precursor molecule Lipid II, followed by translocation of Lipid II to the periplasm and incorporation of this molecule into the existing PG structure (Squeglia et al., 2018, Turapov et al., 2018). (Figure 1.6).

The bulk of glucose and fructose in a bacterial cell is converted to D-fructose-6-phosphate upon entering the cell (Squeglia et al., 2018). In the cytoplasm, the enzymes GlmS (transfer an amino group), GlmM (mutase) and GlmU (carries out acetylation and urydilation) use D-fructose-6-phosphate as a substrate to form uridine-diphospho-*N*-acetylglucosamine (UDP- GlcNAc), the first essential precursor of bacterial PG synthesis (Squeglia et al., 2018). UDP- GlcNAc is converted to UDP-MurNAc by MurA and MurB before five sidechain residues are added by a series of ATP-dependent Mur ligases (Jankute et al., 2015).

MurC adds the first amino acid (L-Ala) to UDP-MurNAc. MurD then adds D-Glu. Subsequently, MurE adds meso-Diaminopimelic acid (m-DAP) before MurF adds a D-Ala-D-Ala dipeptide. The resulting structure is lipid I (Jankute et al., 2015). MurX (MraY), catalyses the transfer of Lipid I to decaprenyl phosphate. MurG then catalyses the addition of GlcNAc to Lipid I to form Lipid II. Lipid II is translocated to the periplasm via MurJ/FtsW, a flippase, Figure 1.6 (Squeglia et al., 2018). In the periplasmic space, Penicillin-binding proteins (PonA1 and PonA2) catalyse the transglycosylation and transpeptidation reactions, which allow glycan strand polymerisation and peptide crosslinking between side chains respectively, thus incorporating new PG subunits into the pre-existing PG polymer (Figure 1.6) (Sauvage et al., 2008, Squeglia et al., 2018).

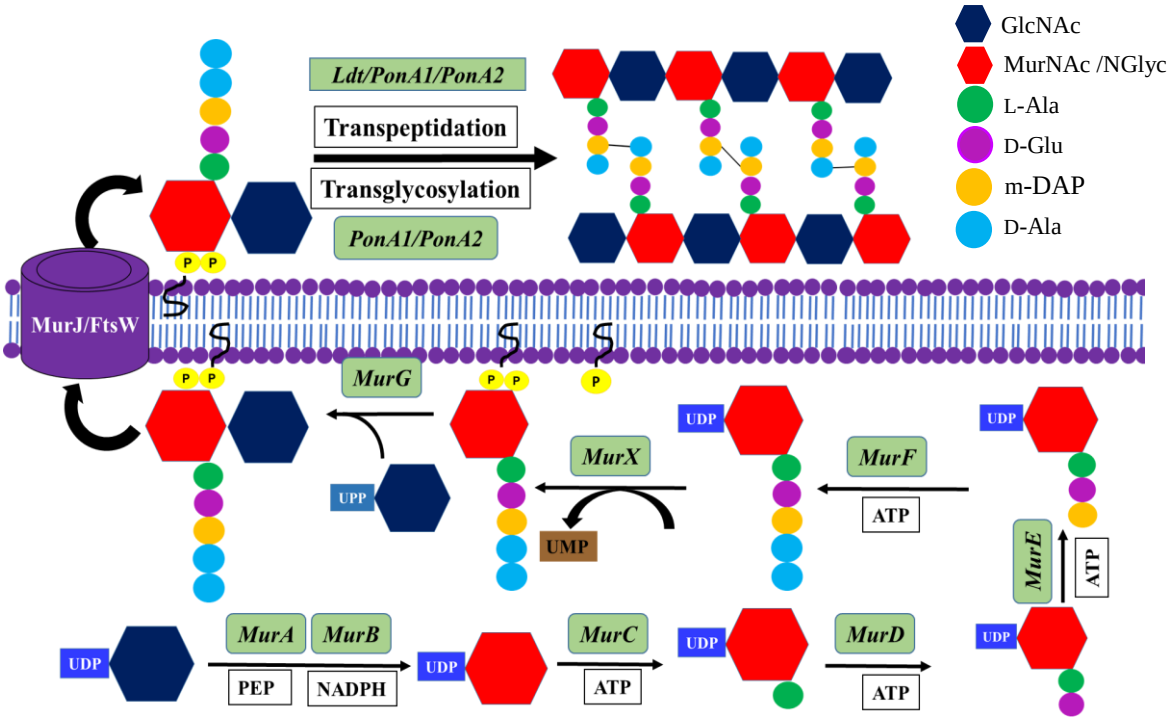


Figure 1.6. The biosynthesis of PG in *Mycobacterium tuberculosis*. Image adapted from Squeglia *et al*., (2018). MurA and MurB convert the PG precursor, UDP- GlcNAc to UDP-MurNAc. MurC-F subsequently adds amino acid residues to UDP-MurNAc, forming Lipid I. MurX catalyses the transfer of Lipid I to decaprenyl phosphate and MurG adds GlcNAc to Lipid I, forming Lipid II. MurJ/FtsW translocates Lipid II to the periplasm, where it is incorporated into an existing PG polymer by Penicillin-binding proteins (PonA1 and PonA2) through transglycosylation and transpeptidation reactions.

In bacteria, PG synthesis generally occurs at sites of cell division and cell extension, also including sites of cell wall repair. In contrast to other rod-shaped organisms such as *B. subtillis* or *E. coli*, which utilize lateral expansion of PG biosynthesis for cell extension, mycobacterial species and other actinomycetes extend from the polar regions. Polar PG synthesis is consistently carried out in the older pole (one inherited from the mother cell) throughout all growth phases, however in the new pole, it is delayed during the lag phase and later carried out at high rates in the log phase (Aldridge et al., 2012, Hannebelle et al., 2020). The polar extension is asymmetrical in mycobacteria and this results in daughter cells of different lengths and this has been associated with cell heterogeneity and phenotypic tolerance to drugs within the mycobacterial population (Aldridge et al., 2012). In addition to asymmetric cell division, other molecular factors drive singe-cell heterogeneity and variation in mycobacteria. As an example, Rego et al. (2017) reported that the deletion of the gene encoding LamA (a protein involved in promoting cell asymmetry) in Msm is associated with decreased survival in the presence of RIF.

1.9. PG modifications and their roles in mycobacterial cell walls

In mycobacterial species, PG undergoes several modifications in both the glycan strand and the peptide stem, which promotes survival in the host. Concerning the glycan strand, modifications include *N*-glycosylation, *O*-acetylation and *N*-deacetylation (Brott and Clarke, 2019). Mycobacterial MurNAc residues contain a combination of *N*-acetyl and *N*-glycolyl modifications, and it is believed that the *N*-glycolyl modification allows for additional hydrogen bonding (Figure 1.7), which strengthens the mesh-like structure of PG (Moynihan et al., 2019). *N*-glycolyl modifications occur in the cytoplasm via the actions of UDP-MurNAc hydroxylase (NamH), a monooxygenase that oxidizes the acetamido group in the soluble PG precursor using oxygen and NADPH (Raymond et al., 2005). The MurNAc and GlucNAc residues undergo respective *O*-acetylation (the acetylation of the C-6 hydroxyl of MurNAc) and *N*-deacetylation (the removal of a nitrogen atom from the acetyl group) modifications which confer resistance to the activity of host produced lysozymes (Brott and Clarke, 2019). The glycan strands are cross-linked by peptide stems, which are linked to the strand via covalent bonds between MurNAc lactyl groups and *N*-termini of L-Alanine. For the peptide component, the peptide stems consist of L-Ala, D-Glu, meso-diaminopimelic acid (m-DAP) and D-Ala amino acids. The D-amino acids render bacteria resistant to host proteases, an important feature in pathogenesis (Alvarez et al., 2014). The cross-linking (ca. 80% of the PG is cross-linked) and

formation of DAP–DAP covalent linkages (commonly referred to as 3-3 crosslinks) by *M. tuberculosis*, allows for the survival of the pathogen in macrophages for extended periods (Lavollay et al., 2008). Efficient cross-linking requires an amidation modification in the PG stem peptide that constitutes the addition of an amide (NH_2) group to α- and ε-carboxyl groups of D-isoGlu and DAP by amidotransferases. Ngadjeua et al. (2018) showed that amidation of DAP by amidotransferase AsnB (Rv2201), was required for mycobacterial growth whilst amidation of the D-isoGlu is catalyzed by the MurT-GatD bi-enzmye complex (Maitra et al., 2021). These, and other, characteristics of PG components contribute to the pathogenicity and survival of Mtb; therefore, targeting enzymes that modulate this structure may serve as a useful avenue for drug discovery.

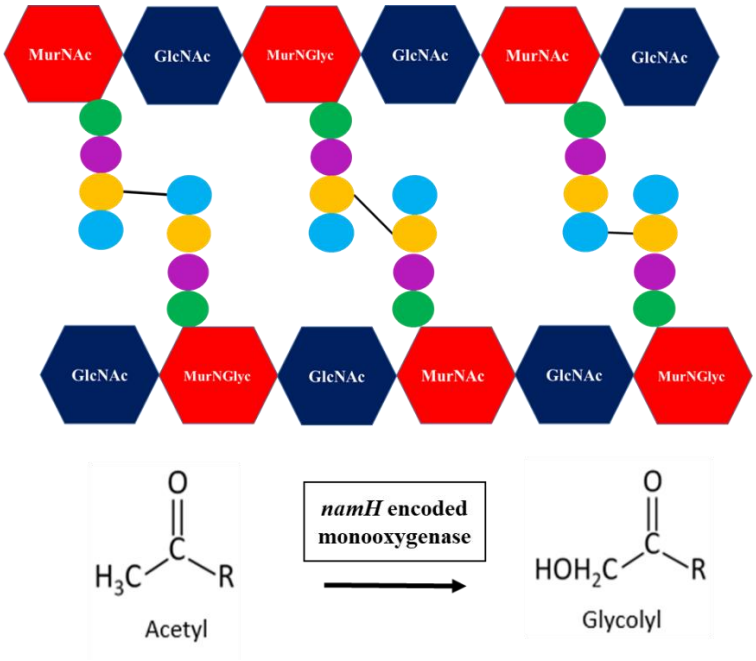


Figure 1.7. Schematic diagram showing *N*-glycolyl modifications in mycobacterial PG. Modifications are carried out in the cytoplasm by the monooxygenase, UDP-MurNAc hydroxylase (NamH) which converts the acetyl group into a glycolyl group via oxidation.

1.10. PG remodelling during cell growth and division

PG remodelling involves the biosynthesis and breakdown of PG by enzymes in a coordinated manner to allow for vital bacterial processes such as cell growth/elongation, cell division, and cellular communication (Moynihan et al., 2019, Senzani et al., 2017). The activity of select PG remodelling enzymes is given in Figure 1.8. For the growth and elongation of individual

mycobacterial cells, existing bonds in the PG polymer must be broken to allow for the addition of new PG material at the cell poles (Wheeler et al., 2015). With respect to cell division, PG is synthesized at the mid-cell and leads to the formation of septa, which are then subsequently degraded to allow for daughter cell separation. In addition, remodelling allows for the insertion of cell wall components such as efflux pumps and porins (Blair et al., 2015, Uehara and Bernhardt, 2011). The degradation products of PG (termed muropeptides) can function as signalling molecules and play a role in the resuscitation of Mtb from the non-replicative state (Mir et al., 2011). Moreover, in other organisms, muropeptides are involved in the induction of β-lactamase activity and interact with the host immune system employing NOD-like receptors (Frirdich and Gaynor, 2013, Shah et al., 2008, Vötsch and Templin, 2001). Given these essential roles of PG hydrolases, their dysregulation can lead to atypical growth and division, or cell lysis. PG synthases and hydrolases are vital components of bacteria and are discussed further below.

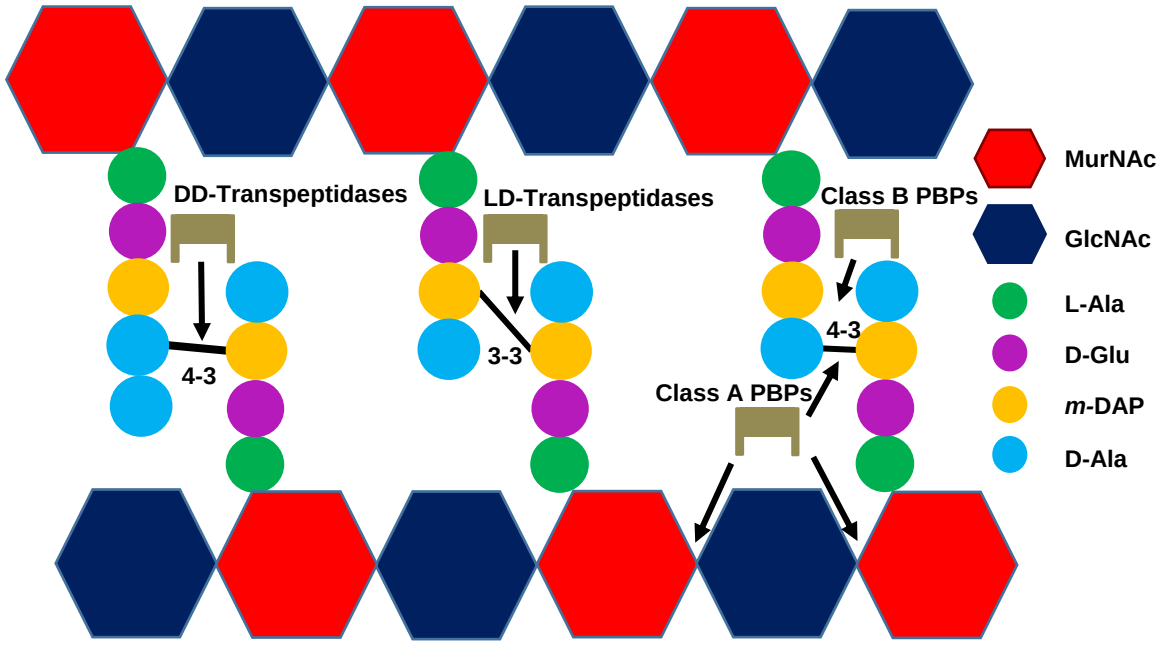


Figure 1.8. Various PG synthases and the bonds arising from their actions on the PG molecule. Class A PBPs possess both transglycosylation and transpeptidation activity, respectively, synthesizing the β-1,4-glycosidic bond between MurNAc and GlcNAc, and 4-3 peptide crosslinks. Class B PBP/DD-transpeptidases activity forms 4-3 crosslinks. LD-Transpeptidases catalyse the formation of 3-3 crosslinks.

1.11. PG polymerization and PG synthases

Transglycosylation and transpeptidation reactions are the hallmarks of PG polymerization. Transglycosylation reactions result in the formation of the β-1,4-glycosidic bond between MurNAc and GlcNAc residues in an alternating manner by Penicillin Binding Proteins (PBPs) and monofunctional glycosyltransferases (Caveney et al., 2018, van Heijenoort, 2001). Transpeptidation reactions involve the crosslinking of adjacent glycan strands through 4-3 and 3-3 linkages via PBPs and LD-transpeptidases (Kumar et al., 2012, Catalão et al., 2019). Typically, bacterial PG transpeptidation is characterised by an abundance of 4-3 crosslinking, which comprises the formation of an amide bond via the linking of a carbonyl at the acyl donor stem of the 4th position D-Ala to the side-chain amino group of an acyl acceptor stem at the 3rd position m-DAP of an adjacent pentapeptide by PBPs with D, D-transpeptidase activity (Ngadjeua et al., 2018). The 4-3 crosslinks increase the vulnerability of bacteria to β-lactam antibiotics, which mimic the acyl group of D-Ala residues, and bind the PBP at the serine-containing active site (Catalão et al., 2019). However, in the case of mycobacterial species, PG transpeptidation is characterized by cross-linking with 3-3 covalent linkages, constituting around 80% of all crosslinks (Kumar et al., 2012, Gokulan and Varughese, 2019). 3-3 crosslinking occurs between the m-DAP on the third position of a peptide side chain and m-DAP on a similar position of an adjacent pentapeptide (Catalão et al., 2019, Caveney et al., 2018). Baranowski et al. (2018) showed that the deletion of all L, D-transpeptidases from Msm resulted in the formation of localised spherical blebs, the loss of ability to maintain rod shape and eventual cell death. This finding highlighted the importance of 3-3 crosslinks in mycobacterial physiology and survival. Similarly, in Mtb, deletion of the L, D-transpeptidases, LdtMt1 and LdtMt2, was associated with an increased sensitivity to β-lactam antibiotics (Schoonmaker et al., 2014).

In Mtb, PG polymerization is carried out by the class A PBPs, PonA1 and PonA2, and class B PBPs, PbpA and PBP3 (Arora et al., 2018). PonA1 and PonA2 are bifunctional synthases possessing transglycosylation and transpeptidation activity. PonA1, encoded by *Rv0050* was found to be the major PG synthase in Mtb (Gao et al., 2019). The depletion of PonA1 resulted in impaired growth and atypical cell morphology (Kieser et al., 2015). Degradation of PG, particularly at the septum in mycobacteria is catalyzed by an NlpC-60-type endopeptidase, RipA, whose activity is activated by interaction with a soluble lytic transglycosylase, RpfB (Nikitushkin et al., 2015). In this regard, PonA1 competes with RpfB for the binding of RipA to coordinate septal PG degradation this modulates cell division and elongation (Hett et al.,

2010). PbpA and Pbp3 are monofunctional synthases with transpeptidation activity (Arora et al., 2018). In various organisms, Class B PBPs have been found to form complexes with SEDS (Shape, Elongation, Division and Sporulation) proteins to carry out PG polymerization. This includes FtsW-PBP3 in *E. coli*, FtsW-PBP1 in *Streptococcus aureus* and FtsW-FtsI (PBP) in *Caulobacter crescentus* (Lariviere et al., 2019, Leclercq et al., 2017, Reichmann et al., 2019). In Mtb, PbpA was found to form a complex with RodA for PG polymerization, and this interaction was found to regulate cell length (Arora et al., 2018). In all bacteria where they exist, PG synthases function in harmony with PG hydrolases to carry out PG remodelling.

1.12. PG hydrolases

PG hydrolases are degradative enzymes that are divided into three main groups, namely glycosidases, peptidases, and *N*-acetylmuramyl-L-alanine amidases (Prigozhin et al., 2013). Glycosidases cleave covalent bonds between the glycan strand; peptidases cleave between peptide bonds; and *N*-acetylmuramyl-L-alanine amidases remove peptides from glycan strands (Prigozhin et al., 2013). These activities are outlined in Figure 1.9.

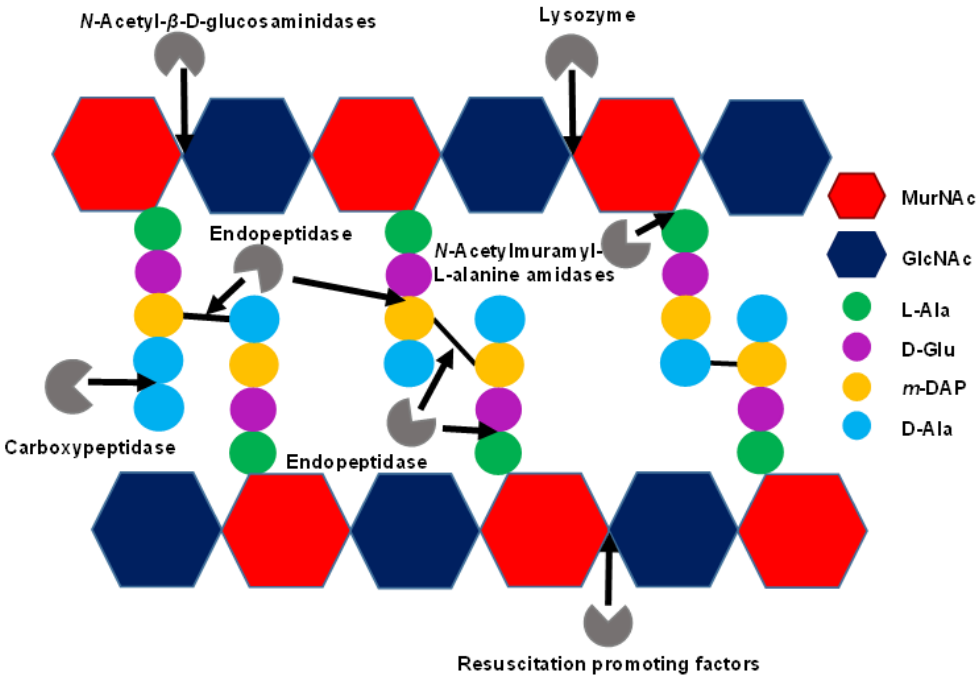


Figure 1.9. Various PG hydrolases and their cleavage locations on the PG molecule. Image adapted from Vollmer et al. (2008).

1.12.1. Glycosidases

The enzymes in this group include *N*-acetyl-β-D-muramidases, *N*-acetyl-β-D-glucosaminidases and lytic transglycosylases (Do et al., 2020a). *N*-acetyl-β-D-muramidases cleave the β-1, 4-glycosidic bond between MurNAc and GlcNAc residues in PG. *N*-acetyl-β-D-glucosaminidases cleave between GlcNAc and MurNAc residues of PG. This enzyme makes use of GlcNAc-1, 6-anhydroMurNAc muropeptides for recycling and activation of β-lactamases (Vötsch and Templin, 2001). Lytic transglycosylases cleave the β-1,4-glycosidic bond between MurNAc and GlcNAc residues similarly to *N*-acetyl-β-D-muramidases but the cleavage is non-hydrolytic and results in the production of a 1,6-anhydro ring at the MurNAc residue (Do et al., 2020a). This ring plays a role in signalling, recycling, and induction of the β-lactam degrading β-Lactamases (Moynihan et al., 2019, Vötsch and Templin, 2001). Resuscitation-promoting factors (Rpfs) possess a catalytic domain that is similar to that of lytic transglycosylases (Nikitushkin et al., 2015). In Mtb, the joint action of RpfB and the peptidase, RipA, results in the formation of the disaccharide-dipeptide, *N*-acetylglucosaminyl-β(1-4)-*N*-glycolyl-1,6-anhydromuramyl-L-alanyl-D-isoglutamate, which is the minimum product required to resuscitate Mtb from the state of non-replication and low metabolic activity (Nikitushkin et al., 2015).

1.12.2. Peptidases

PG peptidases can be further classified into endopeptidases and carboxypeptidases, depending on the specific cleavage site. Endopeptidases cleave within the pentapeptide and can be classified as either DD-endopeptidases (cleave between m-DAP and D-Ala), LD-endopeptidases (cleaves between L-Ala and D-Glu) or DL- endopeptidases (cut between D-Glu and m-DAP) (Vollmer et al., 2008). Mtb possesses the *Rv1477-Rv1478* operon, which encodes two NlpC/60-like domain containing DL- endopeptidases, RipA and RipB (Böth et al., 2011). RipA is not only involved in bacterial resuscitation, it is has been shown to play a role in persistence in mice and is the major PG hydrolase required for cell division in Mtb (Healy et al., 2020, Nikitushkin et al., 2015). Carboxypeptidases cleave the *C*-terminal amino acids from pentapeptide sidechains. In this case, LD-Carboxypeptidases (LD-transpeptidases) cleave between and L- and D- form amino acids, and DD-carboxypeptidases cleave bonds between two D-amino acids (Rolain et al., 2012, Sharma et al., 2016). Msm cells devoid of all L, D-transpeptidases form localised spherical blebs; and cannot maintain rod shape, with decreased viability (Baranowski et al., 2018).

In Msm, DD-carboxypeptidases were found to be dispensable for growth, except for MSMEG_6113 (DacB), which was found to be part of a highly conserved operon that is essential for growth (Kumar et al., 2012, Ealand et al., 2019). Additionally, Ealand et al. (2019) showed that DacB is essential for mycobacterial growth and that it is involved in the localization of PG synthesis, as the transcriptional repression of *dacB* resulted in PG incorporation at a single pole instead of both poles in Msm.

1.12.3. Amidases

N-acetylmuramyl-L-alanine amidases are a group of zinc metalloenzymes that cleave the amide bond between MurNAc and L-alanine in the first position of the pentapeptide (Sharma et al., 2016). Amidases can be classified into either amidase_2 or amidase_3 domain-containing enzymes (Senzani et al., 2017). Amidase_2 domain containing enzymes are generally associated with bacteriophages and eukaryotic amidases, whereas Amidase_3 domains - containing amidases are limited to bacteria and bacteriophages (Prigozhin et al., 2013). Amidases are implicated in cell division in various organisms; a brief summary is given below, as these enzymes will be discussed in further detail in Chapter 3.

In *Staphylococcus aureus*, the hydrolysis of un-crosslinked PG by the LytH amidase, in complex with a membrane protein, ActH, controls cell growth and division by regulating PBP2 mediated cell growth and controlling FtsZ placement, respectively (Do et al., 2020b). The catalytic activity of amidases results in the formation of denuded (that is lacking any PG stem peptides) glycan strands, which are densely concentrated at the septum (Alcorlo et al., 2019). These glycans are recognised by SPOR (sporulation-related repeat) domain-containing proteins, which subsequently act on the strand. Alcorlo et al. (2019) showed that RlpA (a lytic transglycosylase from *Pseudomonas aeruginosa*) binds denuded glycan strands via the SPOR domain to effect efficient cell division and maintain rod shape.

To date, five amidases have been identified in Msm and four amidases have been identified in Mtb (Cole et al., 1998, Machowski et al., 2014, Senzani, 2018). In Msm, Ami1 (MSMEG_6281) was found to play a role in cell division. Deletion of *ami1* resulted in the inability of daughter cells to separate, forming cellular chains with multiple septa (Senzani et al., 2017). Additionally, Ami1 is involved in fatty acid metabolism and biofilm formation (Miao et al., 2020).

Biochemical analysis of Ami2/CwlM (MSMEG_6935) in Msm revealed that it is essential for survival in addition to regulating MurA, an enzyme involved in the first step of PG biosynthesis (Boutte et al., 2016). Similarly, the Ami2 homologue in Mtb, Rv3595, is also essential for growth and exists in two forms, i.e. cytoplasmic and membrane-bound (Turapov et al., 2018). The membrane-bound state is non-phosphorylated, associated with MurJ (MviN) and may play a role in lipid II transport, whereas the cytoplasmic form is the main substrate of PknB and acts as the regulator of MurA via phosphorylation (Turapov et al., 2018). Despite these recent reports, the biological functions of Mtb amidases remain largely unknown. In this PhD study, we aimed to characterise the role of Ami1 and its regulation in Mtb cell division, proliferation and survival. The dissertation research is divided into two broad sections with the first comprising phenotypic characterization of an amidase defective mutant to determine the biological function of Ami1. The second component focused on regulation of the *ami1* gene in Mtb using a combination of bioinformatics and experimental approaches. The appending hypotheses, along with the aims and objectives are outlined in chapter 3 and chapter 4 respectively.

Space left intentionally blank

Chapter 2: General Experimental Methods and Associated Materials

2. General experimental methods and associated materials

2.1. Bacterial growth conditions

2.1.1. Growth conditions for *E. coli* strains

E. coli strains were cultured in Luria-Bertani (LB) broth or Luria agar (LA) at 37 °C, supplemented with the appropriate antibiotic. Antibiotic concentrations used were as follows: Ampicillin (Amp) 100 μg/ml, Kanamycin (Kan) 50 μg/ml and Hygromycin (Hyg) 200 μg/ml. *E. coli* strains cultured in LB were grown with shaking at 250 rpm unless stated otherwise.

2.1.2. Growth conditions for Msm strains

Msm strains were cultured in Middlebrook 7H9 liquid media supplemented with 0.2 % glucose, 0.5 % glycerol, 0.085 % NaCl, and 0.05 % Tween 80 (herein referred to as 7H9) or, if required, on Middlebrook 7H10 solid media supplemented with 0.2 % glucose, 0.5 % glycerol, and 0.085 % NaCl (herein referred to as 7H10) at 37 °C, supplemented with appropriate antibiotic. Antibiotic concentrations used were as follows: Hyg 50 μg/ml and Kan 25 μg/ml. M. smegmatis strains cultured in 7H9 were grown with shaking at 100 rpm.

2.1.3. Growth conditions of Mtb strains

Mtb strains were cultured in Middlebrook 7H9 liquid media supplemented with Middlebrook OADC enrichment, 0.5 % glycerol, and 0.05 % Tween 80 (herein referred to as 7H9) or, if required, on Middlebrook 7H11 solid media supplemented with Middlebrook OADC enrichment and 0.5 % glycerol containing appropriate antibiotic (herein referred to as 7H11) at 37 °C. Where appropriate, antibiotics were added at the following concentrations: Kan 25 μg/ml and Hyg 50 μg/ml.

2.2. DNA extractions

2.2.1. Mtb genomic DNA (gDNA) extraction

2.2.1.1. Cetyltrimethylammonium bromide (CTAB) for gDNA extraction

Mtb cells were grown on 7H11 plates until a bacterial lawn was formed. Cells were harvested by scraping and were re-suspended in 500 µl TE buffer (10 mM Tris-HCL, 10 mM EDTA; pH 10). The cells were heat-killed at 80ºC for 1 hr and then cooled to room temperature. A 70 µl aliquot of lysozyme (10 mg/ml) was added and the cells were incubated at 37ºC for 1 hr. Thereafter, 6 µl of proteinase K (10 mg/ml) and 70 µl SDS (10%) were added and the sample was incubated at 65ºC for 1-2 hrs. To this, 100 µl of pre-warmed 5 M NaCl and 80 µl, pre-warmed CTAB/NaCl (10%:4.1%) was added and mixed by vortexing, followed by and incubation at 65ºC for 15 min and the sample was frozen at -80ºC for 20 min. An equal volume of chloroform:isoamyl alcohol (24:1) was added, mixed vigorously and centrifuged at 12 470 × g for 10 min. The top aqueous layer was transferred into a sterile Eppendorf tube. Isopropanol (0.6 volumes of the sample) was added and the sample was centrifuged at 12 470 × g for 20 min. The supernatant was discarded and the pellet was washed by adding 500 µl of 70% ethanol, followed by centrifugation at 12 470 × g for 5 min. The supernatant was discarded and the pellet was vacuum dried at 60ºC for 10 min using the Eppendorf Concentrator 5301. Finally, the DNA pellet was re-suspended in 100 µl sterile distilled water (dH_2O) and incubated at 65ºC for 10 min. The gDNA was quantified using the NanoDrop (ND-1000) and stored at -20ºC until use.

2.2.1.2. Small scale gDNA extraction for PCR in Mtb

Small-scale gDNA extractions were conducted to obtain crude lysates to serve as PCR templates. A single colony was picked from an agar plate and re-suspended in 100 µl dH_2O. The sample was incubated at 95ºC for 5 min and 100 µl of chloroform was added and the sample was mixed vigorously by vortexing, followed by centrifugation at 12 470 × g for 5 min. The top, aqueous phase (containing gDNA) was transferred into a sterile Eppendorf tube and immediately used.

2.2.2. Plasmid DNA extraction from *E. coli*

2.2.2.1. Large scale plasmid extraction (Nucleobond Xtra Midi plasmid kit)

Large-scale plasmid extraction was performed using the Nucleobond Xtra Midi DNA extraction kit (Macherey-Nagel) and vector preparation was carried out as per manufacturer's instructions. Briefly, *E. coli* strains that carried the plasmids requiring purification were grown overnight at 37°C in 50 ml of LB media, which was supplemented with appropriate antibiotics. After harvesting cells by centrifugation at 1180 × g for 15 minutes, the supernatant was discarded and the cell pellet was resuspended in 4 ml of Buffer S1 (50 mM Tris-HCl, 10 mM EDTA, 100 µg/ml RNase-A, pH 8.0). Thereafter, 4 ml of Buffer S2 (200 mM NaOH, 1% SDS) was added and the mixture was inverted several times incubated at room temperature for 3 minutes. Following this, 4 ml of Buffer S3 (2.8 M KAc, pH 5.1) was added, mixed by inversion and incubated on ice for 5 minutes. This neutralized lysate was centrifuged at 1180 × *g* for 30 minutes in preparation for column purification. A Nucleobond Ax100 column was equilibrated with 2.5 ml of Buffer N2 (100 mM Tris, 15% ethanol, 900 mM KCl, 0.15% Triton X-100, adjusted to pH 6.3 with H_3PO_4). The supernatant resulting from centrifugation of the lysate was passed through the column. Following this, 10 ml of the wash Buffer N3 (100 mM Tris, 15% ethanol, 1.15 M KCl, adjusted to pH 6.3 with H_3PO_4) was used to wash the column. The plasmid DNA was eluted in 5 ml of Buffer N5 (100 mM Tris, 15% ethanol, 1 M KCl, adjusted to pH 8.5 with H_3PO_4) and precipitated through the addition of 3.5 ml of isopropanol. The DNA was collected by centrifugation of the mixture at 12 470 × g for 30 minutes. The isolated DNA pellet was washed with 500 µl 70% ethanol and centrifuged at 15 000 x g for 5 min. The supernatant was discarded and the pellet was vacuum dried at 60^{o}C for 10 min using the Eppendorf Concentrator 5301. The pellet was re-suspended in 25 µl sterile dH_2O and incubating at 65^{o}C for 10 min. The gDNA was quantified using the NanoDrop (ND-1000) and stored at -20^{o}C.

2.2.2.2. Small scale plasmid extraction (alkaline lysis)

Small scale plasmid extraction was performed by using the alkaline lysis method (Birnboim and Doly, 1979). A 5 ml pre-culture of *E. coli* was grown in LB at 37^{o}C overnight and thereafter, 2 ml of the culture was centrifuged at 12 470 × g for 5 min. The supernatant was discarded and the pellet was re-suspended in 100 µl of solution I (25 mM Tris-HCl, 10 mM EDTA, 50 mM glucose; pH 8) and incubated on ice for 10 min. Thereafter, 200 µl of freshly prepared solution II (0.2 M NaOH, 1% SDS) was added and mixed by inversion, and the sample

was incubated at room temperature for 5 min. Subsequently, 150 µl of pre-chilled solution III (3 M potassium acetate, 11.5% acetic acid) was added and the suspension was incubated for 5 min on ice. The suspension was centrifuged at 12 470 × g for 5 min and the supernatant was transferred into a sterile Eppendorf tube. Thereafter, 4 µl of RNase A (10 mg/ml) was added to the suspension and incubated at 42^{o}C for 10 min, followed by the addition of isopropanol at a volume equal to that of the sample. The mixture was centrifuged at 12 470 × g for 20 min. The supernatant was discarded and the pellet was washed with 500 µl 70% ethanol and centrifuged at 12 470 × g for 5 min. The supernatant was discarded and the pellet was vacuum dried and re-suspended in 25 µl sterile dH_2O. The gDNA was quantified using the NanoDrop (ND-1000) and stored at -20^{o}C.

2.2.3. Ethanol precipitation for purification of genomic and plasmid DNA

Ethanol precipitation was used to remove residual contaminants from the isolated DNA. This was achieved by adding 0.1 volume of 3 M sodium acetate to the DNA solution. This was followed by adding 2.5 volumes of pre-chilled 100% ethanol to the sample and mixing the sample by inversion. The sample was incubated at -20^{o}C for at least 30 min and thereafter, centrifuged at 12 470 × g for 20 min. The supernatant was discarded and the pellet was washed with 500 µl 70% ethanol and centrifuged at 12 470 × g for 5 min. The supernatant was discarded and the pellet was vacuum dried and re-suspended in 100 µl sterile dH_2O. The gDNA was quantified using the NanoDrop (ND-1000) and stored at -20^{o}C.

2.3. DNA manipulation/cloning

2.3.1. Polymerase Chain Reaction (PCR)

2.3.1.1. Roche FastStart Taq DNA PCR

The Roche Fast-Start kit (Roche Applied Science) was used to confirm gene knockouts in mutant strains. PCR reactions were carried out in 50 µl volumes comprising 1 × Roche FastStart Taq DNA polymerase buffer, 2 mM $MgCl_2$, 1 × GC rich buffer, 0.2 mM dNTPs, 1 µM of forward and reverse primers, ~100 ng DNA template, 1 U FastStart Taq DNA polymerase and dH_2O. Reactions were carried out in a thermo-cycler (Bio-Rad Laboratories) with cycling conditions as follows: Initial denaturation at 95^{o}C for 4 min; followed by 30-35 cycles of denaturation at 95^{o}C for 30 sec, annealing at primer dependent temperature (55-65^{o}C) for 30 sec and elongation at 72^{o}C for a period that is dependent on the product length (FastStart

Taq DNA polymerase amplifies at 60 sec/kb); thereafter, the final elongation at 72ºC for 7 min. PCR products were viewed on a 0.8-1% agarose gel.

2.3.1.2. NEB Q5 High-Fidelity DNA PCR

The NEB Q5® High-Fidelity kit (New England Biolab) was used to generate DNA fragments for cloning. The kit makes use of the Q5 High-Fidelity DNA polymerase, which maintains proof reading capacity that prevents the introduction of mutations thus, ensuring sequence fidelity. PCR reactions were carried out in 50 µl volumes comprising 1 × Q5 Reaction Buffer, 1 × Q5 High GC Enhancer, 0.2 mM dNTPs, 0.5 µM forward and reverse primers, ~100 ng DNA template, 1 U Q5 High-Fidelity DNA polymerase and dH_2O. Reactions were carried out in a thermo-cycler (Bio-Rad Laboratories) with cycling conditions as follows: Initial denaturation at 98ºC for 30 sec; followed by 30-35 cycles of denaturation at 98ºC for 10 sec, annealing at primer dependent temperature (55-72ºC) for 30 sec and elongation at 72ºC for a period that is dependent on the product length (Q5 High-Fidelity DNA polymerase amplifies at 30 sec/kb); thereafter, the final elongation at 72ºC for 2 min. PCR products were viewed on a 0.8-1% agarose gel.

2.3.2. Restriction digests

Restriction digests were performed using NEB (NewEngland Biolab) or/and Roche (Roche Applied Sciences) enzymes and were carried out according to the manufacturer's instructions. Reactions were conducted in 20 µl volumes, unless stated otherwise, comprising 1 x restriction buffer, 1 U restriction enzyme, appropriate DNA (0.5-1 µg for plasmid DNA and 1-3 µg for gDNA) and dH_2O. Restrictions were usually carried out at 37ºC for 1 hr, unless stated otherwise. Restriction digests were terminated by heat inactivating the enzymes at appropriate temperatures as prescribed by the manufacturer. Digestion products were viewed on a 0.8-1% agarose gel.

2.3.3. Plasmid dephosphorylation

Antarctic Phosphatase (NEB) was used for the removal of 5' phosphate groups from the termini of linearized plasmids in order to prevent self-ligation and reduce false positive clones. Each dephosphorylation reaction was conducted in a volume of 20 µl consisting of 1 × Antarctic Phosphatase buffer (NEB), 1 U Antarctic Phosphatase, 1-3 µg plasmid DNA and dH_2O. The

reaction was performed at 37ºC for 15-30 min. The reaction was stopped by heat-inactivation at 70ºC for 5 min.

2.3.4. Agarose gel electrophoresis

Agarose gel electrophoresis was used to separate DNA into distinct sizes (bands). Agarose gels with 0.8% and 2% agarose strength were respectively used for the separation of high molecular weight DNA and low molecular weight DNA, along with the appropriate DNA molecular weight markers. Each agarose gel comprised of 1 × TAE buffer (40 mM Tris-acetate, 1 mM EDTA) and 0.5 µg/ml ethidium bromide. Electrophoresis was performed in 1 × TAE buffer at 80 – 100 V in electrophoresis tanks (Bio-Rab laboratories). Bands were visualised using a G: Box SYNGENE system along with the GeneSnap image acquisition software (Syngene).

2.3.5. DNA fragment purification

The NucleoSpin Gel and PCR Clean-Up kit (Macherey-Nagel) was used to remove impurities (enzymes, primers, RNA) from DNA. Additionally, it was used to purify desired DNA fragments from an agarose gel after electrophoresis. Purification was carried out as per manufacturer's instruction. In the case of PCR clean up, 2 × volumes of Buffer NTI was added to 1 × volume of the DNA sample and mixed. Thereafter, the mixture was transferred to a NucleoSpin column that was placed in a 2 ml collection tube and centrifuged at 11 000 × g for 30 sec. The flow-through was discarded and the column was placed back into the collection tube and if needed, the remaining sample was loaded and the centrifugation was repeated. The column was washed by adding 700 µl Buffer NT3 and centrifuging at 11 000 × g for 30 sec. The flow-through was discarded and the column was placed back into the collection tube and the NT3 step was repeated for optimal cleaning. Thereafter, the sample was centrifuged at 11 000 × g for 1 min and then the column was transferred to a 1.5 ml Eppendorf tube. Fifteen-thirty µl of Buffer NE was applied directly to the column membrane and incubated at room temperature for 1 min and the centrifuged at 11 000 × g for 1 min for elution.

The column was discarded and the DNA was stored on ice or stored at -20ºC for later use. In the case of gel purification, the DNA fragment of interest was excised from the agarose gel with the aid of a scalpel and UV exposure. The weight of the gel slice was measured and the gel slice was transferred to a 1.5 ml Eppendorf tube. For every 100 mg of gel slice, 200 µl of

Buffer NTI was added and the tube was incubated at 50°C for the required time to dissolve the gel. From this point on, purification was carried out as mentioned above.

2.3.5. DNA ligation

DNA fragments were ligated using the T4 DNA ligase enzyme (NEB). The optimal ratio of vector DNA to insert DNA is required for successful ligation. The ratio was determined using the following equation:

Amount of insert (ng) = 50ng (plasmid) × size of insert (bp)/ size of vector (bp)

Ligation reactions were performed in 20 µl reactions, comprising 1 × ligation buffer, 5 U T4 DNA ligase, 50 ng vector DNA, appropriate amount of DNA insert and dH_2O. The reactions were conducted at room temperature for 10-120 min or alternatively, at 16°C overnight. Ligation reactions were stopped by heat-inactivation at 65°C for 10 min. Ligations were viewed on a 0.8-1% agarose gel to determine their success.

2.4. Bacterial Transformations

2.4.1. Transformation of chemically competent *E. coli* DH5α cells

2.4.1.1. Preparation of chemically competent *E. coli* DH5α cells

Chemically competent cells were prepared by growing DH5α cells overnight in 5 ml 2 × TY at 37°C with shaking at 100-120 rpm. The overnight culture was transferred to new 2 × TY broth such that it was 0.1 volumes of the total broth. The culture was then incubated at 37°C with shaking at 100-120 rpm for ca. 3 hrs to allow growth to reach the log phase (OD600nm 0.3-0.6). DH5α cells were collected by centrifugation at 4 000 × g for 5 min at 4°C and thereafter kept at ice-cold conditions for subsequent steps. The supernatant was discarded and the cells were gently re-suspended in ice cold 0.1 M $MgCl_2$ (10 ml), and placed on ice for 10 min.

The cells were collected by centrifuged at 4 000 × g for 5 min at 4°C and the supernatant was discarded. Cells were then re-suspended in 10 ml of ice cold 0.1 M $CaCl_2$ and left on ice for 30 min and thereafter at centrifuged at 4 000 × g for 5 min at 4°C. At this point, the cells were re-suspended in 2 ml of 0.1 M $CaCl_2$ and used for transformations.

2.4.1.2. Transformation chemically competent *E. coli* DH5α cells by heat shock

For heat shock transformations, 2-20 µl of plasmid/ligation reaction was added to 200 µl of chemically competent *E. coli* DH5α cells and incubated on ice for 15 min. The mixture was heat shocked at 42^{o}C for 90 s and immediately incubated on ice for 5 min. Thereafter, 800 µl 2 × TY broth was added and the cells were incubated at 37^{o}C for 60 min, before plating on LA plates with the appropriate antibiotic. LA plates were incubated at 37^{o}C overnight.

2.4.2. Mtb electroporations

An Mtb culture grown to stationary phase (OD600nm ≥ 1) was inoculated into 100 ml 7H9 and grown to the log phase (OD600nm 0.8-1). At this point, the culture was supplemented with glycine to a final concentration of 1.5%, and then incubated at 37°C for 16 hrs. The cells were harvested at 4 000 × g for 10 min at room temperature and the supernatant discarded. The pellet was subjected to four washes in 40 ml of 10% glycerol washes at room temperature and finally re-suspended in 2 ml of 10% glycerol. At this point, the cells were ready for electroporation. For electroporations, 1-5 µg of plasmid DNA was UV-irradiated (100 mJ/cm2) then immediately inoculated into a 400 µl aliquot of electro-competent Mtb cells. The cell suspension was transferred to a 0.2 cm electroporation cuvette (Bio-Rad laboratories) and pulsed using the following conditions: 2500 V, 25 µF, 0.2 cm and 1000 Ω using the GenePulserX cell (Bio-Rad Laboratories). Cells were rescued immediately with 800 µl 7H9 and incubated at 37°C overnight. Thereafter, cells were plated on 7H11 media containing the appropriate antibiotics, followed by incubation for 3-6 weeks at 37°C to allow CFU growth.

2.5. Monitoring gene expression

2.5.1. RNA Extraction in Mtb

RNA extraction was performed using the NucleoSpin RNA purification Kit (Macherey-Nagel) according to the manufacturer's instructions. Mtb cultures were grown to OD600nm 0.6-0.8 (unless stated otherwise).

Cells were harvested by centrifugation 4 000 x g for 10 min at room temperature. The pellet was re-suspended in a mixture of 350 µl lysis buffer and 3.5 µl β-mercaptoethanol and transferred to lysis matrix B tubes (IEPSA) and ribolysed 3 times using the FastPrep Savant FP-120 Ribolyser for 1 min at speeds of 6 m/sec, with 2 min ice incubation between each ribolysis. The lysate was transferred to the lipid filters tubes and centrifuged at 11 000 × g for

30 sec. Three hundred and fifty microlitres of 70 % ethanol was added to the flow-through and the sample was transferred to nucleic acid binding columns placed in 2 ml collection tubes and centrifuged at 11 000 × g for 30 sec, followed by the removal of the flow-through. Thereafter, 350 µl of membrane desalting buffer (MBD) was added to the column, centrifuged at 11 000 × g for 30 sec and the flow-through was discarded. The column membrane was subjected to 90 µl of a rDNAse reaction mixture of 50 µg/ ml rDNAse and rDNAse Reaction buffer (1:9) and was incubated for 15 min at room temperature. The column was washed by adding 200 µl of Buffer RA2 into the membrane and centrifuging for 30 sec at 11 000 × g. Further washing was done by adding 600 µl Buffer RA3, with centrifugation at 11 000 × g for 30 sec, and 250 µl Buffer RA3 with centrifugation at 11 000 × g for 2 min. The column was then placed in a sterile Eppendorf tube and RNA was eluted by adding 60 µl of RNAse free water on the membrane, incubating at room temperature for 10 min and centrifugation at 11 000 × g for 1 min. The RNA was then quantified using the NanoDrop and stored at -80ºC awaiting further use.

2.5.2. Complementary DNA (cDNA) synthesis from total RNA

The Superscript IV reverse transcriptase kit (Invitrogen) was used for cDNA synthesis. Prior to reverse transcription (RT), a 25 µl reaction comprising of ≥ 1 µg RNA and a mixture of 2.5 µM reverse primers (for reverse transcription of the gene of interest and a house-keeping gene). The sample was annealed in a thermal cycler (Bio-Rad) using the following conditions: 94ºC for 90 sec, 65ºC for 3 min, and 57ºC for 3 min and thereafter, placed on ice. Separately, two 12.5 µl RT reaction samples (RT-positive and RT-negative) were prepared. The RT-positive comprised 5 µl of 5 x first-strand buffer, 4 mM $MgCl_2$, 0.1 mM Dithiothreitol (DTT), 1 µl of Superscript IV (SSIV) and 0.4 mM dNTPs.

The RT-negative reaction consisted of similar components with the exception that SSIV is replaced with sterile dH_2O. Thereafter, the annealed 25 µl reaction was split into two 12.5 µl aliquots, which were then added to the 12.5 µl RT reactions. The conditions for the RT reaction were as follows: 55ºC for 30-50 min; 80ºC for 5 min. The cDNA was used immediately used for quantitative PCR or stored at -80ºC for later use.

2.5.3. Quantitative PCR (qPCR)

The Bio-Rad SsoFast Evergreen Supermix (Bio-Rad Laboratories) was used for qPCR. Reactions were carried out in 20 µl volumes comprising 10 µl of SsoFast Evergreen Supermix, 0.375 µM forward and reverse primers, 1 µl cDNA and nuclease-free water. Reactions were performed in the CFX96 Real-Time PCR detection system using the following parameters: 98^{o}C for 2 min; 40 cycles of denaturation at 98^{o}C for 5 sec, annealing at primer dependent temperatures for 5 sec, elongation at 72^{o}C for 5 sec and SYBR Green quantification. This was followed by a melt curve analysis starting from 50^{o}C to 95^{o}C, with gradual increases of 0.5^{o}C every 0.05 sec and SYBR Green quantification at every point. Bio-Rad CFX Manager v3.0 was used for processing raw data. The calculated concentration (Sq) values for each reaction, based on genomic DNA standard curves (prepared via 10-fold genome equivalent standard dilutions), were copied into Excel for further analysis. The calculated expression of the gene of interest (GOI) were normalized to the reference gene (*sigA*) using the following formula: Sq of GOI/Sq of *sigA*.

Space left intentionally blank

Chapter 3: Characterization of an *ami1*-deficient mutant of *Mycobacterium tuberculosis*

3.1. Introduction

For successful proliferation, bacteria have to maintain growth and normal functioning while adapting to challenges presented by the environment. The PG structure is vital in allowing these adaptations because in addition to conferring rigidity and facilitating resistance to osmotic pressure, it is constantly remodelled to allow growth and division and in response to environmental influences, promoting bacterial survival and/or virulence. In this section of the dissertation, the work focusing on evaluating the biological function of Ami1 in Mtb is described. To provide further context, the functions of amidases in a select set of organisms is described in the next sections.

3.1.1. Amidases in *E. coli*

The *E.coli* genome encodes five amidases, designated AmiA, AmiB, AmiC, AmiD and AmpD (Heijenoort, 2011). AmiA, B, and C are soluble periplasmic enzymes, AmpD is a soluble cytoplasmic enzyme, whereas AmiD is a lipoprotein anchored in the outer membrane (Heidrich et al., 2001, Lindquist et al., 1989, Park and Uehara, 2008). AmiA, B, and C belong to the amidase_3 family (PF01520) and are associated with cell division, whereas AmiD and AmpD are members of the amidase_2 family (PF01510), involved in PG recycling (Vollmer et al., 2008, Heijenoort, 2011). Individually, AmiA, AmiB, or AmiC are dispensable for cell division, however, mutant strains lacking all three genes display severe cell chaining (Heidrich et al., 2001, Priyadarshini et al., 2007). These observations suggested a functional redundancy in the activity of these proteins. However, extensive studies have revealed subtle differences in the activity of these proteins. Subcellular localization profiles of AmiA, B and C tagged with the green fluorescent protein (GFP) showed that AmiB and AmiC are concentrated at the invaginating septum before cell division, whereas AmiA is evenly distributed around the cell periphery throughout the cell cycle, (Bernhardt and de Boer, 2003, Peters et al., 2011). Priyadarshini et al. (2006) showed that AmiC preferentially cleaves PG tetrapetides over pentapeptides, whereas AmiA and AmiB are non-discriminant. Furthermore, deletion of the DD-carboxypeptidase PBP5 increased the concentration of PG pentapeptides. When PBP5 was deleted in a mutant strain lacking *amiC*, the level of cell chaining increased whereas, mutants

lacking either *amiA* or *amiB* were unaffected by the additional PBP5 deletion. The LytM domain containing proteins EnvC, NlpD, and ActS regulate the activity of AmiA, B and C during cell division (Uehara et al., 2009, Uehara et al., 2010, Mueller et al., 2021, Chodisetti et al., 2022). More specifically, ActS preferentially activates AmiB, and to a lesser level, AmiC to promote cell division under acidic growth conditions (Mueller et al., 2021).

The role of amidase_3 domain containing amidases in *E. coli* is not limited to cell division but also maintenance of the cell wall. A mutant strain with a triple deletion of *amiA, amiB* and *amiC* displayed an increased cell wall permeability resulting in greater susceptibility to sodium dodecyl sulphate and vancomycin (Heidrich et al., 2002). The amidase activator, ActS activates AmiC when the bacterium encounters cell wall stress (Gurnani Serrano et al., 2021, Chodisetti et al., 2022). AmiB and AmiC are also activated by ActS to maintain cell wall integrity under acidic conditions, as evidenced by an increased resistance to Triton-X in strains expressing AmiB or AmiC only (Mueller et al., 2021).

During growth, *E.coli* recycles approximately 50% of its PG in each generation (Doyle et al., 1988, Uehara and Park, 2007). The anhydromuropeptide, GlcNAc-1,6-anhMurNAc-L-Ala-D-Glu-Dap-D-Ala- is a major PG degradation product during recycling (Rousseau et al., 2023, Uehara and Park, 2007). The catalytic activities of the amidase_2 domain containing amidases, AmiD and AmpD implicate these enzymes in PG recycling because they hydrolyse muropeptides (soluble PG fragments consisting of the GlcNAc-Mur*NAc* residue and the peptide strand) (Heijenoort, 2011). AmpD specifically acts on 1, 6-anhydro-MurNAc residues whereas AmiD hydrolyzes muropeptides with or without a 1, 6-anhydro functional group on the MurNAc (Jacobs et al., 1995, Uehara and Park, 2007, Pennartz et al., 2009).

3.1.2. Amidases in *Bacillus subtilis*

The life cycle of *Bacillus* species typically involves vegetative growth and spore formation (Errington, 2003). Amidases have differential roles during these stages of growth and survival. For example, during vegetative growth, amidases play important roles in cell division, as seen in *E. coli*, whereas during spore formation, these enzymes are facilitate morphological changes. These roles are discussed further below.

The genome of *B. subtilis* encodes five amidases belonging to the amidase_2 family, designated BlyA, CwlA, CwlH, XlyA, and XlyB, and four amidases belonging to the amidase_3 family, designated LytC (CwlB), CwlC, CwlD, and YqiI (Smith et al., 2000). Despite the presence of

catalytic activity in amidase_2 family enzymes, their biological roles of remain largely unknown (Regamey and Karamata, 1998, Kuroda et al., 1991, Nugroho et al., 1999, Longchamp et al., 1994). Enzymes of the amidase_2 family are postulated to be of viral origin, given that their expression can be driven by prophage elements (Regamey and Karamata, 1998, Kuroda et al., 1991, Nugroho et al., 1999, Longchamp et al., 1994). Enzymes of the amidase_3 family are required for sporulation, protection against high osmolarity and cell division. LytC [CwlB] was one of the first hydrolases to be identified and purified in *B. subtillis* (Rogers et al., 1984). Inactivation of CwlB resulted in increased resistance to lysis, suggesting possible involvement in the regulation of cell autolysis during sporulation (Kuroda and Sekiguchi, 1991). Rashid et al. (1995) observed that the activity of LytC [CwlB] remains constant throughout the vegetative state. LytC and the glucosaminidase, LytD are the most abundant PG hydrolases in *B. subtilis*. Blackman et al. (1998) showed that single deletion mutants lacking either *lytC* or *lytD* displayed subtle increases in cell chain length relative to the parental strain; however, the *lytC, lytD* double mutant strain displayed extensive cell chains, pointing to a synergistic interaction between the two. LytC [CwlB] is the only amidase_3 family enzyme known to be involved in *B. subtilis* cell division thus far, whereas the remaining amidase_3 enzymes are involved in maintenance of the cell wall structure sporulation and recovery from sporulation (Blackman et al., 1998, Kuroda et al., 1993, Atrih et al., 1996, Smith et al., 2000).

Sporulation is a process in which *Bacillus* species form endospores in response to unfavourable environmental conditions such as nutrient scarcity (Errington, 1993). Endospores remain dormant until conditions become favourable for growth. The beginning of sporulation is characterized by the asymmetric formation a septum at the cell pole, dividing the cell into the mother cell (the larger portion of cell) and the forespore (the smaller part which will be the future spore) (Piggot and Hilbert, 2004). Thereafter, the mother cell coats the forespore with multiple PG layers and provides all components required for spore maturation. When required, it undergoes autolysis, releasing the endospore (Meador-Parton and Popham, 2000). Endospores consists of two types of PG layers differing in structure: an inner primary PG, which will be part of the cell wall of the new cell in the vegetative state post germination; and an outer spore PG cortex, which is characterised by either a complete absence of peptide side chains (forming muramic-δ-lactam) or the exhibition of L-Ala side chains (Warth and Strominger, 1969, Warth and Strominger, 1972). Deletion of CwlC did not affect mother cell lysis, spore properties or spore germination; however, CwlC expression increased at the beginning of sporulation (Kuroda et al., 1993). Strains with a double deletion of *cwlC-lytC* and

cwlC-cwlH, and a triple deletion mutant of *cwlC-lytC-cwlH* displayed significant decrease in mother cell lysis, suggesting that this process requires the action of multiple hydrolases, with CwlC as the main enzyme (Smith and Foster, 1995).

The PG cortex of endospores is required for maintaining spore core dehydration, heat resistance, and dormancy (Popham et al., 1999). The reduced number of peptide side chains lowers the level PG cross-linking in the spore cortex allowing the flexibility required for spore core dehydration (Atrih et al., 1996, Lewis et al., 1960). The deletion of the gene encoding for CwlD leads to the absence of muramic-δ-lactam residues, suggesting that it is the amidase required for spore core dehydration (Atrih et al., 1996). However, another study revealed that the loss of *cwlD* and *dacB* genes in *B. subtilis* increased cross-linking in spore peptidoglycan (PG) with no significant effect on spore core hydration. (Popham et al., 1999). Although CwlD has no direct effect on core hydration, it is involved in maintaining the spore PG structure. The maintenance of the endospore cortex PG by CwlD results in spore resilience against heat and hydrogen peroxide stress (Gilmore *et al*., 2004). A study by Sekiguchi et al. (1995) revealed that a *cwlD* mutant was incapable of spore germination, and that germination could only be restored by adding lysozyme or SDS to the cells, showing that CwlD is required for spore germination to restore vegetative growth. While CwlD maintains spore PG, the additional amidase Yqil may be involved in maintaining PG under stress during vegetative growth as expression of Yqil was upregulated in *B. subtilis* cells cultured in media with a high salinity (1.2 M NaCl) (Steil et al., 2003).

3.1.3. Amidases is *Staphylococcus* species

Staphylococcus species, particularly *Staphylococcus aureus* and *Staphylococcus epidermis* contribute to a significant number of opportunistic infections in healthcare settings (Vermassen et al., 2019b). The *S. aureus* genome encodes four enzymes with amidase activity, namely AtlA, SleI, LytN and LytH (Kuroda et al., 2001, Götz et al., 2014, Kajimura et al., 2005, Vermassen et al., 2019a). LytH is an amidase-3 domain-containing enzyme and it is the only amidase in *S.aureus* that has mono-functional amidase hydrolase activity, whereas the other three display bifunctional hydrolase activity. AtlA possesses a single domain with glucosaminidase activity (GHF-73) and an amidase_2 domain, and both domains are functionally independent (Götz et al., 2014). SleI and LytN both possess a CHAP (cysteine, histidine-dependent amidohydrolase peptidase) domain, which is bifunctional for peptidase

and amidase activity (Kajimura et al., 2005, Frankel and Schneewind, 2012, Bateman and Rawlings, 2003). *S. epidermis* encodes a single monofunctional amidase with amidase-3 activity, (correlating to lytH in *S. aureus*) and two bifunctional hydrolases with amidase activity: one hydrolase with glucosaminidase and amidase-2 activity (AtlE), and one hydrolase with peptidase and CHAP activity, corresponding to the Slei in *S. aureus* (Vermassen et al., 2019b).

Atl is a major hydrolase in *S. aureus* (AtlA) and *S. epidermis* (AltE) (Vermassen et al., 2019b). Mutant strains with single deletions of either the amidase (Δ*atl*$_{AM}$) or the glucosaminidase (Δ*atl*$_{GL}$) domain did not affect cell growth, but had defective cell division, with Δ*atl*$_{AM}$ showing a more pronounced division defect (Bose et al., 2012). The same study also revealed that both mutant strains (Δ*atl*$_{AM}$ and Δ*atl*$_{GL}$) were incapable of forming biofilm structures. A more recent study showed that the glucosamidase domain of AtlA was able to process denuded PG, revealing that glucosaminidase activity is dependent on amidase activity for efficient cell division (Nega et al., 2020). The interaction of AtlA with vitronectin in *S. aureus*, and *S. epidermis* and the ability of AtlA to elicit protective immunity in TH1 and TH2 cells, highlights the importance of this hydrolase in virulence and immune responses (Hussain et al., 2015, Nair et al., 2015).

In *S. aureus*, the bifunctional hydrolase SleI preferentially displays amidase activity. A transposon mutagenesis screen associated the *slei* gene with cell division and this phenotype was exacerbated in a double deletion mutant lacking *slei* and *atlA*, suggesting that the two proteins are synergistic during cell division (Kajimura et al., 2005). SleI has also been shown to contribute to colonization and virulence in *S. aureus* mouse infection models as a mutant strain lacking *slei* resulted in in reduced pathogenesis (Kajimura et al., 2005). In *S. epidermis*, Slei interacts with the extracellular matrix proteins fibronectin, vitronectin and fibrinogen suggesting an additional role in colonization (Heilmann et al., 2003). Methicillin Resistant *Staphylococcus aureus* (MRSA) possess β-lactam resistance due to the acquisition of the *mecA* gene encoding PBP2a, a transpeptidase enzyme displaying poor affinity for β-lactams (Thalsø-Madsen et al., 2019). The MRSA USA300 mutant strain lacking *slei* phenocopies the mutant strain lacking *mecA,* which is characterized by an increased susceptibility to β-lactams (Thalsø-Madsen et al., 2019). Mutation of LytN results in cell growth defects and disrupts the PG cross-wall (septum) during cell division (Frankel et al., 2011). A recent study by Do et al. (2020b) showed that the deletion of *lytH* in *S. aureus* led to slowed cell growth and enlarged cells incapable of cell division. Furthermore, cells were characterised by mislocalised septa and FtsZ

proteins. These cell-division phenotypes were reversed by suppressing the PG synthase PBP2, suggesting that cell growth is regulated by LytH activity in *S.aureus* (Do et al., 2020b).

3.1.4. Mycobacterial amidases

In chapter 1, we described the published literature on mycobacterial amidases and their demonstrated roles in cell division and growth. The reader is referred to section 1.12.3 of chapter 1 for further details. Unpublished work from our lab on amidases in Msm demonstrated that Ami2 (also annotated as CwlM) localised to a single cell pole in wild type cells (Senzani, 2018, Boutte et al., 2016). This was consistent with the subsequent demonstration that this protein is important for activating PG synthesis at the cell pole, in a PknB-dependent manner. In a separate study, our laboratory deleted putative amidase-encoding genes *ami3*, *ami4* and *ami5* in Msm. Deletion of *ami3* resulted in cell division defects that were also associated with mislocalization of DivIVA, in a manner akin to that seen in an *ami1* defective mutant (Sikhosana, 2018, Senzani et al., 2017) . This mutant also displayed increased susceptibility to antibiotics and a more permeable cell wall. In contrast, deletion of the gene encoding Ami4 resulted in twisted, atypical cells, which died after the first cell division event. Mutation of Ami5 resulted in stunted growth suggesting that this enzyme is important for cell growth/elongation (Sikhosana, 2018). These observations, together with published literature outlined earlier, point to functional specialization of amidases in mycobacteria.

3.1.5. Amidases and the immune response

In the previous sections, we highlighted the role of amidases in bacterial growth and division; in response to antibiotics; and in host colonization and pathogenicity. In this section, we expand on the roles of amidases with a focus on pathogen-host interactions for several bacterial pathogens. Bacteria release muropeptides, via processing of the cell wall, for various reasons including cell signalling and PG recycling. These PG fragments can be recognised by the host immune system (Johnson et al., 2013). The innate immune system recognizes PG components via the Toll-like receptor (TLR) system, the NOD receptor system and PG recognition proteins, all of which are discussed below.

The TLR system

TLRs are transmembrane proteins found in a variety of eukaryotic and prokaryotic cells. The TLR system consists of 11 receptors, with each containing an extracellular TLR domain and an intracellular Toll/IL-1 receptor (TIR) domain (Takeda and Akira, 2005). The TLR domain consists of leucine-rich repeat (LRR) regions, which facilitate interactions with pathogen, associated molecular patterns (PAMPs) such as PG. The TLR domain facilitates pro-inflammatory signalling via the myeloid differentiation primary response protein MYD88 and TLR domain-containing adapter molecule 1 (Kieser and Kagan, 2017). TLR2 was initially shown to be the primary ligand required for PG recognition in the TRL system (Yoshimura et al., 1999, Takeuchi et al., 1999, Ozinsky et al., 2000). However, a study by Travassos et al. (2004) revealed that TLR2 primarily interacts with lipoproteins and lipoteichoic acids (LTAs) which co-purify with PG. Since then, the role of TLR2 PG recognition remains controversial as some studies support TLR2-PG recognition citing the recognition of PG fragments by TLR2 whereas opposing studies show that TLR2 recognition is poor when LTAs are absent (Dziarski and Gupta, 2005, Asong et al., 2009, Iyer et al., 2010, Volz et al., 2010). Nonetheless, recognition by TLR leads to the activation of Nuclear factor-κB (NF-κB), a component that is also activated by NOD-like PG recognition receptors.

NOD receptor system

Nucleotide-binding oligomerization domain (NOD)-like receptors (NLRs) belong to a family of intracellular receptors characterized by three motifs, namely a C-terminal leucine rich repeat (LRR) domain; a central nucleotide-binding domain (NBD domain); and a variable N-terminal effector domain (Inohara and Nuñez, 2003). The PG recognising receptors NOD1 and NOD2 belong to the NLRC family of NLRs and contain one (CARD4) and two (CARD15) N-terminal caspase recruitment domains (CARD), respectively (Keestra-Gounder and Tsolis, 2017). NOD1 recognises the γ-D-glutamyl-mDAP from Gram-negative bacteria and some Gram-positive bacteria, whereas NOD2 recognizes muramyl dipeptides (MDP) from both Gram-positive and Gram-negative bacteria (Chamaillard et al., 2003, Girardin et al., 2003a, Girardin et al., 2003b). PG recognition by NOD1 and NOD2 leads to oligomerization and interaction of these receptors with the scaffolding kinase receptor-interacting protein (RIP2) to activate NF-κB and MAPK pathways (Ogura et al., 2001, Inohara et al., 2003, Bertin et al., 1999).

The activation of NF-κB is a shared response in PG recognition by the TLR and the NOD systems. This pathway involves the activation and recruitment of TAK1/TAB complex, which results in an enhanced activity of the IκB Kinase (IKK) complex. This in turn results in phosphorylation and degradation of the inhibitor of NF-κB (IκB), (Takeda and Akira, 2005). These events allow for the release and translocation of NF-κB transcription factors to the nucleus thereby inducing the expression of proinflammatory cytokines such as TNF-α and IL-12 (Zhong et al., 2013)

PG recognition proteins

The mammalian immune system expresses four secreted soluble PG recognising enzymes (PGLYRP1–PGLYRP4) that recognize the muramyl pentapeptide or tetrapeptide. These proteins possess bactericidal activity (Wolf and Underhill, 2018). PGLYRP2 also possesses PG amidase activity that can directly hydrolyse PG bonds, suggesting that the immune system produces PGLYRP2 as a sentinel molecule that can affect bacterial viability (Wang et al., 2003). Although the immune system possesses advanced PG recognition systems, bacterial pathogens are able to evade recognition to promote proliferation, possibly via several PG-associated hydrolases. In the enteric pathogen, *Salmonella typhimurium*, a mutant strain with a defective AmpD was associated with the accumulation of muropeptides. This was postulated to trigger the production of reactive nitrogen species by murine macrophage derived J774-A. 1 cells (Folkesson et al., 2005). The same study further showed that *ampD* mutants displayed a reduced ability to invade J774-A1 cells and decreased intracellular survival (Folkesson et al., 2005). The amidase homologue in *Listeria monocytogenes* promotes the adhesion to mouse hepatocytes (Asano et al., 2012).

With respect to mycobacteria, a recent study from our group demonstrated that deletion of ami1 or ami4 from Mtb resulted in altered immune responses in bone marrow-derived macrophages (BMDM) and the C57BL/6 mice. Deletion of either of these amidases resulted in increased pro-inflammatory responses in BMDMs whilst infection of the Δ*ami1* mutant in mice led to differential induction of pro-inflammatory cytokines and certain chemokine (Kieswetter et al., 2021). This effect was only seen during acute infection. In contrast, the Δami4 mutant did not alter cytokine and chemokine responses significantly. These data confirm the notion that mycobacterial amidases are functionally specialised. Herein, we explore the role of Ami1 in Mtb growth and survival.

Hypothesis

Ami1 homologues, including amidase_3 domain containing proteins, are implicated in cell division and survival following exposure to antibiotics and virulence in various bacterial species. From these previous studies, we hypothesized that the Ami1 homologue in Mtb is required for cell division, antibiotic tolerance and intracellular survival during infection. It should be noted that during the course of our study, Healy et al. (2020) published findings which revealed that the Ami1 homologue in Mtb is dispensable for cell division *in vitro* and is required for maintaining Mtb persistence in chronic infections in mice. Thus, our hypothesis was formulated before the findings of the aforementioned study were published. In this context, we still present the work that was done to assess if the *ami1* defective mutant in Mtb had growth or division defects.

Aims and Objectives

Primary aim: To investigate the role of Ami1 in cell division and proliferation of Mtb.

Objective 1: Genetic characterization of strains, specifically:

- Genotyping of an *ami1* defective strain in Mtb, together with wild type and genetically complemented counterparts, via PCR and Southern Blotting.
- Transcriptional analysis of Mtb strains for *ami1* gene expression.

Objective 2: To determine the role of Ami1 in Mtb cell growth, PG synthesis and cell division under normal *in vitro* growth conditions, specifically:

- Monitor the growth kinetics of H37RvS, H37*Δami1S* and H37*Δami1S*::*ami1* in 7H9 growth media.
- Assess PG synthesis via fluorescence microscopy using a PG mimicking fluorogenic probe.
- Assess Mtb cell length via light microscopy.
- Assess localization of cell elongation proteins.
- Assess cell division markers.

Objective 3: To determine the role of Ami1 in Mtb cell viability under carbon limiting conditions, specifically:

- Monitor the growth kinetics of H37RvS, H37*Δami1S* and H37*Δami1S*::*ami1* in Sauton's minimal growth media with 1% glycerol as a primary carbon source and in the absence of a carbon source.

Objective 4: To determine the role of Ami1 in Mtb survival under antibiotic stress, specifically:

- Perform minimum inhibitory concentration (MIC) assays on Mtb using various antibiotics
- Monitor kill kinetics of selected antibiotics in Mtb strains.
- Monitor Ami1 expression in response to selected antibiotic stress.

Objective 5: To determine the role of Ami1 in Mtb survival during macrophage infection, specifically:

- Monitor the survival of H37RvS, H37*Δami1S* and H37*Δami1S*::*ami1* in U937 human macrophages

Space left intentionally blank

3.2. Methods

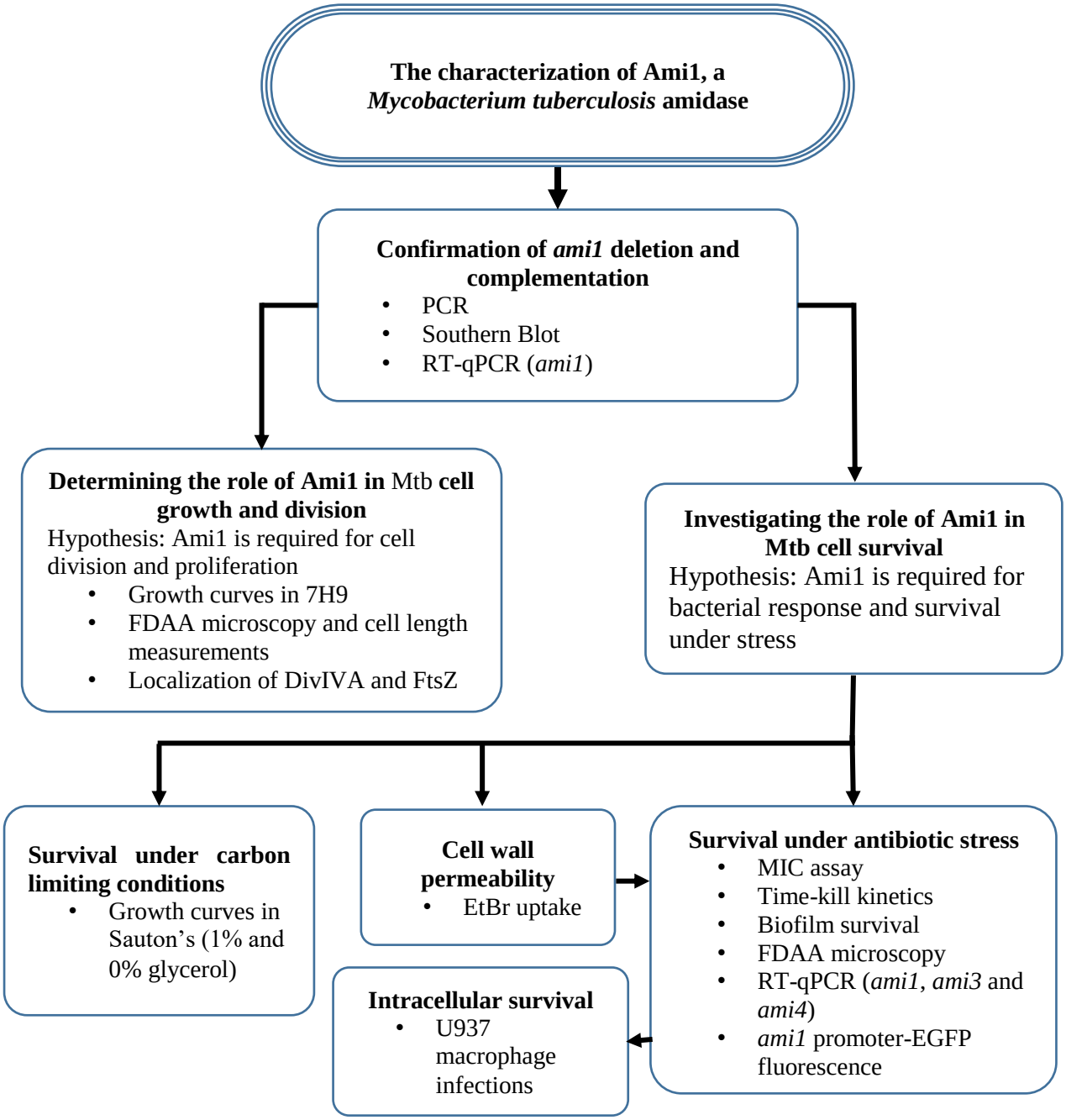


Figure 3.2. An overview of the methodology used in this study.

General methods that were used in this chapter are given in Chapter 2. Additional methods that were specific to work described herein are given in the next sections.

Table 3.2.1. Bacterial strains used in this study

Bacterial strain	Description	Reference
E. coli DH5α	*SupE44 ΔlacU169 hsdR17 recA1 endA1 gyrA96 thi-1 relA1*	Promega, Madison, WI
Mtb H37RvS	A virulent laboratory Mtb isolate ATCC 25618	CBTBR lab stock
Mtb H37*Δami1S*	An H37RvS mutant with the *ami1* gene deletion	Senzani (2018)
Mtb H37*Δami1S::ami1*	Derivative of H37*Δami1S* carrying pAmi1TB integrated at the bacterial attB phage attachment site, Hyg^R	Senzani (2018)
Mtb H37_*-5Cami1_EGFP*	Derivative of H37RvS carrying p-*5Cami1_EGFP* integrated at the bacterial attB phage attachment site, Hyg^R	This study
Mtb H37_*-5CsigA_EGFP*	Derivative of H37RvS carrying p-*5CsigA_EGFP* integrated at the bacterial attB phage attachment site, Hyg^R	This study
Msm MC^2155	High frequency transformation mutant of Msm ATCC 607	Snapper et al. (1990)

Hyg^R: Hygromycin resistance, Kan^R: Kanamycin resistance

Table 3.2.2. Standard PCR primers used in this study

Gene	Primers (5'-3')	Position	Amplicon
ami1	F: GCGCGCGCAAGCTTGCCATCTTCGTCACCTGC	382-400 bp US	1126 bp *ami1* including a 400 bp UP the *ami1* start codon and the 726 bp *ami1* gene
	R: GCCGCCGCGTTAACCTAACGCGCCTGGCCCTG	708-726 bp DS	
-*5Cami1*	F: GTGGGTACCCGGCATACCCGGCATACC	482-500 bp US	500 bp upstream of the *ami1* gene
	R: GTGACTAGTCCATGGCGAACCCGACAC	0-18 bp US	
-*5CsigA*	F: GTGGGTACCAACGGGACGTTGATACCC	500-482 bp US	500 bp upstream the *sigA* gene
	R: GTGACTAGTCCATATACACCCCTTCGG	0-18 bp US	

Restriction sites indicated in red. US: Upstream. DS:Downstream

Table 3.2.3. PCR primers for confirming pMV306 (and it variations) integration into the Mtb genome.

Forward primer (5'-3')	Reverse primer (5'-3')	Size (bp)
attBS1: ACGTGGCGGTCCCTACCG	attL2: CTTGGATCCCGCTGCGC	282
attBS2: ACAGGATTTGAACCTGCGGC	attL4: ATTTCTTGCAGACCCCTGGA	320

Please see figure 3.3.9 for the genomic position of these primers post integration.

Table 3.2.4. Plasmids used in this study

Plasmid	Description	Reference
pTweety_DivIVA_GFP	Derivative of DivIVA (plus native promoter /150 bp upstream of start codon),carrying an in-frame C-terminal rseGFP tag; Kan^R	CBTBR lab stock/ Maphatsoe (2017)
pFtsZGFP	Derivative of FtsZ (plus native promoter /150 bp upstream of start codon),carrying an in-frame C-terminal rseGFP tag; Hyg^R	CBTBR lab stock/ Maphatsoe (2017)
pEGFP	Derivative of pMV306(H) (an integrating plasmid) carrying an *EGFP* gene, Hyg^R	CBTBR lab stock
p-*5Cami1_EGFP*	Derivative of pEGFP carrying the *ami1* promoter region (500bp up stream) upstream the *EGFP* gene, Hyg^R	This study
p-*5CsigA_EGFP*	Derivative of pEGFP carrying the *sigA* promoter region (500bp up stream) upstream the *EGFP* gene, Hyg^R	This study

Hyg^R: Hygromycin resistance, Kan^R: Kanamycin resistance

Table 3.2.5. Standard RT-qPCR primers used in this study

Gene	Primers (5'-3')	Position	Amplicon (bp)
ami1	F: CGGATTCCACGTCAACTACTC	402-420 bp DS	186 bp
	R: GACGGATATTGGGCTAGGTTC	569-587 bp DS	
ami3	F: AGCTCGTACACCACGTTTCC	1030-1048 bp DS	118 bp
	R: TCTCGTCCATCACAGCGTAG	1149-1147 bp DS	
ami4	F: AGATCGTGAGCATGCGAGA	398-426 bp DS	136 bp
	R: CAGTCCATCGACAGGTTTCC	515-533 bp DS	
sigA	F: TGCAGTCGGTGCTGGACAC	1379-1397 bp DS	195 bp
	R: CGCGCAGGACCTGTGAGCGG	1555-1573 bp DS	

DS:Downstream

3.2.1. Confirmation of ami1 deletion and complementation

3.2.1.1. PCR genotyping

Genomic DNA extracted from the Mtb strains H37RvS, H37*ami1S* and H37*ami1S*::*ami1* was respectively used as the template in FastStart Taq DNA PCR (as described in Section 2.3.1.1) reactions using ami1 primers (Table 3.2.2) to amplify the 1126 bp region which includes *ami1* (726 bp) and 400 bp upstream the *ami1* start codon. The cycling conditions were as follows: Initial denaturation at 95^{o}C for 4 min; followed by 34 cycles of denaturation at 95^{o}C for 30 sec, annealing at 60^{o}C for 30 sec and elongation at 72^{o}C for 90 sec; thereafter, the final elongation at 72^{o}C for 7 min.

3.2.1.2. Southern Blot Hybridization

3.2.1.2.1. Electro-blotting

Genomic DNA (2-5 µg) of H37RvS, H37*ami1S* and H37*ami1S*::*ami1* was digested (as described in section 2.3.2) overnight and was separated on a 0.8% agarose gel with Roche marker IV (Roche) for ca. 2 hrs. An image of the digested DNA was captured using the G-Box SYNGENE system. Thereafter, the gel was incubated in depurination solution (0.2 M HCl) for 15 min at room temperature with gentle shaking. The gel was washed twice with dH_2O and then soaked in denaturation solution (0.5 M NaOH, 1.5 M NaCl) for 30 min at room temperature with gentle shaking. The gel was briefly equilibrated in 1 × TBE buffer (89 mM Tris-Borate, 2 mM EDTA, pH 8.3). The gel was over-layered with a Hybond™-N nitrocellulose membrane and thereafter, sandwiched between 4 Whitman filter papers and 2 sponges that were pre-soaked in 1 × TBE buffer and enclosed in a cassette (Bio-Rad Laboratories). The cassette was then loaded on a SB10 tank (Bio-Rad Laboratories) containing 1 × TBE. Electro-blotting was conducted at 600 mA for 2 hrs to transfer DNA to the nitrocellulose membrane. DNA was crosslinked to the membrane via UV irradiation at 2000 mJ/cm^2 with the UV Stratalinker 1800 (Stratagene). The membrane was stored in 1 × maleic acid buffer before further use.

3.2.1.2.2. DNA Probe Synthesis

The PCR DIG Probe Synthesis kit (Roche Applied Science) was used to synthesize Alkali-labile digoxigenin (DIG)-dUTP *ami1* probe as per manufacturer's instructions. This was achieved by performing two 50 µl Fast start Taq (section 2.3.1.1.) PCR reactions (labelled and unlabelled) were prepared as follows: 1 × PCR buffer with 2 mM $MgCl_2$, 1 × GC rich buffer, 0.2mM dNTPs (for the unlabelled reaction)/ 0.1 mM dNTPs (supplemented with 1 × PCR DIG

labelling mix for the labelled reaction); 1 µM of *ami1* forward and reverse primers (Table 3.2.2), ~100 ng H37RvS DNA template, 2.5 U FastStart Taq DNA polymerase and dH_2O. Reaction conditions used are mentioned in section 2.3.1.1. DIG labelling was confirmed by running labelled and unlabelled PCR products on a 1% agarose gel. For a successful labelling, the DIG labelled amplicon was expected to be slightly larger in molecular weight relative to the unlabelled product.

3.2.1.2.3. Hybridization and Immunological detection

The hybridization of the *ami1* DIG labelled probe to DNA cross-linked nitrocellulose membrane was performed using the DNA High Prime DNA labelling and Detection Starter kit II (Roche Applied Sciences) as per manufacturer's instructions. Briefly, the DNA cross-linked nitrocellulose membrane was soaked in 12 ml DIG Easy Hybridization solution for 30 min at 42°C. The *ami1* DIG labelled probe was denatured by boiling at 95°C for 10 min immediately followed by cooling on ice. Thereafter, the probe was added to the membrane containing DIG Easy Hybridization solution at a concentration of 2 µl/ml. Hybridization was carried out overnight at a probe specific temperature. The mixture containing the DIG Easy Hybridization solution and probe was transferred into a 50 ml Falcon tube and stored at -20 ºC for future use. Thereafter, the membrane was washed twice in Solution I (2 × SSC (300 mM NaCl, 30 mM Sodium citrate); 0.1 % SDS) for 5 min at room temperature with gentle shaking. The membrane was also washed twice with solution II (0.5 × SSC; 0.1 % SDS) for 15 min per wash at 68 ºC. It was then placed in wash buffer (0.1 M maleic acid buffer; 0.3 % Tween 20) for 5 min at room temperature, followed by incubation in 1 × blocking solution (comprising of a 1 in10 dilution of 10 × blocking solution (Roche Applied Sciences) in 0.1 M maleic acid buffer) for 30 min at room temperature with gentle shaking. The membrane was incubated in antibody blocking solution (2 µl Anti-Digoxigenin-AP (Roche Applied Sciences) in 20 ml 1 × blocking solution and) for 30 min at room temperature, followed by two washes in wash buffer for 15 min at room temperature with shaking. The membrane was then equilibrated in detection buffer (0.1 M Tris-HCl, 0.1 M NaCl in dH2O; pH 9.5) for 5 min at room temperature with gentle shaking. Thereafter, the membrane was transferred to a hybridization bag (Roche Applied Science) with the DNA side facing up and 1 ml chloro-5-substituted adamantyl- 1, 2-dioxetane phosphate (CSPD) substrate was added and evenly applied on the DNA containing side of the membrane. Excess CSPD was removed and the membrane incubated for 10 min in the dark at room temperature. The hybridization bag was the sealed and incubated at 37ºC for 10 min in the dark. Thereafter, the membrane was then exposed to X-ray film (Thermo Scientific) at least

2 hrs and X-ray films were manually developed through incubation in developing solution (30 sec), rinsing in dH_2O (30 sec) and fixing solution (30 sec), followed by rinsing in dH_2O for 30 sec. The film was hung to dry to develop the image.

3.2.1.3. RT-qPCR for monitoring Ami1 expression

H37RvS, H37*ami1S* and H37*ami1S*::*ami1* cultures were grown to OD600nm 0.6 at 37^{o}C in 25 ml of 7H9 media, and where necessary, supplemented with appropriate antibiotics. These cultures were used to monitor the transcription of *ami1* in each strain as outlined in section 2.5. The housekeeping gene, *sigA* was used as a reference for constitutive expression. RT-qPCR primers for *ami1* and *sigA* are outlined in table 3.2.5.

3.2.2. Determining the role of Ami1 in Mtb cell growth and division

3.2.2.1. Growth Rate Analysis

H37RvS, H37*ami1S* and H37*ami1S*::*ami1* cultures were grown to OD600nm 0.6-0.8 at 37^{o}C in 5 ml of 7H9 media, and where necessary, supplemented with appropriate antibiotics. Pre-cultures were then diluted to OD600nm of 0.05 in 50 ml of 7H9, containing the appropriate antibiotics. Thereafter, the cultures were incubated at 37^{o}C and the growth rates were assessed daily (for 14-15 days) by recording OD600nm readings and plating 10-fold dilutions of culture on 7H11 agar plates for CFU/ml determination. Plates were incubated at 37°C for 3-6 weeks and scored.

3.2.2.1. Microscopy

3.2.2.1.1. Tetramethylrhodamine-3-amino-d-alanine (TADA) fluorescence Microscopy

TADA was used to stain for spatial localization of new PG synthesis. Samples were prepared by adding 0.1 mM of TADA to 2 ml of H37RvS, H37*ami1S* and H37*ami1S*::*ami1* grown to the log phase (OD600nm of 0.6-0.8) in 7H9 (containing the appropriate antibiotic) and left for 3 hrs at 37^{o}C. Cells were collected by centrifugation at 12 470 × g for 5 min and the supernatant was discarded. The cells were subjected to three washes with 500 µl of 0.01 M Phosphate buffer saline (PBS) and re-suspended in 2.5% glutaraldehyde overnight at 4^{o}C. The cells were collected as mentioned before and re-suspended in 50 µl 0.01 M PBS. Thereafter, 10 µl of the cells was spotted on 2% flattened agarose pads on glass slides and viewed under a fluorescence microscope (Nikon). With the exception of TADA staining, sample preparation performed in the same manner for all microscopy in this thesis.

3.2.2.1.2. Measuring cell length and fluorescence intensity

Cell lengths were measured using the Nikon Elements Software, and three hundred (N=300) cells were counted for each strain. In order to measure fluorescence intensity, microscopic images were converted into .TIFF format images (to preserve original optical data) using the Nikon Elements Software. Subsequently, fluorescence intensity along the length of each cell was analysed using the ImageJ (Fiji) software. The intensity analysis function (ctrl+k) was used to obtain plot co-ordinates of fluorescence intensity across the drawn line (y) with respect to pixel length of the line (x). The x and y plot coordinates were transferred to Excel whereby, pixel length was normalised to a % of cell length and average fluorescence intensity of the cells were calculated. The fluorescence intensity of 300 cells for each strain was analysed. Thereafter, the data was plotted in Graphpad Prism, using the locally weighted scatterplot smoothing (LOWESS) function to plot the average fluorescence of 300 cells for each strain.

3.2.3. Assessing H37*Δami1S* Survival under carbohydrate limiting conditions

3.2.3.1. Carbohydrate starvation assay

H37RvS, H37*Δami1S* and H37*Δami1S*::*ami1*were grown to an OD600nm of 0.6 at 37ºC in 7H9 in 5 ml flasks and cells were harvested by centrifugation at 4000 x g for 8 min. Cells were subjected to two washes with 10 ml of PBS and pelleted after the final wash. Thereafter, the bacterial pellets were resuspended 5 ml of respective Sauton's minimal media (0.05% potassium phosphate monobasic, 0.0001% zinc sulfate, 0.05% ammonium sulfate, 0.05% magnesium sulfate heptahydrate, 0.2% citric acid, 0.005% ferric ammonium citrate, 0.02% tyloxapol) with either 6% glycerol or 0% glycerol at 37 °C. Pre-cultures were then diluted to OD600nm of 0.05 in 50 ml of the respective Sauton's media. Growth rates were assessed daily by recording OD600nm readings and plating 10-fold dilutions of culture on 7H11 agar plates for CFU/ml determination. Plates were incubated at 37°C for 3-6 weeks and scored.

3.2.4. Monitoring the effect of *ami1* deletion on Mtb cell wall permeability

3.2.4.1. Ethidium bromide (EtBr) diffusion assay

H37RvS, H37*Δami1S* and H37*Δami1S*::*ami1* were grown to an OD600nm of 0.8, in a volume of 25 ml in 50 ml flasks. The cells were harvested at 4 000 x g, washed twice in 10 ml of PBS and resuspended in PBS containing 0.4 % glucose. The OD600nm of the cells was adjusted to

0.4 and 95 µl of the samples were transferred to flat, clear-bottom, black 96-well plates (Greiner Bio). EtBr was added to a final concentration of 8 µg/ml to cells in a final volume of 100 µl. EtBr fluorescence emission was measured at Ex530nm; Em585nm, with a Spectra Max Gemini EM microplate reader (Molecular Devices) at 60 sec intervals for 60 min.

3.2.5. Survival under antibiotic stress

3.2.5.1. Antibiotic stress assays

3.2.5.1.1. Minimum Inhibitory Concentration (MIC) assay

The minimum concentration of antibiotics required to inhibit the growth of Mtb strains was determined using the MIC assay. H37RvS, H37*Δami1S* and H37*Δami1S*::*ami1* cultures were grown to an OD600nm of 0.3 at 37ºC, followed by a 100-fold dilution in fresh 7H9 media. Thereafter, cells were transferred to round bottom 96-well plates (Thermo Scientific) in 50 µl aliquots and arranged such that each individual MIC experiment spanned over 24 wells. For each experiment, the first well consisted of 100 µl of the antibiotic in question; which was the serially diluted in a 2-fold manner from well 1 through to 24 across 2 rows (in each plate, whereby a single row consists of 12 wells). The final volume of 50 µl was removed after the dilution in well 24. The plates were sealed and incubated for 7 days at 37 ˚C after which, the MIC of the particular antibiotic was determined by observing growth.

3.2.5.1.2. Antibiotic time-kill assays in Mtb

Time-kill assays were performed to observe antibiotic kill-kinetics on Mtb growth. H37RvS, H37*Δami1S* and H37*Δami1S*::*ami1* cultures were grown at 37ºC to an OD600nm of 0.6, in a final volume of 50 ml 7H9 media. The desired antibiotic was added at a concentration that is 100x ≥ the MIC, as determined above, and the sample was gently mixed by swirling the flask and incubated at 37ºC. Bacterial survival was assessed by plating 10-fold dilutions of culture on 7H11 agar plates for CFU/ml determination. Sampling for assessing survival was assessed daily for 7 days. Plates were incubated at 37°C for 3-6 weeks and scored. In certain cases, samples were extracted at days 0 (prior antibiotic addition), 1, 2 and 7 post antibiotic addition for assessing gene expression (as outlined in section 2.5).

3.2.5.2. Biofilm response to INH and RIF stress

H37RvS, H37*Δami1S* and H37*Δami1S*::*ami1* were grown to an OD600nm of 1 in 7H9 media and harvested at 4000 × g for 10 min. The cells were resuspended with an equal volume of Sauton's minimal media (0.05% potassium phosphate monobasic, 0.0001% zinc sulfate, 0.05% ammonium sulfate, 0.05% magnesium sulfate heptahydrate, 0.2% citric acid, 0.005% ferric ammonium citrate, 0.02% tyloxapol and 6% glycerol). Separately, 2 ml aliquots of fresh Sauton's media were added to each well of a 24 well plate (Thermo-Fischer). Thereafter, 20 µl aliquots of the Mtb strain were added to the plates. The plates were sealed with parafilm and incubated at 37°C for 8 weeks. For antibiotic survival assays, 32 µl/ml isoniazid and 0.25 µl/ml were added to the wells without disturbing the biofilms incubated at 37°C. Survival was monitored at 2-4 days post drug exposure by disrupting the biofilms with the addition of Tween-80 at a final concentration of 0.1% to remove cell clumps. Cells were harvested and resuspended in 1 × PBS before serial dilutions were performed for plating on 7H11 for CFU/ml determination.

Quantification of biofilm formation was done using crystal violet staining. After biofilm structures had formed, 1 ml of a 0.1% crystal violet solution (prefiltered through a 0.2-m filter) was added to each biofilm well and incubated at room temperature for 10 min. Planktonic bacteria and liquid media were removed by pipetting, while keeping the pellicle intact. The wells were allowed to dry at room temperature for 15 min. Thereafter, 1 ml of 95% ethanol was subsequently added, mixed by pipetting, and left to incubate at room temperature for 15 min. The contents of each well were briefly mixed and then diluted 100-fold in 95% ethanol before measuring the absorbance at 600 nm (Spekol 1500; Analytik Jena).

3.2.5.3. TADA fluorescence Microscopy for Mtb strains exposed to INH

H37*Δami1S* and H37*Δami1S*::*ami1* cultures were grown at 37ºC to an OD600nm of 0.6, in a final volume of 5 ml 7H9 media. The cultures were exposed 32 µl/ml isoniazid overnight at 37ºC. The cells were pelleted at 12 470 × g for 5 min and resuspended in 2 ml of 7H9 media containing 32 µl/ml isoniazid. Thereafter, TADA fluorescence microscopy and cell length analyses were performed as outlined in section 3.2.2.1.

3.2.5.4. RT-qPCR for monitoring ami1, ami3 and ami4 expression post INH exposure

Antibiotic time-kill assay with INH were performed on H37RvS, H37*ami1S* and H37*ami1S*::*ami1* cultures as outlined in section 3.2.5.1.2 and RNA samples were collected at

days, 0, 1, 2 and 7 post INH exposure. These samples were used to monitor the transcription of *ami1*, *ami3* and *ami4* in each strain as outlined in section 2.5. The housekeeping gene, *sigA* was used as a reference for constitutive expression. RT-qPCR primers for *ami1*, *ami3*, *ami4* and *sigA* are outlined in table 3.2.5.

3.2.5.5. Validation of *ami1* expression via EGFP fluorescence driven by *ami1* promoter

To validate the expression of *ami1*, the promoter regions of *ami1* and *sigA* (500 bp upstream the transcriptional start site) were cloned upstream the gene coding the green fluorescent protein, EGFP in a pMV306H plasmid. The *-5Cami1 and -5CsigA* primers (Table 3.2.2) were used to amplify the 500 bp upstream region of each respective gene via the NEB Q5 High-Fidelity DNA PCR as outlined in section 2.3.1.2. The cycling conditions were as follows: Initial denaturation at 98ºC for 30 sec; followed by 34 cycles of denaturation at 98ºC for 10 sec, annealing at 60ºC for 30 sec and elongation at 72ºC for 30 sec; thereafter, the final elongation at 72ºC for 2 min. Thereafter, *-5Cami1 and -5CsigA* were cloned into pEGFP as outlined in Section 2.3 to yield p-*5Cami1_EGFP* and p-*5CsigA_EGFP* respectively. These constructs were electroporated into H37RvS, as outlined in section 2.4.2, to produce the Mtb strains, H37_-*5Cami1_EGFP* and H37_-*5CsigA_EGFP*. Thereafter, H37_-*5Cami1_EGFP* and H37_-*5CsigA_EGFP* were grown to an OD600nm of 0.6 in 7H9 media supplemented with hygromycin (50 µg/ml). The strains were divided into two sets; one set was exposed to 32 µl/ml isoniazid whereas, the other set served as a non-exposed control. The strains were incubated overnight at 37ºC. Thereafter, the strains were washed in three times in 1 × PBS before being resuspended in 1 × PBS with 0.4% glucose. The OD600nm adjusted to 0.4 and 100 µl of the samples were transferred to flat, clear-bottom, black 96-well plates (Greiner Bio). EGFP fluorescence emission was measured at Ex488nm; Em509nm, with a Spectra Max Gemini EM microplate reader (Molecular Devices).

3.2.6. Transposon mutagenesis for identifying genes that are conditionally essential with *ami1* under isoniazid stress

Transposon mutagenesis was attempted to identify genes conditionally essential with *ami1* under isoniazid stress and was carried out as outlined by Siegrist and Rubin (2009) and Griffin et al. (2011). The method makes use of the ΦMycoMarT7 phage to introduce transposons into the Mtb genome.

3.2.6.1. Phage Stock Preparation and titering

Top agar was prepared by dissolving 0.6 g LA and 0.3 g 7H9 powders in 100 ml of dH_2O and autoclaving; following this, $CaCl_2$ was added to a final concentration of 2 mM, the media was left to cool to 42ºC. An Msm culture was grown in 7H9 at 37ºC to the stationary phase (OD600nm ≥ 1) with shaking at 100 rpm and 500 µl of the cells transferred to a 1.5 ml Eppendorf tube. The cells were harvested by centrifugation for 1 min at 13 000 rpm. The pellet was washed twice with an equal volume of MP buffer (50 mM Tris-HCl, pH 7.5; 150 mM NaCl; 10 mM $MgSO_4$, 2 mM $CaCl_2$), followed by re-suspension in 500 µl of MP buffer. A 5 µl aliquot of the ΦMycoMarT7 mycobacteriophage was added to 45 µl of MP buffer to create a 10-fold dilution of the phage stock. This was then serially diluted up to 10^{-9}. The washed cells were added to the phage dilutions up to a volume of 100 µl. Thereafter, the phage-bacteria mixtures were incubated at 37ºC for 30 min to allow transduction. Subsequently, the samples were added to 3.5 ml of cooled top agar (ca. 42ºC), and poured onto 7H10 plates, followed by incubation at 30ºC for 48 hours to induce plaque formation. To extract the phage, 3 ml MP buffer was added to plates and gently agitated at 4ºC for 4 hours and the suspension was collected, sterilised (with the aid of a syringe with a 0.2-mm filter), and stored at 4ºC. To increase the phage titer stocks, the aforementioned process was repeated and optimized until the phage titer was greater than 5×10^{10} phage/ ml.

3.2.6.2. Bacterial transduction and transposon library construction

M. tuberculosis cultures were grown in 50 ml 7H9 media to an OD_{600nm} of 0.8 and cells were harvested at 3900 × g for 10 min and washed with 50 ml MP buffer. After washing, cells were re-suspended in 5 ml MP buffer, and a 200 ml aliquot was removed to serve as a control (no phage). Subsequently, ca. 1×10^{11} phage was added and incubated for 3 hours at 37ºC. The transduced cells were frozen into 200 µl aliquots of 10% glycerol at –80ºC. Samples were thawed and 10-fold dilutions were prepared in media and plated on 7H10 agar plates, which were incubated at 37ºC for 3 to 4 weeks. Emerging colonies were enumerated to determine transduction efficiency and library coverage.

3.2.7. Assessing the role of Ami in Mtb intracellular survival

3.2.7.1. Culturing of U937 human macrophage (U937 Mϕ) cells

A single 1 ml frozen stock of U937 monocyte cells was thawed at 37ºC and inoculated in 20 ml of Roswell Park Memorial Institute (RPMI) 1640 media, supplemented with 10 % Fetal Bovine Serum (FBS). The cells were incubated for 48-72 hrs and harvested through centrifugation at 200 × g for 5 min. Thereafter, cells were gently resuspended in 5 ml fresh media and inoculated into 45 ml of fresh RPMI in a 50 ml cell culture flask and incubated at 37 ˚C in 5 % CO2 for 48 hrs. Thereafter, the macrophage population was assessed using an inverted microscope and a cell counter (Countess 3, Invitrogen). Cell counting entailed adding a 2 µl aliquot of the cell suspension into 98 µl of 0.4 % trypan blue solution, and spotting a 10 µl aliquot of this solution on a haemocytometer, which was subsequently analysed in the cell counter, whereby unstained cells represented viable cells. The desired concentration of viable cells was $\geq 1 \times 10^6$ cells/ml, which was achievable after 48 hrs of incubation. However, if the desired concentration was not achieved, the media was replaced with fresh RPMI for further cell growth. Media replacement involved centrifugation at 200 × g for 5 min, discarding the supernatant, gently resuspending cells in 5 ml fresh media and inoculating into 45 ml of fresh RPMI in a 50 ml cell culture flask and incubating at 37 ˚C.

3.2.7.2. Preparing plates for infections

Once the U937 monocyte cell population reached a concentration of $\geq 1 \times 10^6$ cells/ml, the growth medium was then replaced as outlined in section 3.2.7.1 however, in this instance, 100 nM of phorbol myristate acetate (PMA) was added to the growth medium to induce cell differentiation into macrophages and cell surface attachment. The cell suspension was adjusted to ca.1 x10^6 cells/ml using RPMI containing PMA The cell suspensions were transferred to 12 well plates at volumes of 1 ml per well and incubated at 37ºC until the cells were differentiated into U937 Mϕ and the well cell surface was confluent (48 hrs). At this point, U937 Mϕ were used directly for Mtb infections. Alternatively, U937 Mϕ were activated by replacing the growth media with RPMI containing 150 U of IFN-γ through gentle pipetting. This was followed by an overnight incubation at 37ºC prior Mtb infections.

3.2.7.3. Infection of U937 Mϕ with Mtb

H37RvS, H37*Δami1S* and H37*Δami1S*::*ami1* cultures were grown to an OD600nm of 0.5 (ca. 5×10^8 CFU/ml) and the bacterial cells were adjusted to 10 x 10^6 CFU/ml using fresh RPMI media and stored at room temperature. The RPMI media was removed from the 12 well plates containing confluent U937 Mϕ (ca. 1×10^6 cells/ml), and was replaced with RPMI containing 1×10^7 CFU/ml Mtb. Each Mtb strain was infected in triplicate and the uninfected controls were prepared in triplicate (In a 12-well plate, 3 wells were respectively assigned to H37RvS, H37*Δami1S*, H37*Δami1S*::*ami1* and the uninfected control). This was followed by an incubation at 37ºC for 4 hrs to allow for bacterial phagocytosis. Subsequently, the media was discarded and the cells were washed twice in PBS. This was followed by the addition of 2 ml fresh macrophage media to each well and an incubation at 37ºC. There were four 12-well plates and each plate was assigned a single time point (4, 24, 48 and 168 hrs respectively). A single plate was sacrificed per time point for use in determining bacterial survival and alternatively for macrophage RNA extraction. Experiments were conducted in triplicate.

3.2.7.4. Assessing bacterial survival via CFU enumeration

The 12-well plates with infected macrophages where washed twice with PBS and lysed with 0.1 % SDS in PBS. Serial dilutions of the lysates were conducted from 10^{-2} to 10^{-5} in 7H9 and were plated on 7H11 media. The 7H11 plates were incubated at 37ºC for 4-5 weeks before the plates were scored. The same was applied to the uninfected controls to ensure that macrophages were not contaminated.

3.3. Results

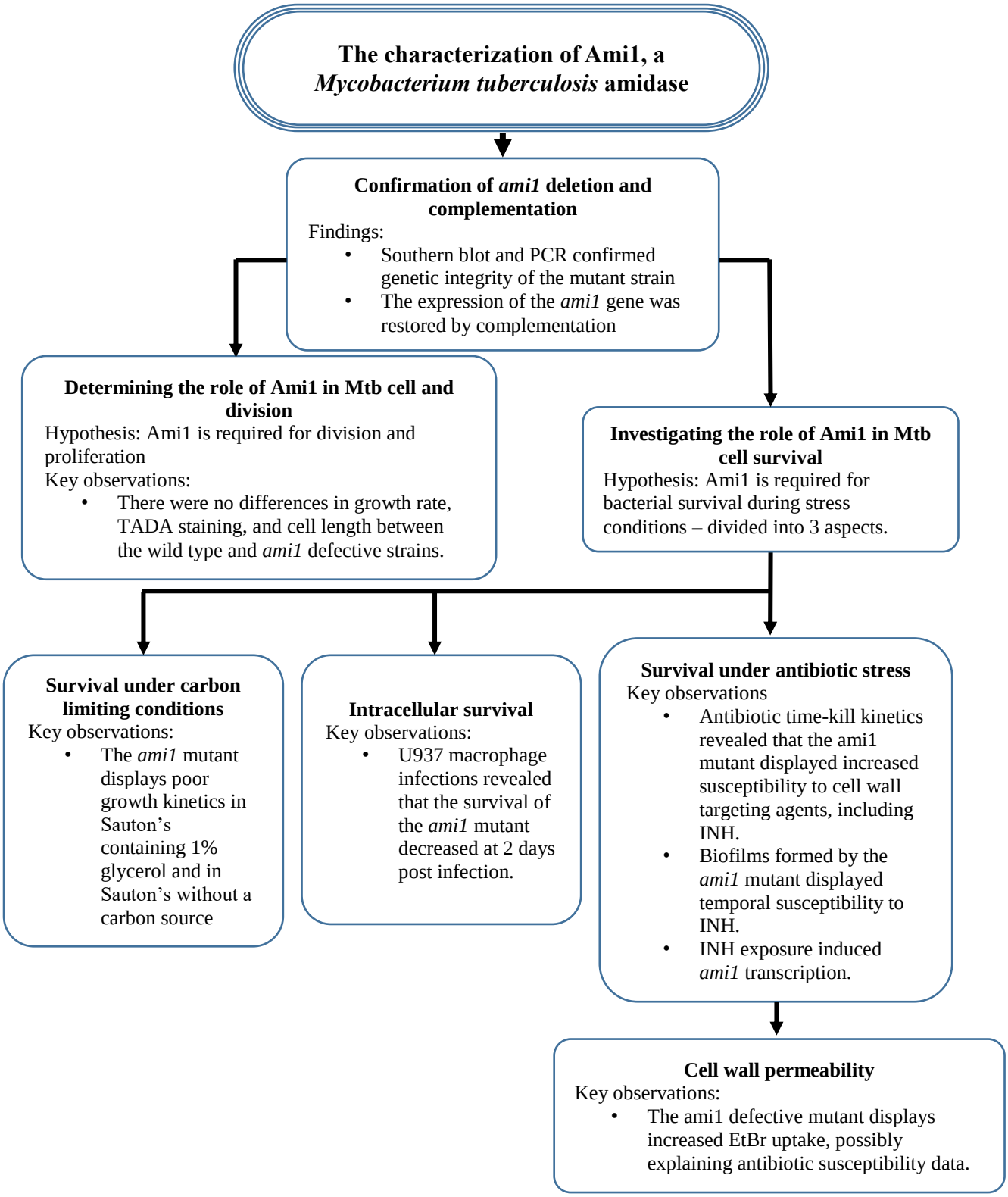
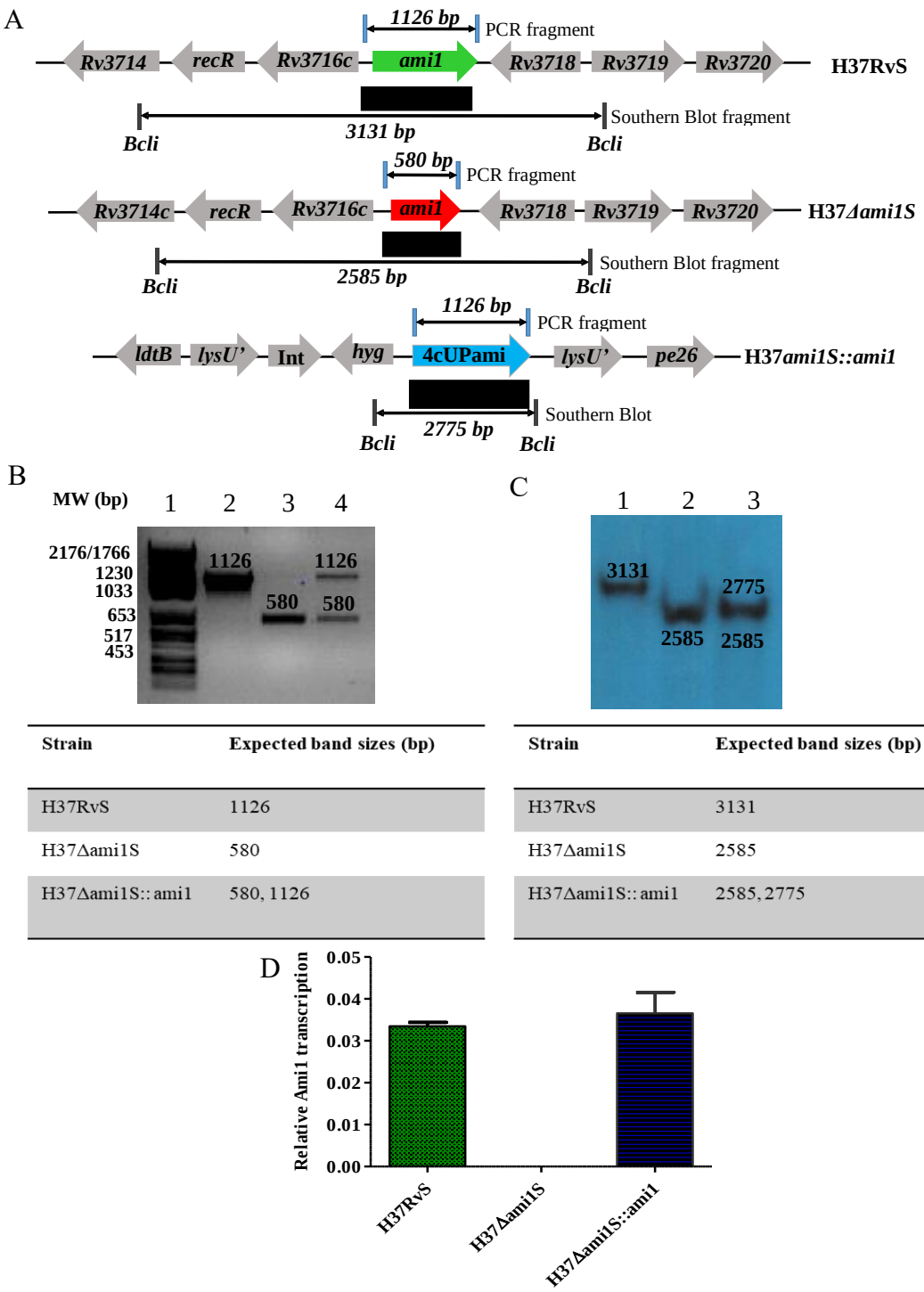


Figure 3.3. An overview of the findings of this study.

3.3.1. Confirmation of *ami1* gene deletion in the mutant strain H37*Δami1S*

The Mtb strains used in this study, H37RvS (wild type), H37*Δami1S* (ami1 deletion mutant), and H37*Δami1S*::*ami1* (genetically complemented derivative, Table 3.2.1) were provided by Dr Sibusiso Senzani, as part of his PhD work at the Centre of Excellence for Biomedical TB Research (CBTBR) (Senzani, 2018). Before further investigations of the role of Ami1 in Mtb, the strains were confirmed by genotyping and transcriptional phenotyping via PCR, Southern blotting, and qPCR (Figure 3.3.1). These data confirmed that the H37*Δami1S* mutant strain contains an *ami1* gene deletion and that H37*Δami1S*::*ami1* was indeed complemented with the *ami1* gene (Figure 3.3.1 B and C). However, it was noted that the expected bands for H37*Δami1S*::*ami1* were close in size to give distinct band and thus, strains were also confirmed by qPCR. Transcriptional profiling confirmed expression of the *ami1* gene in the genetically complemented and wild type strains (Figure 3.3.1 D). These strains, together with the H37RvS wild-type strain, were used in downstream phenotypic experiments to determine the biological function of Ami1.

Space left intentionally blank



Strain	Expected band sizes (bp)
H37RvS	1126
H37Δami1S	580
H37Δami1S:: ami1	580, 1126

Strain	Expected band sizes (bp)
H37RvS	3131
H37Δami1S	2585
H37Δami1S:: ami1	2585, 2775

Figure 3.3.1. Genotyping and *ami1* transcriptional analysis in H37RvS, H37*Δami1S*, and H37*Δami1S*::*ami1*. (A) Schematic diagram representing genomic probe sites for PCR and Southern blot genotyping. The solid black box represents the Southern blot probe (B) PCR genotyping of Mtb strains [Lane 1: DNA molecular marker VI, Lane 2: H37RvS, Lane 3: H37*Δami1S*, Lane 4: H37*Δami1S*::*ami1*]. The 1126 bp product represents the full-length *ami1* gene whereas the 580 bp product represents the deletion *ami1* allele in the knockout strain. (C) Southern blot genotyping of Mtb strains. H37RvS (Lane 1), H37*Δami1S* (Lane 2) and H37*Δami1S*::*ami1* (Lane 3) using the restriction enzyme *BclI*. The observed fragments correspond with the expected band sizes. D) RT-qPCR

displaying transcription of *ami1*. The absence of *ami1* transcription in H37*Δami1S* confirms *ami1* gene deletion; and restoration of transcription in H37*Δami1S*::*ami1* confirms successful *ami1* complementation.

3.3.2. Deletion of *ami1* has no effect on *in vitro* cell growth, elongation, and division in nutrient rich media

The effect of *ami1* deletion on cell growth was assessed by monitoring the growth kinetics of H37RvS, H37*Δami1S*, and H37*Δami1S*::*ami1 in vitro* in 7H9 growth media. There were no significant differences in growth kinetics between the Mtb strains, as assessed by absorbance (OD600nm) readings (Figure 3.3.2 A) and log CFU/ml (Figure 3.3.2 B). As mycobacterial species grow and elongate by incorporating PG at the cell poles, the effect of *ami1* deletion on cell elongation was determined by monitoring PG incorporation in via fluorescence microscopy using the fluorogenic probe, TADA. This is a fluorogenic monopeptide probe that mimics the D-ala residue and is incorporated into the PG via PG crosslinking (Figure 3.3.3 A and B). Mycobacterial cells extend by incorporating nascent PG at the cell poles. Thus in this context, TADA can be used to report on cell extension by assessing PG incorporation at cell poles. To assess spatial incorporation of PG in the *ami1* mutant, we stained cells with TADA and monitored probe fluorescence using microscopy. There were no significant differences in TADA incorporation between H37RvS, *H37Δami1S*, and *H37Δami1S*::*ami1* as all the strains incorporated the fluorogenic probe at the cell poles (Figure 3.3.4 A). We further assessed staining patterns by plotting fluorescence intensity across the lateral axis of the cell and noted cell staining at the poles at equivalent levels between wild type and mutant strains (Figure 3.3.4 B). Based on the cell division defects noted in the Ami1 mutant in Msm (Senzani et al., 2017), we hypothesized that the ami1 mutant in Mtb may have septation abnormalities, leading to longer cells/cell chains. To assess this, cell length measurements of 300 cells per strain was conducted via phase contrast microscopy. There were no notable differences observed in cell length between H37RvS, *H37Δami1S*, and *H37Δami1S*::*ami1* (Figure 3.3.4 C).

Deletion of *ami1* in Msm resulted in ectopic localization of the cell elongation apparatus, particularly DivIVA, a tropomyosin-like protein that localizes to negative curvature of mycobacterial cells and binds enzymes required for biosynthesis of different polymers in the cell wall, including PG (Meniche et al., 2014). In addition, in the inability to degrade the septum disrupted the kinetics of FtsZ ring formation. FtsZ, an actin like protein in bacteria is central to septum formation and degradation (Chauhan et al., 2006). Based on these findings, we next

sought to investigate if these two key mediators of cell elongation and division localized correctly in the *ami1* Mtb mutant.

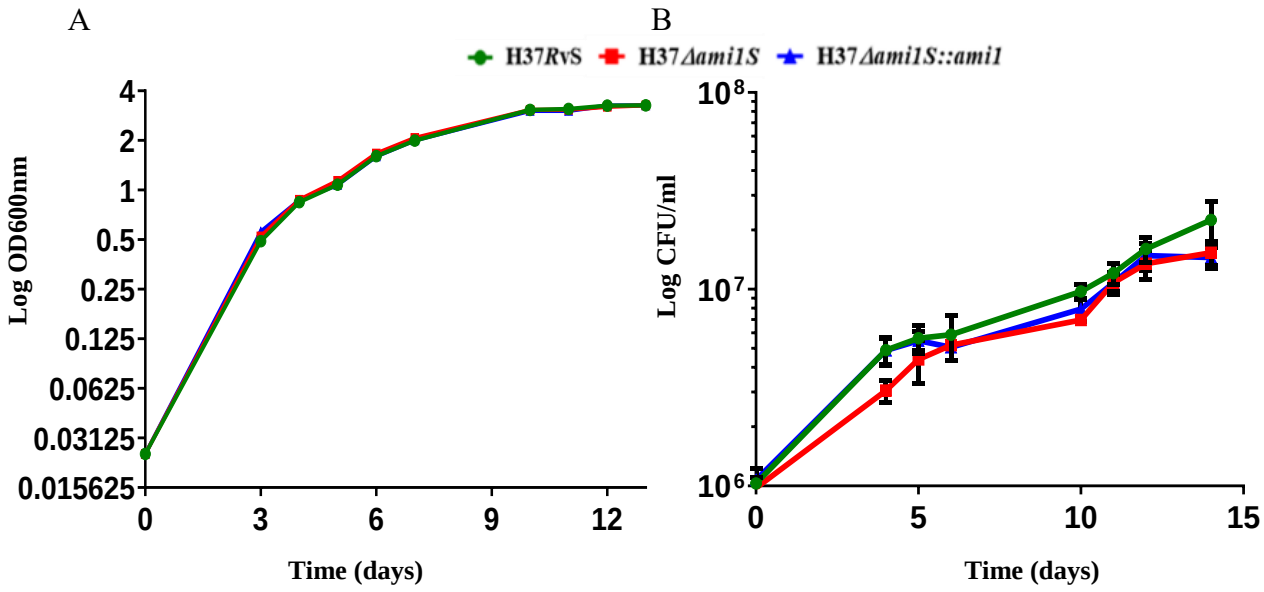


Figure 3.3.2. Growth kinetics of Mtb strains. H37RvS, H37Δami1S and H37Δ*ami1S*::*ami1* cultured in 7H9 media at 37 ˚C, assessed over 7 days. (A) Mtb growth kinetics as a function of Absorbance (OD600nm). (B) Mtb growth kinetics as a function of log CFU/ml. Error bars represent the standard error of the mean (SEM) for three biological replicates. There were no differences in growth kinetics across the three Mtb strains.

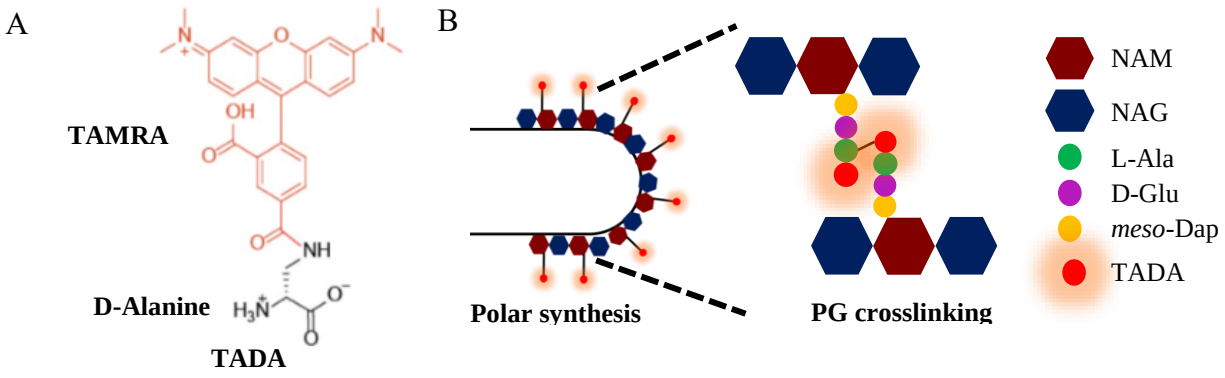


Figure 3.3.3. Schematic diagrams showing the PG incorporation mechanism of fluorescent D-ala analogue TADA. (A) The structure of the TADA fluorescent PG probe. (B) TADA is incorporated in mycobacterial cells during growth; it is crosslinked into the fourth position of the PG peptide LD-Transpeptidases.

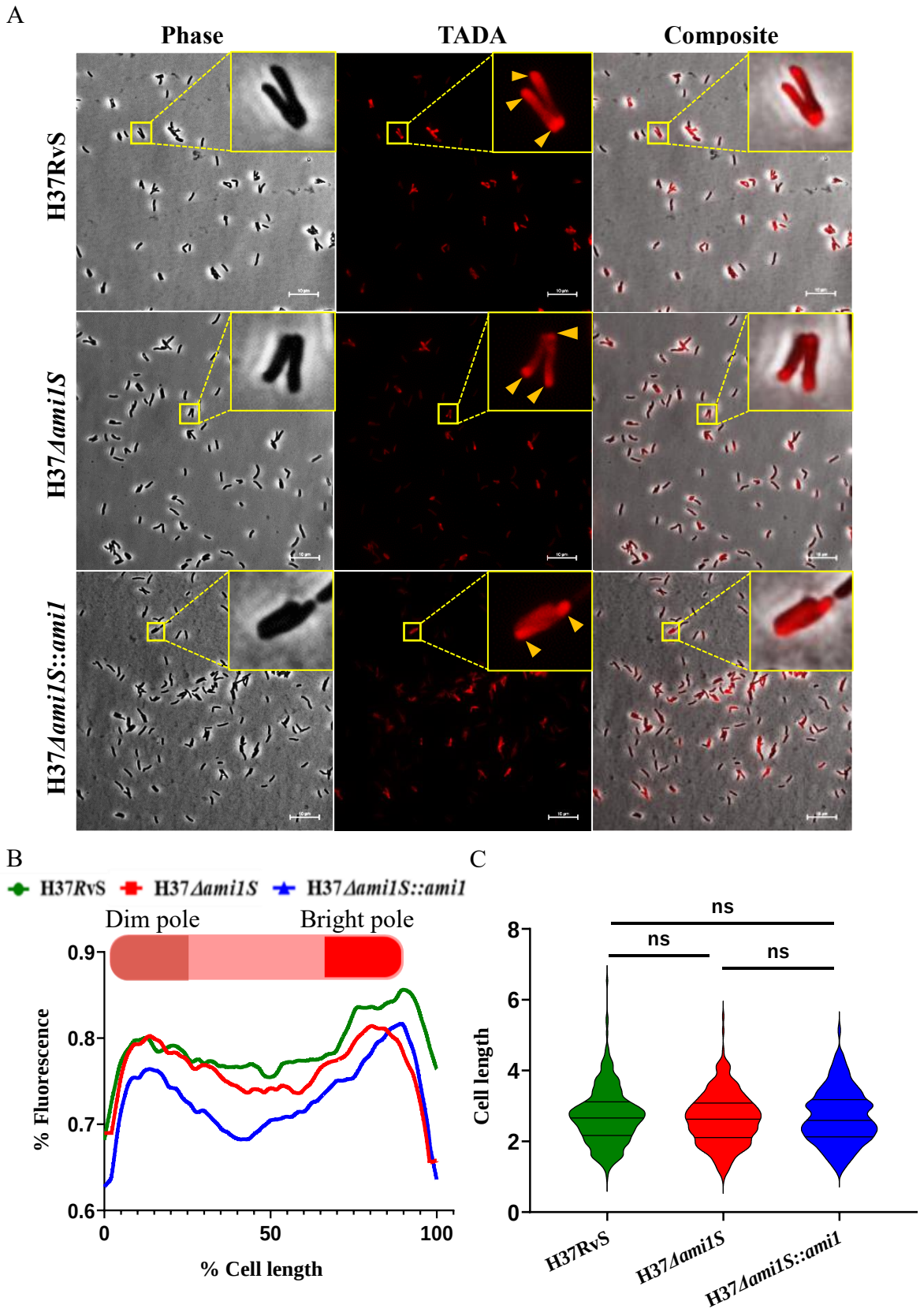
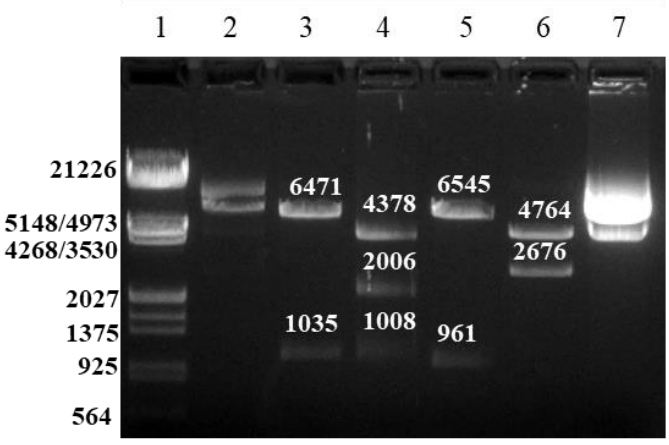


Figure 3.3.4. Assessment of TADA staining and cell lengths of *Mtb* strains. H37RvS, H37*Δami1S* and H37*Δami1S*::*ami1* were grown in 7H9 media and stained with TADA. A) Fluorescent images depicting TADA at

cell poles (yellow arrow). B) Line graph showing the TADA staining pattern across the lateral axis of the cell. C) Measurement of cell lengths in strains. At least 300 cells (N=300) were counted per strain. Scale bar 10 µM. Statistical analysis for cell lengths was conducted using the Student's t-test. ns; Not significant.

The mycobacterial integrating plasmids, pTweety_DivIVA_GFP and pFtsZGFP, were initially constructed by Ms Masethabela Maphatsoe as part of her MSc project and form part of the lab stock (Maphatsoe, 2017). These constructs enable localization of Msm DivIVA and FtsZ respectively. Both constructs were screened by restriction digests to assess genetic integrity before further work was done. Restriction mapping yielded expected fragment sizes (Figure 3.3.5 and 3.3.6). Thereafter, pTweety_DivIVA_GFP was electroporated into all three Mtb strains and the resulting strains were imaged using fluorescent microscopy.



Restriction enzyme	Fragment size (bp)
AccI	4647, 1912, 575, 198
BamHI	6471, 1035
BspI	4387, 2006, 1008, 105
HindIII	6545, 961
Xhoi	4764, 2676, 66

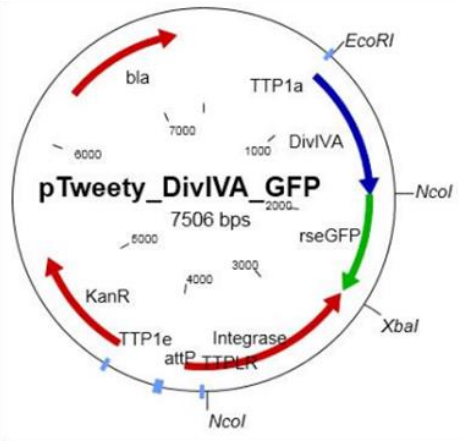
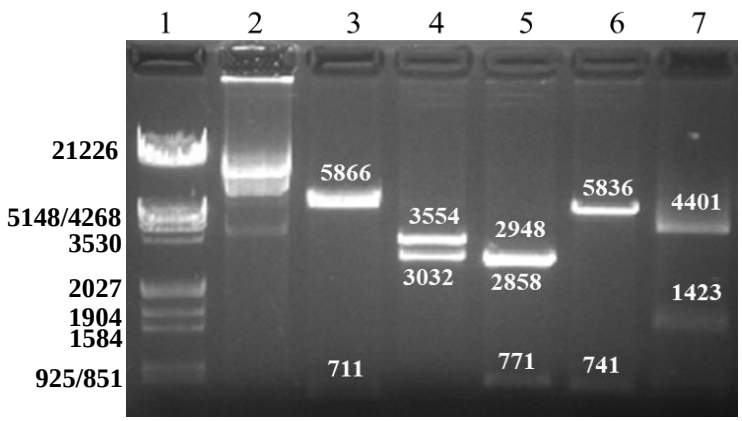
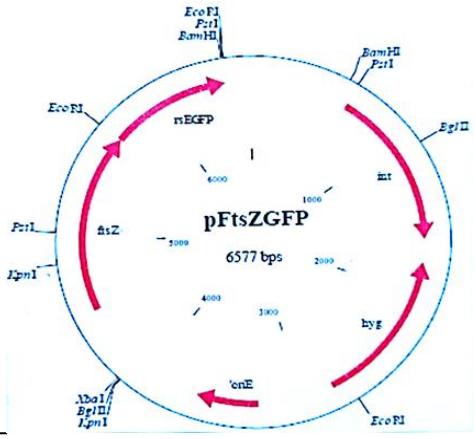


Figure 3.3.5. PTweety_DivIV_GFP restriction mapping to confirm plasmid integrity. 1- Molecular weight marker III, 2-*AccI*, 3-*BamHI*, 4-*BspHI*, 5-*HindIII*, 6-*XhoI*, 7-uncut plasmid. With the exception of *AccI*, all restriction enzymes produced expected band sizes. It appeared that *AccI* did not cut the DNA.





Restriction enzyme	Expected band size
BamHI	5866, 711
BglII	3554, 3023
EcoRI	2948, 2858
KpnI	5836, 741
PstI	4401, 1423, 753

Figure 3.3.6. pFtsZGFP restrictions to confirm plasmid integrity. 1- Molecular weight marker III, 2-uncut plasmid, 3- *BamHI*, 4-*BglI*, 5-*EcoRI*, 6-*KpnI*, 7-*PstI*. All restriction enzymes produced expected band sizes. The expected 753 fragment in *PstI* digestions was too faint for observation.

We found that DivIVA-GFP localizes the cell poles in all strains (Figure 3.3.7). Following this, the localization of FtsZ-GFP was attempted but no fluorescent signals were noted in the cells carrying pFtsZGFP, which was electroporated into H37RvS and H37*Δami1S* (Figure 3.3.8 A). This construct yielded clear FtsZ rings in Msm (Figure 3.3.8 B, as performed by Maphatsoe (2017)) and in this context, it was unclear why no localization was observed in Mtb. To ensure genetic integrity of the strains carrying pFtsZGFP, we confirmed integration of the plasmid in the bacterial chromosome using PCR targeted at the integration junctions using the AttBS2, AttL4 and AttBS1, AttL2 primer pairs (Shown in Table 3.2.3) which amplify a 320 bp segment and a 282 bp segment respectively (Figure 3.3.9). The 320 bp segment was successfully amplified but repeated attempts did not yield the 282 bp fragment (Figure 3.3.10). Given that one junction was amplified, and considering the strain grew in the presence of the appropriate antibiotic, successful incorporation of the plasmid was considered as confirmed. In this context, it remains unclear why no localization was observed, however; because pFtsZGFP was derived from Msm, it is possible that it may not be expressed similarly in Mtb. For example, despite

the high sequence homology between the Ribosomal protein S1 (RpsA) in Msm and Mtb, the Msm RpsA homologue has low affinity to pyrazinoic acid (POA), a bactericidal pyrazinamide by-product, hence the natural resistance against the drug (Antiparra et al., 2020). We had used Msm FtsZ based of the high sequence similarity of the protein sequence (91.56%) between Mtb and Msm.

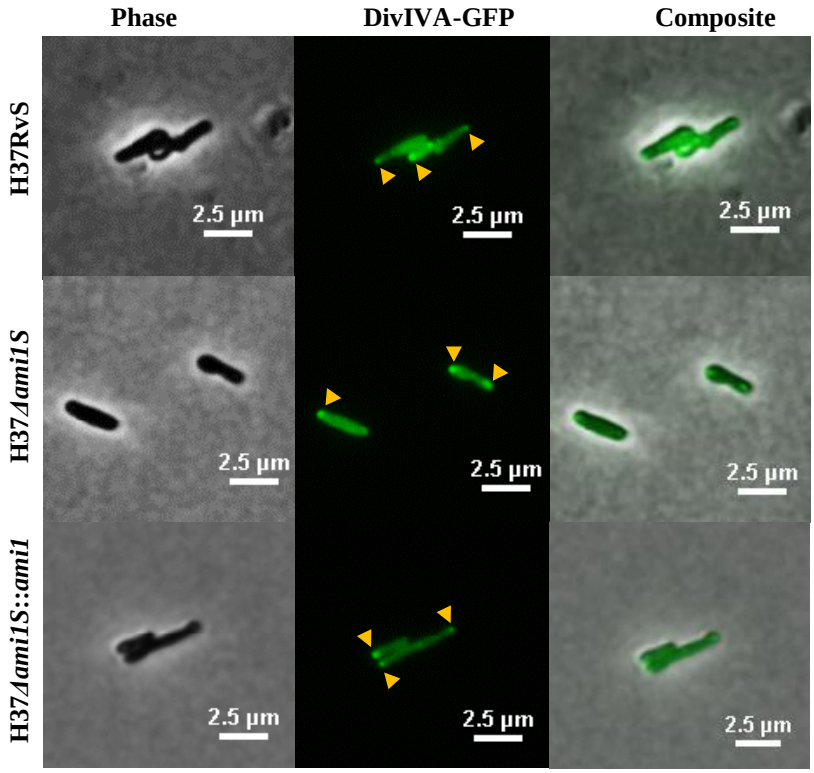


Figure 3.3.7. DivIVA-GFP localization in *M. tuberculosis* strains. H37RvS, H37*Δami1S*, and H37*Δami1S*::*ami1* carrying pTweety_DivIVA-GFP were grown to OD600nm and DivIVA_GFP fluorescence was analysed at Em488nm; Ex509nm. Yellow arrows depict DivIVA localization. Scale bar 2.5 µM

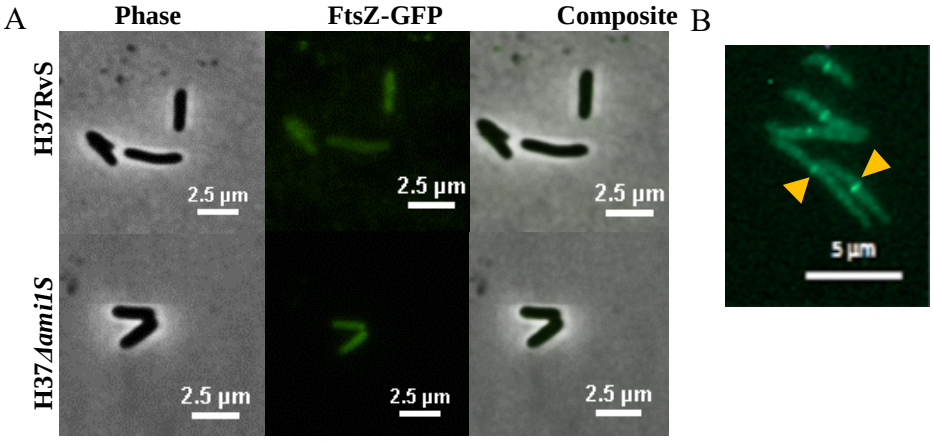


Figure 3.3.8. FtsZ-GFP localization in *M. tuberculosis* strains. A) H37RvS and H37*Δami1S* carrying pFtsZ-

GFP. Both strains were grown to OD600nm and FtsZ_GFP fluorescence was analysed at Em488nm; Ex509nm. Scale bar 2.5 µM. B) pFtsZ-GFP localization in Msm, previously performed by Maphatsoe (2017). Yellow arrows depict FtsZ localization. Scale bar 5 µM.

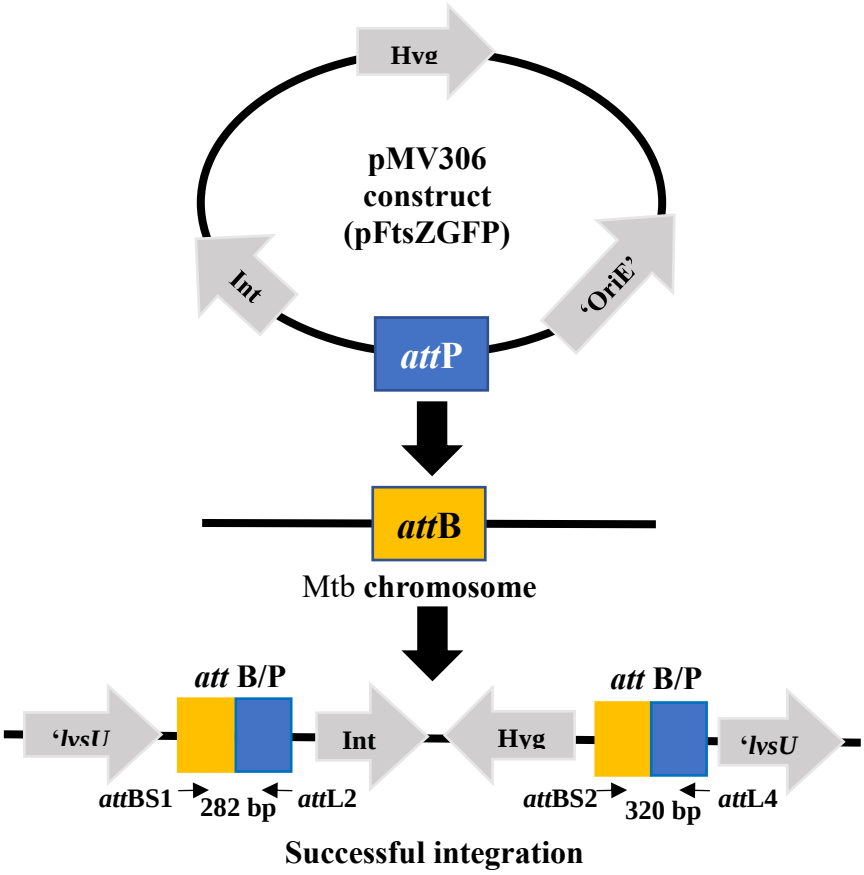
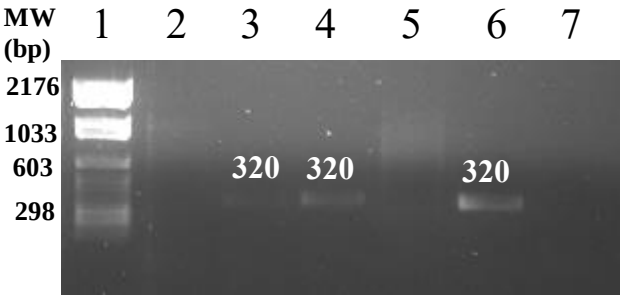


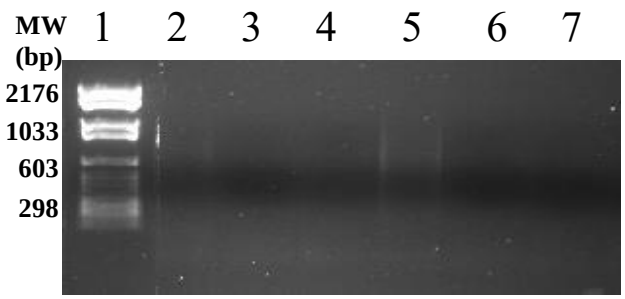
Figure 3.3.9. Schematic showing pMV_FtsZGFP integration into H37RvS and H37Δami1S. The AttBS2, AttL4 and AttBS1, AttL2 primer pairs amplifying a 320 bp segment and a 282 bp segment respectively, to allow the confirmation of plasmid integration.

Space left intentionally blank



PCR step	Temperature	Period
Initial denaturation	65°C	5 min
Denaturation	65°C	30 sec
Annealing	55°C	30 sec
Extension	72°C	90 sec
Final extension	72°C	7 min

***att*BS2-*att*L4, Expected band size: 320 bp**



PCR step	Temperature	Period
Initial denaturation	65°C	5 min
Denaturation	65°C	30 sec
Annealing	61°C	30 sec
Extension	72°C	90 sec
Final extension	72°C	7 min

***att*BS1-*att*L2, Expected band size: 282 bp**

Figure 3.3.10. Confirmation of pMV_FtsZGFP integration into H37RvS and H37Δami1S. Left panel: *att*BS2-*att*L4 fragment amplification (1- Molecular weight marker VI, 2-H37RvS DNA, 3-4 H37RvS_pFtsZGFP DNA, 5- H37*Δami1S* DNA, 6-7- H37*Δami1S*_pFtsZGFP DNA). Right panel: *att*BS1-*att*L2 fragment amplification)1- Molecular weight marker VI, 2-H37RvS DNA, 3-4 H37RvS_pFtsZGFP DNA, 5- H37*Δami1S* DNA, 6-7- H37*Δami1S*_pFtsZGFP DNA).

3.3.3. H37*Δami1S* displayed poor growth in Sauton's media (1% and 0% glycerol)

Mtb is an intracellular pathogen that encounters nutrient deprivation during colonization of the human host. Considering this, the effect of *ami1* gene deletion on bacterial growth under carbon limiting conditions was assessed by monitoring the growth of H37RvS, *H37Δami1S*, and *H37Δami1S*::*ami1* in Sauton's minimal growth media (pH 7.0) with either 1% glycerol as the sole carbon source or without any source of carbon. H37*Δami1S* displayed poor growth kinetics in both variations of Sauton's minimal growth media compared to both H37RvS and *H37Δami1S*::*ami1*, as assessed by absorbance (OD600nm) readings and CFUs (Figure 3.3.11 A and B for 1% glycerol and Figure 3.3.11. C and D for no carbon source).

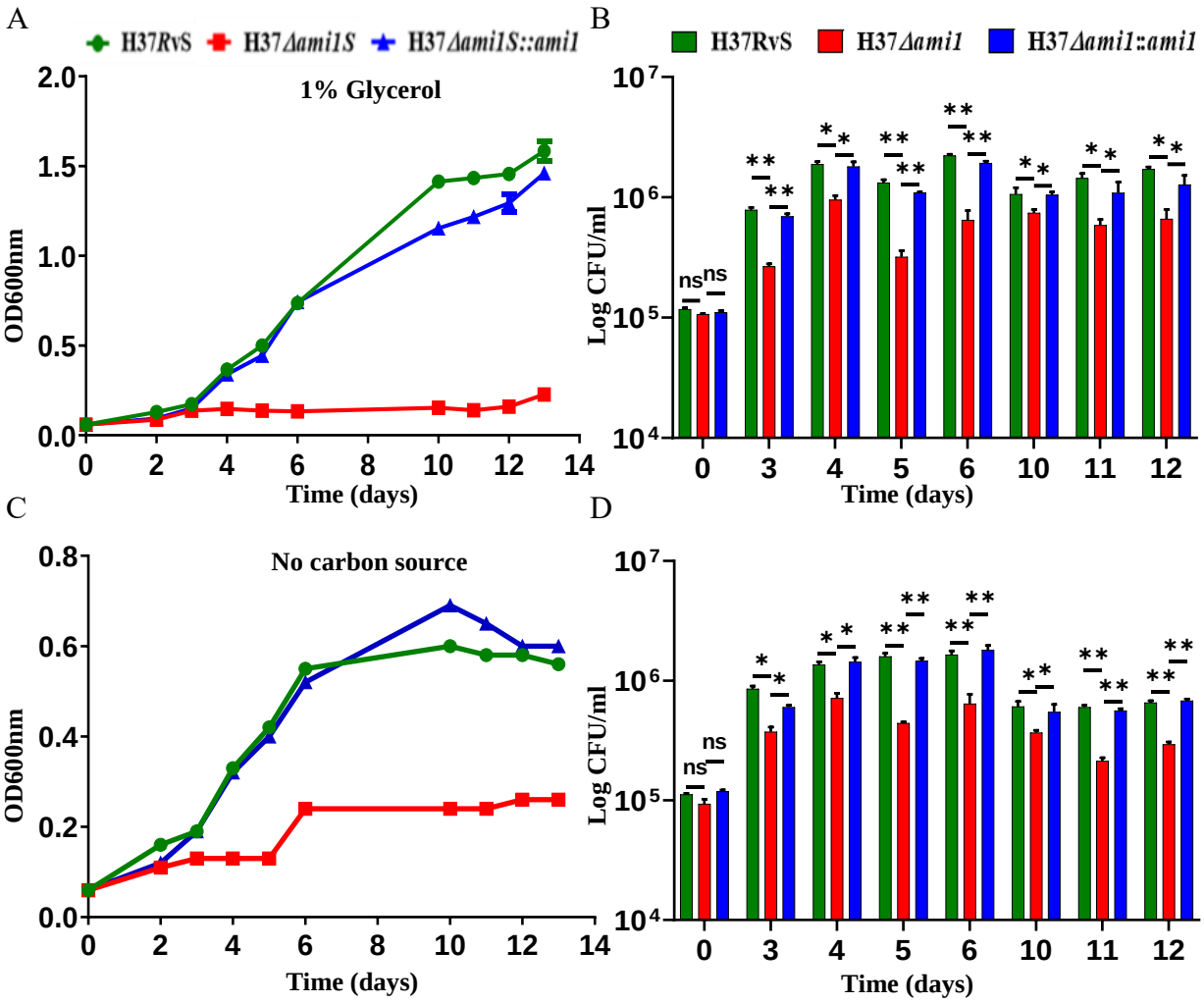


Figure 3.3.11. Growth assessment of the ami1 mutant strains under nutrient limited conditions. Shown are the growth kinetics of H37RvS, H37*Δami1S* and H37*Δami1S*::*ami1* in Sauton's minimal media either with 1% glycerol as the sole carbon source (A and B for ODs and CFUs respectively) or no carbon source (C and D for ODs and CFUs respectively). Error bars represent the standard error of the mean (SEM) for three biological replicates. Statistical analysis was conducted using the Student's t-test, *: P<0,05. **: P<0.001.

3.3.4. H37*Δami1S* displays increased EtBr uptake

Having established that the *ami1* defective mutant of Mtb displayed grow defects under nutrient limiting condition, attention was subsequently focused on investigating whether the mutant had a defective cell wall. PG hydrolases are required in remodelling to maintain cell wall homeostasis and in this context; loss of Ami1 could lead to defects. Ethidium bromide (EtBr) uptake in the H37RvS, H37*Δami1S* and H37*Δami1S*::*ami1* strains was used as a proxy to monitor cell wall permeability. Altered uptake of EtBr would point to an altered cell wall. The *ami1* mutant strain displayed a significantly higher EtBr uptake compared to H37RvS and H37*Δami1S*::*ami1*, confirming increased cell wall permeability (Figure 3.3.12). EtBr uptake

plots were subjected to polynomial curve fitting, with Mtb strains displaying coefficient values (R^2) of 0.9976 (H37RvS) 0.9988, (H37*Δami1S*), and 0.9963 (H37*Δami1S*::*ami1*), suggesting a good fit (R^2 values closer 1 are desirable). With exception of the starting points, H37*Δami1S* curve does not intercept with those of H37RvS and H37*Δami1S*::*ami1*, indicating that the observed difference in EtBr uptake is statistically significant.

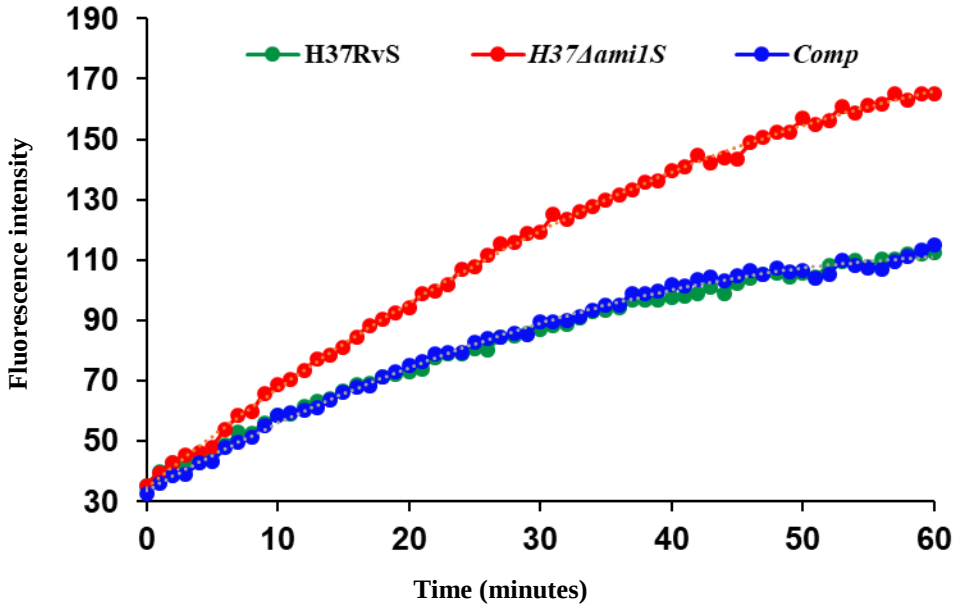


Figure 3.3.12. Assessment of ethidium bromide uptake in the *ami1* mutant of Mtb. Shown is a line graph indicating EtBr (8 µg/mL) diffusion into the cytoplasm of Mtb strains H37RvS, H37Δ*ami1S* and H37Δ*ami1S*::ami1. Background fluorescence was subtracted when plotting values. Each line represents three biological replicates. Strains were subject to polynomial curve fitting. H37RvS: $y = -0{,}0141x^2 + 2{,}0764x + 37{,}67$ $R^2 = 0{,}9976$; H37Δ*ami1S*: $y = 2E - 05x^3 - 0{,}0235x^2 + 3{,}5224x + 34{,}526$ $R^2 = 0{,}9988$; H37Δ*ami1S*::ami1: $y = -0{,}0187x^2 + 2{,}4069x + 33{,}657$ $R^2 = 0{,}9963$.

3.3.5. The *ami1* mutant of Mtb displays increased susceptibility to Lysozyme, Vancomycin, Ethionamide and INH in time-kill assays

Susceptibility assessments of the ami1 mutant

Considering the increased uptake of EtBr, we hypothesized that the ami1 mutant would display increased susceptibility to various antibiotics into the cell. H37RvS, H37*Δami1S* and H37*Δami1S*::*ami1* were grown in 7H9 media and were exposed to various antibiotics in minimum inhibitory concentration (MIC) broth microdilution assays (Table 3.3.1). There were no differences in MIC values between the Mtb strains for all drugs tested, with the exception of RIF, where H37*Δami1S* displayed at least, a ca. 4-fold decrease in MIC value, indicating increased drug susceptibility, Table 3.3.1.

Table 3.3.1. Minimum inhibitory concentration (MIC) values for antibiotics targeting various biological processes, such as DNA replication, protein translation and cell wall synthesis.

Drug	**MIC (µg/ml)**		
	H37RvS	H37*Δami1S*	H37*Δami1S*::*ami1*
Azaserine	1-2	2	2
Ciprofloxacin	0.25	0.25	0.5
D-cycloserine	8-16	8-16	8-16
Amoxicillin	4-8	4-8	8-16
Erythromycin	16	8-16	4-16
Ethambutol (EMB)	2	2	2-6
Ethionamide (ETO)	0.8	0.8	0.8
Isoniazid (INH)	0.0625	0.0625	0.0625-0.125
Kanamycin (KAN)	2-4	4	4
Lysozyme (LYS)	31.25	31.25	31.25
Rifampicin (RIF)	0.00025-0.001*	0.00006*	0.0005-0.001*

Data are from three independent biological replicates. *: $P < 0.05$

In addition to broth microdilution, the drug susceptibility of the *ami1* mutant of Mtb was also tested using time kill assays. This approach was based on prior work which assessed the temporal susceptibility of H37RvS to INH and RIF (de Steenwinkel et al., 2010). Cell wall targeting antibiotics were given preference in Mtb time kill assays, in addition to using agents that target other components of bacterial metabolism. Lysozyme (LYS) and vancomycin (VANC) were selected because they target the PG component of the cell wall. Ethionamide (ETO), was selected because it is an anti-mycobacterial agent that targets the MA component of the cell wall; INH was selected because it is a first-line TB drug that targets the MA component of the well; and lastly RIF and kanamycin (KAN) were selected as non-cell wall targeting controls. The modes of action for these drugs are indicated in the inserts in Figure 3.3.13. Drug concentrations were used at ≥ 100x the MIC (Table 3.3.1) to allow for effectivity against Mtb at log phase (OD600nm = 0.6), which is approximately 2 x 10^7 cells/ml. Only lysozyme was used at a concentration of ≥ 10x the MIC (Table 3.3.1) due to its enzymatic nature, with higher concentrations killing Mtb rapidly. Using this approach, H37*Δami1S* displayed a significant increase in susceptibility to cell wall targeting agents, INH, ETO, VANC, and LYS between day 0 and day 4 (Figure 3.3.13 A, B, C, and E).

H37Δ*ami1S* was not able to recover from day 4 post exposure in the presence of ETO and VANC as noted by the absence of colonies at day 7 (Figure 3.3.13 B-C). The recovery of H37Δ*ami1S* at 7 days post INH exposure was curious, suggestive of the emergence of drug resistant mutant in culture. To evaluate this, three colonies were picked from the day 7 plate, with three colonies taken from the day 0 plate as controls, and all samples were subjected to DNA extraction. The resulting DNA was genotyped on the Hain Line Probe Assay (LPA) that reports on genetic resistance to INH and RIF. The LPA blots are given in Appendix D, with the data summarized in Table 3.3.2. Hain LPA assays confirmed that colonies emerging from all strains at day 7 were still genetically susceptible to INH, suggesting that they represented phenotypically resistant populations. There were no differences in survival between the H37RvS, H37*Δami1S* and H37*Δami1S*::*ami1* following exposure to RIF and KAN, which respectively target transcription and translation (3.3.13 D and F). It was noted that the survival of H37Δ*ami1S* starts to decrease at 7 days post exposure to RIF, however, this observation was not significant (Figure 3.3.13 F).

Space left intentionally blank

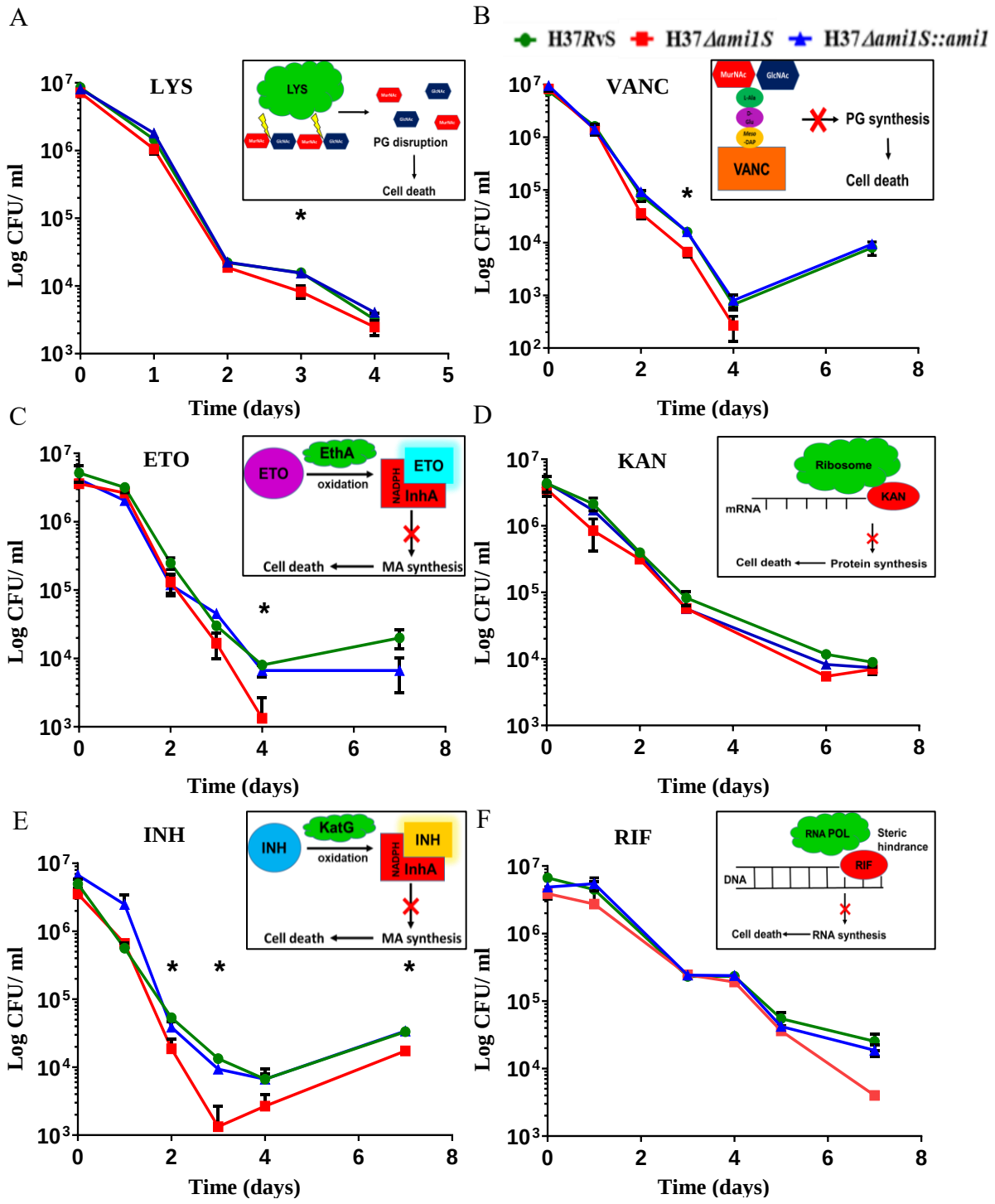


Figure 3.3.13. Drug susceptibility assessments of the ami1 mutants using time-kill curves. Graphs show survival of H37RvS, H37Δ*ami1S* and H37Δ*ami1S::ami1* exposed to 32 µg/ml INH, 0.25 µg/ml RIF, 80µg/ml ETO, 400 µg/ml kanamycin, 400 µg/ml VANC and 1 mg/ml lysozyme. Antibiotic used are displayed with schematic diagrams of their mechanisms of action. Antibiotics were not removed from the media post addition. Error bars represent the standard error of the mean (SEM) for three biological replicates. Statistical analysis was conducted using the student's t-test *: $p < 0.05$. Statistical significance only shown for H37RvS and H37Δ*ami1S* comparisons.

Table 3.3.2. Hain line probe assay to determine drug susceptibility of strains exposed to INH (sampled from the time-kill assays at day zero [T0] and day seven [T7]). See Appendix D for data sheet.

Mtb strain	Replicate	INH		RIF	
		Sensitive	**Resistant**	**Sensitive**	**Resistant**
H37RvS	R1 T_0	✓	-	✓	-
	R1 T_7	✓	-	✓	-
	R2 T_0	✓	-	✓	-
	R2 T_7	✓	-	✓	-
	R3 T_0	✓	-	✓	-
	R3 T_7	✓	-	✓	-
H37*Δami1S*	R1 T_0	✓	-	✓	-
	R1 T_7	✓	-	✓	-
	R2 T_0	✓	-	✓	-
	R2 T_7	✓	-	✓	-
	R3 T_0	✓	-	✓	-
	R3 T_7	✓	-	✓	-
H37*Δami1S*::*ami1*	R1 T_0	✓	-	✓	-
	R1 T_7	✓	-	✓	-
	R2 T_0	✓	-	✓	-
	R2 T_7	✓	-	✓	-
	R3 T_0	✓	-	✓	-
	R3 T_7	✓	-	✓	-

Assessment of biofilm formation and associated drug tolerance

It is established in mycobacteria that biofilm formation confers drug tolerance to bacteria (Ojha et al., 2008). Thus, to further study the effect of *ami1* gene deletion on antibiotic survival biofilms were established and exposed to first-line TB drugs INH and RIF. The hypothesis here was that the *ami1* mutant would be deficient in the establishment of drug tolerant bacteria in the biofilm. Although there were differences in wrinkling pattern between the wild-type and

both the mutant and complement strains, these differences did not affect biofilm mass formation (Figure 3.3.14 panel A and B). Consistent with the data from INH time-kill kinetics (Figure 3.3.13 E), cells derived from biofilms from the H37Δ*ami1S* strain displayed an increase in susceptibility to INH at 2 and 3 days post exposure (Figure 3.3.14 C). The *ami1* mutant strain also displayed a delayed non-significant decrease in survival at 4 days after exposure to RIF (Figure 3.3.14 D), in correspondence to the RIF time-kill kinetics (Figure 3.3.13 F). These observations confirmed that *ami1* mutant did indeed display defects in tolerance to INH.

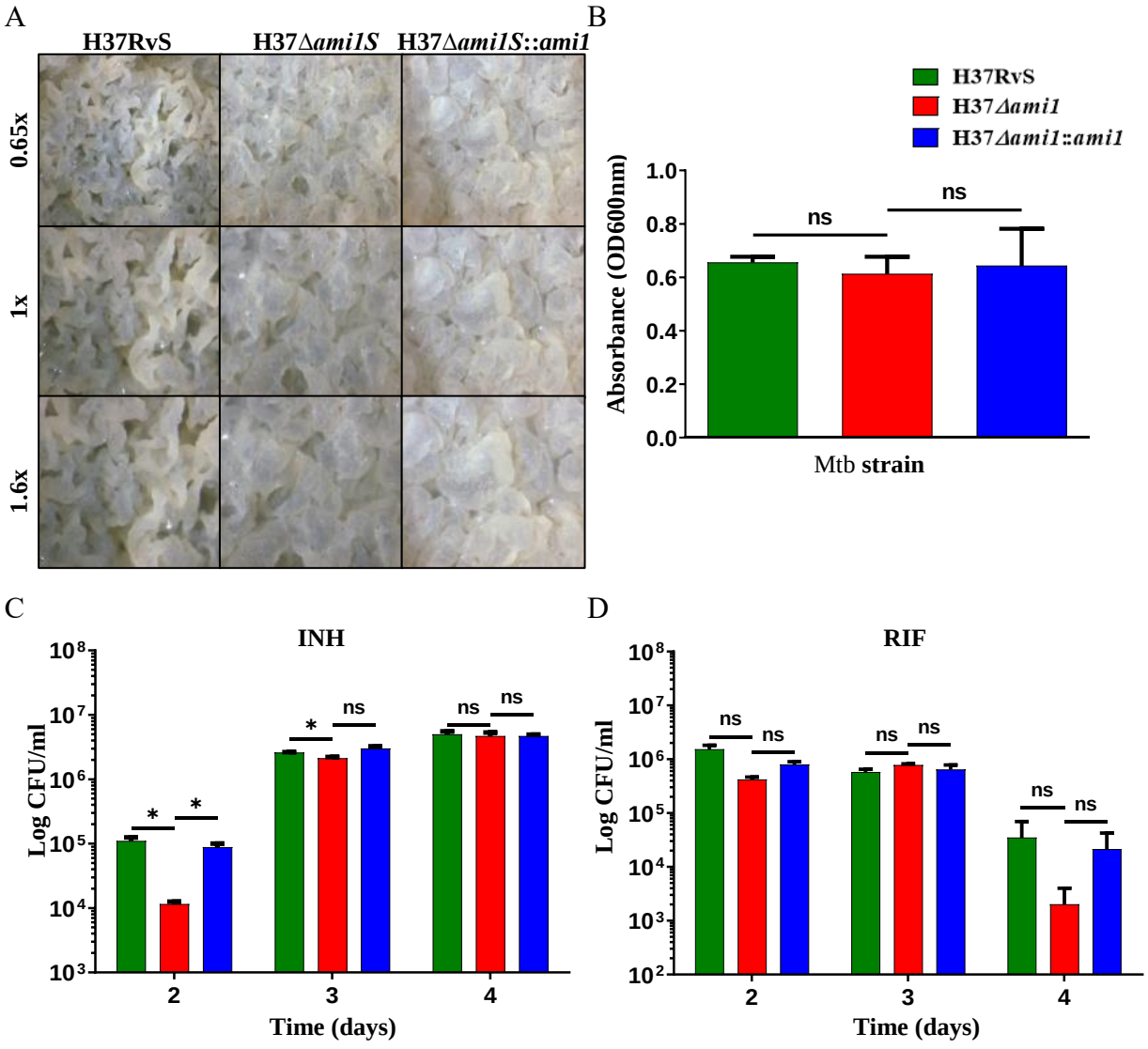


Figure 3.3.14. Biofilm formation and associated drug tolerance in the *ami1* mutant. (A) Morphology of pellicle biofilms formed by Mtb strains. (B) Quantification of biofilm mass using crystal violet staining (C) Response of biofilm -derived cells to INH exposure at 32 µg/ml (D) Response of biofilm-derived cells to RIF exposure at 0,25 µg/ml. Error bars represent the standard error of the mean (SEM) for three biological replicates. Statistical analysis was conducted using the student's t-test *: P< 0,05.

TADA staining of INH treated Mtb

To investigate if the effect of INH treatment was associated with defects in spatial localization of PG, INH cells were stained with TADA. Staining patterns of H37RvS, H37Δ*ami1S* and H37Δ*ami1S*::*ami1* exposed to INH show the distribution of TADA towards the side wall instead of the cell poles, as seen in cells grown in standard media (Figure 3.3.15 panel A and B). The observed staining pattern indicates possible repair of INH damaged PG. Interestingly, the H37Δ*ami1S* displayed a decrease in cell length when exposed to INH, in comparison to H37RvS and H37Δ*ami1S*::*ami1* (Figure 3.3.15 panel C).

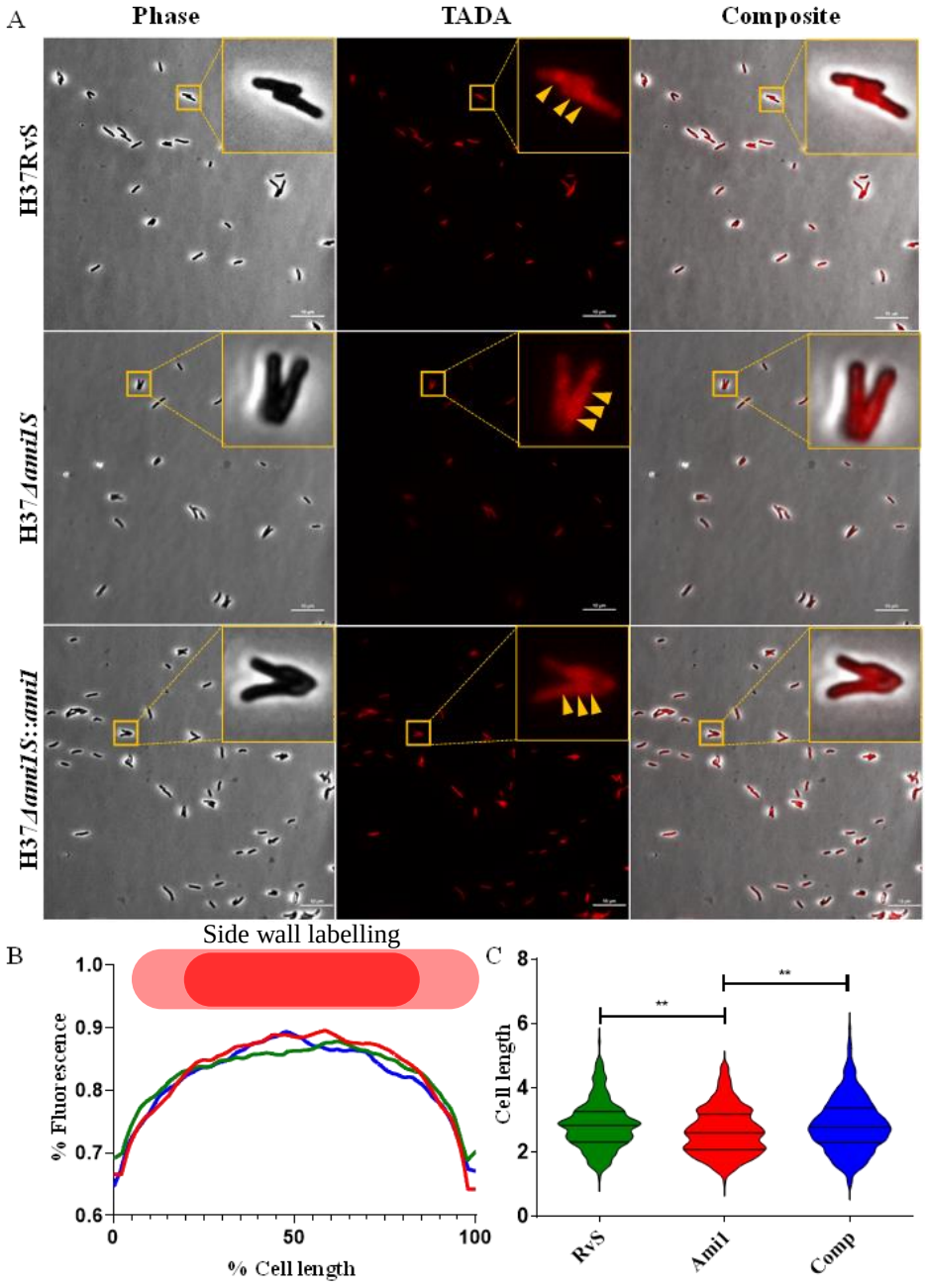


Figure 3.3.15. TADA fluorescence microscopy of *Mtb* strains exposed to INH. A) Micrographs depicting Mtb cells, incubated in the presence of 32 µg/ml INH, and stained with TADA. The cells were grown up to an

OD600nm of 0.6 and exposed to INH for 24 hours, followed by TADA staining. Yellow arrows depict localization of TADA to the sidewall. B) Line graph showing the TADA staining pattern across the lateral axis of the cell between the *Mtb* strains. C) Measurements of cell length in cells treated with INH. At least 300 cells (N=300) were counted per strain. Scale bar 10 uM Error bars represent the standard error of the mean (SEM) for three independent experiments. Statistical analysis was conducted using the Student's t-test, **: $p<0.001$

3.3.6. INH exposure induces *ami1* transcription in H37RvS

Up to this point in our research, there was a growing body of evidence from our work suggesting that Ami1 in Mtb plays an important role in the bacterial response to INH. Next, this effect was interrogated further by analysing *ami1* transcription in H37RvS exposed to first-line TB drugs, INH and RIF via qPCR. The transcription of *ami1* was normalized to the transcription of *sigA*, a constitutively expressed housekeeping gene. The transcription of *ami1* significantly increased at 1 day after exposure to 32 µg/ml INH but did not increase at any time point after exposure to 0.25 µg/ml RIF (Figure 3.3.16 A), suggesting that the effect was specific for INH.

Given these observations, the multiple reports of the redundant nature of amidases in other bacterial species ((Heidrich et al., 2002, Priyadarshini et al., 2007), the transcription of amidases, *ami3* and *ami4* was also analysed under INH stress to observe if Mtb *amidase* display any redundancy in response to INH. It was observed that the transcription of *ami3* and *ami4* did not increase in response INH (Figure 3.3.16 B), showing that *ami1* is the only amidase that is specifically expressed in response to INH stress.

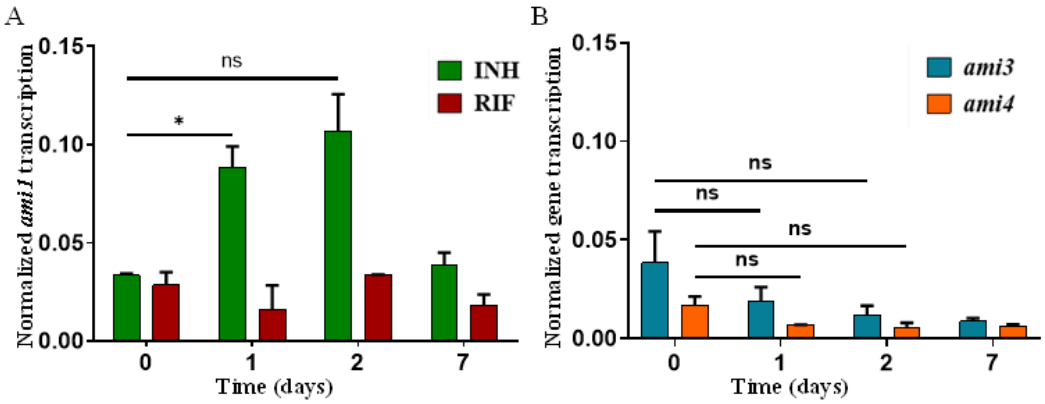
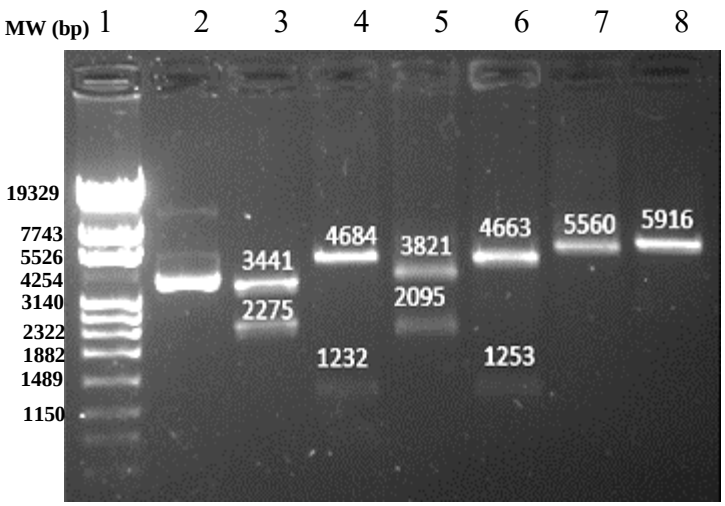


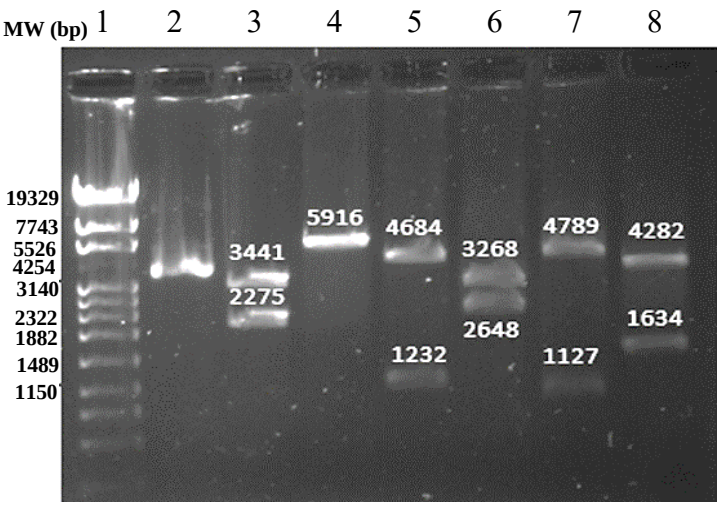
Figure 3.3.16. Transcriptional analysis of amidase-encoding genes in Mtb. (A) Normalized *ami1* expression in H37RvS when exposed to 32µg/ml of INH and 0,25 µg/ml of RIF. (B) Expression of *ami3* and *ami4* in H37RvS when exposed to 32µg/ml INH. Amidase transcription was normalized to the transcription of *sigA*, a basally

express gene. Error bars represent the standard error of the mean (SEM) for three biological replicates. Statistical analysis was conducted using the student's t-test *: $P < 0.05$.

To further validate these observations, the 500 bp promoter regions of the *ami1* and *sigA* genes were cloned upstream of the gene encoding EGFP in pMV306H to produce plasmids p-5C*ami1_EGFP* and p-5C*sigA_EGFP*. The constructs were subjected to restriction enzyme screening for the confirmation of successful cloning. Restriction digests of p-5C*ami1_EGFP* and p-5C*sigA_EGFP* yielded the expected fragments sizes for all enzymes used, with the exception of p-5C*ami1_EGFP PvuI* digests, in which the expected 365 bp band could not be visualised because band sizes below 400 bp were not visible on the 1% agarose gel (Figure 3.3.17 panels A and B). Both p-5C*ami1_EGFP* and p-5C*sigA_EGFP* constructs were electroporated into H37RvS to yield the reporter strains H37_-5C*ami1_EGFP* and H37_-5C*sigA_EGFP*. Reporter strains were then exposed to 32µg/ml INH and fluorescence was measured on a plate reader (Ex488nm; Em509nm, Figure 3.3.18 panel A). As expected, The H37_-5C*ami1_EGFP* strain displayed a significant increase in fluorescence intensity in the presence of INH relative to the negative INH control, signalling an increase in *ami1* transcription (Figure 3.3.18 panel B). Additionally, there were no significant differences in fluorescence intensity of the H37_-5C*sigA_EGFP* strain in the presence and absence of INH, signalling the basal transcription of *sigA* under these conditions (Figure 3.3.18 panel B).

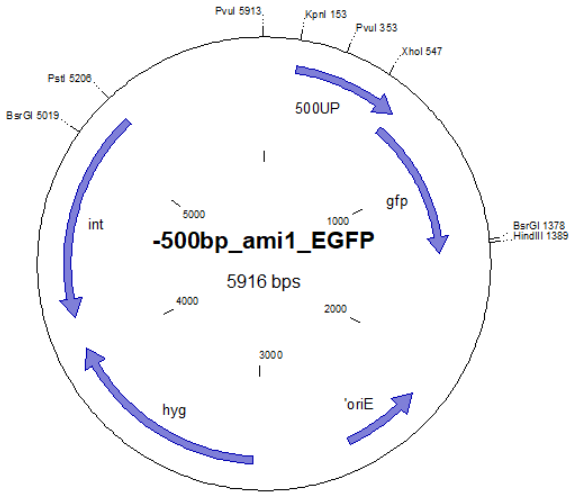
Space left intentionally blank





Restriction enzymes	Expected band sizes
BsrGI	3441, 2275
HindIII, KpnI	4684, 1232
HindIII, PstI	3821, 2095
PstI, XhoI	4663, 1253
PvuI	5560, 365
XhoI	5916

Restriction enzyme	Expected band size
BsrGI	3441, 2275
HindIII	5916
HindIII, KpnI	4684, 1232
EcoRI, NcoI	3268, 2648
PstI	4789, 1127
PvuII	4282, 1634



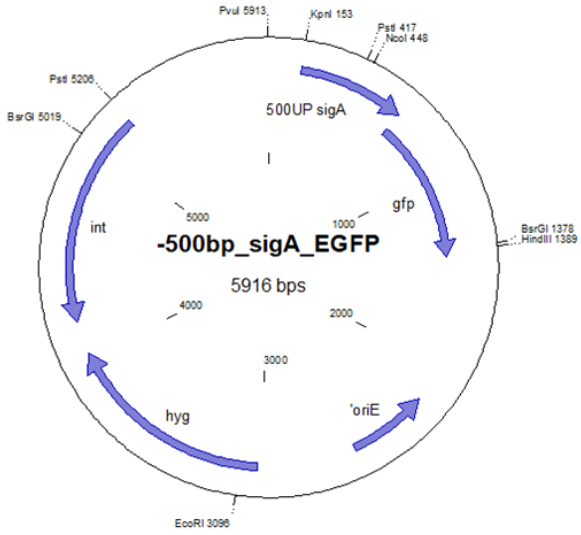
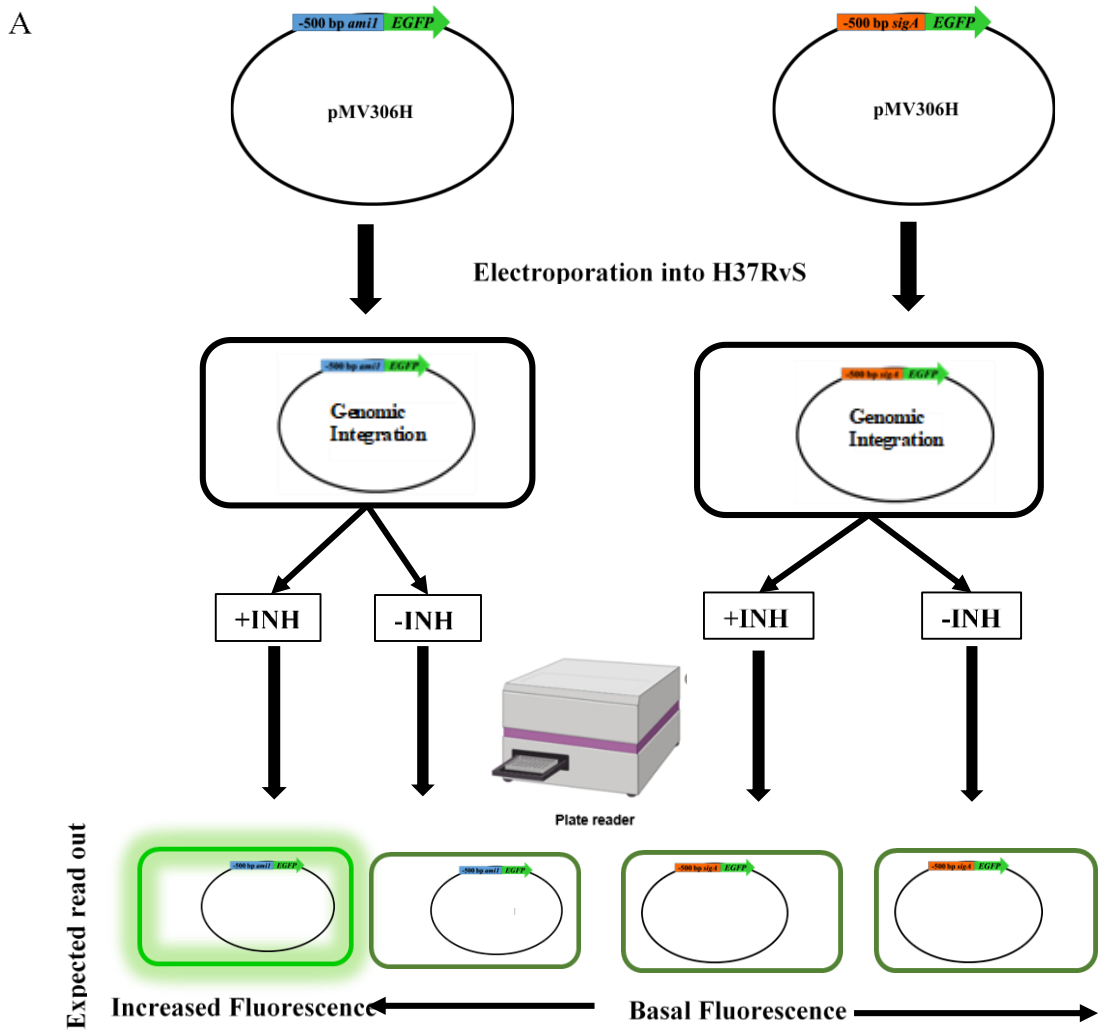
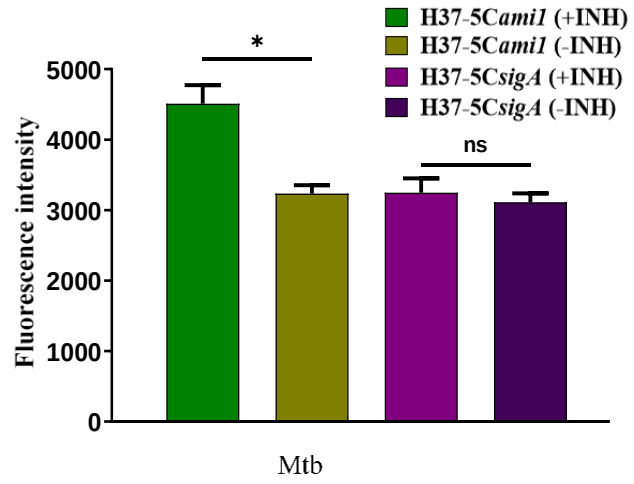


Figure 3.3.17. Restriction digests of -5C*ami1*_EGFP and -5C*sigA*_EGFP to confirm successful cloning. (A) Restriction digests of -5C*ami1*_EGFP (Lane 1: DNA molecular marker IV, Lane 2: Undigested construct, Lane 3: *BsrGI*, Lane 4: *HindIII* and *Kpni*, Lane 5: *HindIII* and *PstI*, Lane 6: *PstI* and *XhoI*, Lane 7: *PvuI*, Lane 8: *XhoI*). The expected 365 bp band in the *PvuI* digest could not be visualised because band sizes below 400 bp were not visible on the 1% agarose gel. (B) Restriction digests of -5C*sigA*_EGFP (Lane 1: DNA molecular marker IV, Lane 2: Undigested construct, Lane 3: *BsrGI*, Lane 4: *HindIII*, Lane 5: *HindIII* and *KpnI*, Lane 6: *NcoI* and *EcoRI*, Lane 7: *PstI*, Lane 8: *PvuI*).





Mtb strain	Description
H37RvS	The wild type laboratory strain of *Mtb*
H37_-5C*ami1*_EGFP	Derivative of H37RvS with an integrating plasmid carrying the putative *ami1* promoter region (500bp US) upstream an EGFP gene
H37_-5C*sigA*_EGFP	Derivative of H37RvS with an integrating plasmid carrying the putative *sigA* promoter region (500bp US) upstream an EGFP gene

Figure 3.3.18. Fluorescence intensity of H37_-5C*ami 1*_EGFP and H37_-5C*sigA*_EGFP strains reporting on the expression of the *ami1* and *sigA*. (A) Schematic representation of the EGFP experimental rationale with reporter strains. (B) Bar graph showing fluorescence intensity of H37_-5C*ami1*_EGFP and H37_-5C*sigA*_EGFP in the presence and absence of INH. Reporter strains were grown to the log phase (OD600nm of 0.6-0.8), and exposed to 32 µg/ml INH for 24 hrs. Fluorescence was assessed using a plate reader. Background fluorescence

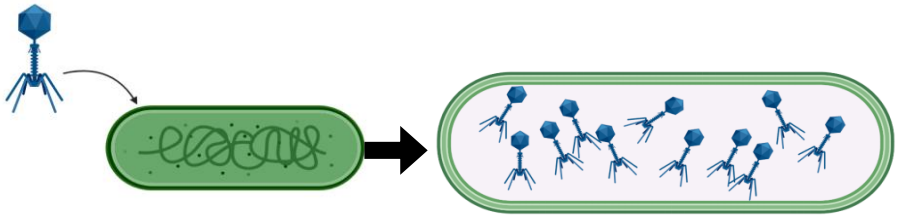
was subtracted (using H37RvS as a blank). Error bars represent the standard error of the mean (SEM) for biological triplicates. Statistical analysis was conducted using the student's t-test *: $P < 0.05$. ns: Not significant.

3.3.7. Attempts to generate transposon libraries in the ami1 mutant of Mtb

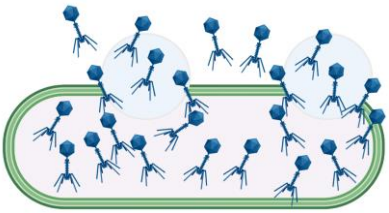
To further investigate the mechanistic basis of role Ami1 plays in response to INH treatment, we next attempted to generate transposon libraries in the mutant. We were able to obtain ΦMycoMarT7 phage titer stocks (between $1 \times 10^{11}$and 1×10^{12} PFU/ml) that are well over the recommended minimum of 5×10^{10} PFU/ml (Figure 3.3.19 A). Before we could construct transposon libraries for Mtb strains under INH stress, we attempted to construct transposon library in H37RvS under normal growth conditions in 7H9, to assess the fitness of the ΦMycoMarT7 in infecting Mtb strains. We discovered that the ΦMycoMarT7 stock we have displayed reduced fitness as it had a transduction efficiency (between 1×10^{2} and 3×10^{3} CFU) that was lower that the required threshold for sufficient coverage ($\geq 1 \times 10^{5}$). This was not only observed in H37RvS, but also in H37Δ*ami1* and H37Δ*ami1*::*ami1* (Figure 3.3.19 B). At this point, another study was published reporting synthetic lethality of RipA in the *ami1* mutant of Mtb (Healy et al., 2020). Hence, no further attempts were made to improve on this method.

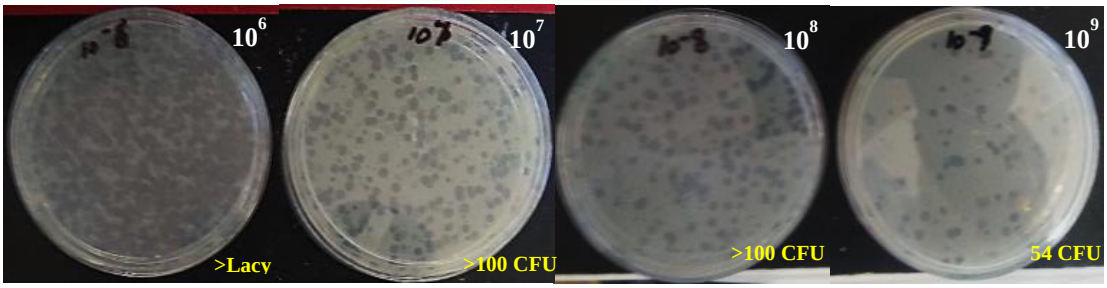
Space left intentionally blank

A



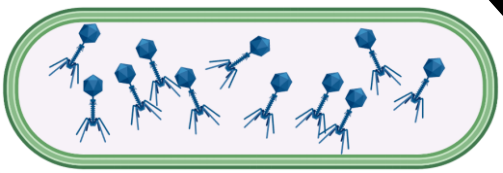
Phage transduction in Msm **at 37°C**

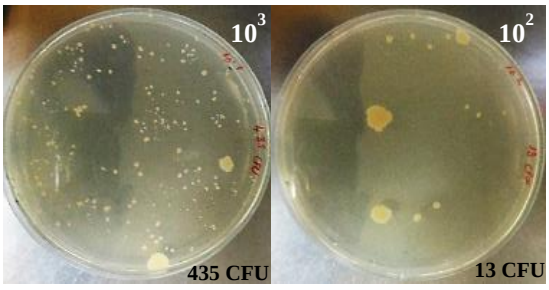




Induction of lysis in Msm **at 30°C. (Viral titer at 2,78 x 10^{11} PFU/ml)**

B





Transduction efficiency

Attempts	H37RvS	H37*Δami1*	H37*Δami1*::*ami1*
1	2,48 x 10^3	-	-
2	1,62 x 10^2	-	-
3	2,88 x 10^3	-	-
4	1,37 x 10^3	1,07 x 10^3	3,85 x 10^2
5	9,32 x 10^2	1,17 x 10^3	1,33 x 10^3

Phage transduction in *M. tuberculosis* at 37°C to create a library. R

Figure 3.3.19. Transposon mutagenesis in the *ami1* mutant. A) Transposon ΦMycoMarT7 phage stock preparation. B) ΦMycoMarT7 phage transductions in Mtb. Shown are representative plates with kanamycin resistant colonies and a table reporting on the transduction efficiencies from different attempts.

3.3.8. The survival of H37*Δami1S* is reduced in activated U937Mϕ

Finally, we sought to investigate the role of Ami1 in Mtb intracellular survival in IFN-γ stimulated and non-stimulated U937 human monocyte derived macrophages (U937Mϕ). There were no differences in intracellular survival across all strains in non-stimulated U937Mϕ (Fig 3.3.20 panel A). In contrast, the intracellular survival of H37*Δami1S* was reduced when compared to H37RvS and H37*Δami1S*::*ami1* in IFN-γ stimulated U937Mϕ at 48 hrs post infection but this effect was abrogated at 7 days post infection (Fig 3.3.20 panel B). The recovery of H37*Δami1S* day 7 possibly stems from the depletion of IFN-γ, consequently leading to a reduced immune response by U937Mϕ cells. IFN-γ stimulation does not affect the level of IFN-γ inherently expressed by U937Mϕ (Ucla et al., 1990), and thus, the observed immune response in figure Fig 3.3.20B is driven by externally added IFN-γ. Alternatively, the recovery of H37*Δami1S* at day 7 may possibly arise from the inability of U937Mϕ to mount a complete immune response over time. For example, activated U937Mϕ have been shown to be permissive for the growth live attenuated BCG overtime, displaying an inability to mount a complete immune response (Passmore et al., 2001).

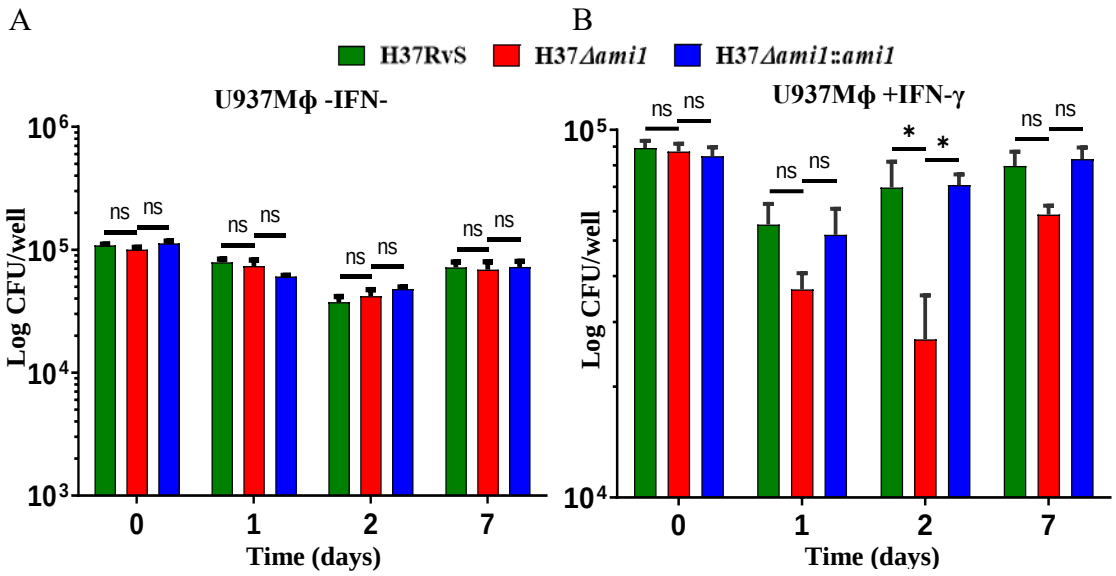


Figure 3.3.20. Survival of the ami1 mutant in macrophages. A) Intracellular survival of Mtb strains post infection of unactivated human U937 macrophages (U937 Mϕ). B) Intracellular survival of Mtb in IFN-γ activated U937Mϕ. Error bars represent the standard error of the mean (SEM) for three independent experiments. Statistical analysis was conducted using the Student's t-test, *: $P < 0.05$.

3.4 Discussion

Mycobacteria possess a unique cell wall structure and as a result, a large number of enzymes are required to co-ordinate cell growth and division whilst maintaining cell viability. The PG component of the bacterial cell wall is a rich source of drug targets with several existing antibiotics targeting it. For example, antibiotics such as β-lactams (penicillin, methicillin, and amoxicillin) and non-β-lactams (vancomycin) inhibit PG biosynthesis ultimately arresting cell growth in a variety of organisms. In mycobacterial species, β-lactams are ineffective due to the presence of several β-lactamases which rapidly degrade the peptide bond of the characteristic four-membered β-lactam ring resulting in antibiotic resistance (Flores et al., 2005).

In this study, we focused on characterizing a single class of PG-associated enzymes, namely the *N*-acetylmuramyl-L-alanine amidases, in Mtb. In general, these enzymes are classified as zinc metalloenzymes that are hydrolyse the amide bond between the glycan strand and stem peptide in PG (Vollmer et al., 2008, Heijenoort, 2011). In a previous study from our lab, we showed that Ami1, in Msm, was required for cell division. Deletion of *ami1* resulted in the formation of cellular chains, which remained viable. Where daughter cells failed to divide, lateral branching was evident. Interestingly, lateral budding was shown to due to the mislocalization of DivIVA, one of the major proteins driving polar elongation. Moreover, the failure of daughter cell division led to dysregulation of FtsZ, another major protein involved in cytokinesis. Msm cells lacking Ami1 were more susceptible to β-lactams (ampicillin, erythromycin, cefotaxime), non-β-lactams (vancomycin), rifampicin, cephalosporins (cefoxitin, ceftriaxone, cefapirin) – all of which were attributed to an increased cell wall permeability (Senani et al, 2018). More recently, Healy *et al* (2020) showed that the Ami1 homologue in Mtb (Rv3717) was dispensable for cell division but still required for persistence during chronic infection in mice. In Mtb, the D,L-endopeptidase RipA was shown to dispensable for growth but necessary for efficient cell division *in vitro* and *in vivo* (akin to the Ami1 homologue in Msm). Likewise, depletion of this major cell division enzyme sensitized Mtb to rifampicin and other cell wall-targeting antibiotics. The Mtb Ami1 homologue did however play a minor role in cell division in cells lacking RipA but this partial redundancy was not enough to compensate for the loss of RipA, particularly during infection (Healy et al., 2020).

In this study, deletion of *ami1* in Mtb, decreased the intracellular survival of Mtb in human U937 macrophages, corroborating findings from Healy et al (2020) in which Ami1 was required for the intracellular survival in the lungs of CB57BL/6 mice (Healy et al., 2020). Similarly, mouse stomach infections with the human gastric pathogen, *Helicobacter pylori* devoid of the *amiA* amidase gene (the only amidase in this organism), revealed that AmiA is required for colonization (Chaput et al., 2016). In other work, Frirdich et al. (2019) showed that the enteric pathogen, *Campylobacter jejuni* (*C. jejuni*) changes its morphology from helical to coccoid in response to adverse conditions. This change in morphorlogy required the amidase, AmiA and the DL-carboxypeptidase Pgp1 to act on the PG. Furthermore, the coccoid PG severely reduced Nod1 and Nod2 signaling in human embryonic kidney HEK293T cells compared to the PG from the helical form (Frirdich et al., 2019). Interestingly, the genome of the obligate intracelluar pathogen *Mycobacterium leprae* encodes two amidase genes, namely Ami1 and Ami2. As *M. leprae* is considered a minimal/reducitonist genome, retention of two amidases is likely to be significant, further supporting that Ami1 may be vital for the intracellular survival of mycobacterial species (Küssau et al., 2020). Collectively, the observations from previous studies, together with this study, highlight the importance of Ami1 in bacterial survival, virulence and immune evassion during infection.

We also assessed the impact of *ami1* deletion on bacterial growth and noted no differences relative to the wild type strain when grown in nutreint-rich media. Moreover, biofilm formation was unaffected by the deletion of *ami1* except when these were exposed to high concentrations of isoniazid or rifampicin. Over the time-course tested (2, 3 or 4 days of exposure), the mutant strain lacking *ami1* appearted to be less tolerant to isoniazid only. When the strains were grown in Sauton's minimal media (with or without a carbon source), growth of the *ami1* deletion mutant was significantly attenauted. These observations suggested that *ami1* may also play a role in PG recycling or in the selective metabolism of available carbon sources, such fatty acids from MA. To support a role for PG recycling, the ability of Mtb Ami1 to hydrolyse PG fragments, but not polymerised PG has been reported (Kumar et al., 2013). The deletion *ami1* in Msm led to the upregulation of *fadD32*, *fabD*, *kasB*, and *inhA*, all of which are genes involved in fatty acid metabolism (Miao et al., 2020). In *Mycobacterium abscessus*, there is evidence that the Ami1 homologue is specifically involved in PG remodelling. Following deletion of *ami1*, a slight increase in the susceptibility to β-lactam antibiotics was observed whereas the drug susceptibility profiles of antibiotics not targeting PG remained unaltered. This suggested that *ami1* deletion triggered a specific cell wall modification in PG rather than

general permeabilty (Küssau et al., 2020). In contrast, and as previously reported by Healy et al (2020), the deletion of *ami1* in Mtb (in our study) resulted in increased cell wall permeability. In both studies, the deltion of *ami1* was assocaited with increased susceptibilities to rifampicin and cell wall targeting antibiotics. Genetic complemetion with *ami1* restored drug suspectibility profiles to that of the wild type strain. Simiarly, in *Pseudomonas aeruginosa*, a mutant strain lacking the *amiB* amidase gene displayed an increased cell wall permeability and concomitant increased susceptibility to various cell wall-targeting antibiotics including gentamicin, tobramycin, vancomycin, and meropenem (Yakhnina et al., 2015). A more recent study in *Mycobacterium abscessus* demonstrated that a strain lacking the *ami1* homologue was also more susceptible to killing by cell wall damiging agents, including SDS, imipenem, cefuroxine and cefamandole (Küssau et al., 2020). We next sought to establish whether cell wall-targeting antibiotic potency would diminish differentilly over time. The mutant strain lacking *ami1* displayed an increased susceptibility to lysozyme, vancomycin, ethionamide and isonaizid. More specifically, in the wild-type and genetically complemented strains expressing *ami1*, cells were able to rebound growth after 7 days when exposed to vancomycin and ethionanide, an effect that was not seen in the *ami1* mutant strain. This suggested weakening of the cell wall as a result of *ami1* deletion. Interestingly, when strains were exposed to isonazid, the mutant strain lacking *ami1* was severely attenuated during the early stages of expoure (3 days). At 7 days, the mutant strain was able to recover to wild type levels but given that this was not associated with genetic drug resistance, we postualte that *ami1* is required for persistence in Mtb. In Msm, it was shown via microfluidics that persister cells can divide in the presence of isoniazid (Wakamoto et al., 2013). Thus is possible that Mtb persisters can do the same.

The INH-specific response of a PG-associated amidase in Mtb was intriguing and led us to investigating the observation further. We subsequently assessed the expression of three amidase homolgues (*ami1*, *ami3* and *ami4*) following exposure to isoniazid and showed that only *ami1* was induced over time, whereas the transcription of *ami3* and *ami4* remained largely unaffected. A previous study showed that when using the transcriptional regulator induced phenotype (TRIP) screen, *ami1* was part of the gene cluster upregulated in Mtb exposed to isoniazid (Ma et al., 2021). In certain instances, amidases are not strictly redundant but rather have specialist roles depending on environmental conditions, which could offer insights in the mechanism of *ami1* relative to *ami3* and *ami4*. For example. AmiB in *E.coli* is preferentially activated by the enzyme ActS in response to acidic conditions (Mueller et al., 2021). In *B.*

subtillis, only the transcription of the amidase, Yqil was upregulated in response to osmotic stress (Steil et al., 2003).

Collectively, our data point to an important role for Ami1 in Mtb for survival under nutrient limited conditions and for developing tolerance to INH. These effects were associated with the presence of an altered cell wall in the *ami1* mutant. The specific response of *ami1* to isoniazid exposure led us to identifying and characterizing putative transcriptional regulators of *ami1*, which will be discussed in the next chapter.

Space left intentionally blank

Chapter 4: Characterization of putative regulators of the *ami1* gene in *Mycobacterium tuberculosis*

4.1. Introduction

Careful regulation of PG hydrolases is not only required for preventing cell autolysis but also to facilitate essential cellular processes such a cell extension and division. Via the regulation of PG hydrolases, bacteria are readily able to adapt to external environment cues thus ensuring survival. In this chapter, we discuss the transcriptional and/or translation regulation of bacterial PG amidases and then explore mechanisms governing the regulation of the *ami1* gene in Mtb.

4.1.1. Regulation of amidase activity at protein level

LytM domain containing proteins

The active sites of most bacterial amidases involved in cell division contain auto-inhibitory domains as part of regulatory mechanisms preventing unregulated amidase activity (Yang et al., 2012). Rocaboy et al. (2013) demonstrated that the amidase-3 domain of AmiC in *E.coli* contains an α-helix that inhibits amidase activity via three potential mechanisms: 1) by blocking substrate entry via steric hindrance; 2) by chelating zinc ions before they reach the active site; or 3) by forming stable interactions in the catalytic site. Furthermore, they showed that expression of AmiC with a defective α-helix resulted in an active amidase enzyme that did not require activation. The active site of AmiB in *Bartonella henselae* is occluded by a conserved α-helix, AmiB variants with amino acid substitutions in this conserved α-helix similarly exhibited activity with the need for activation (Yang et al., 2012). In Mtb, it is postulated that a β-hairpin regulates the amidase activity of Ami1 by occluding the active site, preventing substrate entry (Kumar et al., 2013). These observations suggest that the auto inhibition of amidases via modifications in the structural elements of the active site requires external factors to effect conformational changes to activate these enzymes. Consistent with this, Yang et al. (2012) demonstrated that EnvC and NlpD in *E. coli* effect conformational changes that remove the auto inhibitory domains away from the active site. Rocaboy et al., (2013) showed that NlpD directly interacts with AmiC in *E. coli*, supporting the premise of allosteric activation of amidases by LytM domain containing proteins.

LytM domain (Pfam, peptidase_M23) containing endopeptidases have previously been shown to activate amidases in various bacterial species (Uehara et al., 2009, Ercoli et al., 2015, Möll et al., 2014). These enzymes are characterised by a degenerate M23 domain, which lacks Zn^{2+}

coordinating residues required for endopeptidase activity (Meisner et al., 2012, Peters et al., 2013). The genome of *E.coli* encodes four LytM domain-containing proteins, namely EnvC, NlpD, ActC (formerly known as YgeR), and YebA (Uehara et al., 2009, Uehara et al., 2010, Singh et al., 2012, Mueller et al., 2021). EnvC and NlpD are the most extensively studied amidase activators, with evidence that they regulate the activities of *E. coli* AmiA, B and C during cell division. More specifically, EnvC is thought to activate AmiA and B whereas NlpD activates AmiC (Uehara et al., 2009, Uehara et al., 2010). However, a very recent study in *E.coli* revealed that EnvC and NlpD are capable of activating AmiA, B, and C (Mueller et al., 2021). A third LytM protein, ActS, has also been shown to activate *E. coli* amidases but it is likely that it has a specialist role under conditions of environmental stress such as growth in acidic conditions (Mueller et al., 2021). Despite ActS being able to activate all three amidases, it preferentially activates AmiC (Chodisetti et al., 2022). YebA is the only amidase activator with a catalytically active LytM domain, exhibiting DD-endopeptidase activity (Singh et al., 2012). The role of YebA in cell division is minor relative to EnvC/NlpD as evidenced by the subtle cell division defects seen in a *ΔyebAΔygeR* strain relative to a *ΔEnvCΔnlpD* strain (Uehara et al., 2009). The deletion of the *yebA* homologue in *Haemophilus influenzae* resulted in defective cell division, membrane blebbing and a disrupted cell wall architecture (Ercoli et al., 2015). Conversely, in *H. influenza*, EnvC is not the main cell division amidase activator as gene deletion resulted in a dramatic decrease in cell surface proteins, suggesting that EnvC possible mediates cell surface protein transport through PG (Ercoli et al., 2015). The same study showed that the *ΔnlpD* mutant displayed a weakened adherence to epithelial cells and an inability to produce mature biofilms.

The human pathogen, *Vibrio cholera* encodes a single amidase (AmiB) that is activated by both the equivalent EnvC and NlpD homologues (Möll et al., 2014).The same study demonstrated that at least one activator is required for efficient cell division, similar to *E.coli* (Uehara et al., 2009, Uehara et al., 2010). Moreover, Möll et al. (2014) showed that the activation of amidase activity by EnvC or NlpD is dependent on environmental conditions. For example, NlpD specifically regulated amidase activity during intestinal colonization in mouse models and in response to bile salts.

The AmiB homologue in *Pseudomonas aeruginosa* is essential for growth and division. Depletion of AmiB results in growth and division defects, as well as an increased cell wall permeability and susceptibility to drugs including gentamicin, tobramycin, vancomycin, and meropenem (Yakhnina et al., 2015). Collectively, these studies demonstrate that LytM domain

containing enzymes are regulators of amidase activity, which is essential during the processes of cell growth and division, antibiotic resistance, and virulence. In addition to LytM proteins, there are activation mechanisms that are independent of LytM.

Non-LytM domain containing proteins that regulate amidase activity

In *B. subtilis*, the cell wall binding protein, CwbA was shown to specifically stimulate the activity of amidases CwlA and CwlB (Kuroda and Sekiguchi, 1992). CwbA does not possess catalytic activity and is homologous to the N-terminal, non-catalytic domain of CwlB as opposed to a degenerate LytM domain (Kuroda and Sekiguchi, 1992) In the spore forming *Clostridioides difficile*, the lipoprotein GerS allosterically binds the CwlD amidase allowing the binding of Zn^{2+}, thereby activating the enzyme (Alves Feliciano et al., 2021). The ClpXP protease regulates Slei amidase activity in *S. aureus*. In a mutant stain lacking ClpXP activity, Slei activity was unregulated (and high), which resulted in an increased resistance to β-lactam antibiotics (Thalsø-Madsen et al., 2019). The *S. aureus* membrane associated protein ActH, is a regulator of LytH because deletion of the gene encoding ActH led to retarded cell growth and enlarged cells that were incapable dividing – morphologies which phenocopy the Δ*lytH* mutant (Do et al., 2020b). In Msm, the HtrA protease interacts with the lipoprotein LppZ to cleave cytoplasmic Ami3 so that it accumulates in the cytoplasm thereby minimizing cell toxicity due to autolysis of the external PG (Wu et al., 2019).

4.1.2. Regulation of amidase activity at transcriptional level

Sigma factors

Bacterial sigma (σ) factors regulate gene expression by inducing transcription through interaction with the core RNA polymerase (Helmann and Moran, 2002). Bacteria produce a variety of σ factors that regulate genes involved in specialised bacterial processes or that regulate the basal expression of housekeeping genes. In *B. subtilis*, the genome encodes at least 17 σ factors that regulate sporulation genes, amongst others, in response to adverse environmental conditions (Britton et al., 2002). The biological role of amidases in *B. subtilis* sporulation was previously discussed in section 3.1.2. In this section, we discuss the transcriptional regulation of amidases via sigma factors during sporulation and in the vegetative state.

Cell division in the vegetative state is regulated by σ factor D, which controls the transcription of LytC (CwlB) and the glucosamidase LytD (Blackman et al., 1998). In the vegetative state, cells can adopt two morphologies, namely as individual motile cells with flagella, or as nonmotile cell chains (Kearns and Losick, 2005). Chen et al. (2009) demonstrated that σ factor D induces the expression of LytC (CwlB) to influence flagella motility. Sporulation specific σ factor K, drives the expression of CwlH, which is associated with mother cell lysis and spore germination (Nugroho et al., 1999). In addition, multiple σ factors can regulate the activity of a single amidase at different time points. For example, during the initiation of sporulation, CwlD expression is driven by σ factor E, whereas σ factor G drives CwlD expression post sporulation (Sekiguchi et al., 1995). Given that CwlD is involved in maintenance of the endospore PG cortex, it is possible that σ factor E drives CwlD expression to form endospores, whereas σ factor G would induce CwlD expression to alter endospore PG cortex to promote spore germination (Sekiguchi et al., 1995, Atrih et al., 1996, Gilmore et al., 2004).

Two component systems

There are not many examples of two-component systems involved in amidase regulation. The WalK/WalR two-component system in *S. aureus* is a transcriptional activator of the amidase, SleI. Depletion WalKR proteins decreases PG synthesis and biofilm formation (Dubrac et al., 2007). In *E. coli* and *Salmonella*, the transcription of *amiA*, *amiC* and *mar* is regulated by the CpxR/CpxA two-component system in which the CpxR TF interacts with the -10 bp and -35 bp region upstream of the amidase encoding genes to regulate responses to a variety of periplasmic stresses such as cationic antimicrobial peptides (CAMPs)(Weatherspoon-Griffin et al., 2011).

In this chapter, we explore mechanisms of regulation for the *ami1* gene in Mtb.

Hypothesis

In the previous chapter, we demonstrated that *ami1* is transcriptionally (and specifically) induced in the presence of INH. Based on this, we hypothesize that the genome of Mtb encodes a transcription factor (s) or regulator (s) that bind to the upstream region or within the *ami1* gene and that these respond directly to INH to effect changes in the expression of *ami1*.

Primary aim: To identify and study the transcriptional regulators of Ami1.

Objective 1: Conduct bioinformatics analysis of amidase regulators by:

- Searching the TB database (weblink) for possible *ami1* transcriptional regulators.
- Conducting secondary structure predictions for putative regulators and identification of binding sites.

Objective 2: Clone and express recombinant forms of putative regulators, specifically:

- Clone open reading frames for regulators in an, E. coli recombinant expression system.
- Test expression conditions to optimize yield of proteins.
- Purify regulators.

Objective 3: Characterize regulators using electrophoretic mobility shift assays (EMSA), specifically:

- Establish EMSA conditions and test binding of recombinant regulators to the promoter region.

Objective 4: Characterize regulators in Mtb, specifically:

- Monitor the phenotypic effects of over expressing putative Ami1 regulators in H37RvS.

Space left intentionally blank

4.2. Methods

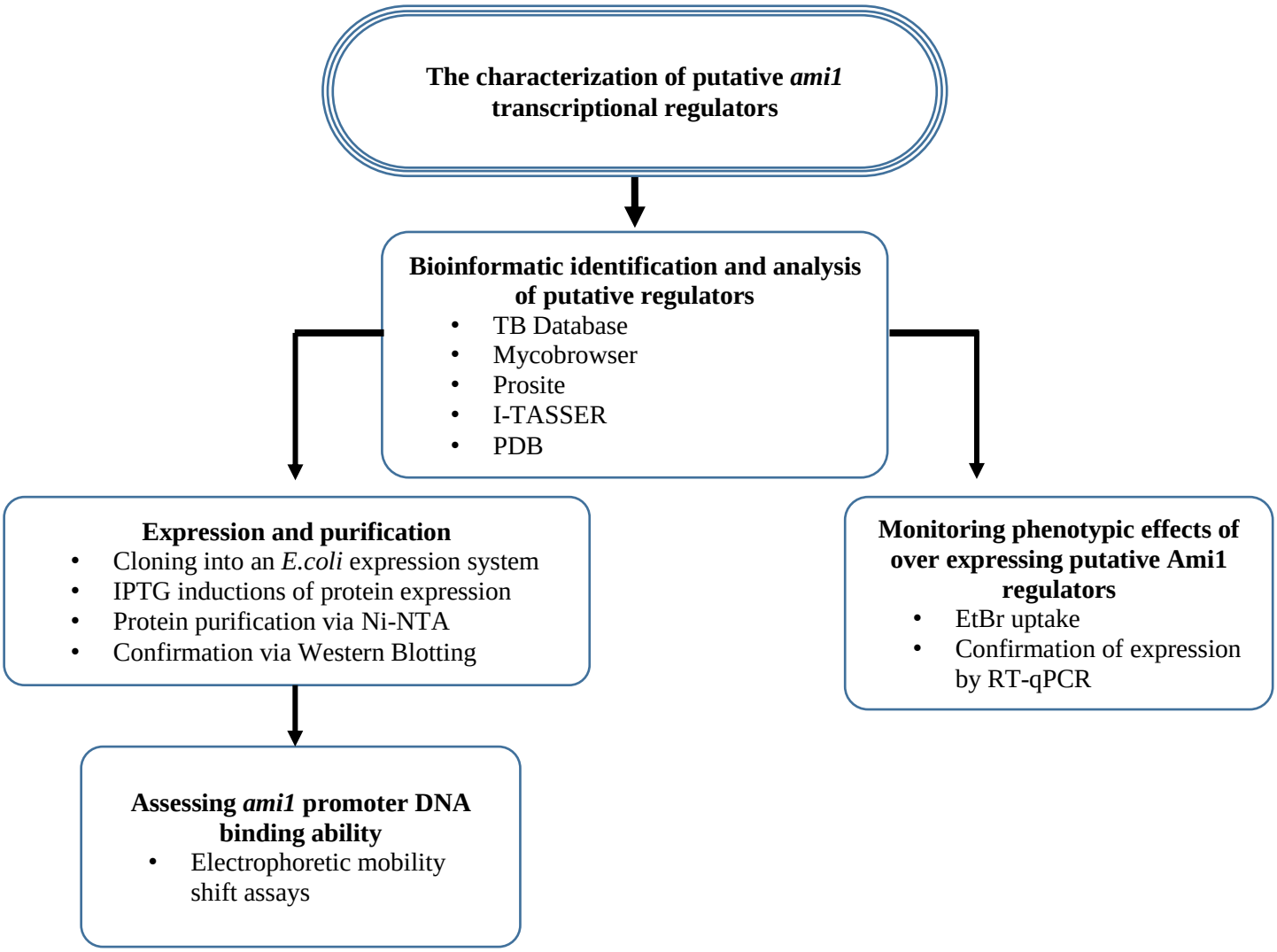


Figure 4.1. An overview of the methodology used in this study.

Table 4.2.1. Bacterial strains used in this study

Bacterial strain	Description	Reference
E. coli DH5α	*SupE44 ΔlacU169 hsdR17 recA1 endA1 gyrA96* *thi-1 relA1*	Promega, Madison, WI
E. coli BL21 (DE3)	Lysogen of the bacteriophage DE3, *lacI*, *lacUV5* promoter, *T7RNApol*	TaKaRa Bio
E. coli BL21_Rv1423	A derivative of *E. coli* BL21 (DE3) with a pET_Rv1423 expression plasmid, Kan^R	This study
E. coli BL21_Rv1776c	A derivative of *E. coli* BL21 (DE3) with a pET_Rv1776c expression plasmid, Kan^R	This study
E. coli K12Δ*lacizya*::Δ*envC*,Δ*nlpD* (Δ*envC*_Δ*nlpD*)	*E. coli* cell division-defective strain lacking *envC* and *nlpD* genes, Kan^R.	Uehara et al. (2009)
E. coli Δ*envC*_Δ*nlpD*::Rv3717	Derivative of Δ*envC*_Δ*nlpD* expressing the Mtb *ami1* gene	This study
Mtb H37*_Rv1423*	Derivative of H37RvS carrying a pEXNF*_Rv1423* episomal expression plasmid, Hyg^R	This study
Mtb H37*_Rv1776c*	Derivative of H37RvS carrying a pEXNF*_Rv1776c* episomal expression plasmid, Hyg^R	This study

Hyg^R: Hygromycin resistance, Kan^R: Kanamycin resistance

Space left intentionally blank

Table 4.2.2. Standard PCR primers used in this study

Gene	Primers (5'-3')	Position	Amplicon
pFLAG *Rv1423*	F: GTGTGTACAATGACGACCGATGTCAAA	1-18 bp DS	972 bp
	R: GTGTGTACACCGGCGTCTTCCAGC	954-972 DS	
pFLAG *Rv1776c*	F: GTGTGTACAGTGCCGGGTAACGAT	1-18 bp DS	555 bp
	R: GTGTGTACACCGCTTTGCTCGGCAAAC	537-555 bp DS	
pET29a+ *Rv1423*	F: GTGGAATTCATGACGACCGATGTCAAA	1-18 bp DS	972 bp
	R: GTGAAGCTTGGCGTCTTCCAGCAGATC	954-972 DS	
pET29a+ *Rv1776c*	F: GTGGAATTCATGCCGGGTAACGATTGG	1-18 bp DS	555 bp
	R: GTGAAGCTTGCTTTGCTCGGCAAACGC	537-555 bp DS	

Restriction sites highlighted in red. Restriction sites indicated in red. US: Upstream. DS:Downstream. Primer start codons are highlighted in yellow. Primer stop codons are highlighted in green.

Space left intentionally blank

Table 4.2.3. Plasmids used in this study

Plasmid	Description	Reference
pFLAGEM	*E. coli-Mycobacterium* episomal shuttle vector carrying a 3X FLAG epitope sequence downstream Pmyc-*tetO*; Hyg^R	CBTBR lab stock
pRv1423FLAG	A derivative of pFLAGEM carrying a *Rv1423* gene	This study
pRv1776cFLAG	A derivative of pFLAGEM carrying a *Rv1776c* gene	This study
pET29a+	Protein expression plasmid with T7*lac* signalling sequence, f1 origin of replication, a C-terminal His-tag and a Thrombin protease sequence, Kan^R	Novagen
pET_Rv1423	A derivative of pET29a+with a *Rv1423* gene, Kan^R	This study
pET_Rv1776c	A derivative of pET29a+with a *Rv1776c* gene, Kan^R	This study
pEXNF_*Rv1423*	An expression vector with a FLAG tag at the *Rv1423* N-terminus and an ATC inducible promoter, Hyg^R	Rustad et al., 2014
pEXNF _*Rv1776c*	An expression vector with a FLAG tag at the *Rv1776c* N-terminus and an ATC inducible promoter, Hyg^R	Rustad et al., 2014
p-4CAmi1	Derivative of pMV306 carrying the *ami1* gene and its promoter region (400bp up stream), Hyg^R	CBTBR lab stock

Hyg^R: Hygromycin resistance, Kan^R: Kanamycin resistance

Table 4.2.4. Standard RT qPCR primers used in this study

Gene	Primers (5'-3')		Amplicon (bp)
ami1	F: CGGATTCCACGTCAACTACTC	402-420 bp DS	186 bp starting at 402 bp downstream the *ami1* start codon
	R: GACGGATATTGGGCTAGGTTC	569-587 bp DS	
Rv1423	F: TTGGAGATCCTCGGCGATA	742-759 bp DS	131 bp starting at 742 bp downstream the *Rv1423* start codon
	R: GCTACAGCGTCTTTCGTCAT	854-872bp DS	
Rv1776c	F: ACTTTGCTACCGAGCTCAC	398-416 bp DS	114 bp starting at 398 bp downstream the *Rv1776c* start codon
	R: GTTCGGCTTCGTCGTTCT	493-511 bp DS	
sigA	F: TGCAGTCGGTGCTGGACAC	1379-1397 bp DS	195 bp starting at 1379 bp downstream the *sigA* start codon
	R: CGCGCAGGACCTGTGAGCGG	1555-1573 bp DS	

DS:Downstream

4.2.1. Investigating Ami1 transcription regulator

4.2.1.1. *In sillico* identification and analysis of putative Ami1 transcription regulators

The TB Database (http://tbdb.bu.edu/tbdb_sysbio/OperonBrowser.html) was used to predict the transcriptional regulators of Ami1 and their DNA binding sites. Two amino acid sequences for Rv1776c and Rv1423 respectively were retrieved from Mycobrowser (https://mycobrowser.epfl.ch/) for use in structural prediction studies. The PROSITE database (https://prosite.expasy.org/) and the Iterative Threading ASSEmbly Refinement (I-TASSER) database (https://zhanggroup.org/I-TASSER/) were used for the prediction of the protein secondary structure and structural homology modelling respectively.

4.2.2. Expression and purification of FLAG-tagged Rv1423 and Rv1776c

The *Rv1423* and *Rv1776c* genes were amplified as outlined in Section 2.3.1.2 using the primers described in Table 4.2.2. The cycling conditions were as follows: Initial denaturation at 95^{o}C for 4 min; followed by 34 cycles of denaturation at 95^{o}C for 30 sec, annealing at (60^{o}C for Rv1776c and 65^{o}C for Rv1423) for 30 sec and elongation at 72^{o}C for 90 sec; thereafter, the final elongation at 72^{o}C for 7 min. Thereafter, Both *Rv1423* and *Rv1776c* were cloned into the pFLAGEM plasmid (Table 4.2.3) using the restriction sites *BsrGI* and *BsiWI* as described in section 2.3. This would allow for the C-terminal tagging of both mycobacterial proteins. Recombinant plasmids were transformed into *E. coli* DH5α (Table 4.2.1) cells as outlined in

section 2.4.1. *E. coli* DH5α cells expressing 3× FLAG tagged Rv1423 and Rv1776c were cultured up to an OD600nm of 0.8 in 50 ml of LB media supplemented with hygromycin (200 µg/ml). The cells were then pelleted at 4000 × g for 10 min and resuspended in 1 ml of the B-PER (bacterial protein extraction reagent) (Thermo-Fischer) cocktail containing protease inhibitor. Cells were lysed with a French press (Constant systems, Ltd) at 1.9 kBar. The cell lysate was collected and centrifuged at 11 000 × g for 15 min at 4°C to harvest the insoluble cell lysate fraction and any intact cells. The insoluble fraction was re-suspended in 1 ml of lysis buffer. The desired protein was expected to be in the soluble fraction. All cell fractions were analysed by SDS-PAGE gels (Section 4.2.4). Anti-FLAG M2® magnetic beads (Sigma) were used to purify FLAG-tagged proteins as per manufacturers' instructions and analysed by SDS-PAGE. FLAG-tagged Rv1423 and Rv1776c purifications were confirmed by Western blots (Section 4.2.5) using ANTI-FLAG M2 Monoclonal Antibody (Sigma).

4.2.3. Expression and purification of His-tagged Rv1423 and Rv1776c

4.2.3.1. Induction of protein expression

The *Rv1423* and *Rv1776c* genes were amplified using the primers described in Table 4.2.2 under the cycling conditions described in 4.2.2. *Rv1423* and *Rv1776c* were cloned into the pET29a+ plasmid (encoding a histidine hexamer sequence, HHHHHH) using the restriction sites *EcoRV* and *HindIII* as described in section 2.3. This would allow for the C-terminal tagging of both proteins. Recombinant plasmids were transformed into *E. coli* DH5α cells and subsequently into *E. coli* BL21 cells as outlined in section 2.4.1. Protein expression was induced at 37°C for 4 hrs or at 20°C overnight with 1 mM isopropyl β-D-1-thiogalactopyranoside (IPTG). A single colony of an *E. coli* BL21 (DE3) strain expressing the desired protein was grown in a 5 ml pre-culture of LB containing the appropriate antibiotic at 37°C overnight with shaking at 200 rpm. Thereafter, the pre-culture was inoculated into a 100 ml or 1 L of media and grown up to an OD600nm of 0.5 at 37°C with shaking at 200 rpm. Prior to the addition of IPTG, a 1 ml aliquot of culture was collected and harvested at 11 000 × g for 5 min at room temperature. The cells were then re-suspended in 200 µl B-PER and frozen overnight at -20°C. This served as the uninduced control. To the remaining culture, 1 mM IPTG was added, which was further incubated either at 37°C for 4 hrs or at 20°C overnight with shaking at 200 rpm. After the induction of recombinant protein expression, 1 ml aliquots of the culture were collected at various times for monitoring expression. These samples were

resuspended in B-PER in a manner similar to the uninduced control and run on a SDS PAGE gel.

4.2.3.2. Cell lysis

Post the induction of protein expression (section 4.2.3.1); cells were harvested at 4000 x g for 15 min at 4°C. The cells were then re-suspended in the desired volume (depending on the scale of protein induction) of lysis buffer/equilibration buffer (50 mM Na_2HPO_4, 150 mM NaCl, 5 mM imidazole, 5% (v/v) glycerol; pH 6.8) supplemented with complete protease inhibitor cocktail (Roche) to prevent protein degradation by proteases during cell lysis (1 tablet per 10 ml lysis buffer). Cells were lysed with a French press (Constant systems, Ltd) using the following settings: 1.9 kBar in batches of 6 ml at a time. The cell lysate was collected and centrifuged at 11 000 × g for 15 min at 4°C to harvest the insoluble cell lysate fraction and any intact cells. The insoluble fraction was re-suspended in 1 ml of lysis buffer.

4.2.3.3. Protein purification with Nickel-NTA (Ni-NTA) column

Purification was carried out using an 8 ml his-select Ni-NTA column connected to a Biologic LP system (Bio-Rad) as described below.

4.2.3.3.1. Ni-NTA column preparation

The column was stripped by washing with 8-10 column volumes of 50 mM EDTA, pH 8 followed by a wash with at least 3-5 column volumes of 0.5 M NaOH. Thereafter, the column was washed with 5-8 column volumes of binding buffer (50 mM Na_2HPO_4, 0.3 M NaCl, 10 mM imidazole, pH 7.8) and 5-8 column volumes of dH_2O. Subsequently, the column was recharged with 3-4 column volumes of 50 mM $NiCl_2$ and followed by a wash with 5 column volumes dH_2O, and 5 column volumes of binding buffer before use or storage in 20% ethanol.

4.2.3.3.2. Protein purification

After the Ni-NTA column had been stripped and recharged as outlined in section 4.2.3.3.1, it was equilibrated by washing with 30 ml of equilibration buffer (50 mM Na_2HPO_4, 150 mM NaCl, 5 mM imidazole, 5% (v/v) glycerol, pH 7.8) at a flow rate of 1 ml/minute. The soluble cell lysate obtained as outlined in sections 4.2.3.2 was loaded onto the equilibrated his-select Ni-NTA column, followed by a wash with 70 ml of the equilibration buffer, both at a flow rate of 1 ml/minute. A 20 ml volume of flow-through containing unbound proteins was collected

immediately after commencing the wash with equilibration buffer. After the wash, the desired His-tagged protein was eluted off the column with a 40 ml gradient of 250 to 500 mM imidazole, with buffer A (50 mM Na_2HPO_4, 150 mM NaCl, 250 mM imidazole, 5% (v/v) glycerol, pH 7.8) and buffer B (50 mM Na_2HPO_4, 150 mM NaCl, 500 mM imidazole, 5% (v/v) glycerol, pH 7.8), at a flow rate of 1 ml/minute. The eluate was collected in 1 ml fractions with the aid of the Fraction Collector-2110 (Bio-Rad) and quantified on the NanoDrop (ND-1000). An elution profile was developed from the quantification and eluates where peak protein quantifications where visualised on an SDS-PAGE gel, as described in section 4.2.4.

4.2.3.3.2. High salt wash

The high salt wash technique was used to clean protein eluates and to lessen the binding of non-specific proteins to the His-select Ni-NTA column. Eluates obtained as outlined in the previous section and were pooled together and loaded onto 8 ml of pre-equilibrated his-select Ni-NTA column at a flow rate of 1 ml/minute. Equilibrated involved washing with 30 ml of equilibration buffer, charging with 30 ml 50 mM of $NiCl_2$, followed by a further 60 ml wash with the equilibration buffer, all at a flow rate of 1 ml/minute. After the pooled protein had been loaded, the his-select Ni-NTA was washed using 60 ml high salt wash buffer 50 mM Na_2HPO_4, 0.3 M NaCl, 20 mM imidazole, pH 7.8). A 20 ml volume of flow through was collected immediately after commencing the high salt wash. Thereafter, the His-tagged protein was re-eluted off the column with a 40 ml gradient of 250 to 500 mM imidazole, with buffer A and buffer B at a flow rate of 1 ml/minute, as described in the prior section. The eluate was collected and quantitated as described in section 4.2.3.3.1. The eluates were visualised on an SDS-PAGE gel, as described in section 4.2.4.

4.2.4. Sodium dodecyl sulfate–polyacrylamide gel electrophoresis (SDS-PAGE)

SDS-PAGE gels were used for the visualisation of protein fractions and cell lysates. SDS-PAGE gels of the desired concentration were prepared by mixing Tris-HCl buffer, 40% (w/v) bisacrylamide, 10% (w/v) SDS, 10% (w/v) ammonium persulfate (APS) and TEMED to a final concentration of 0.125 M Tris-HCl, 0.1% (w/v) SDS, 0.1% (w/v) APS and 0.1% (v/v) TEMED, as described in Table 4.2.5. The resolving gel was cast first in the Bio-Rad casting system and a small volume of isopropanol was added to level the gel. The gel was left to solidify at room temperature for 30 min. The isopropanol was poured off the gel and dH_2O was used to rinse

off the remaining isopropanol. The stacking gel was prepared and poured on top of the resolving gel in the casting system, followed by the insertion of a well comb. The stacking gel was also left to solidify at room temperature for 30 min. The gel was placed in Mini protean tetra cell tanks (Bio-Rad laboratories), which was subsequently filled with 1x SDS-PAGE running buffer (25 mM Tris, 192 mM glycine, 0.1% (w/v) SDS, pH 7.5). Before loading, protein samples were mixed with 5× SDS-PAGE loading dye (62.5 mM Tris-HCl, 10% (v/v) glycerol, 2% (w/v) SDS, 5% (v/v) β- mercaptoethanol, 5% (w/v) bromophenol blue) at a ratio of 4:1 and samples were then boiled at 95°C for 5 min. Samples were loaded into the wells of the stacking gel along with the PAGE-Plus pre-stained protein ladder (Thermo Scientific). SDS-PAGE gels were run at 80-100 V at room temperature for 2-3 hrs. SDS-PAGE gels were either visualised by staining with Coomassie R250 dye or used for western blots (Section 4.2.5). For visualisation, SDS-PAGE gels were rinsed with dH_2O and stained with Coomassie R250 stain (0.1% (w/v) Coomassie R250, 40% (v/v) methanol and 10% (v/v) acetic acid) overnight. Thereafter, the stain was poured off and stored for repeated usage and the gels were then washed with dH_2O and de-stained at room temperature in destaining solution (40% (v/v) methanol and 10% (v/v) acetic acid) with gentle agitation.

Table 4.2.5. SDS-PAGE gel recipes.

Component	4% stacking gel	12% resolving gel	15% resolving gel
dH_2O	3.15 ml	6.9 ml	5.7 ml
40% (w/v) bisacrylamide	0.5 ml	4.8 ml	6 ml
0.5 M Tris-HCl pH 6.8 (stacking)/1.5 M Tris-HCl pH 8.8 (resolving)	1.25 ml	4 ml	4 ml
10% (w/v) SDS	50 µl	160 µl	160 µl
10% (w/v) APS	50 µl	160 µl	160 µl
TEMED	5 µl	16 µl	16 µl

4.2.5. Western Blot analysis

Western blot with an anti-His conjugate antibody (Sigma) was used to verify the expression of His-tagged proteins. An SDS-PAGE gel with the protein samples was rinsed in dH_2O and layered with a methanol-equilibrated polyvinylidene fluoride (PVDF) membrane (Bio-Rad).

The gel and the membrane were sandwiched between four Whatman filter papers and placed in the transblot transfer cassette (Bio-Rad). Transfer of proteins from the SDS-PAGE gel to the PVDF membrane was performed at 2.5 A for 10 min. The PVDF membrane was incubated in blocking solution (5% (w/v) skim milk powder, 20 mM Tris, 140 mM sodium chloride, 0.1% (v/v) Tween 20, pH 7.6) overnight at 4°C. The anti-his conjugate antibody was added to the blocking solution in a 1:25 000 antibody to blocking solution ratio and incubated at room temperature for 30 min to allow antibody binding. The membrane was washed three times in TBST wash buffer (20 mM Tris, 140 mM sodium chloride, 0.1% (v/v) Tween 20, pH 7.6) for 5 min on a rocking platform at room temperature. This allowed for the removal of unbound antibody. The membrane was placed in a hybridisation bag and 1 ml chemiluminescent peroxidase substrate (CPSD) was added onto the membrane and incubated at room temperature for 10 min. Excess CPSD was then removed and the hybridisation bag was sealed. Thereafter, the membrane was exposed to X-ray film (Kodak Biomax Light or CL-Xposure™ Film-Thermo Scientific) for 30 sec to 2 min. The X-ray film was developed manually by washing in X-ray film developer (Axim) for 30 sec followed by dH_2O for 30 sec. The X-ray film was then incubated in fixative (Axim) for 30 sec, rinsed in dH_2O for 30 sec and then air-dried.

4.2.6. Electrophoretic mobility shift assay (EMSA)

EMSAs were performed to observe if putative transcription regulators of *ami1* were able to bind the promoter regions of *ami1*. EMSAs were performed in 10% PAGE gels (Table 4.2.6) with a mixture of 40% (w/v) bisacrylamide, 5x Tri-borate EDTA (TBE) buffer (AMRESCO), triethylene glycol, 10% (w/v) ammonium persulfate (APS) and TEMED to a final concentration of 1x TBE, 20 % triethylene glycol, 0.1% (w/v) APS and 0.2% (v/v) TEMED. For the binding reaction, a 5× binding buffer (10 mM HEPES, pH 7.5, 1 mM $MgCl_2$, 100mM KCl, 10% (w/v) glycerol and 0.1 mg/ml BSA) was prepared. The binding reaction contained a final concentration of 1× Binding buffer, 0.5µM DNA and a various titrated concentrations of the desired protein and dH_2O. The binding reactions were performed at 4^oC. Samples were mixed with 5× loading dye with no SDS (62.5 mM Tris-HCl, 10% (v/v) glycerol, 5% (w/v) bromophenol blue) at a ratio of 4:1 and ran on a PAGE gel at 160 V at 4^oC. For visualisation, the gels were stained post PAGE with SyBr green (30µl in 30 ml TBE).

Table 4.2.6 PAGE gel recipes for a 10 ml gel.

Component	10 % resolving gel
dH_2O	2.6 ml
40% (w/v) bisacrylamide	3.4 ml
20% triethylene glycol	2 ml
TBE	2 ml
10% (w/v) APS	75 µl
TEMED	25 µl

4.2.7. EtBr uptake

The EtBr uptake assay was performed on Mtb strains as outlined in Chapter 3 (section 3.2.4.1).

4.2.8 RT-qPCR for monitoring ami1, ami3 and ami4 expression post INH exposure

Mtb strains, H37_*Rv1423* and H37_*Rv1776c* (Table 4.2.1), were respectively induced to express Rv1423 and Rv1776c, by adding ATC at 50, 100 and 200 ng/ml. RNA samples were collected for assessing the transcription of *ami1*, *Rv1423* and *Rv1776c* at each concentration as outlined in section 2.5. Gene expression was also monitored in controls that were not exposed to ATC. The housekeeping gene, *sigA* was used as a reference for constitutive expression. RT-qPCR primers for *ami1*, *Rv1423* and *Rv1776c* are outlined in table 4.2.4.

4.2.9. Heterologous expression of Ami1 in *E.coli*

The mycobacterial pMV_-4CAmi1 plasmid (the recombinant plasmid containing the Mtb *ami1* gene and its associated 400 bp upstream region) was transformed into the wild-type *E. coli* strain and an *E. coli* strain lacking envC and *nlpD* as described in section 2.4.1. The phenotypes of *E. coli* heterologously expressing Mtb *ami1* were monitored by phase contrast microscopy.

4.3. Results

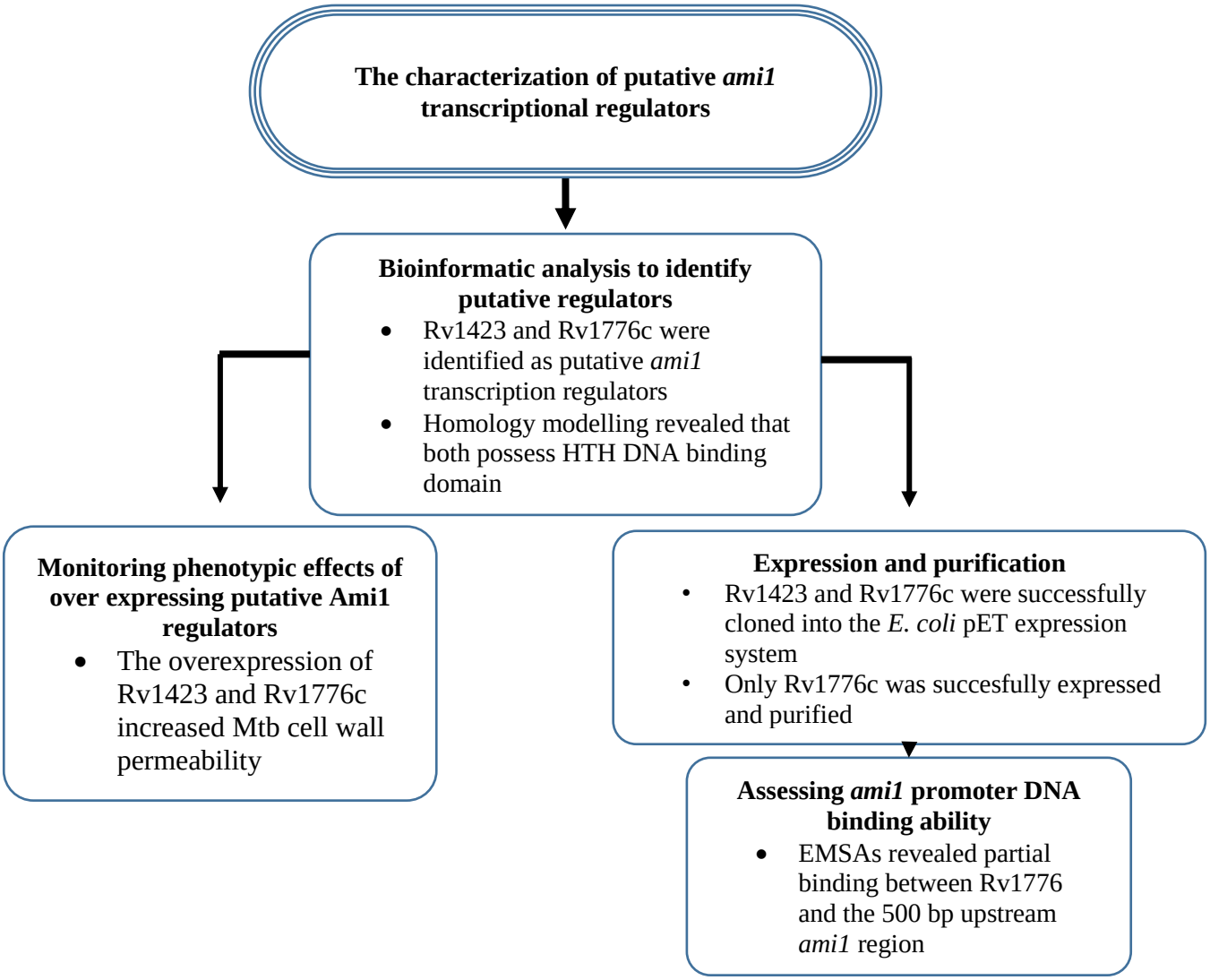
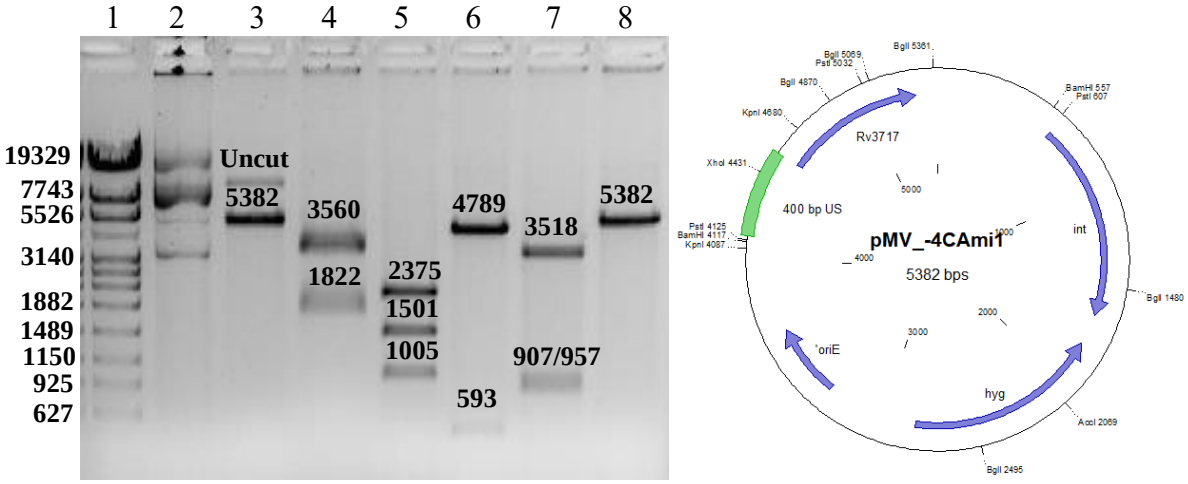


Figure 4.2. An overview of the findings of this study.

4.3.1. Preliminary data to determine regulatory mechanisms for Ami1 in Mtb.

As mentioned in the introduction, amidases in a variety of organisms are regulated through allosteric mechanisms. In these cases, amidases are produced in an inactive form. To investigate whether a similar situation prevails in mycobacteria, we opted to attempt heterologous expression of the Mtb Ami1 in the *E. coli envC-nlpD* mutant, which displays a cell chaining phenotype due to the inability to degrade the septum. Here the hypothesis was that if the Mtb amidase was active, and did not need activation by EnvC/NlpD, and if it were expressed in *E. coli*, it would resolve the chaining defect. We first cloned the *ami1* gene into a mycobacterial integrating vector (restriction mapping confirmed in Figure 4.3.1) and transformed this into the *E. coli* mutant.



Restriction enzyme	Expected band size
AccI	5382
BamHI	3560, 1822
BglI	2305, 1501, 1005
KpnI	4789, 593
PstI	3518, 957, 907
XhoI	5382

Figure 4.3.1. Restriction digests of pMV_-4CAmi1. Restriction mapping confirmed the cloning of *ami1* and the 400bp region upstream the *ami1* start site, into pMV306H. Lane 1: DNA molecular marker IV, Lane 2: Undigested construct, Lane 3: *AccI*, Lane 4: *BamHI*, Lane 5: BglI, Lane 6: *KpnI*, Lane 7: *PstI*, Lane 8: *XhoI*. All restriction digests produced DNA fragments with the expected sizes. It should be noted that *AccI* did not completely digest the plasmid.

This heterologous expression experiment revealed that insertion of a plasmid carrying the Mtb *ami1* gene into the *E. coli* Envc-NlpD defective mutant resolved the chaining defect, suggesting that the Mtb Ami1 is active, Figure 4.3.2 This experiment did have limitations in that heterologous expression is challenging for a variety of reasons and drawing firm conclusions is difficult. Nevertheless, these observations prompted us to search for transcriptional regulators of the *ami1* gene.

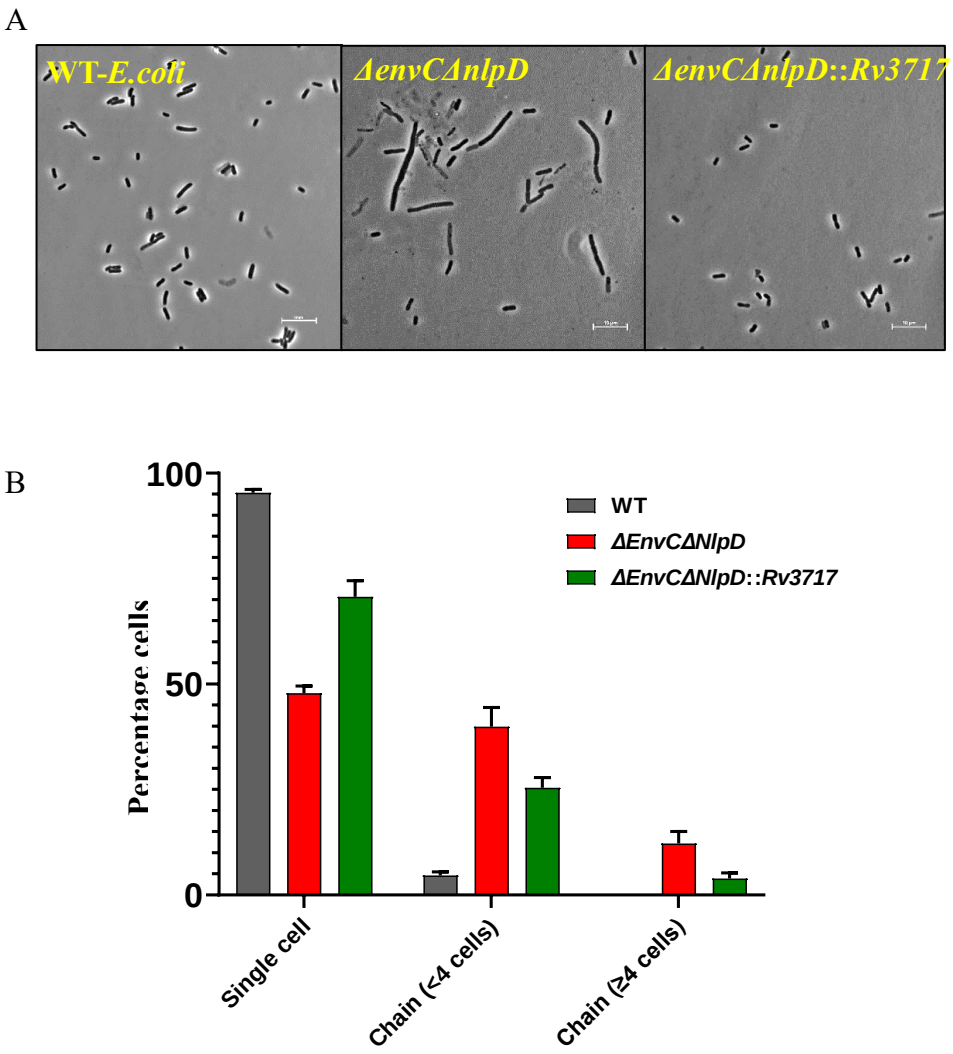


Figure 4.3.2. The activity of Ami1 is not dependent on amidase activators, EnvC and NlpD. A plasmid containing the Mtb *ami1* gene (*Rv3717*) was transformed into the *E. coli* strain, *ΔenvCΔnlpD,* which is devoid of amidases activators EnvC and NlpD. (A) Phase contrast micrographs of *E. coli* strains, WT, *ΔenvCΔnlpD*, and *ΔenvCΔnlpD*::*Rv3717*. (B) Bar graph showing the percentage of cells, displaying chaining. Scale bar 10 µM.

4.3.2. Identification and characterization of putative *ami1* transcriptional regulators

The observed increase in *ami1* transcription in response to INH led to the investigation of possible regulators of *ami1* transcription. By probing the TB Database for transcriptional regulators of the ami1 gene, Rv1776c and Rv1423, were identified as possible negative regulators (repressors) of *ami1* transcription (Figure 4.3.3) (http://tbdb.bu.edu/cgi-bin/GeneDetails.html?id=SRv3717). Using this approach, the regulators were predicted along with their DNA binding sites based on previous chromatin immunoprecipitation sequencing (ChipSeq) studies in Mtb (Galagan, 2013). Thereafter, the DNA sequences of the predicted *ami1* transcriptional regulators along with other relevant protein information were obtained from the Mycobrowser database (https://mycobrowser.epfl.ch/), a repository for sequences and information about mycobacterial species (Table 4.3.1).

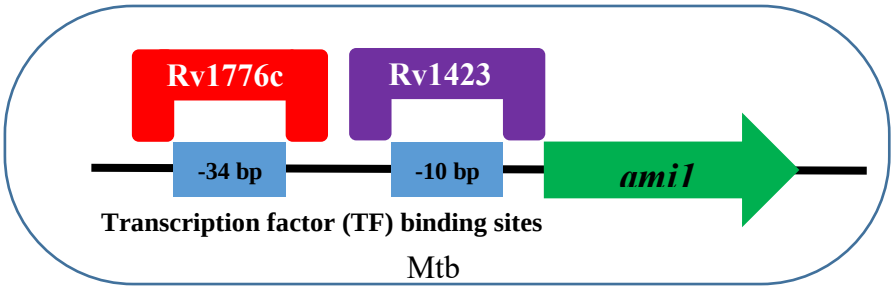


Figure 4.3.3. Two transcriptional regulators for *ami1* gene expression in Mtb. Identified putative *ami1* transcription regulators, Rv1776c and Rv1423 along with their predicted binding sites, as determined by the TB Database (©2013 Galagan Lab, Boston University; ©2010 Broad Institute and Stanford School of Medicine).

Table 4.3.1. Attributes of Rv1776c and Rv1423 as determined by Mycobrowser.

Locus	**Rv1776c**	**Rv1423**
Gene length	561 bp	978 bp
Protein length	186 amino acids	325 amino acids
Molecular mass	20.3 kDa	34.93 kDa≈ 35 kDa
Isoelectric point (pI)	9.0417	10.56

Secondary structure predictions on the PROSITE database (https://prosite.expasy.org/) and on I-TASSER (https://zhanggroup.org/I-TASSER/) revealed that both Rv1776c and Rv1423 respectively possess the HTH DNA binding domain at the N-terminal and C-terminal (Figure 4.3.4 panels A and C). Furthermore, the tertiary structure predictions on I-TASSER revealed

that Rv1776c and Rv1423 are respectively homologous to Rv3249c, a TF of Mtb (PDB 5D1W), and WhiA, a TF of *Thermatoga maritima* (PDB 3hyiA) (Figure 4.3.4 panels B and D). DNA binding predictions showed that Rv1776c and Rv1423 are respectively homologous to PA2196, a TF *Pseudomonas aeruginosa* (4L62A), and I-Dmol, an endonuclease from *Desulfurococcus mucosus* (PDB 4unB), highlighting the putative DNA binding ability of these proteins (Figure 4.3.4 B and D).

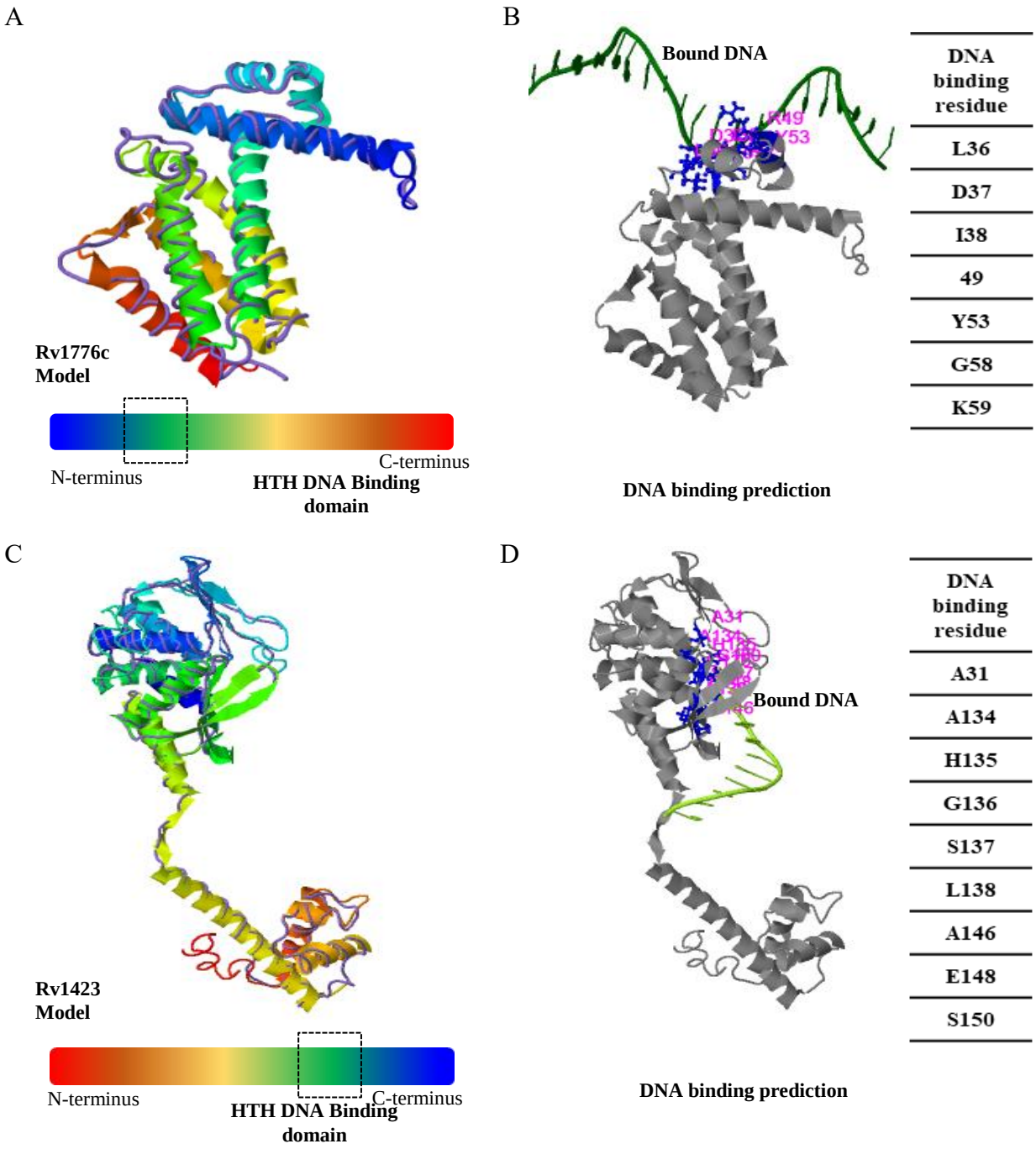
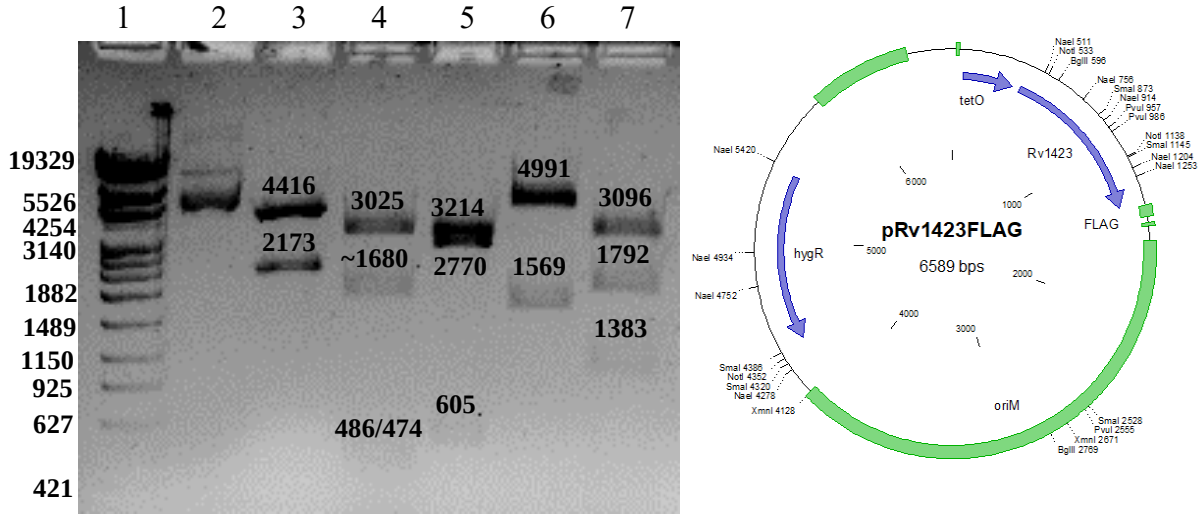


Figure 4.3.4. Predicted structural and DNA binding models for Rv1776c and Rv1423 (A) The predicted Rv1776c model aligned with crystal monomeric structure of Rv3249c (PDB 5D1W). (B) Homology based DNA

binding prediction of Rv1776c, based on PDB 4L62A (PA2196 of *Pseudomonas. aeruginosa*). (C) The predicted model for Rv1423 aligned with 3hyiA (WhiA from *Thermatoga maritima*). (D) Homology based DNA binding prediction of Rv1423 based on PDB 4unB (an endonuclease from *Desulfurococcus mucosus*). DNA binding residues are also shown. Refer to the text for details on how the model was constructed.

4.3.2. Expression and purification of Rv1423 and Rv1776c using *E. coli* expression systems

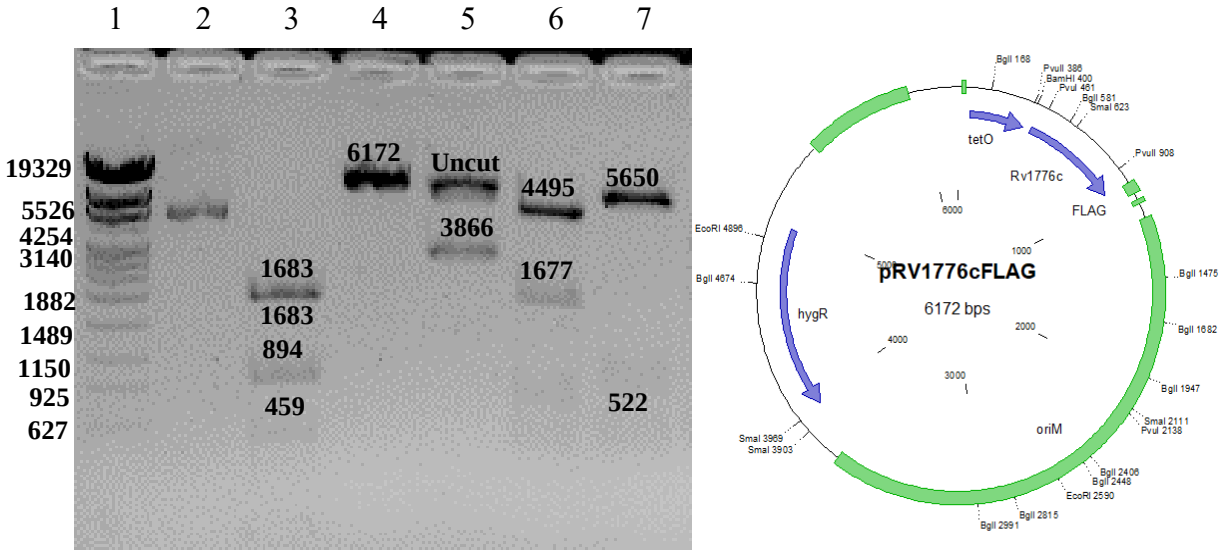
Based on the modelling predictions of Rv1776c and Rv1423, the genes encoding these putative regulators were cloned into expression systems for recombinant protein production in *E.coli*. Prior work in our lab generated a vector (pFLAGEM) that allows for in-frame fusion of mycobacterial proteins with the FLAG tag. The resulting proteins can be purified from *E. coli* using FLAG-tag magnetic beads (Narrandes et al., 2015). The open reading frames for Rv1776c and Rv1423 were cloned into pFLAGEM. Restriction mapping of constructs yielded the expected banding patterns (Figure 4.3.5 and 4.3.6).



Restriction Enzyme	Expected bands (pRv1423F) Forward	Expected bands (pFLAG)	Expected bands (pRv1423F) Reverse
BglII	4416, 2173	5606	5037, 1552
NaeI	3025, 1680, 486, 474, 290	4464, 4896, 474, 182	2976, 1729, 486, 474, 290
NotI	3214, 2770, 605	5606	3074, 2910, 605
PvuI	4991, 1569	5606	4861, 1699, 29
SmaI	3086, 1792, 1383, 272, 66	3748, 1792, 66	2871, 1792, 1588

Figure 4.3.5. Restriction digests of pRv1423FLAG. Lane 1: DNA molecular marker IV, Lane 2: Undigested construct, Lane 3: *BglI*, Lane 4: *NaeI*, Lane 5: *NotI*, Lane 6: *PvuI*, Lane 7: *SmaI*, All restriction digests produced

DNA fragments with the expected sizes. Rv1423 was successfully cloned into pFLAG in the forward conformation.



Restriction Enzyme	Expected bands (pRv1776cF) Forward	Expected bands (pFLAG)	Expected bands (pRv1776cF) Reverse
BglI	1683, 1666, 894, 459, 413	1683, 1666, 741, 459, 367	1683, 1666, 665, 642, 459, 367
BamHI	6172	5606	6172
EcoRI	3866, 2306	3300, 2306	3866, 2306
PvuI	4995, 1677	5606	4965, 1203
PvuII	5650, 522	5606	6070, 102

Figure 4.3.6. Restriction digests of pRv1776FLAG. Lane 1: DNA molecular marker IV, Lane 2: Undigested construct, Lane 3: *BglI*, Lane 4: *BamHI*, Lane 5: *NotI*, Lane 6: *PvuI*, Lane 7: *SmaI*, All restriction digests produced DNA fragments with the expected sizes. *EcoRI* did not produce the 2306 fragment due to inefficient restriction. *PvuI* restrictions allow for a clear distinction between the forward and the reverse conformation. The presence of the 1677 bp fragment in this plasmid confirmed that Rv1776c was cloned in the forward conformation. Faint non-specific fragments were identified in *PvuI* and *PvuII* restrictions (red lines).

However, expression analysis using this system did not yield any detectable proteins when screened with the anti-FLAG antibody (4.3.7 A-C). Due to time constraints, we were not able to troubleshoot this experiment by using a positive control and thus, we decided to change expression systems and shifted to using pET29A, which generates a His-tagged recombinant protein.

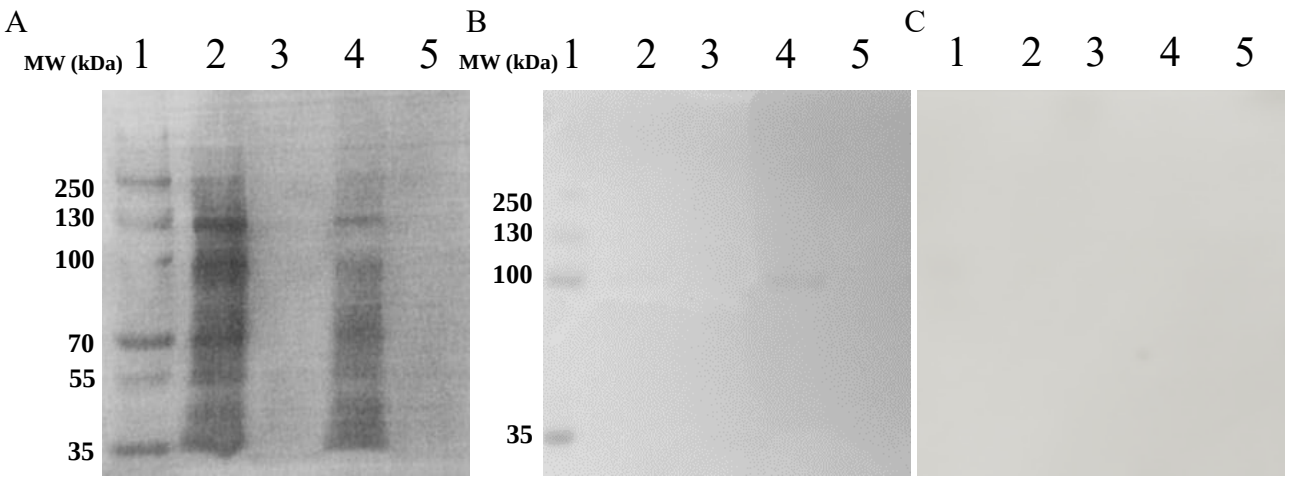
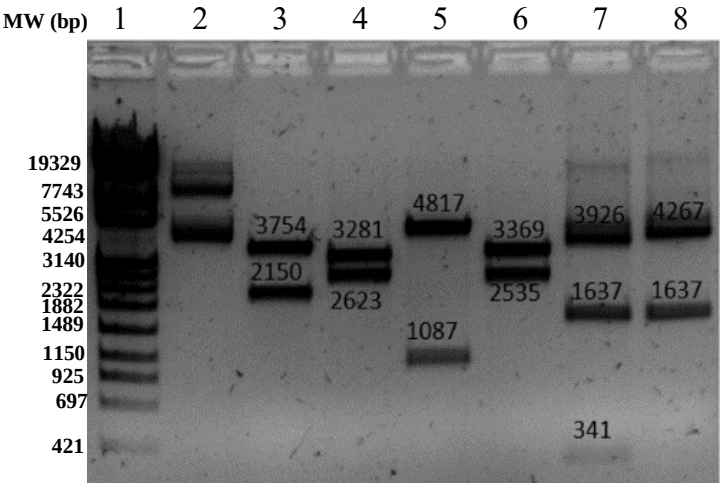


Figure 4.3.7. Expression and purification of Rv1423 and Rv1776 using the pFLAG system. A) Cell lysates of *E.coli* expressing pRv1423FLAG and pRv1776CFLAG (10% SDS-PAGE). Lane 1: Protein marker, Lane 2: Rv1423 soluble cell lysate, Lane 3: Rv1423 insoluble cell lysate Lane 4: Rv1776c soluble cell lysate, Lane 5: Rv1776c insoluble cell lysate. B) Purification of Rv1423 and Rv1776c using M2 anti FLAG beads (10% SDS-PAGE). Lane 1: Protein marker, Lane 2: Rv1423 derived from soluble cell lysate, Lane 3: Rv1423 derived from insoluble cell lysate Lane 4: Rv1776c derived from soluble cell lysate, Lane 5: Rv1776c derived from insoluble cell lysate. Western blot analysis, confirming expression of FLAG tagged Rv1423 and Rv1776c using Anti-FLAG monoclonal antibodies. Expression and purification of Rv1423 and Rv1776c via the pFLAG system was unsuccessful.

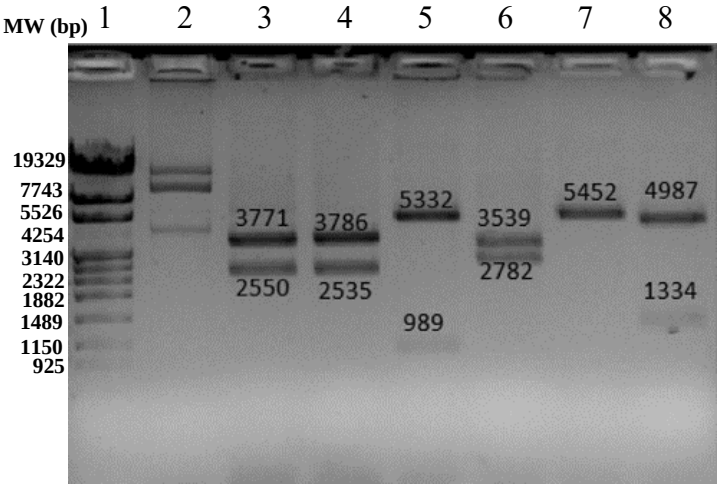
The cloning of *Rv1776c* and *Rv1423* into pET29a+ resulted in the constructs, pET*Rv1776c* and pET*Rv1423*. The constructs were subjected to restriction digest screening for the confirmation of successful cloning. Restriction digests of pET*Rv1776c* and pET*Rv1423* resulted in the expected fragments sizes for all enzymes used, signifying successful cloning (Figure 4.3.8 A and B). Subsequently, the *E. coli* BL21 (DE3) strain was transformed with the constructs. This strain is a lysogen of the bacteriophage DE3, possessing the *lacI* gene, and the *lacUV5* promoter (inducible by IPTG to drive protein expression). The expression of Rv1423 and Rv1776c proteins was induced with 100 µM IPTG for 4 hrs at 37^{o}C. Samples were collected for the detection of recombinant proteins at hourly intervals. IPTG inductions in BL21_*Rv1776c* led to the successful expression of recombinant Rv1776c, which migrated to the correct molecular weight (20.3 kDa) and was found in the soluble fraction of the cell lysate, allowing for purification under non-denaturing conditions (Figure 4.3.9 A-B). In contrast, IPTG inductions in BL21_*Rv1423* did not produce the expected protein at 35 kDa, which would correspond to recombinant Rv1423, despite optimization at different IPTG concentrations (Figure 4.3.9

panels C and D; Appendix E). Therefore, from this point on, protein purification studies focused on Rv1776c.

A

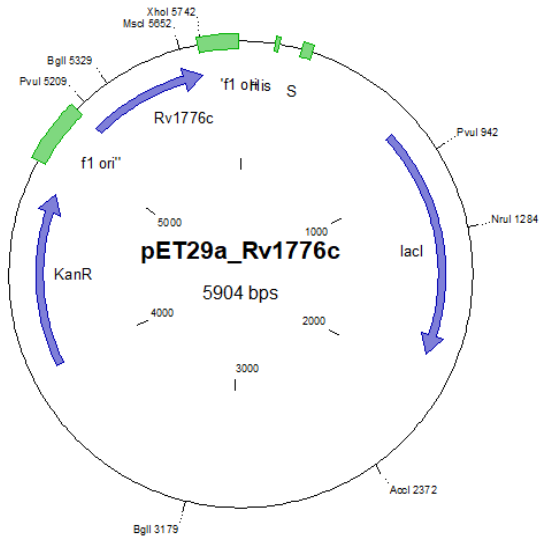


B



Restriction enzyme	Expected band sizes
BglI	3754, 2150
AccI, MscI	3281, 2623
AccI, NruI	4817, 1087
AccI, XhoI	3369. 2535
PvuI, NruI	3926, 1637, 341
PvuI	4267, 1637

Restriction enzyme	Expected band sizes
AccI, HindIII	3771, 2550
AccI, XhoI	3786, 2535
NcoI, HindIII	5332, 989
NcoI, AccI	3539, 2782
NotI	5452
HpaI, NdeI	4987, 1334



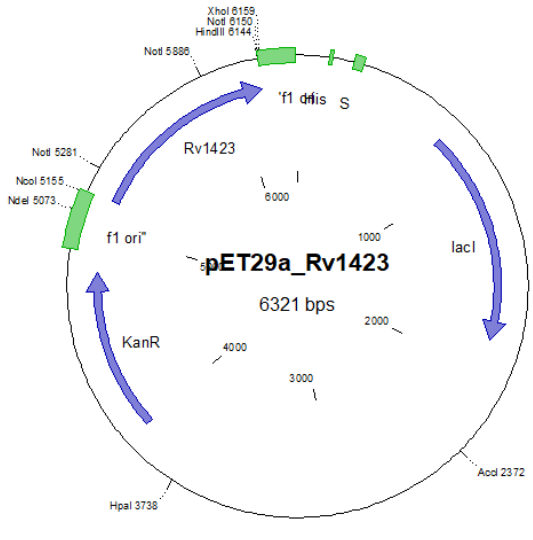


Figure 4.3.8. Restriction digests of pETRv1776c and pETRv1423 confirming successful cloning. (A) Restriction digests of pETRv1776c (Lane 1: DNA molecular marker IV, Lane 2: Undigested construct, Lane 3: *BglI*, Lane 4: *AccI* and *MscI*, Lane 5: *AccI* and *NruI*, Lane 6: *AccI* and *XhoI*, Lane 7: *PvuI* and *NruI*, Lane 8: *PvuII*). (B) Restriction digests of pETRv1423 (Lane 1: DNA molecular marker IV, Lane 2: Undigested construct,

Lane 3: *AccI* and *HindIII*, Lane 4: *AccI* and *XhoI*, Lane 5: *NcoI* and *HindIII*, Lane 6: *NcoI* and *AccI*, Lane 7: *NotI*, Lane 8: *HpaI* and *NdeI*).

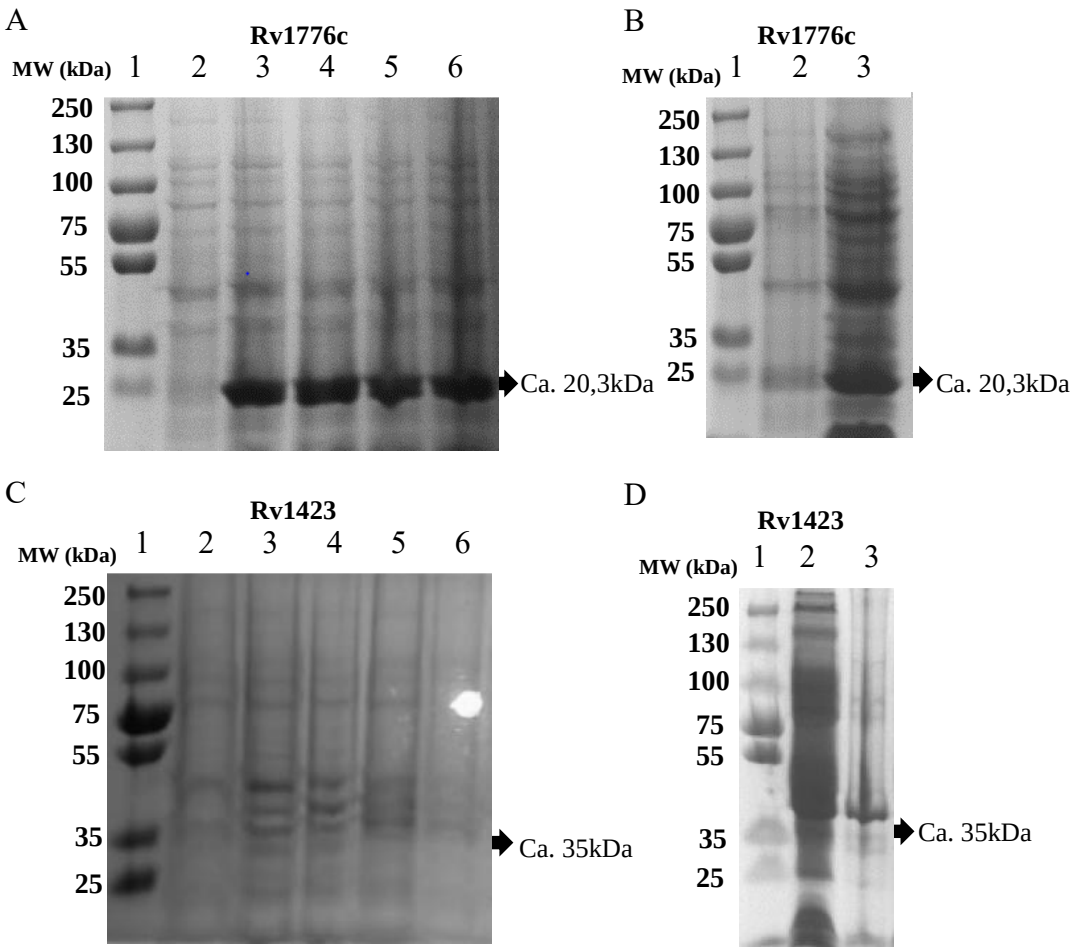


Figure 4.3.9. Induction of Rv1776c and Rv1423 protein expression. (A) IPTG induction of Rv1776c protein expression (Lane 1: Protein marker, Lane 2: Sample before induction, Lane 3: 1hr post induction, Lane 4: 2 hrs post induction, Lane 5: 3 hrs post induction, Lane 6: 4 hrs post induction). (B) Whole cell lysate of Rv1776c 4 hrs post IPTG induction (Lane 1: Protein ladder, Lane 2: Insoluble cell lysate, Lane 3: Soluble lysate). (C) IPTG induction of Rv1423 protein expression (Lane 1: Protein marker, Lane 2: Sample before induction, Lane 3: 1hr post induction, Lane 4: 2 hrs post induction, Lane 5: 3 hrs post induction, Lane 6: 4 hrs post induction). (D) Whole cell lysate of Rv1423 4 hrs post IPTG induction (Lane 1: Protein ladder, Lane 2: Insoluble cell lysate, Lane 3: Soluble lysate).

The C-terminal His-tag on the pET29a+ plasmid was used to purify the expressed protein. Recombinant Rv1776c was successfully purified using a Ni-NTA column (Figure 4.3.10 panels A and B). Western blot analysis using the His-conjugate antibody confirmed that the purified protein was His-tagged (Figure 4.3.10 C).

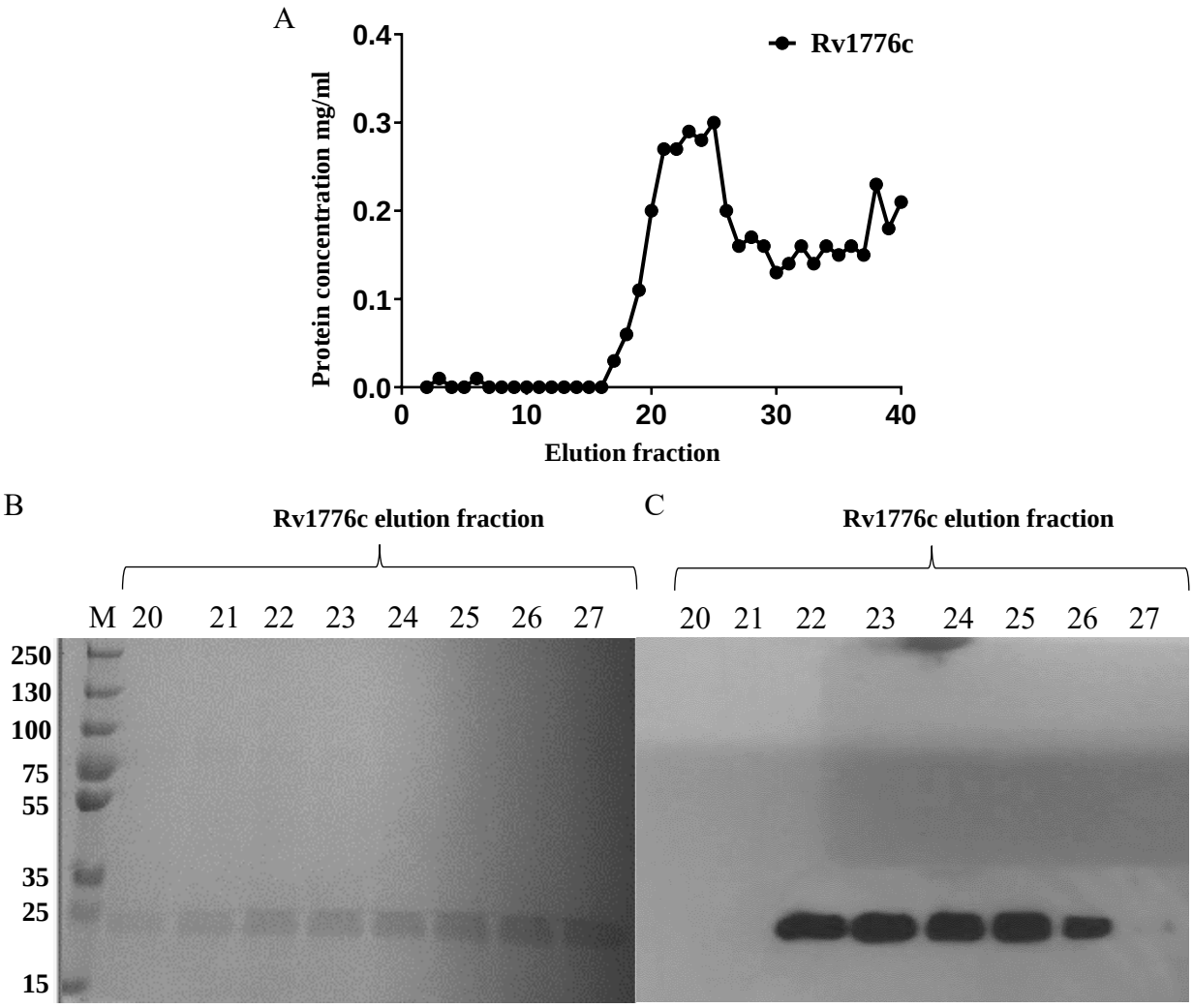


Figure 4.3.10. Purification of the Rv1776c protein. (A) A Ni-NTA elution profile showing elution fractions, 20-27 as possible eluates of Rv1776c due to increased protein concentration. (B) SDS-PAGE of the putative Rv1776c eluates (fractions 20-27). (C) Western blot analysis confirming the purified protein was His-tagged.

4.3.3. Assessing *ami1* promoter DNA binding ability

Once purified, Rv1776c was used in DNA binding assays to determine if it bound a 500 bp DNA fragment that comprised the promoter region of the *ami1* gene. An EMSA revealed that the purified Rv1776c protein bound this region as evidenced by a shift in molecular weight when the protein was present (Figure 4.3.11). As only a small proportion of the substrate DNA bound Rv1776c, we next attempted to optimize this EMSA assay by using different binding reaction length, buffer concentration, buffer pH, and reaction temperature. However, these experiments largely yielded no binding as evidenced by the lack of a band between the 697 and 421 bp markers in the gels shown in Appendix F. We did note the accumulation of a high

molecular weight product in the wells of some gels, in addition to depletion of the substrate, but had no definitive evidence that this comprised the *ami1*-Rv1776 DNA-Protein complex.

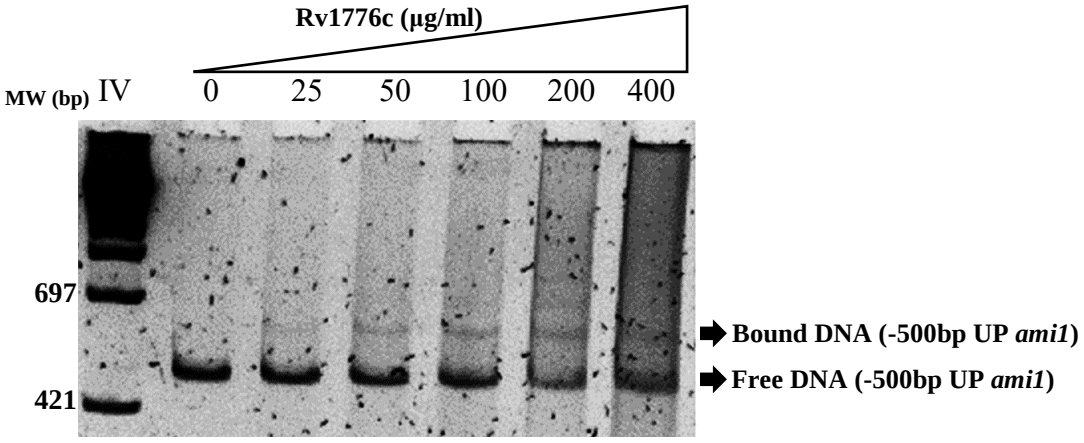


Figure 4.3.11. EMSA assessing the DNA binding ability of Rv1776c to the -500bp upstream promoter region of *ami1* of Rv1776c. Rv1776c displays binding to the 500 bp upstream promoter region of *ami1*.

4.3.4. Monitoring phenotypic effects of over expressing putative Ami1 regulators

Based on the binding results for Rv1776c, we next sought to determine whether this putative negative regulator could substantively repress *ami1* gene expression when over-expressed in Mtb. We also included Rv1423 in this analysis. The model system used for these experiments was based on monitoring ethidium bromide (EtBr) diffusion into cells. Given that loss of *ami1* resulted in increased diffusion of EtBr into the cell, we hypothesized the overexpression of these negative regulators would phenocopy the *ami1* mutant phenotype in this regard.

The plasmids, pEXNF_*Rv1776* and pEXNF_*Rv1423* were used for overexpressing Rv1776c and Rv1423 respectively. These were obtained from the Mtb Transcription factor inducer (TFI) library that allows the anhydrotetracycline (ATC) inducible overexpression of Mtb transcription factors (Rustad et al., 2014; Ma et al., 2020). pEXNF_*Rv1776* and pEXNF_*Rv1423* were electroporated into Mtb H37RvS to produce the corresponding strains, H37_*Rv1776c* and H37_*Rv1423*. Thereafter, H37_*Rv1776c* and H37_*Rv1423* were grown in 7H9 containing 100 ng/ml ATC to induce overexpression of Rv1776c and Rv1423 respectively (Figure 4.3.12. A). Both ATC induced H37_*Rv1776c* and H37_*Rv1423* displayed increased EtBr uptake when compared to the corresponding non-induced strains, suggesting that these regulators reduce levels of Ami1 (Figure. 4.3.12 B-C).

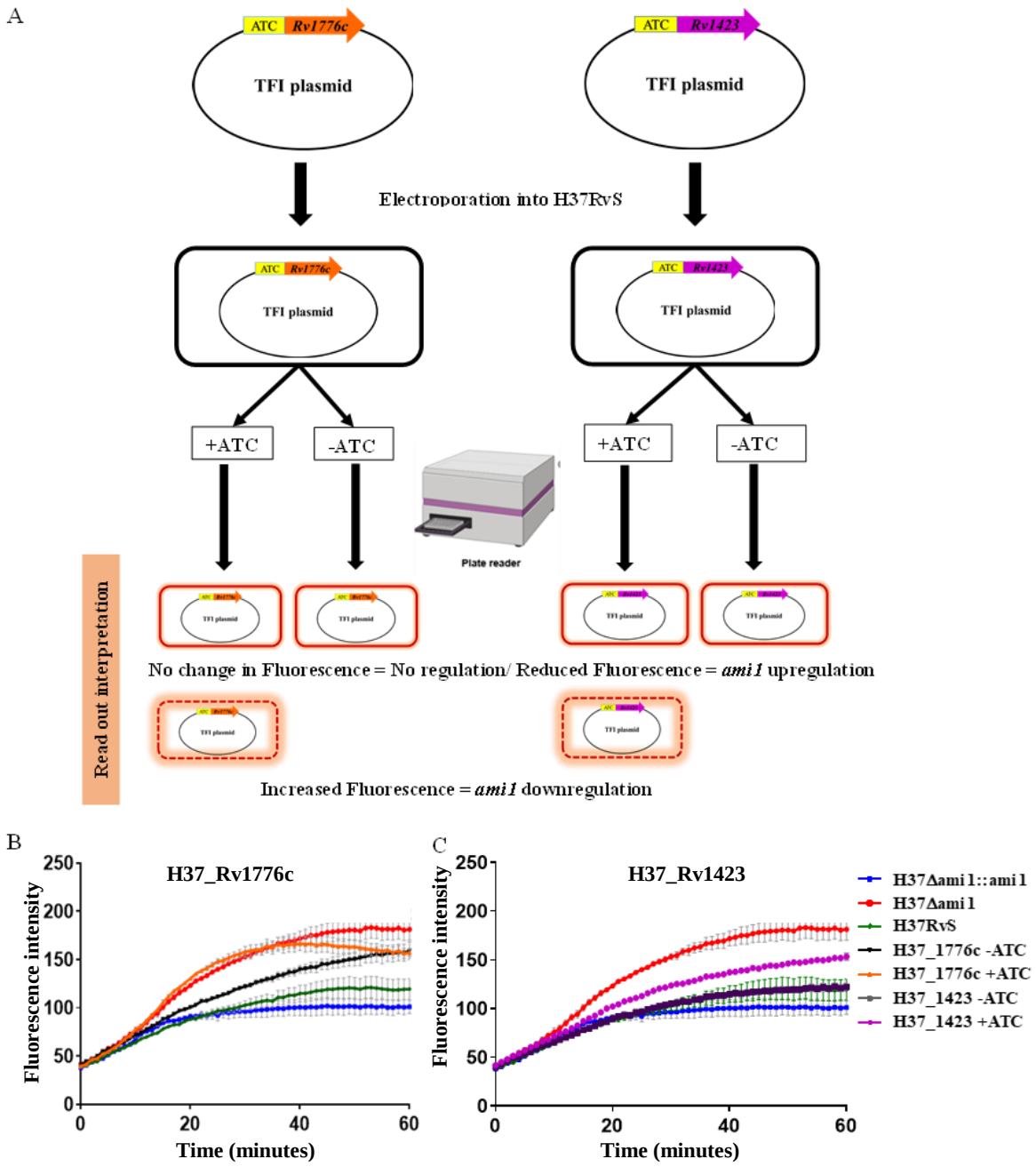


Figure 4.3.12. EtBr uptake of Mtb strains. A) Schematic of experimental approach for monitoring Ethidium Bromide (EtBr) uptake in Mtb. B) Over expression of Rv1776c. C) Over expression of Rv1423. Wild type H37RvS (green), H37Δami1 (*ami1* mutant red), H37Δami1::ami1 (genetically complemented *ami1* mutant, blue), H37_*Rv1776c* (wild type with Rv1776c over expressed [+ATC orange] with Rv1776c with no inducer [-ATC black] and H37_*Rv1423* (wild type with Rv1423 over expressed [+ATC magenta] Rv1423 with no inducer [-ATC green]. Data were subjected to polynomial curve fitting to determine statistical significance. H37_*Rv1776c* [+ATC]: $y = -0{,}0727x^2 + 6{,}3999x + 27{,}773$ $R^2 = 0{,}9889$. H37_*Rv1776c* [-ATC]: $y= -0{,}0257x^2 +3{,}5105x + 39{,}924$ $R^2 = 0{,}9995$. H37_*Rv1423* [+ATC]: $y= -0{,}0298x^2 + 3{,}6293x + 39{,}917$ $R^2 = 0{,}9985$. H37_*Rv1423* [-ATC]: $y = -0{,}0268x^2 + 2{,}9446x + 39{,}845$ $R^2 = 0{,}9988$. Differences were non-significant at points of intersection.

To confirm that the regulators were indeed over expressed, and to assess whether the consequent effects on *ami1* gene expression, we conducted quantitative real time PCR. Addition of ATC to induce regulator expression in H37_*Rv1776c* and H37_*Rv1423* did not yield increased expression of the Rv1776c (Figure 4.3.13 A), however overexpression was associated with a reduction in *ami1* gene but this effect was not statistically significant (Figure 4.3.13 B). In contrast, a significant increase in Rv1423 expression was noted upon incremental addition of the inducer (Figure 4.3.13 C), which led to a statistically non-significant reduction in *ami1* gene expression (Figure 4.3.13 D).

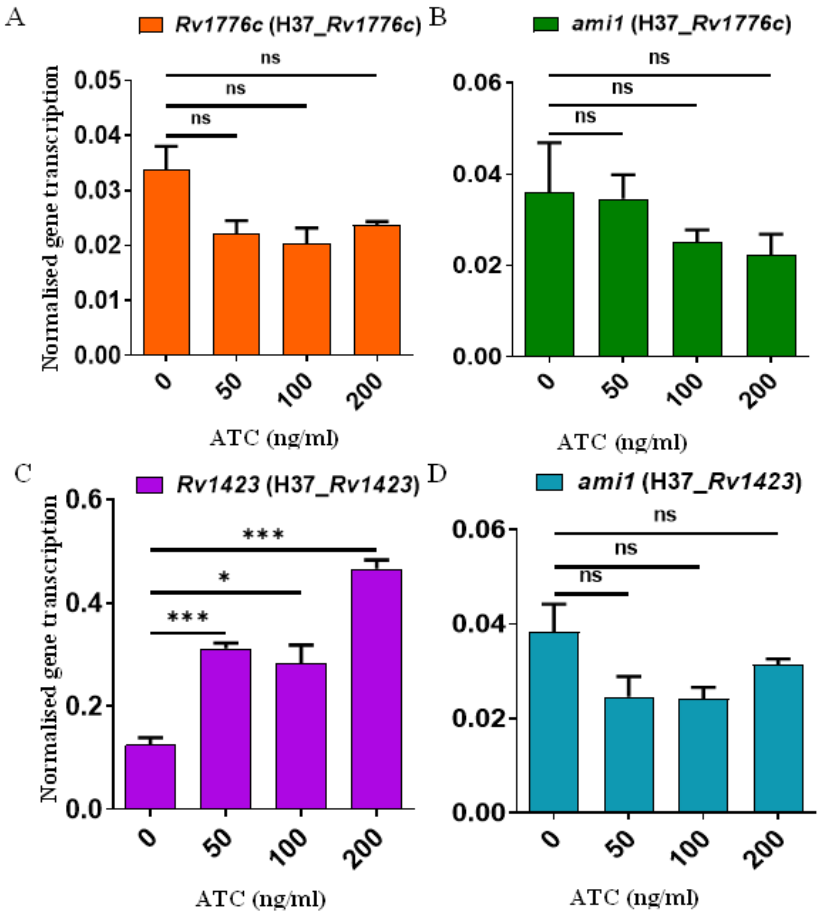


Figure 4.3.13. Assessment of *ami1* transcription in *Mtb* strains overexpressing Rv1423 and Rv1776c. H37_*Rv1776c* and H37_*Rv1423* were exposed to ATC at varying concentrations (0, 50, 100 and 100 ng/ml). The expression of *Rv1423*, *Rv1776c* and *ami1* were monitored at all ATC concentrations. The transcription of *ami1* and *Rv1776c* was decreased with increasing ATC concentration in H37_*Rv1776c*. In H37_*Rv1423*, the transcription of *ami1* decreases with increasing ATC concentration whereas, *Rv1423* expression increases with increasing ATC concentration. Error bars represent the standard error of the mean (SEM) for three biological replicates. Statistical analysis was conducted using the student's t-test *: $p < 0.05$.

4.4. Discussion

Bacterial morphology varies widely across species and this is largely due to the different PG-based cell wall structures. Despite PG being highly conserved, consisting of long glycan chains cross-linked via peptide sidechains, the mature cell wall is chemically diverse (Do et al. 2020) PG hydrolases and cell wall remodelling enzymes alter glycan length, the level and type of cross-links, and the various PG modifications that are all central in defining the cell wall. Therefore, the activity of PG hydrolases need to be tightly regulated as the dysregulation of these enzymes can lead to deleterious effects and ultimately cell death (van Heijenoort, 2011). Several mechanisms exist to prevent unchecked activity of PG hydrolases, which typically entail transcriptional or translation control. For example, the *lytE* and *cwlO* endopeptidase genes of *B. subtilis* are regulated by unknown signals generated during cell wall metabolism (Bisicchia et al., 2007). Alternatively, protein localization may confine certain enzymes with hydrolytic activities to specific sites in the bacterial cell or they may contain tags that direct them to specific cellular compartments. Proteolytic degradation of hydrolases may also contribute to its regulation such as the *E. coli* MepS (an endopeptidase that cleaves cross-links to allow for space required during cell expansion) which is regulated via Prc protease-mediated degradation (Singh et al., 2015). Ultimately, many bacterial genomes encode a large set of PG-associated hydrolases and their regulators, whereby individual enzymes are activated or regulated differentially, but collectively cover the full range of growth conditions to ensure that PG hydrolysis (and biosynthesis) can occur correctly in response to various environmental cues.

In this study, we demonstrated earlier that the *ami1* homologue in Mtb is directly regulated by the first-line anti-TB drug, isoniazid, and we sought to identify the transcriptional regulator (s) driving this response. Prior to this, we surmised that the Mtb Ami1 homologue could be in one of two physiological states: 1) an active form capable of hydrolyzing PG without the need to be activated or 2) an inactive enzyme requiring activation by a yet-to-be determined regulator in mycobacteria. To address this first scenario, we heterologously expressed the Mtb *ami1* gene in an *E. coli* double mutant lacking EnvC and NlpD. In the wild type strain of *E. coli*, the population was predominantly comprised of single cells (indicative of effective cell division) with some cellular chains (>4 cells per chain). In contrast, cells simultaneously lacking EnvC and NlpD grew mainly as cellular chains (> 4 cells per chain). When this double deletion mutant strain was complemented with the Mtb *ami1* gene, the chaining phenotype was partially complemented to wild type levels. The limitations notwithstanding, this suggested that Mtb

Ami1 is able to degrade septal PG and that it exists in an active form that does not require activation (at least not by EnvC or NlpD).

Based on results in chapter 3, we interrogated how a putative active amidase (*ami1* in Mtb) would respond to isoniazid. Using a bioinformatics approach, we identified two putative *ami1* transcriptional regulators, namely Rv1423 and Rv1776c. Protein sequences were used to perform secondary structure predictions and homology modelling for each regulator. Both Rv1423 and Rv1776c were predicted to respectively contain helix-turn-helix (HTH) DNA binding domains at the C-terminal and N-terminal. In *Vibrio cholerae*, the chitin sensor ChiS is transcriptional regulator that plays a role in cell survival via its DNA binding domain (DBD) in the C-terminus. The crystal structure of the ChiS DBD also contains a HTH domain that is similar to other DNA-binding proteins such as the LacI repressor (Klancher et al., 2021). The two-component system, CssS/CssR, in *B. subtilis*, plays a role in overcoming cell envelope stress. The crystal structure of the DNA-binding domain of CssR demonstrated the presence of a winged HTH motif that is conserved in the OmpR/PhoB subfamily of response regulators (Dahal et al., 2021). It is therefore interesting that the two predicted transcriptional regulators of *ami1* in Mtb contain HTH DNA-binding domains and that they possibly regulate *ami1* transcription in response to a cell wall stress induced by isoniazid.

As these data thus far were theoretical or computational, we next sought to produce recombinant forms (using two independent expression systems – FLAG-tagging and pET29a-based His-tagging recombinant protein production in *E. coli*) of each transcriptional regulator for assessing binding activity to the DNA upstream of *ami1*. In the FLAG-tag approach, neither proteins could be successfully purified. The pET29a system proved more useful in that Rv1776c was successfully expressed and purified whereas Rv1423 could not be expressed despite various attempts to optimize the process. One reason why Rv1423 could not be purified may relate to it being classified as WhiB-like (Wbl) family protein. This family of proteins has previously been shown to be difficult to over-express and purify in *E. coli* (Kudhair and Green, 2023). In contrast, a different study revealed that successful expression of Wbl proteins in *E. coli* might require co-expression with a trigger factor (TF) (Kudhair and Green, 2023) which could still apply to Rv1423. Nevertheless, following the purification of Rv1776c, we showed that the protein was able to bind to the 500 bp upstream region of *ami1* using EMSAs. However, binding appeared to be partial despite increasing concentrations of Rv1776c suggesting that Rv1776c is a transcriptional regulator of *ami1* expression. Attempts to improve the binding conditions by adjusting variables such as using varying recombinant protein concentrations or

reaction conditions, failed to yield increased binding. Our previous observation showed that deletion of *ami1* in Mtb resulted in increased cell wall permeability. When we over-expressed Rv1423 and Rv1776c separately in Mtb H37Rv, a similar increase in cell wall permeability was observed, suggesting that Rv1776c and Rv1423 are transcriptional repressors of *ami1*. When we quantitated the amount of Rv1423 transcripts, under the regulation of an ATC-responsive promoter, increasing concentrations of Rv1423 were observed in an ATC concentration-dependent manner. This increased expression of the regulator did lead to reduced expression of *ami1,* however; this effect was not statistically significant. In the same system, Rv1776c decreased in response to increasing concentrations of ATC, an effect that was also associated with decreased *ami1* expression. As these effects were not statistically significant, no conclusions can be made. Given these multiple attempts, through the use of different concentrations of inducer, did not yield increased levels of Rv1776c, we postulate that this regulator could be subjected to some form of downstream regulation to ensure steady-state levels. Consistent with this, a TB Database probe for putative regulators of Rv1776c identified phoP as a downstream transcriptional repressor of Rv1776c. It is part of the phoPR two-component system that regulates virulence gene (Walters et al., 2006).

We postulate that under circumstances when *ami1* is present, these two repressors likely regulate the amount of *ami1* transcripts but when isoniazid is present; the repressors sense the perturbations and release the promoter region driving expression of *ami1*. The mechanism for this remains to be elucidated, however, Rv1776c belongs to the TetR-family of transcriptional factors, a group of proteins involved in the regulation of various processes, including cell division and stress response (Ramos et al., 2005, Cuthbertson and Nodwell, 2013). There are also other examples of amidase transcriptional regulation in other bacterial species including the WalK/WalR two-component system in *S. aureus* (Dubrac et al., 2007). The transcription of *amiA* and *amiC* in both *E. coli* and *Salmonella* is under the control of the CpxR/CpxA two-component system (Weatherspoon-Griffin et al., 2011). Corroborating our findings, deletion of *amiA* and *amiC* in *E. coli* and *Salmonella* results in an increased cell wall permeability and susceptibility to antimicrobial compounds (Weatherspoon-Griffin et al., 2011). Based on these data, it is possible that Rv1776c and Rv1423 form part of a two-component system or form parts of separate two-component systems to drive *ami1* transcription in Mtb, which forms the basis of future studies in our lab.

Chapter 5: Conclusion, limitations and future experiments

5.1. Concluding remarks

In this study, we set out to investigate the biological function of Ami1 in Mtb and were able to demonstrate that this enzyme does not contribute to cell division events such as septal cell wall degradation. Consistent with this, Ami1 appeared to play no role in growth of bacteria in nutrient rich broth, and loss thereof did not affect localization of the DivIVA. We did however; discover that under nutrient limiting conditions, Ami1 plays a critical role in growth. We hypothesize that this relates to the ability of the cell to access nutrients, rather than any specific role in cell division. Given that the activity of many PG hydrolases are associated with antibiotic susceptibility, we went on to explore the role of Ami1 following exposure different classes of antibiotics. Our data revealed a novel role for Ami1 in responses to INH treatment, which was further confirmed through expression analysis indicating that the ami1 gene expression was induced by INH treatment. In the second component of this work, we further explored how this regulation works. Using bioinformatics, we identify two putative new regulators of *ami1* gene expression. A model for these findings is present in Figure 5.1.

Space left intentionally blank

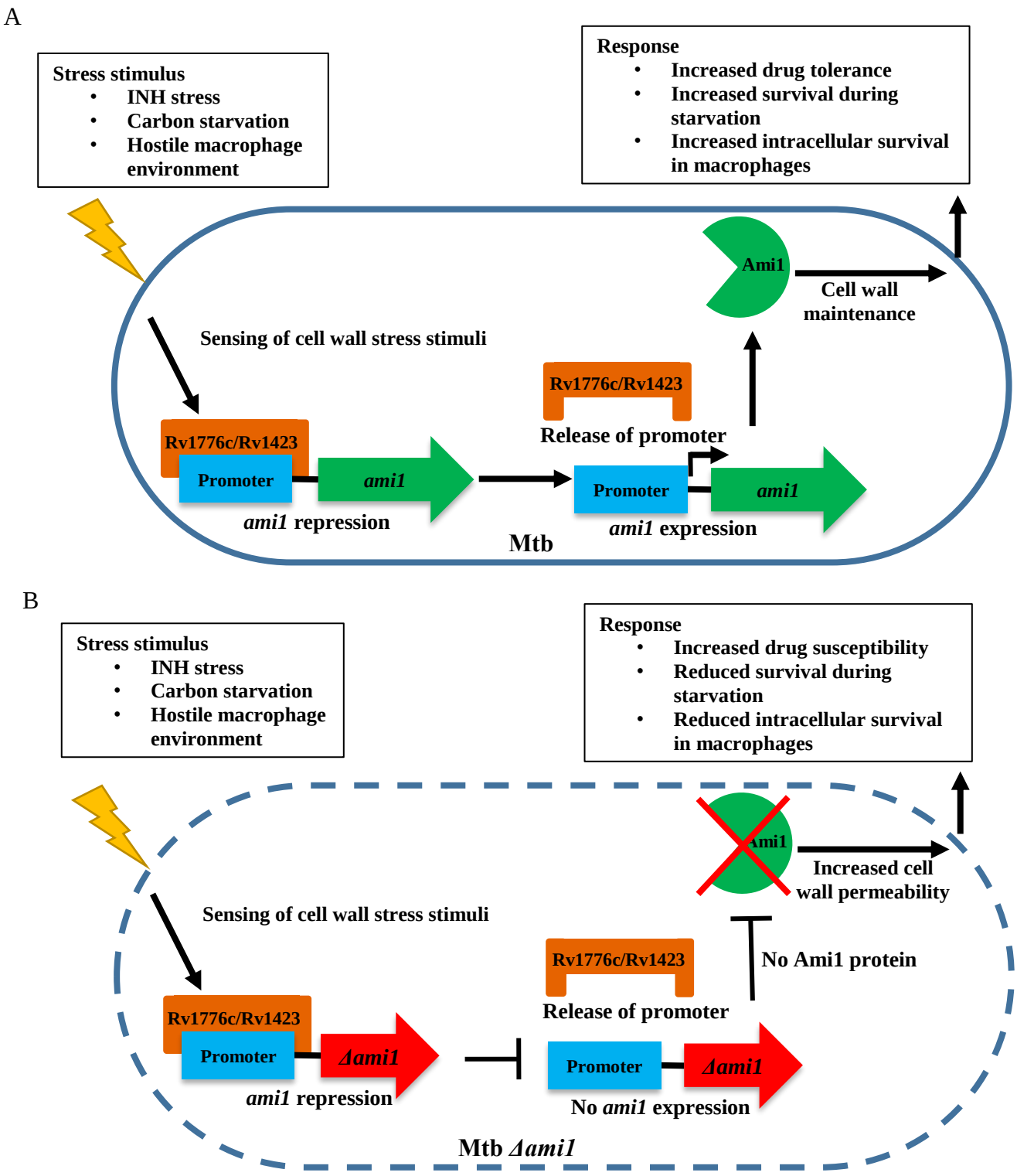


Figure 5.1. Proposed model for the possible role of *ami1* in Mtb. Rv1776c and Rv1423 regulate the ami1 gene via transcriptional repression. However, if the bacterium encounters external stress (Immune assault, antibiotic assault, and starvation). The transcriptional regulators allow ami1 transcription to allow stress response, thus, improving cell survival.

5.2 Limitations

There were several limitations in our work. The increased abundance of Ami1 was imputed from increased gene expression levels. Assessing levels of proteins using antibodies or proteomics would have bolstered these findings. Problems with generating a transposon library limited our ability to explore the mechanistic basis of how Ami1 responds to INH. Regarding putative regulators, not being able to produce recombinant forms of Rv1423 limited our ability to investigate it further. Attempts to improve the EMSA did not yield results that are more robust. One way to establish binding between *ami1* and Rv1776 was through competition binding assays; however, these could not be performed due to time constraints. However, if revised, the assays would include the *csm6* promoter as cold competitive positive control, as it has been demonstrated to interact with Rv1776c (Wei et al., 2023); whereas the *sigA* promoter region would be used as a non-specific negative control. Finally, we imputed the function of the putative regulators through over-expression studies. These appending results would have been bolstered through gene deletion studies.

5.2 Future experiments

Future work should include the assessment of Mtb (H37RvS, H37*Δami1S*, and H37*Δami1S*::*ami1*) transcriptomes under conditions of carbon starvation to understand possible *ami1* interactions and pathways that enable cell survival under these conditions. Genes with significantly altered expression profiles will be investigated further. The possible role of Ami1 in PG recycling could be studied, considering the involvement of Ami1 in Mtb survival in carbon limiting conditions. This would entail the extraction of PG from H37RvS, treating the PG with purified Ami1 protein, and assessing the ability of H37*Δami1S* to grow in minimal media with Ami1-treated PG vs non-treated PG as the sole source of carbon. Given that other studies implicated Ami1 in immune modulation and that, we reported a possible role in intracellular survival, investigating the role of Ami1 in modulating PG detection by NOD1 and NOD2 receptors. The purification and crystallization of Ami1 regulators, Rv1423 and Rv1776c could reveal more about their mechanisms of action. Furthermore, gene deletion studies of said regulators may elucidate the processes that they regulate.

Chapter 6: References

AFSAR, I., GUNES, M., ER, H. & SENER, A. G. 2018. Comparison of culture, microscopic smear and molecular methods in diagnosis of tuberculosis. *Revista espanola de quimioterapia,* 31**,** 435.

AHMED, F., ANDREWS, K., ARSHAD, D. & NEKURI, P. 2020. A New FDA-approved Antibiotic for Drug-resistant Tuberculosis Treatment.

ALCORLO, M., DIK, D. A., DE BENEDETTI, S., MAHASENAN, K. V., LEE, M., DOMÍNGUEZ-GIL, T., HESEK, D., LASTOCHKIN, E., LÓPEZ, D. & BOGGESS, B. 2019. Structural basis of denuded glycan recognition by SPOR domains in bacterial cell division. *Nature communications,* 10**,** 1-13.

ALDERWICK, L. J., HARRISON, J., LLOYD, G. S. & BIRCH, H. L. 2015. The mycobacterial cell wall—peptidoglycan and arabinogalactan. *Cold Spring Harbor perspectives in medicine,* 5**,** a021113.

ALDRIDGE, B. B., FERNANDEZ-SUAREZ, M., HELLER, D., AMBRAVANESWARAN, V., IRIMIA, D., TONER, M. & FORTUNE, S. M. 2012. Asymmetry and aging of mycobacterial cells lead to variable growth and antibiotic susceptibility. *Science,* 335**,** 100-104.

ALMEIDA DA SILVA, P. E. & PALOMINO, J. C. 2011. Molecular basis and mechanisms of drug resistance in Mycobacterium tuberculosis: classical and new drugs. *J Antimicrob Chemother,* 66**,** 1417-30.

ALVAREZ, L., ESPAILLAT, A., HERMOSO, J. A., DE PEDRO, M. A. & CAVA, F. 2014. Peptidoglycan remodeling by the coordinated action of multispecific enzymes. *Microbial drug resistance,* 20**,** 190-198.

ALVES FELICIANO, C., ECKENROTH, B. E., DIAZ, O. R., DOUBLIÉ, S. & SHEN, A. 2021. A lipoprotein allosterically activates the CwlD amidase during Clostridioides difficile spore formation. *PLoS Genetics,* 17**,** e1009791.

AMARAL, E. P., FOREMAN, T. W., NAMASIVAYAM, S., HILLIGAN, K. L., KAUFFMAN, K. D., BARBOSA BOMFIM, C. C., COSTA, D. L., BARRETO-DUARTE, B., GURGEL-ROCHA, C., SANTANA, M. F., CORDEIRO-SANTOS, M., DU BRUYN, E., RIOU, C., ABERMAN, K., WILKINSON, R. J., BARBER, D. L., MAYER-BARBER, K. D., ANDRADE, B. B. & SHER, A. 2022. GPX4 regulates cellular necrosis and host resistance in Mycobacterium tuberculosis infection. *Journal of Experimental Medicine,* 219.

ANTIPARRA, R., SANTOS, M., TOLEDO, A., GILMAN, R. H., KIRWAN, D. E., SHEEN, P. & ZIMIC, M. 2020. EXPRESSION OF Mycobacterium tuberculosis RpsA IN Mycobacterium smegmatis INCREASES SUSCEPTIBILITY TO PYRAZINAMIDE. *bioRxiv***,** 2020.03.31.018390.

ARORA, D., CHAWLA, Y., MALAKAR, B., SINGH, A. & NANDICOORI, V. K. 2018. The transpeptidase PbpA and noncanonical transglycosylase RodA of Mycobacterium tuberculosis play important roles in regulating bacterial cell lengths. *Journal of Biological Chemistry,* 293**,** 6497-6516.

ASANO, K., KAKIZAKI, I. & NAKANE, A. 2012. Interaction of Listeria monocytogenes autolysin amidase with glycosaminoglycans promotes listerial adhesion to mouse hepatocytes. *Biochimie,* 94**,** 1291-1299.

ASONG, J., WOLFERT, M. A., MAITI, K. K., MILLER, D. & BOONS, G.-J. 2009. Binding and cellular activation studies reveal that Toll-like receptor 2 can differentially

recognize peptidoglycan from Gram-positive and Gram-negative bacteria. *Journal of Biological Chemistry,* 284**,** 8643-8653.
ATRIH, A., ZÖLLNER, P., ALLMAIER, G. & FOSTER, S. J. 1996. Structural analysis of Bacillus subtilis 168 endospore peptidoglycan and its role during differentiation. *J Bacteriol,* 178**,** 6173-83.
BALDRIDGE, J., MYERS, K., JOHNSON, D., PERSING, D., CLUFF, C. & HERSHBERG, R. 2006. Monophosphoryl lipid A and synthetic lipid A mimetics as TLR4-based adjuvants and immunomodulators. *Vaccine Adjuvants: Immunological and Clinical Principles***,** 235-255.
BARANOWSKI, C., WELSH, M. A., SHAM, L.-T., ESKANDARIAN, H. A., LIM, H. C., KIESER, K. J., WAGNER, J. C., MCKINNEY, J. D., FANTNER, G. E. & IOERGER, T. R. 2018. Maturing Mycobacterium smegmatis peptidoglycan requires non-canonical crosslinks to maintain shape. *Elife,* 7**,** e37516.
BARRY, C. E., CRICK, D. C. & MCNEIL, M. R. 2007. Targeting the formation of the cell wall core of M. tuberculosis. *Infectious Disorders-Drug Targets (Formerly Current Drug Targets-Infectious Disorders),* 7**,** 182-202.
BATEMAN, A. & RAWLINGS, N. D. 2003. The CHAP domain: a large family of amidases including GSP amidase and peptidoglycan hydrolases. *Trends in Biochemical Sciences,* 28**,** 234-237.
BERNHARDT, T. G. & DE BOER, P. A. 2003. The Escherichia coli amidase AmiC is a periplasmic septal ring component exported via the twin-arginine transport pathway. *Mol Microbiol,* 48**,** 1171-82.
BERTIN, J., NIR, W.-J., FISCHER, C. M., TAYBER, O. V., ERRADA, P. R., GRANT, J. R., KEILTY, J. J., GOSSELIN, M. L., ROBISON, K. E. & WONG, G. H. 1999. Human CARD4 protein is a novel CED-4/Apaf-1 cell death family member that activates NF-κB. *Journal of Biological Chemistry,* 274**,** 12955-12958.
BIRNBOIM, H. C. & DOLY, J. 1979. A rapid alkaline extraction procedure for screening recombinant plasmid DNA. *Nucleic Acids Res,* 7**,** 1513-23.
BISICCHIA, P., NOONE, D., LIOLIOU, E., HOWELL, A., QUIGLEY, S., JENSEN, T., JARMER, H. & DEVINE, K. M. 2007. The essential YycFG two-component system controls cell wall metabolism in Bacillus subtilis. *Mol Microbiol,* 65**,** 180-200.
BLACK, P. A., WARREN, R. M., LOUW, G. E., VAN HELDEN, P. D., VICTOR, T. C. & KANA, B. D. 2014. Energy metabolism and drug efflux in Mycobacterium tuberculosis. *Antimicrobial agents and chemotherapy,* 58**,** 2491-2503.
BLACKMAN, S. A., SMITH, T. J. & FOSTER, S. J. 1998. The role of autolysins during vegetative growth of Bacillus subtilis 168. *Microbiology,* 144**,** 73-82.
BLAIR, J., WEBBER, M. A., BAYLAY, A. J., OGBOLU, D. O. & PIDDOCK, L. J. 2015. Molecular mechanisms of antibiotic resistance. *Nature reviews microbiology,* 13**,** 42-51.
BOSE, J. L., LEHMAN, M. K., FEY, P. D. & BAYLES, K. W. 2012. Contribution of the Staphylococcus aureus Atl AM and GL murein hydrolase activities in cell division, autolysis, and biofilm formation. *PLoS One,* 7**,** e42244.
BOSEDASGUPTA, S. & PIETERS, J. 2014. Inflammatory stimuli reprogram macrophage phagocytosis to macropinocytosis for the rapid elimination of pathogens. *PLoS pathogens,* 10**,** e1003879.
BOSHOFF, H. I. & BARRY III, C. E. 2006. Is the mycobacterial cell wall a hopeless drug target for latent tuberculosis? *Drug Discovery Today: Disease Mechanisms,* 3**,** 237-245.

BÖTH, D., SCHNEIDER, G. & SCHNELL, R. 2011. Peptidoglycan remodeling in Mycobacterium tuberculosis: comparison of structures and catalytic activities of RipA and RipB. *J Mol Biol,* 413**,** 247-60.

BOUTTE, C. C., BAER, C. E., PAPAVINASASUNDARAM, K., LIU, W., CHASE, M. R., MENICHE, X., FORTUNE, S. M., SASSETTI, C. M., IOERGER, T. R. & RUBIN, E. J. 2016. A cytoplasmic peptidoglycan amidase homologue controls mycobacterial cell wall synthesis. *Elife,* 5**,** e14590.

BRENNAN, P. J. 2003. Structure, function, and biogenesis of the cell wall of Mycobacterium tuberculosis. *Tuberculosis,* 83**,** 91-97.

BRITTON, R. A., EICHENBERGER, P., GONZALEZ-PASTOR, J. E., FAWCETT, P., MONSON, R., LOSICK, R. & GROSSMAN, A. D. 2002. Genome-wide analysis of the stationary-phase sigma factor (sigma-H) regulon of Bacillus subtilis. *Journal of bacteriology,* 184**,** 4881-4890.

BROTT, A. S. & CLARKE, A. J. 2019. Peptidoglycan O-acetylation as a virulence factor: Its effect on lysozyme in the innate immune system. *Antibiotics,* 8**,** 94.

BRUCHFELD, J., CORREIA-NEVES, M. & KÄLLENIUS, G. 2015. Tuberculosis and HIV Coinfection. *Cold Spring Harb Perspect Med,* 5**,** a017871.

CAMBAU, E., VIVEIROS, M., MACHADO, D., RASKINE, L., RITTER, C., TORTOLI, E., MATTHYS, V., HOFFNER, S., RICHTER, E. & PEREZ DEL MOLINO, M. 2015. Revisiting susceptibility testing in MDR-TB by a standardized quantitative phenotypic assessment in a European multicentre study. *Journal of Antimicrobial Chemotherapy,* 70**,** 686-696.

CAÑO-MUÑIZ, S., ANTHONY, R., NIEMANN, S. & ALFFENAAR, J. C. 2018. New Approaches and Therapeutic Options for Mycobacterium tuberculosis in a Dormant State. *Clin Microbiol Rev,* 31.

CANTON, J. 2018. Macropinocytosis: new insights into its underappreciated role in innate immune cell surveillance. *Frontiers in immunology,* 9**,** 2286.

CATALÃO, M. J., FILIPE, S. R. & PIMENTEL, M. 2019. Revisiting anti-tuberculosis therapeutic strategies that target the peptidoglycan structure and synthesis. *Frontiers in Microbiology,* 190.

CAVENEY, N. A., LI, F. K. & STRYNADKA, N. C. 2018. Enzyme structures of the bacterial peptidoglycan and wall teichoic acid biogenesis pathways. *Current Opinion in Structural Biology,* 53**,** 45-58.

CHAMAILLARD, M., HASHIMOTO, M., HORIE, Y., MASUMOTO, J., QIU, S., SAAB, L., OGURA, Y., KAWASAKI, A., FUKASE, K. & KUSUMOTO, S. 2003. An essential role for NOD1 in host recognition of bacterial peptidoglycan containing diaminopimelic acid. *Nature immunology,* 4**,** 702-707.

CHAPUT, C., ECOBICHON, C., POURADIER, N., ROUSSELLE, J.-C., NAMANE, A. & BONECA, I. G. 2016. Role of the N-acetylmuramoyl-l-alanyl amidase, AmiA, of Helicobacter pylori in peptidoglycan metabolism, daughter cell separation, and virulence. *Microbial Drug Resistance,* 22**,** 477-486.

CHAUHAN, A., MADIRAJU, M. V., FOL, M., LOFTON, H., MALONEY, E., REYNOLDS, R. & RAJAGOPALAN, M. 2006. Mycobacterium tuberculosis cells growing in macrophages are filamentous and deficient in FtsZ rings. *Journal of bacteriology,* 188**,** 1856-1865.

CHEN, R., GUTTENPLAN, S. B., BLAIR, K. M. & KEARNS, D. B. 2009. Role of the σD-dependent autolysins in Bacillus subtilis population heterogeneity. *Journal of bacteriology,* 191**,** 5775-5784.

CHODISETTI, P. K., BAHADUR, R., AMRUTHA, R. N. & REDDY, M. 2022. A LytM-Domain Factor, ActS, Functions in Two Distinctive Peptidoglycan Hydrolytic Pathways in E. coli. *Front Microbiol,* 13**,** 913949.

COHEN, K. A., MANSON, A. L., DESJARDINS, C. A., ABEEL, T. & EARL, A. M. 2019. Deciphering drug resistance in Mycobacterium tuberculosis using whole-genome sequencing: progress, promise, and challenges. *Genome Medicine,* 11**,** 1-18.

COLE, S., BROSCH, R., PARKHILL, J., GARNIER, T., CHURCHER, C., HARRIS, D., GORDON, S., EIGLMEIER, K., GAS, S. & BARRY, C. R. 1998. Deciphering the biology of Mycobacterium tuberculosis from the complete genome sequence. *Nature,* 396**,** 190-190.

CONDON, N. D., HEDDLESTON, J. M., CHEW, T.-L., LUO, L., MCPHERSON, P. S., IOANNOU, M. S., HODGSON, L., STOW, J. L. & WALL, A. A. 2018. Macropinosome formation by tent pole ruffling in macrophages. *Journal of Cell Biology,* 217**,** 3873-3885.

COTTON, M. F., MADHI, S. A., LUABEYA, A. K., TAMERIS, M., HESSELING, A. C., SHENJE, J., SCHOEMAN, E., HATHERILL, M., DESAI, S., KAPSE, D., BRÜCKNER, S., KOEN, A., JOSE, L., MOULTRIE, A., BHIKHA, S., WALZL, G., GUTSCHMIDT, A., KOTZE, L. A., ALLIES, D. L., LOXTON, A. G., SHALIGRAM, U., ABRAHAM, M., JOHNSTONE, H., GRODE, L., KAUFMANN, S. H. E. & KULKARNI, P. S. 2022. Safety and immunogenicity of VPM1002 versus BCG in South African newborn babies: a randomised, phase 2 non-inferiority double-blind controlled trial. *The Lancet Infectious Diseases,* 22**,** 1472-1483.

CRICK, D. C., MAHAPATRA, S. & BRENNAN, P. J. 2001. Biosynthesis of the arabinogalactan-peptidoglycan complex of Mycobacterium tuberculosis. *Glycobiology,* 11**,** 107r-118r.

CROFTON, J. & MITCHISON, D. 1948. Streptomycin resistance in pulmonary tuberculosis. *British medical journal,* 2**,** 1009.

CUTHBERTSON, L. & NODWELL, J. R. 2013. The TetR family of regulators. *Microbiology and Molecular Biology Reviews,* 77**,** 440-475.

DAFFÉ, M. & DRAPER, P. 1997. The envelope layers of mycobacteria with reference to their pathogenicity. *Advances in microbial physiology,* 39**,** 131-203.

DAHAL, P., KIM, D. Y. & KWON, E. 2021. Crystal structure of the DNA-binding domain of Bacillus subtilis CssR. *Biochemical and Biophysical Research Communications,* 555**,** 26-31.

DAY, T. A., PENN-NICHOLSON, A., LUABEYA, A. K. K., FIORE-GARTLAND, A., DU PLESSIS, N., LOXTON, A. G., VERGARA, J., ROLF, T. A., REID, T. D., TOEFY, A., SHENJE, J., GELDENHUYS, H., TAMERIS, M., MABWE, S., BILEK, N., BEKKER, L. G., DIACON, A., WALZL, G., ASHMAN, J., FREVOL, A., SAGAWA, Z. K., LINDESTAM ARLEHAMN, C., SETTE, A., REED, S. G., COLER, R. N., SCRIBA, T. J. & HATHERILL, M. 2021. Safety and immunogenicity of the adjunct therapeutic vaccine ID93 + GLA-SE in adults who have completed treatment for tuberculosis: a randomised, double-blind, placebo-controlled, phase 2a trial. *Lancet Respir Med,* 9**,** 373-386.

DE STEENWINKEL, J. E., DE KNEGT, G. J., TEN KATE, M. T., VAN BELKUM, A., VERBRUGH, H. A., KREMER, K., VAN SOOLINGEN, D. & BAKKER-WOUDENBERG, I. A. 2010. Time–kill kinetics of anti-tuberculosis drugs, and emergence of resistance, in relation to metabolic activity of Mycobacterium tuberculosis. *Journal of antimicrobial chemotherapy,* 65**,** 2582-2589.

DENG, G., JI, N., SHI, X., ZHANG, W., QIN, Y., SHA, S., YANG, S. & MA, Y. 2020. Effects of Mycobacterium tuberculosis Rv1096 on mycobacterial cell division and modulation on macrophages. *Microb Pathog,* 141**,** 103991.

DILLON, D. C., ALDERSON, M. R., DAY, C. H., LEWINSOHN, D. M., COLER, R., BEMENT, T., CAMPOS-NETO, A., SKEIKY, Y., ORME, I. M. & ROBERTS, A. 1999. Molecular characterization and human T-cell responses to a member of a novel Mycobacterium tuberculosis mtb39 gene family. *Infection and immunity,* 67**,** 2941-2950.

DO, T., PAGE, J. E. & WALKER, S. 2020a. Uncovering the activities, biological roles, and regulation of bacterial cell wall hydrolases and tailoring enzymes. *Journal of Biological Chemistry,* 295**,** 3347-3361.

DO, T., SCHAEFER, K., SANTIAGO, A. G., COE, K. A., FERNANDES, P. B., KAHNE, D., PINHO, M. G. & WALKER, S. 2020b. Staphylococcus aureus cell growth and division are regulated by an amidase that trims peptides from uncrosslinked peptidoglycan. *Nature microbiology,* 5**,** 291-303.

DORMAN, S. E., NAHID, P., KURBATOVA, E. V., GOLDBERG, S. V., BOZEMAN, L., BURMAN, W. J., CHANG, K. C., CHEN, M., COTTON, M., DOOLEY, K. E., ENGLE, M., FENG, P. J., FLETCHER, C. V., HA, P., HEILIG, C. M., JOHNSON, J. L., LESSEM, E., METCHOCK, B., MIRO, J. M., NHUNG, N. V., PETTIT, A. C., PHILLIPS, P. P. J., PODANY, A. T., PURFIELD, A. E., ROBERGEAU, K., SAMANEKA, W., SCOTT, N. A., SIZEMORE, E., VERNON, A., WEINER, M., SWINDELLS, S. & CHAISSON, R. E. 2020. High-dose rifapentine with or without moxifloxacin for shortening treatment of pulmonary tuberculosis: Study protocol for TBTC study 31/ACTG A5349 phase 3 clinical trial. *Contemp Clin Trials,* 90**,** 105938.

DORMAN, S. E., NAHID, P., KURBATOVA, E. V., PHILLIPS, P. P. J., BRYANT, K., DOOLEY, K. E., ENGLE, M., GOLDBERG, S. V., PHAN, H. T. T., HAKIM, J., JOHNSON, J. L., LOURENS, M., MARTINSON, N. A., MUZANYI, G., NARUNSKY, K., NERETTE, S., NGUYEN, N. V., PHAM, T. H., PIERRE, S., PURFIELD, A. E., SAMANEKA, W., SAVIC, R. M., SANNE, I., SCOTT, N. A., SHENJE, J., SIZEMORE, E., VERNON, A., WAJA, Z., WEINER, M., SWINDELLS, S. & CHAISSON, R. E. 2021. Four-Month Rifapentine Regimens with or without Moxifloxacin for Tuberculosis. *N Engl J Med,* 384**,** 1705-1718.

DORMAN, S. E., SCHUMACHER, S. G., ALLAND, D., NABETA, P., ARMSTRONG, D. T., KING, B., HALL, S. L., CHAKRAVORTY, S., CIRILLO, D. M., TUKVADZE, N., BABLISHVILI, N., STEVENS, W., SCOTT, L., RODRIGUES, C., KAZI, M. I., JOLOBA, M., NAKIYINGI, L., NICOL, M. P., GHEBREKRISTOS, Y., ANYANGO, I., MURITHI, W., DIETZE, R., LYRIO PERES, R., SKRAHINA, A., AUCHYNKA, V., CHOPRA, K. K., HANIF, M., LIU, X., YUAN, X., BOEHME, C. C., ELLNER, J. J., DENKINGER, C. M. & STUDY, T. 2018. Xpert MTB/RIF Ultra for detection of Mycobacterium tuberculosis and rifampicin resistance: a prospective multicentre diagnostic accuracy study. *The Lancet. Infectious diseases,* 18**,** 76-84.

DOYLE, R. J., CHALOUPKA, J. & VINTER, V. 1988. Turnover of cell walls in microorganisms. *Microbiological reviews,* 52**,** 554-567.

DRAIN, P. K., BAJEMA, K. L., DOWDY, D., DHEDA, K., NAIDOO, K., SCHUMACHER, S. G., MA, S., MEERMEIER, E., LEWINSOHN, D. M. & SHERMAN, D. R. 2018. Incipient and Subclinical Tuberculosis: a Clinical Review of Early Stages and Progression of Infection. *Clin Microbiol Rev,* 31.

DUBNAU, E., CHAN, J., RAYNAUD, C., MOHAN, V. P., LANÉELLE, M. A., YU, K., QUÉMARD, A., SMITH, I. & DAFFÉ, M. 2000. Oxygenated mycolic acids are

necessary for virulence of Mycobacterium tuberculosis in mice. *Mol Microbiol,* 36**,** 630-7.
DUBRAC, S., BONECA, I. G., POUPEL, O. & MSADEK, T. 2007. New insights into the WalK/WalR (YycG/YycF) essential signal transduction pathway reveal a major role in controlling cell wall metabolism and biofilm formation in Staphylococcus aureus. *Journal of bacteriology,* 189**,** 8257-8269.
DZIARSKI, R. & GUPTA, D. 2005. Staphylococcus aureus peptidoglycan is a toll-like receptor 2 activator: a reevaluation. *Infection and immunity,* 73**,** 5212-5216.
EALAND, C. S., ASMAL, R., MASHIGO, L., CAMPBELL, L. & KANA, B. D. 2019. Characterization of putative DD-carboxypeptidase-encoding genes in Mycobacterium smegmatis. *Scientific reports,* 9**,** 1-11.
ERCOLI, G., TANI, C., PEZZICOLI, A., VACCA, I., MARTINELLI, M., PECETTA, S., PETRACCA, R., RAPPUOLI, R., PIZZA, M., NORAIS, N., SORIANI, M. & ARICÒ, B. 2015. LytM proteins play a crucial role in cell separation, outer membrane composition, and pathogenesis in nontypeable Haemophilus influenzae. *mBio,* 6**,** e02575.
ERRINGTON, J. 1993. Bacillus subtilis sporulation: regulation of gene expression and control of morphogenesis. *Microbiol Rev,* 57**,** 1-33.
ERRINGTON, J. 2003. Regulation of endospore formation in Bacillus subtilis. *Nature Reviews Microbiology,* 1**,** 117-126.
FATIMA, S., KUMARI, A., DAS, G. & DWIVEDI, V. P. 2020. Tuberculosis vaccine: A journey from BCG to present. *Life Sci,* 252**,** 117594.
FLORES, A. R., PARSONS, L. M. & PAVELKA JR, M. S. 2005. Genetic analysis of the β-lactamases of Mycobacterium tuberculosis and Mycobacterium smegmatis and susceptibility to β-lactam antibiotics. *Microbiology,* 151**,** 521-532.
FOLKESSON, A., ERIKSSON, S., ANDERSSON, M., PARK, J. T. & NORMARK, S. 2005. Components of the peptidoglycan-recycling pathway modulate invasion and intracellular survival of Salmonella enterica serovar Typhimurium. *Cellular Microbiology,* 7**,** 147-155.
FRANKEL, M. B., HENDRICKX, A. P., MISSIAKAS, D. M. & SCHNEEWIND, O. 2011. LytN, a murein hydrolase in the cross-wall compartment of Staphylococcus aureus, is involved in proper bacterial growth and envelope assembly. *J Biol Chem,* 286**,** 32593-605.
FRANKEL, M. B. & SCHNEEWIND, O. 2012. Determinants of murein hydrolase targeting to cross-wall of Staphylococcus aureus peptidoglycan. *J Biol Chem,* 287**,** 10460-10471.
FRIRDICH, E., BIBOY, J., PRYJMA, M., LEE, J., HUYNH, S., PARKER, C. T., GIRARDIN, S. E., VOLLMER, W. & GAYNOR, E. C. 2019. The Campylobacter jejuni helical to coccoid transition involves changes to peptidoglycan and the ability to elicit an immune response. *Molecular Microbiology,* 112**,** 280-301.
FRIRDICH, E. & GAYNOR, E. C. 2013. Peptidoglycan hydrolases, bacterial shape, and pathogenesis. *Current opinion in microbiology,* 16**,** 767-778.
GAO, B., WANG, J., HUANG, J., HUANG, X., SHA, W. & QIN, L. 2019. The dynamic region of the peptidoglycan synthase gene, Rv0050, induces the growth rate and morphologic heterogeneity in Mycobacteria. *Infection, Genetics and Evolution,* 72**,** 86-92.
GILMORE, M. E., BANDYOPADHYAY, D., DEAN, A. M., LINNSTAEDT, S. D. & POPHAM, D. L. 2004. Production of muramic δ-lactam in Bacillus subtilis spore peptidoglycan. *Journal of bacteriology,* 186**,** 80-89.

GIRARDIN, S. E., BONECA, I. G., CARNEIRO, L. A., ANTIGNAC, A., JÉHANNO, M., VIALA, J., TEDIN, K., TAHA, M.-K., LABIGNE, A. & ZÄTHRINGER, U. 2003a. Nod1 detects a unique muropeptide from gram-negative bacterial peptidoglycan. *Science,* 300**,** 1584-1587.

GIRARDIN, S. E., BONECA, I. G., VIALA, J., CHAMAILLARD, M., LABIGNE, A., THOMAS, G., PHILPOTT, D. J. & SANSONETTI, P. J. 2003b. Nod2 is a general sensor of peptidoglycan through muramyl dipeptide (MDP) detection. *Journal of Biological Chemistry,* 278**,** 8869-8872.

GLICKMAN, M. S. 2003. The mmaA2 gene of Mycobacterium tuberculosis encodes the distal cyclopropane synthase of the alpha-mycolic acid. *J Biol Chem,* 278**,** 7844-9.

GLICKMAN, M. S., COX, J. S. & JACOBS, W. R., JR. 2000. A novel mycolic acid cyclopropane synthetase is required for cording, persistence, and virulence of Mycobacterium tuberculosis. *Mol Cell,* 5**,** 717-27.

GOKULAN, K. & VARUGHESE, K. I. 2019. Drug resistance in Mycobacterium tuberculosis and targeting the l, d-transpeptidase enzyme. *Drug Development Research,* 80**,** 11-18.

GÖTZ, F., HEILMANN, C. & STEHLE, T. 2014. Functional and structural analysis of the major amidase (Atl) in Staphylococcus. *Int J Med Microbiol,* 304**,** 156-63.

GRIFFIN, J. E., GAWRONSKI, J. D., DEJESUS, M. A., IOERGER, T. R., AKERLEY, B. J. & SASSETTI, C. M. 2011. High-Resolution Phenotypic Profiling Defines Genes Essential for Mycobacterial Growth and Cholesterol Catabolism. *PLOS Pathogens,* 7**,** e1002251.

GRODE, L., SEILER, P., BAUMANN, S., HESS, J., BRINKMANN, V., EDDINE, A. N., MANN, P., GOOSMANN, C., BANDERMANN, S. & SMITH, D. 2005. Increased vaccine efficacy against tuberculosis of recombinant Mycobacterium bovis bacille Calmette-Guerin mutants that secrete listeriolysin. *The Journal of clinical investigation,* 115**,** 2472-2479.

GRÖSCHEL, M. I., PRABOWO, S. A., CARDONA, P.-J., STANFORD, J. L. & WERF, T. S. V. D. 2014. Therapeutic vaccines for tuberculosis—A systematic review. *Vaccine,* 32**,** 3162-3168.

GUIRADO, E., SCHLESINGER, L. S. & KAPLAN, G. Macrophages in tuberculosis: friend or foe. Seminars in immunopathology, 2013. Springer, 563-583.

GUPTA, A., AHMAD, F. J., AHMAD, F., GUPTA, U. D., NATARAJAN, M., KATOCH, V. & BHASKAR, S. 2012. Efficacy of Mycobacterium indicus pranii Immunotherapy as an Adjunct to Chemotherapy for Tuberculosis and Underlying Immune Responses in the Lung. *PLOS ONE,* 7**,** e39215.

GURNANI SERRANO, C. K., WINKLE, M., MARTORANA, A. M., BIBOY, J., MORÈ, N., MOYNIHAN, P., BANZHAF, M., VOLLMER, W. & POLISSI, A. 2021. ActS activates peptidoglycan amidases during outer membrane stress in Escherichia coli. *Molecular Microbiology,* 116**,** 329-342.

HANNEBELLE, M., VEN, J. X., TONIOLO, C., ESKANDARIAN, H. A., VUARIDEL-THURRE, G., MCKINNEY, J. D. & FANTNER, G. E. 2020. A biphasic growth model for cell pole elongation in mycobacteria. *Nature communications,* 11**,** 1-10.

HARRISON, J., LLOYD, G., JOE, M., LOWARY, T. L., REYNOLDS, E., WALTERS-MORGAN, H., BHATT, A., LOVERING, A., BESRA, G. S. & ALDERWICK, L. J. 2016. Lcp1 Is a Phosphotransferase Responsible for Ligating Arabinogalactan to Peptidoglycan in Mycobacterium tuberculosis. *mBio,* 7.

HEALY, C., GOUZY, A. & EHRT, S. 2020. Peptidoglycan hydrolases RipA and Ami1 are critical for replication and persistence of Mycobacterium tuberculosis in the host. *MBio,* 11**,** e03315-19.

HEIDRICH, C., TEMPLIN, M. F., URSINUS, A., MERDANOVIC, M., BERGER, J., SCHWARZ, H., DE PEDRO, M. A. & HÖLTJE, J. V. 2001. Involvement of N-acetylmuramyl-L-alanine amidases in cell separation and antibiotic-induced autolysis of Escherichia coli. *Molecular microbiology,* 41**,** 167-178.

HEIDRICH, C., URSINUS, A., BERGER, J. R., SCHWARZ, H. & HÖLTJE, J.-V. 2002. Effects of multiple deletions of murein hydrolases on viability, septum cleavage, and sensitivity to large toxic molecules in Escherichia coli. *Journal of bacteriology,* 184**,** 6093-6099.

HEIJENOORT, J. V. 2011. Peptidoglycan Hydrolases of Escherichia coli. *Microbiology and Molecular Biology Reviews,* 75**,** 636-663.

HEILMANN, C., THUMM, G., CHHATWAL, G. S., HARTLEIB, J., UEKOTTER, A. & PETERS, G. 2003. Identification and characterization of a novel autolysin (Aae) with adhesive properties from Staphylococcus epidermidis. *Microbiology,* 149**,** 2769-2778.

HELMANN, J. D. & MORAN, C. P. RNA Polymerase and Sigma Factors. 2002.

HETT, E. C., CHAO, M. C. & RUBIN, E. J. 2010. Interaction and modulation of two antagonistic cell wall enzymes of mycobacteria. *PLoS pathogens,* 6**,** e1001020.

HETT, E. C. & RUBIN, E. J. 2008. Bacterial growth and cell division: a mycobacterial perspective. *Microbiology and Molecular Biology Reviews,* 72**,** 126-156.

HEYCKENDORF, J., ANDRES, S., KÖSER, C. U., OLARU, I. D., SCHÖN, T., STUREGÅRD, E., BECKERT, P., SCHLEUSENER, V., KOHL, T. A. & HILLEMANN, D. 2018. What is resistance? Impact of phenotypic versus molecular drug resistance testing on therapy for multi-and extensively drug-resistant tuberculosis. *Antimicrobial agents and chemotherapy,* 62**,** e01550-17.

HMAMA, Z., PEÑA-DÍAZ, S., JOSEPH, S. & AV-GAY, Y. 2015. Immunoevasion and immunosuppression of the macrophage by M ycobacterium tuberculosis. *Immunological reviews,* 264**,** 220-232.

HOAGLAND, D. T., LIU, J., LEE, R. B. & LEE, R. E. 2016. New agents for the treatment of drug-resistant Mycobacterium tuberculosis. *Advanced drug delivery reviews,* 102**,** 55-72.

HUSSAIN, M., STEINBACHER, T., PETERS, G., HEILMANN, C. & BECKER, K. 2015. The adhesive properties of the Staphylococcus lugdunensis multifunctional autolysin AtlL and its role in biofilm formation and internalization. *International Journal of Medical Microbiology,* 305**,** 129-139.

INOHARA, N. & NUÑEZ, G. 2003. NODs: intracellular proteins involved in inflammation and apoptosis. *Nat Rev Immunol,* 3**,** 371-82.

INOHARA, N., OGURA, Y., FONTALBA, A., GUTIERREZ, O., PONS, F., CRESPO, J., FUKASE, K., INAMURA, S., KUSUMOTO, S. & HASHIMOTO, M. 2003. Host recognition of bacterial muramyl dipeptide mediated through NOD2: implications for Crohn′ s disease. *Journal of Biological Chemistry,* 278**,** 5509-5512.

IYER, J. K., KHURANA, T., LANGER, M., WEST, C. M., BALLARD, J. D., METCALF, J. P., MERKEL, T. J. & COGGESHALL, K. M. 2010. Inflammatory cytokine response to Bacillus anthracis peptidoglycan requires phagocytosis and lysosomal trafficking. *Infect Immun,* 78**,** 2418-28.

JACKSON, M., RAYNAUD, C., LANÉELLE, M. A., GUILHOT, C., LAURENT-WINTER, C., ENSERGUEIX, D., GICQUEL, B. & DAFFÉ, M. 1999. Inactivation of the antigen 85C gene profoundly affects the mycolate content and alters the permeability of the Mycobacterium tuberculosis cell envelope. *Mol Microbiol,* 31**,** 1573-87.

JACOBS, C., JORIS, B., JAMIN, M., KLARSOV, K., VAN BEEUMEN, J., MENGIN-LECREULX, D., VAN HEIJENOORT, J., PARK, J. T., NORMARK, S. & FRÈRE, J.-M. 1995. AmpD, essential for both β-lactamase regulation and cell wall recycling,

is a novel cytosolic N-acetylmuramyl-L-alanine amidase. *Molecular Microbiology,* 15**,** 553-559.
JANKUTE, M., COX, J. A., HARRISON, J. & BESRA, G. S. 2015. Assembly of the mycobacterial cell wall. *Annual review of microbiology,* 69**,** 405-423.
JEYANATHAN, M., FRITZ, D. K., AFKHAMI, S., AGUIRRE, E., HOWIE, K. J., ZGANIACZ, A., DVORKIN-GHEVA, A., THOMPSON, M. R., SILVER, R. F., CUSACK, R. P., LICHTY, B. D., O'BYRNE, P. M., KOLB, M., MEDINA, M. F. C., DOLOVICH, M. B., SATIA, I., GAUVREAU, G. M., XING, Z. & SMAILL, F. 2022. Aerosol delivery, but not intramuscular injection, of adenovirus-vectored tuberculosis vaccine induces respiratory-mucosal immunity in humans. *JCI Insight,* 7.
JI, Z., JIAN, M., CHEN, T., LUO, L., LI, L., DAI, X., BAI, R., DING, Z., BI, Y., WEN, S., ZHOU, G., ABI, M.-E., LIU, A. & BAO, F. 2019. Immunogenicity and Safety of the M72/AS01E Candidate Vaccine Against Tuberculosis: A Meta-Analysis. *Frontiers in Immunology,* 10.
JOHNSON, J. W., FISHER, J. F. & MOBASHERY, S. 2013. Bacterial cell-wall recycling. *Annals of the New York Academy of Sciences,* 1277**,** 54-75.
KAJIMURA, J., FUJIWARA, T., YAMADA, S., SUZAWA, Y., NISHIDA, T., OYAMADA, Y., HAYASHI, I., YAMAGISHI, J. I., KOMATSUZAWA, H. & SUGAI, M. 2005. Identification and molecular characterization of an N-acetylmuramyl-l-alanine amidase Sle1 involved in cell separation of Staphylococcus aureus. *Molecular Microbiology,* 58**,** 1087-1101.
KAMARIZA, M., KEYSER, S. G. L., UTZ, A., KNAPP, B. D., EALAND, C., AHN, G., CAMBIER, C. J., CHEN, T., KANA, B., HUANG, K. C. & BERTOZZI, C. R. 2021. Toward Point-of-Care Detection of Mycobacterium tuberculosis: A Brighter Solvatochromic Probe Detects Mycobacteria within Minutes. *JACS Au,* 1**,** 1368-1379.
KAMARIZA, M., SHIEH, P., EALAND, C. S., PETERS, J. S., CHU, B., RODRIGUEZ-RIVERA, F. P., BABU SAIT, M. R., TREUREN, W. V., MARTINSON, N., KALSCHEUER, R., KANA, B. D. & BERTOZZI, C. R. 2018. Rapid detection of Mycobacterium tuberculosis in sputum with a solvatochromic trehalose probe. *Science Translational Medicine,* 10**,** eaam6310.
KAUR, D., GUERIN, M. E., ŠKOVIEROVÁ, H., BRENNAN, P. J. & JACKSON, M. 2009. Biogenesis of the cell wall and other glycoconjugates of Mycobacterium tuberculosis. *Advances in applied microbiology,* 69**,** 23-78.
KEARNS, D. B. & LOSICK, R. 2005. Cell population heterogeneity during growth of Bacillus subtilis. *Genes & development,* 19**,** 3083-3094.
KEESTRA-GOUNDER, A. M. & TSOLIS, R. M. 2017. NOD1 and NOD2: Beyond Peptidoglycan Sensing. *Trends Immunol,* 38**,** 758-767.
KIESER, K. J., BOUTTE, C. C., KESTER, J. C., BAER, C. E., BARCZAK, A. K., MENICHE, X., CHAO, M. C., REGO, E. H., SASSETTI, C. M. & FORTUNE, S. M. 2015. Phosphorylation of the peptidoglycan synthase PonA1 governs the rate of polar elongation in mycobacteria. *PLoS pathogens,* 11**,** e1005010.
KIESER, K. J. & KAGAN, J. C. 2017. Multi-receptor detection of individual bacterial products by the innate immune system. *Nat Rev Immunol,* 17**,** 376-390.
KIESER, K. J. & RUBIN, E. J. 2014. How sisters grow apart: mycobacterial growth and division. *Nature Reviews Microbiology,* 12**,** 550-562.
KIESWETTER, N. S., OZTURK, M., JONES, S.-S., SENZANI, S., CHENGALROYEN, M. D., BROMBACHER, F., KANA, B. & GULER, R. 2021. Deletion of N-acetylmuramyl-L-alanine amidases alters the host immune response to Mycobacterium tuberculosis infection. *Virulence,* 12**,** 1227-1238.

KLANCHER, C. A., MINASOV, G., PODICHETI, R., RUSCH, D. B., DALIA, T. N., SATCHELL, K. J. F., NEIDITCH, M. B. & DALIA, A. B. 2021. The ChiS-Family DNA-Binding Domain Contains a Cryptic Helix-Turn-Helix Variant. *mBio,* 12.

KOCH, A., COX, H. & MIZRAHI, V. 2018. Drug-resistant tuberculosis: challenges and opportunities for diagnosis and treatment. *Current Opinion in pharmacology,* 42**,** 7-15.

KOMMAREDDI, S., ABRAMOWSKY, C. R., SWINEHART, G. L. & HRABAK, L. 1984. Nontuberculous mycobacterial infections: comparison of the fluorescent auramine-O and Ziehl-Neelsen techniques in tissue diagnosis. *Hum Pathol,* 15**,** 1085-9.

KOUL, A., DENDOUGA, N., VERGAUWEN, K., MOLENBERGHS, B., VRANCKX, L., WILLEBRORDS, R., RISTIC, Z., LILL, H., DORANGE, I., GUILLEMONT, J., BALD, D. & ANDRIES, K. 2007. Diarylquinolines target subunit c of mycobacterial ATP synthase. *Nat Chem Biol,* 3**,** 323-4.

KUDHAIR, B. K. & GREEN, J. 2023. Overproduction and purification of Mycobacterium tuberculosis WhiB3 in Escherichia coli is enhanced by co-expression with trigger factor chaperone. *Protein Expression and Purification,* 202**,** 106197.

KUMAR, A., KUMAR, S., KUMAR, D., MISHRA, A., DEWANGAN, R. P., SHRIVASTAVA, P., RAMACHANDRAN, S. & TANEJA, B. 2013. The structure of Rv3717 reveals a novel amidase from Mycobacterium tuberculosis. *Acta Crystallogr D Biol Crystallogr,* 69**,** 2543-54.

KUMAR, P. 2021. A Perspective on the Success and Failure of BCG. *Frontiers in Immunology,* 12.

KUMAR, P., ARORA, K., LLOYD, J. R., LEE, I. Y., NAIR, V., FISCHER, E., BOSHOFF, H. I. & BARRY, C. E., 3RD 2012. Meropenem inhibits D,D-carboxypeptidase activity in Mycobacterium tuberculosis. *Mol Microbiol,* 86**,** 367-81.

KURODA, A., ASAMI, Y. & SEKIGUCHI, J. 1993. Molecular cloning of a sporulation-specific cell wall hydrolase gene of Bacillus subtilis. *J Bacteriol,* 175**,** 6260-8.

KURODA, A., IMAZEKI, M. & SEKIGUCHI, J. 1991. Purification and characterization of a cell wall hydrolase encoded by the cw1A gene of Bacillus subtilis. *FEMS Microbiology Letters,* 81**,** 9-13.

KURODA, A. & SEKIGUCHI, J. 1991. Molecular cloning and sequencing of a major Bacillus subtilis autolysin gene. *Journal of Bacteriology,* 173**,** 7304-7312.

KURODA, A. & SEKIGUCHI, J. 1992. Characterization of the Bacillus subtilis CwbA protein which stimulates cell wall lytic amidases. *FEMS Microbiology Letters,* 95**,** 109-113.

KURODA, M., OHTA, T., UCHIYAMA, I., BABA, T., YUZAWA, H., KOBAYASHI, I., CUI, L., OGUCHI, A., AOKI, K., NAGAI, Y., LIAN, J., ITO, T., KANAMORI, M., MATSUMARU, H., MARUYAMA, A., MURAKAMI, H., HOSOYAMA, A., MIZUTANI-UI, Y., TAKAHASHI, N. K., SAWANO, T., INOUE, R., KAITO, C., SEKIMIZU, K., HIRAKAWA, H., KUHARA, S., GOTO, S., YABUZAKI, J., KANEHISA, M., YAMASHITA, A., OSHIMA, K., FURUYA, K., YOSHINO, C., SHIBA, T., HATTORI, M., OGASAWARA, N., HAYASHI, H. & HIRAMATSU, K. 2001. Whole genome sequencing of meticillin-resistant Staphylococcus aureus. *Lancet,* 357**,** 1225-40.

KÜSSAU, T., VAN WYK, N., JOHANSEN, M. D., ALSARRAF, H. M., NEYRET, A., HAMELA, C., SØRENSEN, K. K., THYGESEN, M. B., BEAUVINEAU, C. & KREMER, L. 2020. Functional characterization of the N-acetylmuramyl-l-alanine amidase, Ami1, from mycobacterium abscessus. *Cells,* 9**,** 2410.

LARIVIERE, P. J., MAHONE, C. R., SANTIAGO-COLLAZO, G., HOWELL, M., DAITCH, A. K., ZEINERT, R., CHIEN, P., BROWN, P. J. B. & GOLEY, E. D.

2019. An Essential Regulator of Bacterial Division Links FtsZ to Cell Wall Synthase Activation. *Current biology : CB,* 29**,** 1460-1470.e4.
LAVOLLAY, M., ARTHUR, M., FOURGEAUD, M., DUBOST, L., MARIE, A., VEZIRIS, N., BLANOT, D., GUTMANN, L. & MAINARDI, J. L. 2008. The peptidoglycan of stationary-phase Mycobacterium tuberculosis predominantly contains cross-links generated by L,D-transpeptidation. *J Bacteriol,* 190**,** 4360-6.
LAWN, S. D., KERKHOFF, A. D., VOGT, M. & WOOD, R. 2012. Diagnostic accuracy of a low-cost, urine antigen, point-of-care screening assay for HIV-associated pulmonary tuberculosis before antiretroviral therapy: a descriptive study. *Lancet Infect Dis,* 12**,** 201-9.
LECLERCQ, S., DEROUAUX, A., OLATUNJI, S., FRAIPONT, C., EGAN, A. J. F., VOLLMER, W., BREUKINK, E. & TERRAK, M. 2017. Interplay between Penicillin-binding proteins and SEDS proteins promotes bacterial cell wall synthesis. *Scientific Reports,* 7**,** 43306.
LEWINSOHN, D., LEWINSOHN, D. & SCRIBA, T. 2017. Polyfunctional CD4 (+) T Cells As Targets for Tuberculosis Vaccination. Front Immunol 8: 1262.
LEWIS, J., SNELL, N. & BURR, H. 1960. Water permeability of bacterial spores and the concept of a contractile cortex. *Science,* 132**,** 544-545.
LIN, X. P., MINTERN, J. D. & GLEESON, P. A. 2020. Macropinocytosis in Different Cell Types: Similarities and Differences. *Membranes (Basel),* 10.
LINDQUIST, S., GALLENI, M., LINDBERG, F. & NORMARK, S. 1989. Signalling proteins in enterobacterial AmpC β-lactamase regulation. *Molecular microbiology,* 3**,** 1091-1102.
LONGCHAMP, P. F., MAUËL, C. & KARAMATA, D. 1994. Lytic enzymes associated with defective prophages of Bacillus subtilis: Sequencing and characterization of the region comprising the N-acetylmuramoyl-L-alanine amidase gene of prophage PBSX. *Microbiology,* 140**,** 1855-1867.
LUABEYA, A. K. K., KAGINA, B. M., TAMERIS, M. D., GELDENHUYS, H., HOFF, S. T., SHI, Z., KROMANN, I., HATHERILL, M., MAHOMED, H. & HANEKOM, W. A. 2015. First-in-human trial of the post-exposure tuberculosis vaccine H56: IC31 in Mycobacterium tuberculosis infected and non-infected healthy adults. *Vaccine,* 33**,** 4130-4140.
MA, S., MORRISON, R., HOBBS, S. J., SONI, V., FARROW-JOHNSON, J., FRANDO, A., FLECK, N., GRUNDNER, C., RHEE, K. Y., RUSTAD, T. R. & SHERMAN, D. R. 2021. Transcriptional regulator-induced phenotype screen reveals drug potentiators in Mycobacterium tuberculosis. *Nat Microbiol,* 6**,** 44-50.
MABHULA, A. & SINGH, V. 2019. Drug-resistance in Mycobacterium tuberculosis: where we stand. *MedChemComm,* 10**,** 1342-1360.
MACHADO, D., COUTO, I. & VIVEIROS, M. 2019. Advances in the molecular diagnosis of tuberculosis: From probes to genomes. *Infect Genet Evol,* 72**,** 93-112.
MACHOWSKI, E. E., SENZANI, S., EALAND, C. & KANA, B. D. 2014. Comparative genomics for mycobacterial peptidoglycan remodelling enzymes reveals extensive genetic multiplicity. *BMC Microbiology,* 14**,** 75.
MACLEAN, E., KOHLI, M., WEBER, S. F., SURESH, A., SCHUMACHER, S. G., DENKINGER, C. M. & PAI, M. 2020. Advances in Molecular Diagnosis of Tuberculosis. *J Clin Microbiol,* 58.
MADAN-LALA, R., SIA, J. K., KING, R., ADEKAMBI, T., MONIN, L., KHADER, S. A., PULENDRAN, B. & RENGARAJAN, J. 2014. Mycobacterium tuberculosis impairs dendritic cell functions through the serine hydrolase Hip1. *J Immunol,* 192**,** 4263-72.

MAHAJAN, R. 2013. Bedaquiline: first FDA-approved tuberculosis drug in 40 years. Medknow.
MAITRA, A., NUKALA, S., DICKMAN, R., MARTIN, L. T., MUNSHI, T., GUPTA, A., SHEPHERD, A. J., ARNVIG, K. B., TABOR, A. B., KEEP, N. H. & BHAKTA, S. 2021. Characterization of the MurT/GatD complex in Mycobacterium tuberculosis towards validating a novel anti-tubercular drug target. *JAC-Antimicrobial Resistance,* 3.
MALINGA, L. & STOLTZ, A. 2016. Efflux Pump Mediated Second-Line Tuberculosis Drug Resistance. *Mycobacterial Diseases,* 6.
MAPHATSOE, M. 2017. *Cellular localization of low-molecular-weight penicillin-binding proteins and other cell wall remodeling enzymes in Mycobacterium smegmatis.* Master of Science, University of the Witwatersrand
MARAIS, B. J. & PAI, M. 2007. New approaches and emerging technologies in the diagnosis of childhood tuberculosis. *Paediatric respiratory reviews,* 8**,** 124-133.
MARTIN, C., AGUILO, N., MARINOVA, D. & GONZALO-ASENSIO, J. 2020. Update on TB Vaccine Pipeline. *Applied Sciences,* 10**,** 2632.
MCNEIL, M., DAFFE, M. & BRENNAN, P. J. 1990. Evidence for the nature of the link between the arabinogalactan and peptidoglycan of mycobacterial cell walls. *J Biol Chem,* 265**,** 18200-6.
MEADOR-PARTON, J. & POPHAM, D. L. 2000. Structural analysis of Bacillus subtilis spore peptidoglycan during sporulation. *J Bacteriol,* 182**,** 4491-9.
MEISNER, J., MAEHIGASHI, T., ANDRÉ, I., DUNHAM, C. M. & MORAN, C. P., JR. 2012. Structure of the basal components of a bacterial transporter. *Proc Natl Acad Sci U S A,* 109**,** 5446-51.
MENICHE, X., OTTEN, R., SIEGRIST, M. S., BAER, C. E., MURPHY, K. C., BERTOZZI, C. R. & SASSETTI, C. M. 2014. Subpolar addition of new cell wall is directed by DivIVA in mycobacteria. *Proc Natl Acad Sci U S A,* 111**,** E3243-51.
MIAO, J., LIU, H., QU, Y., FU, W., QI, K., ZANG, S., HE, J., ZHAO, S., CHEN, S. & JIANG, T. 2020. Effect of peptidoglycan amidase MSMEG_6281 on fatty acid metabolism in Mycobacterium smegmatis. *Microb Pathog,* 140**,** 103939.
MIR, M., ASONG, J., LI, X., CARDOT, J., BOONS, G.-J. & HUSSON, R. N. 2011. The Extracytoplasmic Domain of the Mycobacterium tuberculosis Ser/Thr Kinase PknB Binds Specific Muropeptides and Is Required for PknB Localization. *PLOS Pathogens,* 7**,** e1002182.
MIRZAYEV, F., VINEY, K., LINH, N. N., GONZALEZ-ANGULO, L., GEGIA, M., JARAMILLO, E., ZIGNOL, M. & KASAEVA, T. 2021. World Health Organization recommendations on the treatment of drug-resistant tuberculosis, 2020 update. *European Respiratory Journal,* 57.
MOHANTY, S., JAGANNATHAN, L., GANGULI, G., PADHI, A., ROY, D., ALARIDAH, N., SAHA, P., NONGTHOMBA, U., GODALY, G., GOPAL, R. K., BANERJEE, S. & SONAWANE, A. 2015. A mycobacterial phosphoribosyltransferase promotes bacillary survival by inhibiting oxidative stress and autophagy pathways in macrophages and zebrafish. *J Biol Chem,* 290**,** 13321-43.
MÖLL, A., DÖRR, T., ALVAREZ, L., CHAO, M. C., DAVIS, B. M., CAVA, F. & WALDOR, M. K. 2014. Cell separation in Vibrio cholerae is mediated by a single amidase whose action is modulated by two nonredundant activators. *J Bacteriol,* 196**,** 3937-48.
MOYNIHAN, P., CADBY, I., VEERAPEN, N., JANKUTE, M., CROSATTI, M., MUKAMOLOVA, G., LOVERING, A. & BESRA, G. 2019. The hydrolase LpqI primes mycobacterial peptidoglycan recycling. *Nature Communications,* 10.

MUELLER, E. A., IKEN, A. G., ALI ÖZTÜRK, M., WINKLE, M., SCHMITZ, M., VOLLMER, W., DI VENTURA, B. & LEVIN, P. A. 2021. The active repertoire of Escherichia coli peptidoglycan amidases varies with physiochemical environment. *Mol Microbiol,* 116**,** 311-328.

MUNSERI, P., SAID, J., AMOUR, M., MAGOHE, A., MATEE, M., REES, C. A., MACKENZIE, T., TVAROHA, S., BAILEY-KELLOGG, C., MARO, I., WIELAND-ALTER, W., ADAMS, L. V., HORSBURGH, C. R., NAKAMURA, K., ARBEIT, R. D., PALLANGYO, K. & VON REYN, C. F. 2020. DAR-901 vaccine for the prevention of infection with Mycobacterium tuberculosis among BCG-immunized adolescents in Tanzania: A randomized controlled, double-blind phase 2b trial. *Vaccine,* 38**,** 7239-7245.

NAIR, N., VINOD, V., SURESH, M. K., VIJAYRAJRATNAM, S., BISWAS, L., PEETHAMBARAN, R., VASUDEVAN, A. K. & BISWAS, R. 2015. Amidase, a cell wall hydrolase, elicits protective immunity against Staphylococcus aureus and S. epidermidis. *International journal of biological macromolecules,* 77**,** 314-321.

NARRANDES, N. C., MACHOWSKI, E. E., MIZRAHI, V. & KANA, B. D. 2015. Cleavage of the moaX-encoded fused molybdopterin synthase from Mycobacterium tuberculosis is necessary for activity. *BMC Microbiology,* 15**,** 22.

NEGA, M., TRIBELLI, P. M., HIPP, K., STAHL, M. & GÖTZ, F. 2020. New insights in the coordinated amidase and glucosaminidase activity of the major autolysin (Atl) in Staphylococcus aureus. *Communications Biology,* 3**,** 695.

NELL, A. S., D'LOM, E., BOUIC, P., SABATÉ, M., BOSSER, R., PICAS, J., AMAT, M., CHURCHYARD, G. & CARDONA, P.-J. 2014. Safety, tolerability, and immunogenicity of the novel antituberculous vaccine RUTI: randomized, placebo-controlled phase II clinical trial in patients with latent tuberculosis infection. *PloS one,* 9**,** e89612.

NEMES, E., GELDENHUYS, H., ROZOT, V., RUTKOWSKI, K. T., RATANGEE, F., BILEK, N., MABWE, S., MAKHETHE, L., ERASMUS, M. & TOEFY, A. 2018. Prevention of M. tuberculosis infection with H4: IC31 vaccine or BCG revaccination. *New England Journal of Medicine,* 379**,** 138-149.

NGADJEUA, F., BRAUD, E., SAIDJALOLOV, S., IANNAZZO, L., SCHNAPPINGER, D., EHRT, S., HUGONNET, J. E., MENGIN-LECREULX, D., PATIN, D., ETHÈVE-QUELQUEJEU, M., FONVIELLE, M. & ARTHUR, M. 2018. Critical Impact of Peptidoglycan Precursor Amidation on the Activity of l,d-Transpeptidases from Enterococcus faecium and Mycobacterium tuberculosis. *Chemistry,* 24**,** 5743-5747.

NIEUWENHUIZEN, N. E., KULKARNI, P. S., SHALIGRAM, U., COTTON, M. F., RENTSCH, C. A., EISELE, B., GRODE, L. & KAUFMANN, S. H. E. 2017. The Recombinant Bacille Calmette-Guérin Vaccine VPM1002: Ready for Clinical Efficacy Testing. *Frontiers in immunology,* 8**,** 1147-1147.

NIKITUSHKIN, V. D., DEMINA, G. R., SHLEEVA, M. O., GURYANOVA, S. V., RUGGIERO, A., BERISIO, R. & KAPRELYANTS, A. S. 2015. A product of RpfB and RipA joint enzymatic action promotes the resuscitation of dormant mycobacteria. *Febs j,* 282**,** 2500-11.

NUGROHO, F. A., YAMAMOTO, H., KOBAYASHI, Y. & SEKIGUCHI, J. 1999. Characterization of a new sigma-K-dependent peptidoglycan hydrolase gene that plays a role in Bacillus subtilis mother cell lysis. *J Bacteriol,* 181**,** 6230-7.

OGURA, Y., BONEN, D. K., INOHARA, N., NICOLAE, D. L., CHEN, F. F., RAMOS, R., BRITTON, H., MORAN, T., KARALIUSKAS, R. & DUERR, R. H. 2001. A frameshift mutation in NOD2 associated with susceptibility to Crohn's disease. *Nature,* 411**,** 603-606.

OJHA, A. K., BAUGHN, A. D., SAMBANDAN, D., HSU, T., TRIVELLI, X., GUERARDEL, Y., ALAHARI, A., KREMER, L., JACOBS JR, W. R. & HATFULL, G. F. 2008. Growth of Mycobacterium tuberculosis biofilms containing free mycolic acids and harbouring drug-tolerant bacteria. *Molecular Microbiology,* 69**,** 164-174.

OZINSKY, A., UNDERHILL, D. M., FONTENOT, J. D., HAJJAR, A. M., SMITH, K. D., WILSON, C. B., SCHROEDER, L. & ADEREM, A. 2000. The repertoire for pattern recognition of pathogens by the innate immune system is defined by cooperation between Toll-like receptors. *Proceedings of the National Academy of Sciences,* 97**,** 13766-13771.

PAI, M., BEHR, M. A., DOWDY, D., DHEDA, K., DIVANGAHI, M., BOEHME, C. C., GINSBERG, A., SWAMINATHAN, S., SPIGELMAN, M., GETAHUN, H., MENZIES, D. & RAVIGLIONE, M. 2016. Tuberculosis. *Nature Reviews Disease Primers,* 2**,** 16076.

PARK, J. T. & UEHARA, T. 2008. How bacteria consume their own exoskeletons (turnover and recycling of cell wall peptidoglycan). *Microbiology and Molecular Biology Reviews,* 72**,** 211-227.

PASSMORE, J. S., LUKEY, P. T. & RESS, S. R. 2001. The human macrophage cell line U937 as an in vitro model for selective evaluation of mycobacterial antigen-specific cytotoxic T-cell function. *Immunology,* 102**,** 146-56.

PENNARTZ, A., GÉNÉREUX, C., PARQUET, C., MENGIN-LECREULX, D. & JORIS, B. 2009. Substrate-Induced Inactivation of the Escherichia coli AmiD N-Acetylmuramoyl-l-Alanine Amidase Highlights a New Strategy To Inhibit This Class of Enzyme. *Antimicrobial Agents and Chemotherapy,* 53**,** 2991-2997.

PETERS, J. S., ANDREWS, J. R., HATHERILL, M., HERMANS, S., MARTINEZ, L., SCHURR, E., VAN DER HEIJDEN, Y., WOOD, R., RUSTOMJEE, R. & KANA, B. D. 2019. Advances in the understanding of Mycobacterium tuberculosis transmission in HIV-endemic settings. *Lancet Infect Dis,* 19**,** e65-e76.

PETERS, N. T., DINH, T. & BERNHARDT, T. G. 2011. A fail-safe mechanism in the septal ring assembly pathway generated by the sequential recruitment of cell separation amidases and their activators. *Journal of bacteriology,* 193**,** 4973-4983.

PETERS, N. T., MORLOT, C., YANG, D. C., UEHARA, T., VERNET, T. & BERNHARDT, T. G. 2013. Structure-function analysis of the LytM domain of EnvC, an activator of cell wall remodelling at the Escherichia coli division site. *Mol Microbiol,* 89**,** 690-701.

PETTIT, A. C., PHILLIPS, P. P. J., KURBATOVA, E., VERNON, A., NAHID, P., DAWSON, R., DOOLEY, K. E., SANNE, I., WAJA, Z., MOHAPI, L., PODANY, A. T., SAMANEKA, W., SAVIC, R. M., JOHNSON, J. L., MUZANYI, G., LALLOO, U. G., BRYANT, K., SIZEMORE, E., SCOTT, N., DORMAN, S. E., CHAISSON, R. E. & SWINDELLS, S. 2023. Rifapentine With and Without Moxifloxacin for Pulmonary Tuberculosis in People With Human Immunodeficiency Virus (S31/A5349). *Clin Infect Dis,* 76**,** e580-e589.

PIGGOT, P. J. & HILBERT, D. W. 2004. Sporulation of Bacillus subtilis. *Curr Opin Microbiol,* 7**,** 579-86.

POPHAM, D. L., MEADOR-PARTON, J., COSTELLO, C. E. & SETLOW, P. 1999. Spore peptidoglycan structure in a cwlD dacB double mutant of Bacillus subtilis. *J Bacteriol,* 181**,** 6205-9.

PORTELLI, S., PHELAN, J. E., ASCHER, D. B., CLARK, T. G. & FURNHAM, N. 2018. Understanding molecular consequences of putative drug resistant mutations in Mycobacterium tuberculosis. *Sci Rep,* 8**,** 15356.

PRIGOZHIN, D. M., MAVRICI, D., HUIZAR, J. P., VANSELL, H. J. & ALBER, T. 2013. Structural and biochemical analyses of Mycobacterium tuberculosis N-acetylmuramyl-L-alanine amidase Rv3717 point to a role in peptidoglycan fragment recycling. *The Journal of biological chemistry,* 288**,** 31549-31555.

PRIYADARSHINI, R., DE PEDRO, M. A. & YOUNG, K. D. 2007. Role of peptidoglycan amidases in the development and morphology of the division septum in Escherichia coli. *Journal of bacteriology,* 189**,** 5334-5347.

PRIYADARSHINI, R., POPHAM, D. L. & YOUNG, K. D. 2006. Daughter Cell Separation by Penicillin-Binding Proteins and Peptidoglycan Amidases in Escherichia coli. *Journal of Bacteriology,* 188**,** 5345-5355.

RAMOS, J. L., MARTÍNEZ-BUENO, M., MOLINA-HENARES, A. J., TERÁN, W., WATANABE, K., ZHANG, X., GALLEGOS, M. T., BRENNAN, R. & TOBES, R. 2005. The TetR family of transcriptional repressors. *Microbiology and molecular biology reviews,* 69**,** 326-356.

RAO, V., FUJIWARA, N., PORCELLI, S. A. & GLICKMAN, M. S. 2005. Mycobacterium tuberculosis controls host innate immune activation through cyclopropane modification of a glycolipid effector molecule. *J Exp Med,* 201**,** 535-43.

RASHID, M. H., SATO, N. & SEKIGUCHI, J. 1995. Analysis of the minor autolysins of Bacillus subtilis during vegetative growth by zymography. *FEMS microbiology letters,* 132**,** 131-137.

RASOOL, G., KHAN, A. M., MOHY-UD-DIN, R. & RIAZ, M. 2019. Detection of Mycobacterium tuberculosis in AFB smear-negative sputum specimens through MTB culture and GeneXpert(®) MTB/RIF assay. *Int J Immunopathol Pharmacol,* 33**,** 2058738419827174.

RATNATUNGA, C. N., LUTZKY, V. P., KUPZ, A., DOOLAN, D. L., REID, D. W., FIELD, M., BELL, S. C., THOMSON, R. M. & MILES, J. J. 2020. The rise of non-tuberculosis mycobacterial lung disease. *Frontiers in immunology,* 11**,** 303.

RAYMOND, J. B., MAHAPATRA, S., CRICK, D. C. & PAVELKA, M. S., JR. 2005. Identification of the namH Gene, Encoding the Hydroxylase Responsible for the N-Glycolylation of the Mycobacterial Peptidoglycan *. *Journal of Biological Chemistry,* 280**,** 326-333.

REGAMEY, A. & KARAMATA, D. 1998. The N-acetylmuramoyl-L-alanine amidase encoded by the Bacillus subtilis 168 prophage SPβ. *Microbiology,* 144**,** 885-893.

REGO, E. H., AUDETTE, R. E. & RUBIN, E. J. 2017. Deletion of a mycobacterial divisome factor collapses single-cell phenotypic heterogeneity. *Nature,* 546**,** 153-157.

REICHMANN, N., TAVARES, A., SARAIVA, B., JOUSSELIN, A., REED, P., PEREIRA, A., MONTEIRO, J., SOBRAL, R., VANNIEUWENHZE, M., FERNANDES, F. & PINHO, M. 2019. SEDS–bPBP pairs direct lateral and septal peptidoglycan synthesis in Staphylococcus aureus. *Nature Microbiology,* 4.

ROCABOY, M., HERMAN, R., SAUVAGE, E., REMAUT, H., MOONENS, K., TERRAK, M., CHARLIER, P. & KERFF, F. 2013. The crystal structure of the cell division amidase AmiC reveals the fold of the AMIN domain, a new peptidoglycan binding domain. *Molecular Microbiology,* 90**,** 267-277.

ROGERS, H., TAYLOR, C., RAYTER, S. & WARD, J. 1984. Purification and properties of autolytic endo-β-N-acetylglucosaminidase and the N-acetylmuramyl-L-alanine amidase from Bacillus subtilis strain 168. *Microbiology,* 130**,** 2395-2402.

ROLAIN, T., BERNARD, E., COURTIN, P., BRON, P. A., KLEEREBEZEM, M., CHAPOT-CHARTIER, M.-P. & HOLS, P. 2012. Identification of key peptidoglycan hydrolases for morphogenesis, autolysis, and peptidoglycan composition of Lactobacillus plantarum WCFS1. *Microbial Cell Factories,* 11**,** 137.

ROUSSEAU, A., MICHAUD, J., PRADEAU, S., ARMAND, S., COTTAZ, S., RICHARD, E. & FORT, S. 2023. Hijacking the Peptidoglycan Recycling Pathway of Escherichia coli to Produce Muropeptides. *Chemistry – A European Journal,* 29**,** e202202991.

SABLE, S. B., POSEY, J. E. & SCRIBA, T. J. 2019. Tuberculosis Vaccine Development: Progress in Clinical Evaluation. *Clinical Microbiology Reviews,* 33**,** 10.1128/cmr.00100-19.

SAIGA, H., NIEUWENHUIZEN, N., GENGENBACHER, M., KOEHLER, A.-B., SCHUERER, S., MOURA-ALVES, P., WAGNER, I., MOLLENKOPF, H.-J., DORHOI, A. & KAUFMANN, S. H. 2015. The Recombinant BCG Δ ureC:: hly vaccine targets the AIM2 inflammasome to induce autophagy and inflammation. *The Journal of infectious diseases,* 211**,** 1831-1841.

SAINI, N. K., BAENA, A., NG, T. W., VENKATASWAMY, M. M., KENNEDY, S. C., KUNNATH-VELAYUDHAN, S., CARREÑO, L. J., XU, J., CHAN, J., LARSEN, M. H., JACOBS, W. R. & PORCELLI, S. A. 2016. Suppression of autophagy and antigen presentation by Mycobacterium tuberculosis PE_PGRS47. *Nature Microbiology,* 1**,** 16133.

SAUVAGE, E., KERFF, F., TERRAK, M., AYALA, J. A. & CHARLIER, P. 2008. The penicillin-binding proteins: structure and role in peptidoglycan biosynthesis. *FEMS Microbiol Rev,* 32**,** 234-58.

SCANGA, C. A., MOHAN, V. P., JOSEPH, H., YU, K., CHAN, J. & FLYNN, J. L. 1999. Reactivation of latent tuberculosis: variations on the Cornell murine model. *Infect Immun,* 67**,** 4531-8.

SCHÄFER, G., JACOBS, M., WILKINSON, R. J. & BROWN, G. D. 2009. Non-opsonic recognition of Mycobacterium tuberculosis by phagocytes. *J Innate Immun,* 1**,** 231-43.

SCHAIBLE, U. E., WINAU, F., SIELING, P. A., FISCHER, K., COLLINS, H. L., HAGENS, K., MODLIN, R. L., BRINKMANN, V. & KAUFMANN, S. H. 2003. Apoptosis facilitates antigen presentation to T lymphocytes through MHC-I and CD1 in tuberculosis. *Nature medicine,* 9**,** 1039-1046.

SCHOONMAKER, M. K., BISHAI, W. R. & LAMICHHANE, G. 2014. Nonclassical transpeptidases of Mycobacterium tuberculosis alter cell size, morphology, the cytosolic matrix, protein localization, virulence, and resistance to β-lactams. *Journal of bacteriology,* 196**,** 1394-1402.

SCHRAGER, L. K., VEKEMENS, J., DRAGER, N., LEWINSOHN, D. M. & OLESEN, O. F. 2020. The status of tuberculosis vaccine development. *Lancet Infect Dis,* 20**,** e28-e37.

SCHRAMM, B., NGANABOY, R. C., UWIRAGIYE, P., MUKEBA, D., ABDOUBARA, A., ABDOU, I., NSHIMIYMANA, J.-C., SOUNNA, S., HIFFLER, L., FLEVAUD, L. & HUERGA, H. 2021. Potential value of urine lateral-flow lipoarabinomannan (LAM) test for diagnosing tuberculosis among severely acute malnourished children. *PLOS ONE,* 16**,** e0250933.

SEKIGUCHI, J., AKEO, K., YAMAMOTO, H., KHASANOV, F. K., ALONSO, J. C. & KURODA, A. 1995. Nucleotide sequence and regulation of a new putative cell wall hydrolase gene, cwlD, which affects germination in Bacillus subtilis. *Journal of Bacteriology,* 177**,** 5582-5589.

SENZANI, S. 2018. *Characterisation of mycobacterial amidases and their role in bacterial growth and physiology.* Doctor of Philosophy on medicine Thesis, University of the Witwatersrand.

SENZANI, S., LI, D., BHASKAR, A., EALAND, C., CHANG, J., RIMAL, B., LIU, C., JOON KIM, S., DHAR, N. & KANA, B. 2017. An Amidase_3 domain-containing N-

acetylmuramyl-L-alanine amidase is required for mycobacterial cell division. *Sci Rep*, 7**,** 1140.
SHAH, I. M., LAABERKI, M. H., POPHAM, D. L. & DWORKIN, J. 2008. A eukaryotic-like Ser/Thr kinase signals bacteria to exit dormancy in response to peptidoglycan fragments. *Cell*, 135**,** 486-96.
SHARMA, A. K., KUMAR, S., K, H., DHAKAN, D. B. & SHARMA, V. K. 2016. Prediction of peptidoglycan hydrolases- a new class of antibacterial proteins. *BMC Genomics*, 17**,** 411.
SIA, J. K. & RENGARAJAN, J. 2019. Immunology of Mycobacterium tuberculosis Infections. *Microbiology spectrum*, 7**,** 10.1128/microbiolspec.GPP3-0022-2018.
SIEGRIST, M. S. & RUBIN, E. J. 2009. Phage transposon mutagenesis. *Methods Mol Biol*, 465**,** 311-23.
SIKHOSANA, N. 2018. *Mycobacterium amidases: biological function and putative role in cell wall remodeling.* Master of Science, University of the Witwatersrand.
SINGH, S. K., PARVEEN, S., SAISREE, L. & REDDY, M. 2015. Regulated proteolysis of a cross-link-specific peptidoglycan hydrolase contributes to bacterial morphogenesis. *Proc Natl Acad Sci U S A*, 112**,** 10956-61.
SINGH, S. K., SAISREE, L., AMRUTHA, R. N. & REDDY, M. 2012. Three redundant murein endopeptidases catalyse an essential cleavage step in peptidoglycan synthesis of E scherichia coli K 12. *Molecular microbiology*, 86**,** 1036-1051.
SKEIKY, Y. A., LODES, M. J., GUDERIAN, J. A., MOHAMATH, R., BEMENT, T., ALDERSON, M. R. & REED, S. G. 1999. Cloning, expression, and immunological evaluation of two putative secreted serine protease antigens of Mycobacterium tuberculosis. *Infection and immunity*, 67**,** 3998-4007.
SMAILL, F. & XING, Z. 2014. Human type 5 adenovirus-based tuberculosis vaccine: is the respiratory route of delivery the future? *Expert Review of Vaccines*, 13**,** 927-930.
SMITH, I. 2003. Mycobacterium tuberculosis pathogenesis and molecular determinants of virulence. *Clin Microbiol Rev*, 16**,** 463-96.
SMITH, T. J., BLACKMAN, S. A. & FOSTER, S. J. 2000. Autolysins of Bacillus subtilis: multiple enzymes with multiple functions. *Microbiology (Reading)*, 146 (Pt 2)**,** 249-262.
SMITH, T. J. & FOSTER, S. J. 1995. Characterization of the involvement of two compensatory autolysins in mother cell lysis during sporulation of Bacillus subtilis 168. *J Bacteriol*, 177**,** 3855-62.
SNAPPER, S. B., MELTON, R. E., MUSTAFA, S., KIESER, T. & JACOBS, W. R., JR. 1990. Isolation and characterization of efficient plasmid transformation mutants of Mycobacterium smegmatis. *Mol Microbiol*, 4**,** 1911-9.
SQUEGLIA, F., RUGGIERO, A. & BERISIO, R. 2018. Chemistry of Peptidoglycan in Mycobacterium tuberculosis Life Cycle: An off-the-wall Balance of Synthesis and Degradation. *Chemistry*, 24**,** 2533-2546.
STEIL, L., HOFFMANN, T., BUDDE, I., VÖLKER, U. & BREMER, E. 2003. Genome-wide transcriptional profiling analysis of adaptation of Bacillus subtilis to high salinity. *J Bacteriol*, 185**,** 6358-70.
STEINGART, K. R., NG, V., HENRY, M., HOPEWELL, P. C., RAMSAY, A., CUNNINGHAM, J., URBANCZIK, R., PERKINS, M. D., AZIZ, M. A. & PAI, M. 2006. Sputum processing methods to improve the sensitivity of smear microscopy for tuberculosis: a systematic review. *Lancet Infect Dis*, 6**,** 664-74.
STUTZ, M. D., CLARK, M. P., DOERFLINGER, M. & PELLEGRINI, M. 2018a. Mycobacterium tuberculosis: Rewiring host cell signaling to promote infection. *J Leukoc Biol*, 103**,** 259-268.

STUTZ, M. D., OJAIMI, S., ALLISON, C., PRESTON, S., ARANDJELOVIC, P., HILDEBRAND, J. M., SANDOW, J. J., WEBB, A. I., SILKE, J. & ALEXANDER, W. S. 2018b. Necroptotic signaling is primed in Mycobacterium tuberculosis-infected macrophages, but its pathophysiological consequence in disease is restricted. *Cell Death & Differentiation,* 25**,** 951-965.

TAIT, D. R., HATHERILL, M., VAN DER MEEREN, O., GINSBERG, A. M., VAN BRAKEL, E., SALAUN, B., SCRIBA, T. J., AKITE, E. J., AYLES, H. M., BOLLAERTS, A., DEMOITIÉ, M. A., DIACON, A., EVANS, T. G., GILLARD, P., HELLSTRÖM, E., INNES, J. C., LEMPICKI, M., MALAHLEHA, M., MARTINSON, N., MESIA VELA, D., MUYOYETA, M., NDUBA, V., PASCAL, T. G., TAMERIS, M., THIENEMANN, F., WILKINSON, R. J. & ROMAN, F. 2019. Final Analysis of a Trial of M72/AS01(E) Vaccine to Prevent Tuberculosis. *N Engl J Med,* 381**,** 2429-2439.

TAKAYAMA, K., WANG, C. & BESRA, G. S. 2005. Pathway to synthesis and processing of mycolic acids in Mycobacterium tuberculosis. *Clin Microbiol Rev,* 18**,** 81-101.

TAKEDA, K. & AKIRA, S. 2005. Toll-like receptors in innate immunity. *Int Immunol,* 17**,** 1-14.

TAKEUCHI, O., HOSHINO, K., KAWAI, T., SANJO, H., TAKADA, H., OGAWA, T., TAKEDA, K. & AKIRA, S. 1999. Differential roles of TLR2 and TLR4 in recognition of gram-negative and gram-positive bacterial cell wall components. *Immunity,* 11**,** 443-451.

THALSØ-MADSEN, I., TORRUBIA, F. R., XU, L., PETERSEN, A., JENSEN, C. & FREES, D. 2019. The Sle1 Cell Wall Amidase Is Essential for β-Lactam Resistance in Community-Acquired Methicillin-Resistant Staphylococcus aureus USA300. *Antimicrob Agents Chemother,* 64.

THAU, L., ASUKA, E. & MAHAJAN, K. 2022. Physiology, Opsonization. *StatPearls.* Treasure Island (FL): StatPearls Publishing

Copyright © 2022, StatPearls Publishing LLC.

TKACHUK, A., GUSHCHIN, V., POTAPOV, V., DEMIDENKO, A., LUNIN, V. & GINTSBURG, A. 2017. Multi-subunit BCG booster vaccine GamTBvac: Assessment of immunogenicity and protective efficacy in murine and guinea pig TB models. *PloS one,* 12**,** e0176784.

TURAPOV, O., FORTI, F., KADHIM, B., GHISOTTI, D., SASSINE, J., STRAATMAN-IWANOWSKA, A., BOTTRILL, A. R., MOYNIHAN, P. J., WALLIS, R., BARTHE, P., COHEN-GONSAUD, M., AJUH, P., VOLLMER, W. & MUKAMOLOVA, G. V. 2018. Two Faces of CwlM, an Essential PknB Substrate, in Mycobacterium tuberculosis. *Cell Rep,* 25**,** 57-67.e5.

UCLA, C., ROUX-LOMBARD, P., FEY, S., DAYER, J. & MACH, B. 1990. Interferon gamma drastically modifies the regulation of interleukin 1 genes by endotoxin in U937 cells. *The Journal of clinical investigation,* 85**,** 185-191.

UEHARA, T. & BERNHARDT, T. G. 2011. More than just lysins: peptidoglycan hydrolases tailor the cell wall. *Curr Opin Microbiol,* 14**,** 698-703.

UEHARA, T., DINH, T. & BERNHARDT, T. G. 2009. LytM-domain factors are required for daughter cell separation and rapid ampicillin-induced lysis in Escherichia coli. *Journal of bacteriology,* 191**,** 5094-5107.

UEHARA, T. & PARK, J. T. 2007. An anhydro-N-acetylmuramyl-L-alanine amidase with broad specificity tethered to the outer membrane of Escherichia coli. *Journal of bacteriology,* 189**,** 5634-5641.

UEHARA, T., PARZYCH, K. R., DINH, T. & BERNHARDT, T. G. 2010. Daughter cell separation is controlled by cytokinetic ring-activated cell wall hydrolysis. *The EMBO journal,* 29**,** 1412-1422.

VAN DER MEEREN, O., HATHERILL, M., NDUBA, V., WILKINSON, R. J., MUYOYETA, M., VAN BRAKEL, E., AYLES, H. M., HENOSTROZA, G., THIENEMANN, F., SCRIBA, T. J., DIACON, A., BLATNER, G. L., DEMOITIÉ, M. A., TAMERIS, M., MALAHLEHA, M., INNES, J. C., HELLSTRÖM, E., MARTINSON, N., SINGH, T., AKITE, E. J., KHATOON AZAM, A., BOLLAERTS, A., GINSBERG, A. M., EVANS, T. G., GILLARD, P. & TAIT, D. R. 2018. Phase 2b Controlled Trial of M72/AS01(E) Vaccine to Prevent Tuberculosis. *N Engl J Med,* 379**,** 1621-1634.

VAN HEIJENOORT, J. 2001. Formation of the glycan chains in the synthesis of bacterial peptidoglycan. *Glycobiology,* 11**,** 25r-36r.

VERMASSEN, A., LEROY, S., TALON, R., PROVOT, C., POPOWSKA, M. & DESVAUX, M. 2019a. Cell wall hydrolases in bacteria: insight on the diversity of cell wall amidases, glycosidases and peptidases toward peptidoglycan. *Frontiers in microbiology,* 10**,** 331.

VERMASSEN, A., TALON, R., ANDANT, C., PROVOT, C., DESVAUX, M. & LEROY, S. 2019b. Cell-Wall Hydrolases as Antimicrobials against Staphylococcus Species: Focus on Sle1. *Microorganisms,* 7.

VILAPLANA, C., MONTANÉ, E., PINTO, S., BARRIOCANAL, A., DOMENECH, G., TORRES, F., CARDONA, P. & COSTA, J. 2010. Double-blind, randomized, placebo-controlled Phase I Clinical Trial of the therapeutical antituberculous vaccine RUTI®. *Vaccine,* 28**,** 1106-1116.

VOLLMER, W., JORIS, B., CHARLIER, P. & FOSTER, S. 2008. Bacterial peptidoglycan (murein) hydrolases. *FEMS Microbiology Reviews,* 32**,** 259-286.

VOLZ, T., NEGA, M., BUSCHMANN, J., KAESLER, S., GUENOVA, E., PESCHEL, A., RÖCKEN, M., GÖTZ, F. & BIEDERMANN, T. 2010. Natural Staphylococcus aureus-derived peptidoglycan fragments activate NOD2 and act as potent costimulators of the innate immune system exclusively in the presence of TLR signals. *Faseb j,* 24**,** 4089-102.

VÖTSCH, W. & TEMPLIN, M. 2001. Characterization of a -N-acetylglucosaminidase ofEscherichia coli and Elucidation of Its Role in Muropeptide Recycling and -Lactamase Induction. *The Journal of biological chemistry,* 275**,** 39032-8.

WAKAMOTO, Y., DHAR, N., CHAIT, R., SCHNEIDER, K., SIGNORINO-GELO, F., LEIBLER, S. & MCKINNEY, J. D. 2013. Dynamic Persistence of Antibiotic-Stressed Mycobacteria. *Science,* 339**,** 91-95.

WALTERS, S. B., DUBNAU, E., KOLESNIKOVA, I., LAVAL, F., DAFFE, M. & SMITH, I. 2006. The Mycobacterium tuberculosis PhoPR two-component system regulates genes essential for virulence and complex lipid biosynthesis. *Mol Microbiol,* 60**,** 312-30.

WANG, Z. M., LI, X., COCKLIN, R. R., WANG, M., WANG, M., FUKASE, K., INAMURA, S., KUSUMOTO, S., GUPTA, D. & DZIARSKI, R. 2003. Human peptidoglycan recognition protein-L is an N-acetylmuramoyl-L-alanine amidase. *J Biol Chem,* 278**,** 49044-52.

WARTH, A. & STROMINGER, J. 1972. Structure of the peptidoglycan from spores of Bacillus subtilis. *Biochemistry,* 11**,** 1389-1396.

WARTH, A. D. & STROMINGER, J. L. 1969. Structure of the peptidoglycan of bacterial spores: occurrence of the lactam of muramic acid. *Proc Natl Acad Sci U S A,* 64**,** 528-35.

WEATHERSPOON-GRIFFIN, N., ZHAO, G., KONG, W., KONG, Y., ANDREWS-POLYMENIS, H., MCCLELLAND, M. & SHI, Y. 2011. The CpxR/CpxA two-component system up-regulates two Tat-dependent peptidoglycan amidases to confer bacterial resistance to antimicrobial peptide. *Journal of Biological Chemistry,* 286**,** 5529-5539.

WEI, W., JIANG, X., ZHANG, L., YAN, Y., YAN, J., XU, L., GAO, C.-H. & YANG, M. 2023. Regulation of CRISPR-Associated Genes by Rv1776c (CasR) in Mycobacterium tuberculosis. *Biomolecules,* 13**,** 400.

WHEELER, R., TURNER, R. D., BAILEY, R. G., SALAMAGA, B., MESNAGE, S., MOHAMAD, S. A., HAYHURST, E. J., HORSBURGH, M., HOBBS, J. K. & FOSTER, S. J. 2015. Bacterial Cell Enlargement Requires Control of Cell Wall Stiffness Mediated by Peptidoglycan Hydrolases. *mBio,* 6**,** e00660.

WHO 2019. *Global tuberculosis report 2019,* Geneva, World Health Organization.

WHO 2022. Global tuberculosis report 2022. Geneva: World Health Organization.

WHO, T. 2012. Global tuberculosis report 2012 World Health Organization. *Geneva: http://appswhoint/iris/bitstream/10665/91355/1/9789241564656_eng. pdf*.

WOLF, A. J. & UNDERHILL, D. M. 2018. Peptidoglycan recognition by the innate immune system. *Nat Rev Immunol,* 18**,** 243-254.

WONG, K.-W. & JACOBS, W. R., JR 2013. Mycobacteriumtuberculosis Exploits Human Interferon γ to Stimulate Macrophage Extracellular Trap Formation and Necrosis. *The Journal of Infectious Diseases,* 208**,** 109-119.

WU, K. J., BOUTTE, C. C., IOERGER, T. R. & RUBIN, E. J. 2019. Mycobacterium smegmatis HtrA blocks the toxic activity of a putative cell wall amidase. *Cell reports,* 27**,** 2468-2479. e3.

YAKHNINA, A. A., MCMANUS, H. R. & BERNHARDT, T. G. 2015. The cell wall amidase AmiB is essential for P seudomonas aeruginosa cell division, drug resistance and viability. *Molecular microbiology,* 97**,** 957-973.

YANG, D. C., TAN, K., JOACHIMIAK, A. & BERNHARDT, T. G. 2012. A conformational switch controls cell wall-remodelling enzymes required for bacterial cell division. *Mol Microbiol,* 85**,** 768-81.

YOSHIMURA, A., LIEN, E., INGALLS, R. R., TUOMANEN, E., DZIARSKI, R. & GOLENBOCK, D. 1999. Cutting edge: recognition of Gram-positive bacterial cell wall components by the innate immune system occurs via Toll-like receptor 2. *The Journal of Immunology,* 163**,** 1-5.

YUAN, Y., LEE, R. E., BESRA, G. S., BELISLE, J. T. & BARRY, C. E., 3RD 1995. Identification of a gene involved in the biosynthesis of cyclopropanated mycolic acids in Mycobacterium tuberculosis. *Proc Natl Acad Sci U S A,* 92**,** 6630-4.

ZHONG, Y., KINIO, A. & SALEH, M. 2013. Functions of NOD-like receptors in human diseases. *Frontiers in immunology,* 4**,** 333.

Chapter 7: Appendices

Appendix A: Growth Media Formulations

Lysogeny Agar (LA)

10 g Tryptone, 10 g NaCl, 5 g Yeast extract, 30 g Agar and dH_2O up to 1 l

Lysogeny Broth (LB)

10 g Tryptone, 10 g NaCl, 5 g Yeast extract and dH_2O up to 1 l

2X TY Broth

16 g Tryptone, 5 g NaCl, 10 g Yeast extract and sdH2O up to 1 l

Middlebrook 7H9 media

4.7 g Difco Middlebrook 7H9 powder, 2 ml glycerol, 10 ml 100 × glucose-salt (Msm) or 100 ml Middlebrook OADC (Mtb), 2 ml Tween80 and sdH_2O up to 1 l

Middlebrook 7H10 media

19 g Difco Middlebrook 7H10 powder, 2 ml glycerol, 10 ml 100 × glucose-salt (M. smegmatis) or 100 ml Middlebrook OADC (Mtb) and sdH_2O up to 1 l.

Middlebrook 7H11 media

19 g Difco Middlebrook 7H11 powder, 5 ml glycerol, 100 ml Middlebrook OADC (Mtb) and dH_2O up to 1 l

Media was sterilised by autoclaving at 121 °C for 20 min

Appendix B: Solutions

Solutions for DNA manipulation

1 M Tris-HCl: 60.56 g Tris, pH 8.0 with HCl and dH_2O up to 500 ml

0.5 M EDTA: 18.6 g powder, pH 8.0 with NaOH and dH_2O up to 500 ml

10% SDS: 50 g Sodium Dodecyl Sulfate and dH_2O up to 500 ml

5 M NaOH: 20 g Sodium hydroxide and dH_2O up to 100 ml

Solution I: 50 mM glucose, 25 mM Tris-HCl, 10 mM EDTA, pH 8.0

Solution II: 0.2 M NaOH, 1.0 % SDS

Solution III: 49 g potassium acetate, 11.5 ml glacial acetic acid, and dH_2O up to 100 ml

TE buffer: 1 ml 1 M Tris-HCl, 2 ml 0.5 M EDTA

TAE buffer: 242 g Tris base, 100 ml 0.5 M EDTA, 57.1 ml glacial acetic acid, pH 8.0, 1000 ml final volume dH_2O

Chloroform: Isoamyl alcohol: 24 ml Chloroform, 1 ml Isoamyl alcohol

Phenol: chloroform: 1 ml Phenol, 1 ml Chloroform

3M Sodium acetate: 24.6 g Sodium acetate and sdH2O up to 100 ml

CTAB/NaCl: 4.1 % NaCl, 10 % Cetyltrimethylammonium bromide dissolved in dH2O (filter sterilised)

Southern blotting solutions

Denaturation solution: 0.5 M NaOH, 1.5 M NaCl in dH_2O

Depurination solution: 0.25 M HCl in dH_2O

TBE (5X): 500 ml 10 x Tris-Borate-EDTA solution (Sigma) and 500 ml dH_2O

5 M Sodium citrate: 129.03 g sodium citrate and dH_2O up to 100 ml

SSC (20 ×): 3 M NaCl, 0.3 M sodium citrate in dH_2O

Solution I: 10 ml 20X SSC, 1 ml 10 % SDS, and dH_2O up to 100 ml

Solution II: 2.5 ml 20X SSC, 1 ml 10 % SDS, and dH_2O up to 100 ml

Maleic acid buffer: 116.1 g maleic acid powder, 87.66 g NaCl, pH 7.5 with NaOH pellets and dH_2O up to 1 l

Wash buffer: 0.1M Maleic acid buffer, 0.3 % Tween20

Blocking solution (Roche): 1 × blocking solution in maleic acid buffer

Detection buffer: 0.1M Tris-HCl, 0.1M NaCl in dH_2O (pH 9.5)

Antibody solution (Roche): Dilute 1 in 10 000 in blocking solution

CSPD (Roche): Disodium 2-chloro-5-(4-methoxyspiro (2-dioxetane-3,2 (2-dioxetane-3,2′-(5′-chloro)-tricyclo[3.3.1.1. 3, 7.]decan)-. 4-yl)-1-phenyl phosphate

SDS-PAGE and Western blotting solutions

Running buffer: 303 g Tris, 144 g glycine, 10 g SDS and dH_2O up to 1 l

Coomasie blue: 2 g Coomasie, 400 ml Ethanol and 100 ml acetic acid and dH_2O up to 1 l

De-stain: 400 ml Ethanol, 100 ml acetic acid and dH_2O up to 1 l

Transfer buffer: 3 g Tris, 14.4 g glycine, 1 g SDS, 200 ml methanol and dH_2O up to 1 l

TBS (10×): 24.2 g Tris Base, 80 g NaCl in and dH_2O up to 1 l

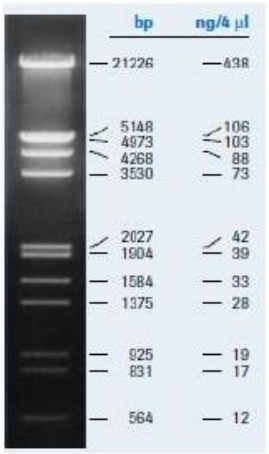
TBST: 100 ml 10 × TBS, 1 ml Tween20 and dH_2O up to 1 l

Blocking solution: 5 g Non-fat dry milk (CellSignal) and TBST up to 100 ml

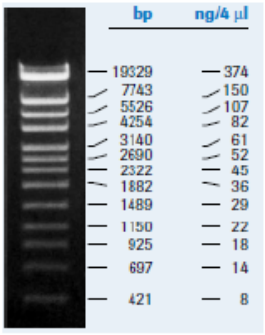
CPS Reagent (Sigma): Chemiluminescent Peroxidase Substrate

Appendix C: Molecular weight Marker

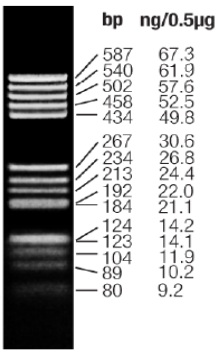
DNA Molecular weight markers



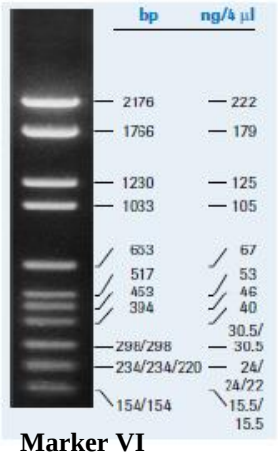
Marker III



Marker IV

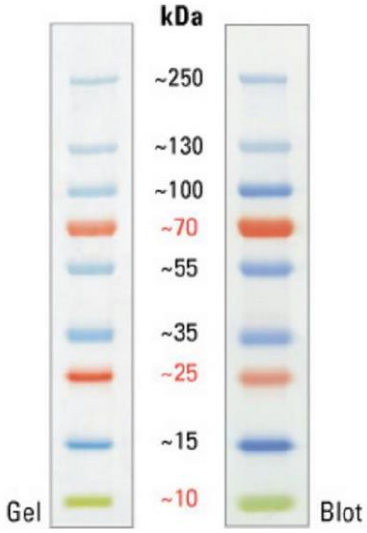


Marker V



Marker VI

Protein Molecular weight markers



PageRuler Plus prestained, protein ladder

Appendix D: Hain-line probe assay data sheet



Figure D1. Data sheet for the Hain-line probe assay performed on Mtb strains derived from the CFUs of the INH time-kill assay (Figure 3.6.1 E). Results confirm that H37RvS, H37*Δami1S*, H37*Δami1S*:: *ami1* did have any genetic resistance to INH via the *InhA* or *katG* genes

Appendix E: Optimization of Rv1423 IPTG inductions

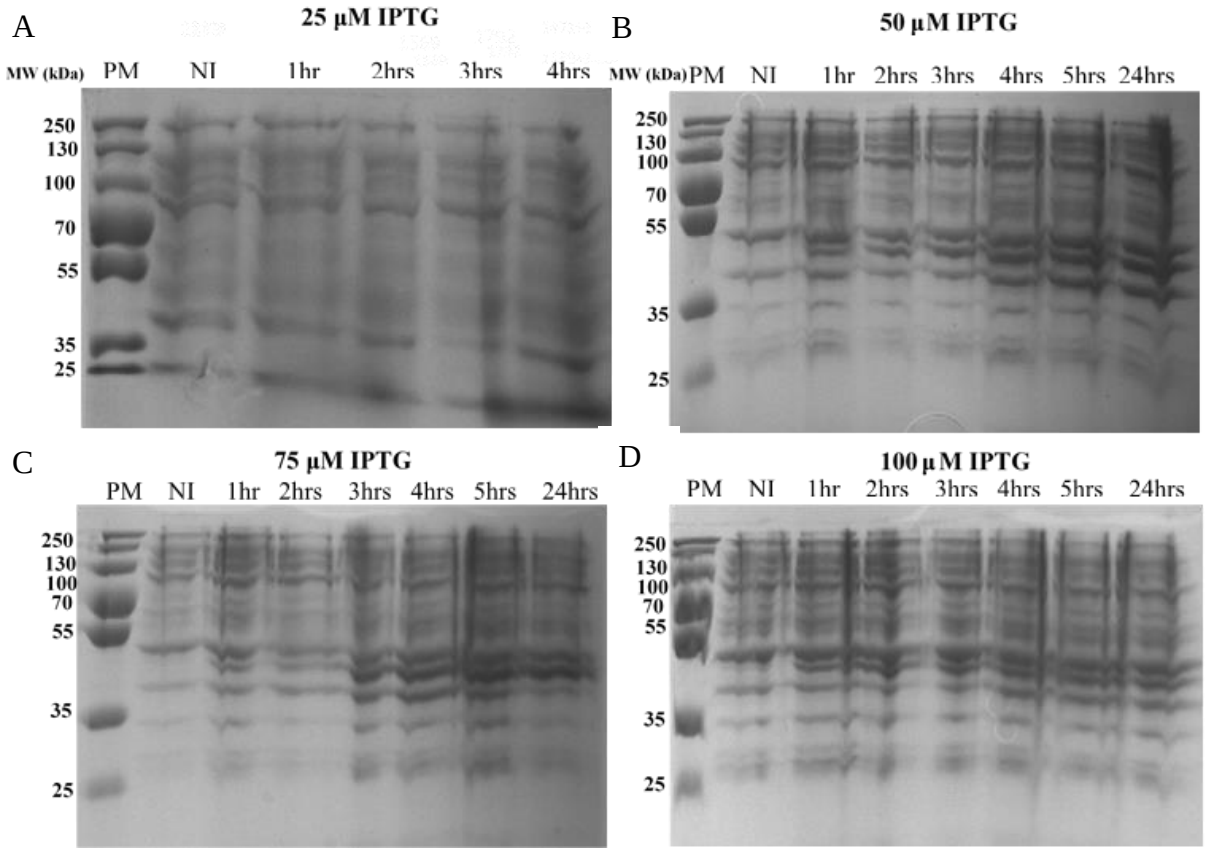


Figure E1. The optimization of IPTG induction of Rv1423 protein expression based on IPTG concentration. Induction of Rv1423 expression at 25 µM (A), 50 µM (B), 75 µM (C) and 100 µM (D) IPTG concentrations.

Appendix F: Optimization of EMSA Rv1776c-500bp UP *ami1* binding

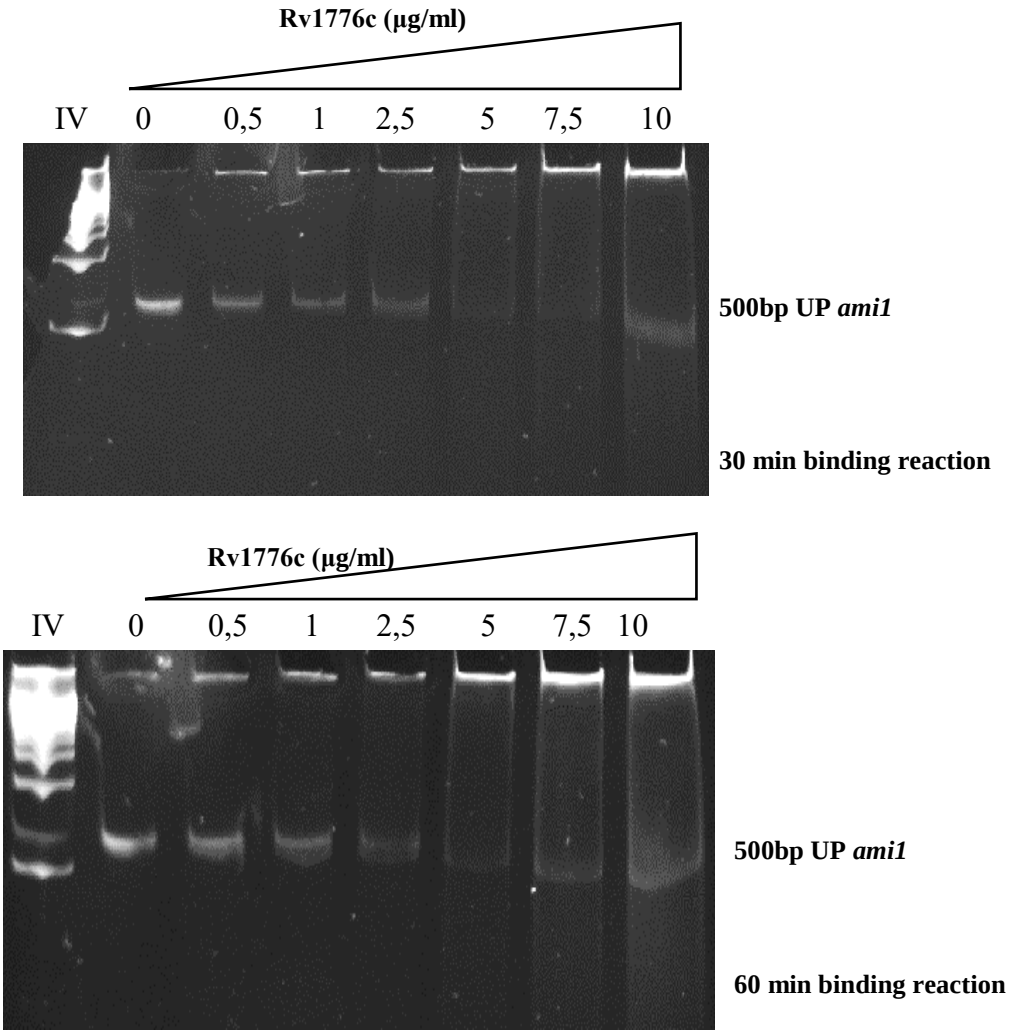


Figure F1. EMSA optimization of EMSA Rv1776c-500bp UP *ami1* binding by reaction length. Binding reaction length did not have an effect on the binding of Rv1776c to the *ami1* promoter region.

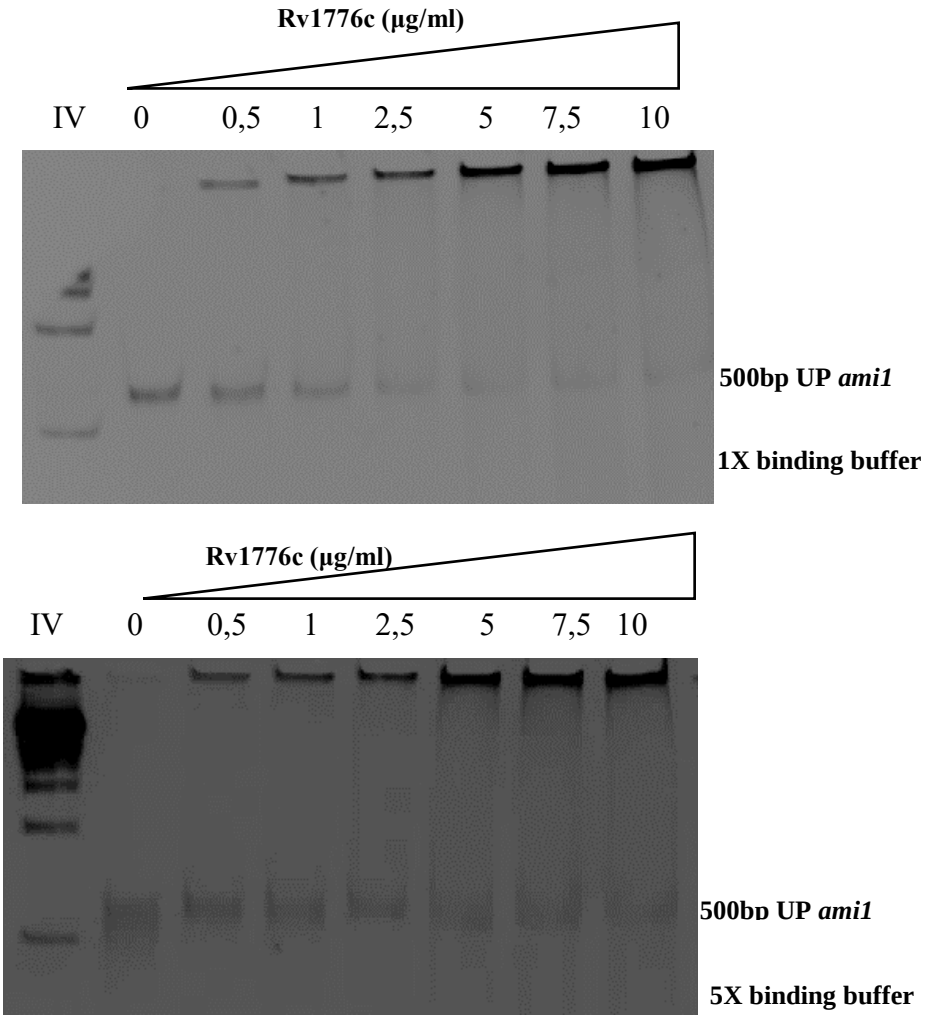


Figure F2. EMSA optimization of EMSA Rv1776c-500bp UP *ami1* binding by buffer concentration. Even though there was no visible band shift, the binding reaction with the 1X binding buffer was much more efficient in reducing the concentration of the 500 bp the *ami1* promoter region as the concentration of Rv1776c increased.

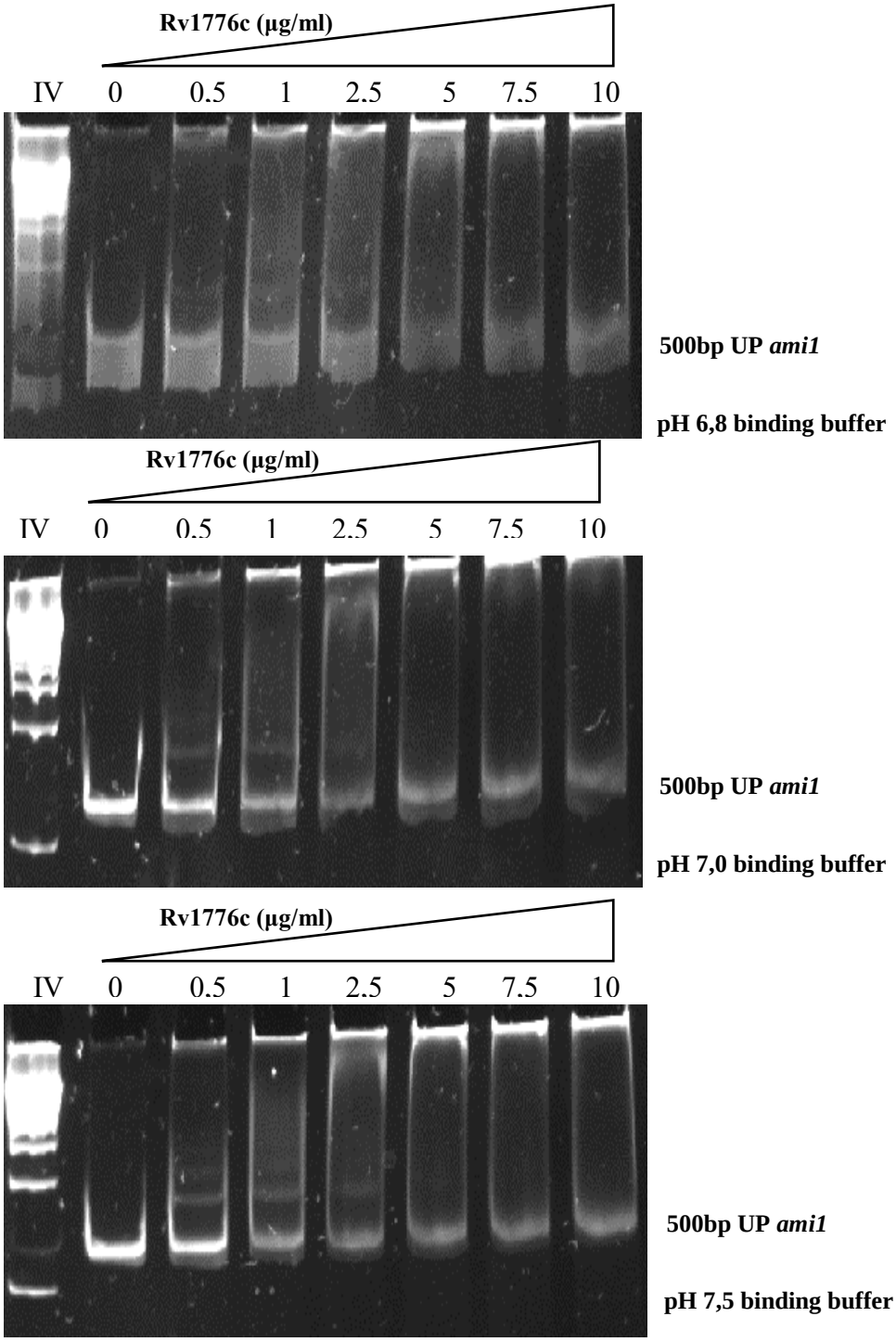


Figure F3. EMSA optimization of EMSA Rv1776c-500bp UP *ami1* binding by buffer pH. The binding reaction with the pH 7.5 was displayed an improved Rv1776c-500bp UP *ami1* binding compared to reactions at pH 6.8 and pH 7, respectively.

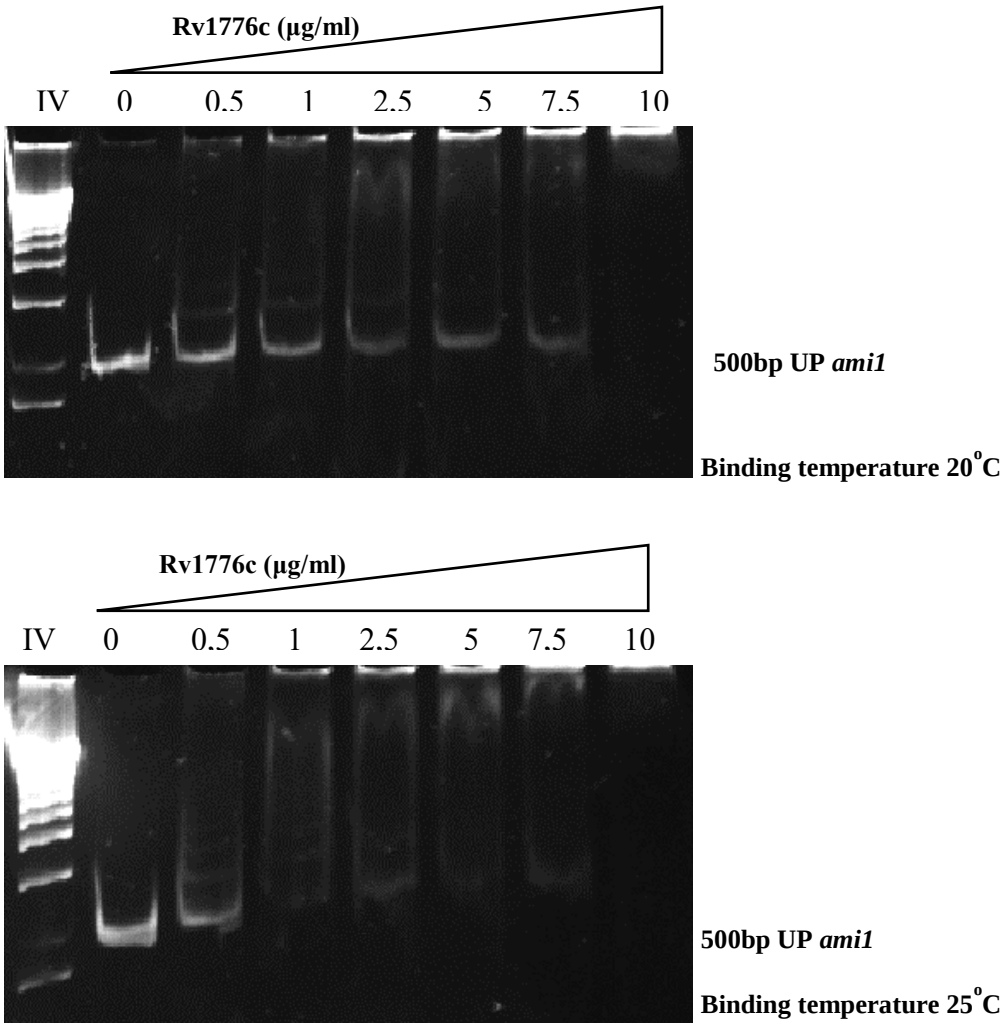


Figure F4. EMSA optimization of EMSA Rv1776c-500bp UP *ami1* binding by adusting binding reaction temperature. Binding reactions at 20ºC displayed improved Rv1776c-500bp UP *ami1* binding compared to the binding reactions at 25ºC.

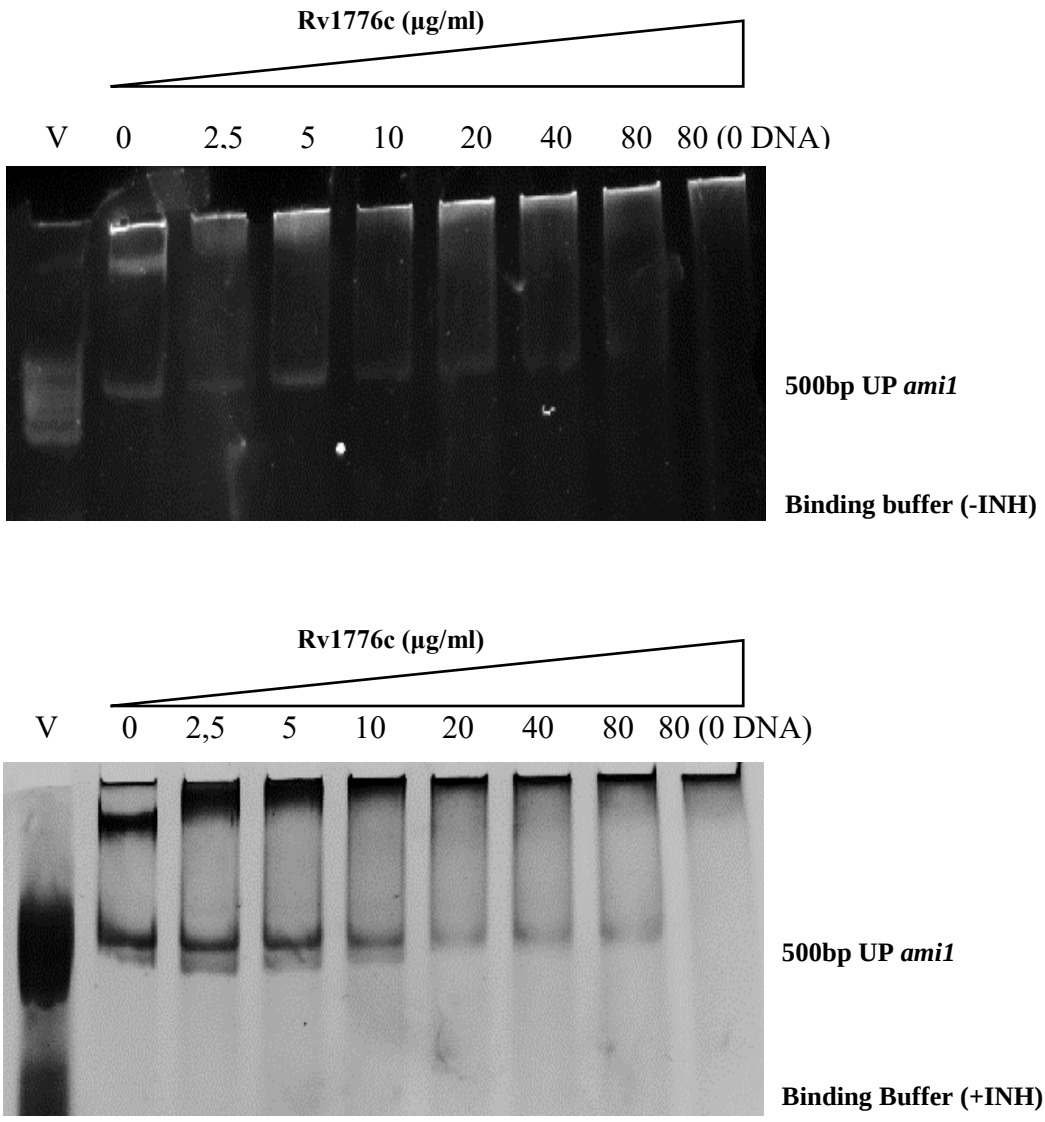


Figure F5. EMSA optimization of EMSA Rv1776c-500bp UP *ami1* binding using INH as possible cofactor.

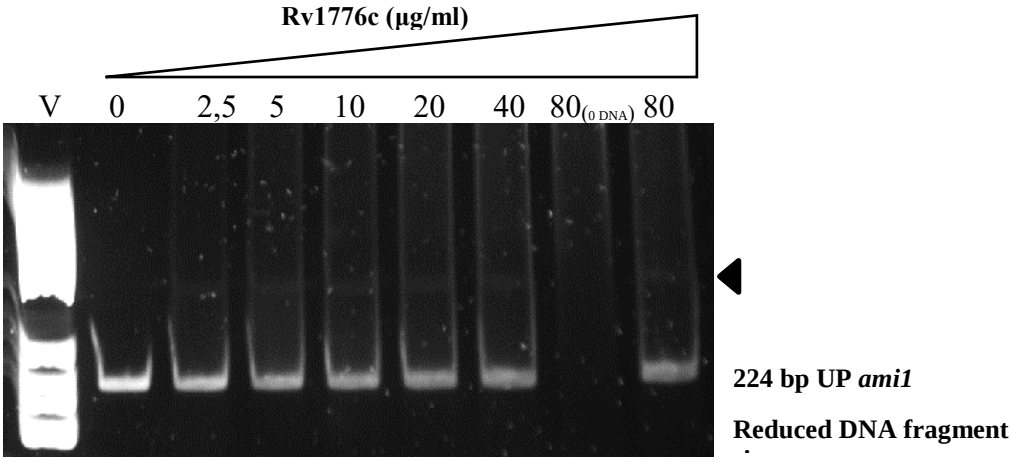


Figure F6. EMSA optimization of EMSA Rv1776c-500bp UP *ami1* binding by reducing DNA fragment size.

Appendix G: Ethics waiver

UNIVERSITY OF THE WITWATERSRAND, JOHANNESBURG

HUMAN RESEARCH ETHICS COMMITTEE (MEDICAL)

Human Research Ethics Committee (Medical)

Research Office Secretariat:
Faculty of Health Sciences, Phillip Tobias Health Sciences Building, 3rd Floor, Office 301/2/4, 29 Princess of Wales Terrace, Parktown, 2193
Private Bag 3, Wits 2050
Office email: HREC-Medical.ResearchOffice@wits.ac.za
Website: www.wits.ac.za/research/about-our-research/ethics-and-research-integrity/

Ref: W-CBP-200206-01 06/02/2020

TO WHOM IT MAY CONCERN:

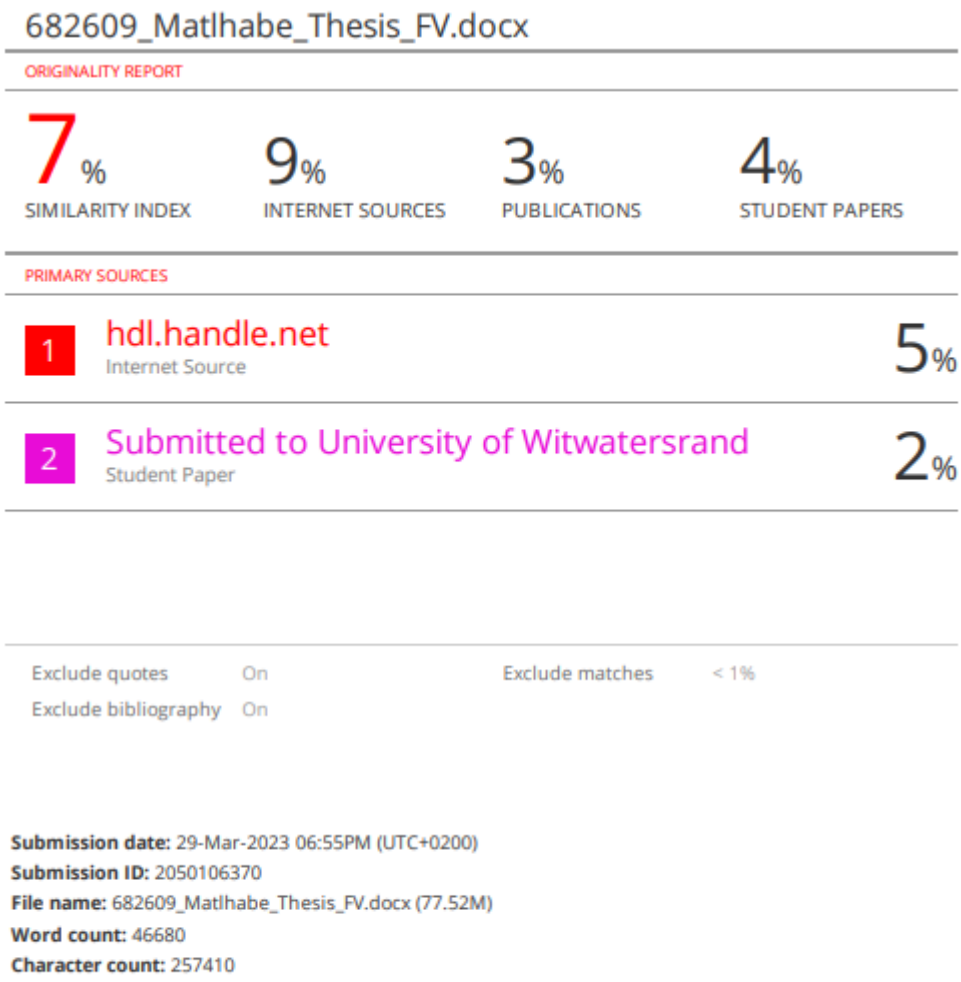
Waiver:	This certifies that the following research does not require clearance from the Human Research Ethics Committee (Medical)
Investigator:	Mr Ofentse Matlhabe
Supervisors:	Prof Bavesh Kana
Department:	Wits Centre of Excellence for Biomedical TB Research
Project title:	The characterisation of *Mycobacterium tuberculosis* amidase-like proteins
Reason:	*In vitro* laboratory study. No human participants, human data or human tissues will be involved in the study.

Dr CB Penny

Chairperson: Human Research Ethics Committee (Medical)

Copy – HREC (Medical) Secretariat: Ms Zanele Ndlovu, Ms Mapula Ramaila and Mr Rhulani Mkansi

Appendix H: Turn it in similarity report



682609_Matlhabe_Thesis_FV.docx

ORIGINALITY REPORT

7%	9%	3%	4%
SIMILARITY INDEX	INTERNET SOURCES	PUBLICATIONS	STUDENT PAPERS

PRIMARY SOURCES

1	hdl.handle.net Internet Source	5%
2	Submitted to University of Witwatersrand Student Paper	2%

Exclude quotes	On	Exclude matches	< 1%
Exclude bibliography	On		

Submission date: 29-Mar-2023 06:55PM (UTC+0200)
Submission ID: 2050106370
File name: 682609_Matlhabe_Thesis_FV.docx (77.52M)
Word count: 46680
Character count: 257410